minerals

Special Issue Reprint

Waste Valorization

Recycling and Recovery of Critical and Strategic Metals

Edited by
Elif Emil Kaya, Srecko Stopic and Duygu Yilmaz

mdpi.com/journal/minerals

MDPI

Waste Valorization: Recycling and Recovery of Critical and Strategic Metals

Waste Valorization: Recycling and Recovery of Critical and Strategic Metals

Guest Editors

Elif Emil Kaya
Srecko Stopic
Duygu Yilmaz

MDPI

Basel • Beijing • Wuhan • Barcelona • Belgrade • Novi Sad • Cluj • Manchester

Guest Editors

Elif Emil Kaya
IME Process Metallurgy and Metal Recycling Department
RWTH Aachen University
Aachen
Germany

Srecko Stopic
IME Process Metallurgy and Metal Recycling Department
RWTH Aachen University
Aachen
Germany

Duygu Yilmaz
Environmental Industrial Processes
IFE, Institute for Energy Technology
Kjeller
Norway

Editorial Office

MDPI AG
Grosspeteranlage 5
4052 Basel, Switzerland

This is a reprint of the Special Issue, published open access by the journal *Minerals* (ISSN 2075-163X), freely accessible at: https://www.mdpi.com/journal/minerals/special_issues/T53K8Q1YYO.

For citation purposes, cite each article independently as indicated on the article page online and as indicated below:

Lastname, A.A.; Lastname, B.B. Article Title. *Journal Name* **Year**, *Volume Number*, Page Range.

ISBN 978-3-7258-8659-3 (Hbk)
ISBN 978-3-7258-8660-9 (PDF)
https://doi.org/10.3390/books978-3-7258-8660-9

© 2026 by the authors. Articles in this reprint are Open Access and distributed under the Creative Commons Attribution (CC BY) license. The reprint as a whole is distributed by MDPI under the terms and conditions of the Creative Commons Attribution-NonCommercial-NoDerivs (CC BY-NC-ND) license (https://creativecommons.org/licenses/by-nc-nd/4.0/).

Contents

Srećko Stopić, Elif Emil-Kaya and Duygu Yilmaz
Waste Valorization: Recycling and Recovery of Critical and Strategic Metals
Reprinted from: *Minerals* **2026**, *16*, 386, https://doi.org/10.3390/min1640386 . . . . . **1**

José Machado Moita Neto, Régis Casimiro Leal, Nivianne Lima dos Santos Araújo and Elaine Aparecida da Silva
Challenges and Opportunities for the Development of Urban Mining in Brazil
Reprinted from: *Minerals* **2025**, *15*, 593, https://doi.org/10.3390/min1560593 . . . . . **6**

Aleksandar N. Nikoloski, Pritam Singh and Tina Chanda Phiri
From Waste to Resource: Critical Mineral Recovery and Environmental Impact Mitigation in Copper Smelting Slag
Reprinted from: *Minerals* **2026**, *16*, 206, https://doi.org/10.3390/min1620206 . . . . . **36**

Mertol Gökelma, Utku Hatipoğlu, Alicia Vallejo-Olivares, Rabia Önen Tüzgel, Olcay Kıvrak, Elif Bazoğlu, et al.
Effects of Size and Mechanical Pre-Treatment on Aluminium Recovery from Municipal Solid Waste Incineration Bottom Ash
Reprinted from: *Minerals* **2024**, *14*, 1006, https://doi.org/10.3390/min14101006 . . . . . **63**

Srecko Stopic, Duško Kostić, Richard Schneider, Magnus Sievers, Florian Wegmann, Elif Emil Kaya, et al.
Recovery of Titanium from Red Mud Using Carbothermic Reduction and High Pressure Leaching of the Slag in an Autoclave
Reprinted from: *Minerals* **2024**, *14*, 1151, https://doi.org/10.3390/min14111151 . . . . . **74**

Furkan Nazlı, Işıl Hasdemir, Emircan Uysal, Halide Nur Dursun, Utku Orçun Gezici, Duygu Yesiltepe Özçelik, et al.
Eco-Friendly Leaching of Spent Lithium-Ion Battery Black Mass Using a Ternary Deep Eutectic Solvent System Based on Choline Chloride, Glycolic Acid, and Ascorbic Acid
Reprinted from: *Minerals* **2025**, *15*, 782, https://doi.org/10.3390/min1580782 . . . . . **88**

Savas Ozun and Ahmet Kerim Guraslan
Enhanced Chromite Recovery from Tailings via a Custom-Designed Shaking Table: Optimization and Performance
Reprinted from: *Minerals* **2025**, *15*, 1100, https://doi.org/10.3390/min15111100 . . . . . **106**

Mahsa Pourmohammad, Josep Oliva, Hernan Anticoi, Carlos Hoffmann Sampaio, Pura Alfonso, César Valderrama, et al.
Recycling Copper (Cu) from Waste Automotive Printed Circuit Boards (WPCBs) After Characterization and Liberation Study by Mineral Processing Techniques
Reprinted from: *Minerals* **2025**, *15*, 1259, https://doi.org/10.3390/min15121259 . . . . . **124**

Stefan Petrović, Nenad Nikolić, Jovica Stojanović, Vesna Cvetkov, Vladimir Simić, Jovana Malbašić, et al.
Preliminary Study of Geochemical, Mineralogical and Magnetic Susceptibility Properties of Flotation Tailings from the Pb-Zn-Cu-Ag Rudnik Mine, Serbia
Reprinted from: *Minerals* **2025**, *15*, 1287, https://doi.org/10.3390/min15121287 . . . . . **146**

minerals

MDPI

Editorial

Waste Valorization: Recycling and Recovery of Critical and Strategic Metals

Srećko Stopić [1,*], Elif Emil-Kaya [2] and Duygu Yilmaz [3]

[1] IME Process Metallurgy and Metal Recycling, RWTH Aachen University, Intzestrasse 3, 52056 Aachen, Germany
[2] Department of Materials Science and Engineering, Norwegian University of Science and Technology, 7034 Trondheim, Norway
[3] Environmental Industrial Processes, Institute for Energy Technology, Instituttveien 18, 2007 Kjeller, Norway
* Correspondence: sstopic@metallurgie.rwth-aachen.de

1. Introduction

This Special Issue focuses on innovative approaches and methodologies for valorizing waste, including mineral waste and end-of-life (EoL) products, through the recycling and recovery of critical and strategic metals, including, but not limited to, rare earth elements, cobalt, copper, nickel, lithium, silver, aluminum, titanium, and silicon. Given the growing demand for these metals in high-tech and green energy industries, sustainable waste management practices are imperative. Key topics include, but are not limited to, the following:

Extraction and Purification processes: Hydrometallurgical techniques for recovering critical and strategic metals from industrial by-products, mineral residues, and EoL products.

Recycling Technologies: Cutting-edge approaches to enhance the efficiency and cost-effectiveness of recycling critical and strategic metals from waste streams such as sludge, red mud, tailings, slag, and EoL products, utilizing pyrometallurgical, hydrometallurgical, and electrometallurgical methods.

Thermodynamical Modeling and Process Simulation: In-depth studies on the thermodynamical aspects of metal extraction processes, including modeling and simulation techniques, to optimize and tailor the recycling techniques.

Economic and Environmental benefits: Comprehensive assessments of the potential economic gains and environmental impacts of critical/strategic metal recovery, fostering a circular economy and sustainability.

Case studies: Practical applications in the valorization of mineral waste and the extraction of critical and strategic raw materials.

Our text provides advances in the understanding of waste valorization. In particular, recycling and the recovery of critical and strategic metals were performed from different materials, such as red mud, using a combined pyrometallurgical and hydrometallurgical strategy. The hydrogen reduction of iron oxides from bauxite residue before a leaching process now offers a chance for an environmentally friendly technology.

2. Contents of This Special Issue

The Special Issues contain eight papers, which are mentioned in our list of contributions. Challenges and opportunities for the development of urban mining in Brazil are reported about the state of the art for these important activities (Contribution 1). This article highlights its unique context compared to other regions. While the European Union

focuses on critical metal supply and advanced Waste Electrical and Electronic Equipment (WEEE) legislation and the circular economy, Brazil's urban mining is primarily driven by waste management and social inclusion. The current investigation was underpinned by the PRISMA extension for Scoping Reviews (PRISMA-ScR framework) using targeted searches on the Web of Science platform for technological processes and the Brazilian scenario, complemented by an analysis of legislative evolution and a Critical Discourse Analysis of national policies. The results indicate that, despite advanced legislation, significant gaps exist between discourse and practice, highlighting the need for technological appropriation, specific public policies that incentivize reverse logistics, and the integration of the informal sector, and overcoming infrastructural challenges. It concludes that Brazil has a unique opportunity to develop an urban mining model that pioneeringly integrates environmental sustainability, technological innovation, and social inclusion, demanding coordinated efforts to overcome existing barriers.

Copper and cobalt are critically important metals for the transition to renewable energy and various aspects of modern life. Their production from primary sources, ores, necessitates metallurgical separation from the unwanted host materials, resulting in the generation of a huge amount of waste. Copper smelting slag is one of these metallurgical wastes, with 39 million tonnes of slag generated and discarded globally each year. These massive amounts of slag occupy a considerable and growing land footprint, often close to residential areas, and present a hazard that potentially releases contaminants into the environment. On the other hand, they also represent a material that often contains a significant residual amount of valuable copper and cobalt. To better understand and address the challenge of reducing the adverse impacts of the waste, as well as the possible commercial opportunity the contained critical metals present, this study reviews global smelting slag production over the last 25 years, its composition, and technical reprocessing options. A summary of the chemical and mineralogical characterization of the copper slag from diverse research is thus provided, as well as a comprehensive overview of the processing strategies for metal recovery from copper slag, such as flotation, pyrometallurgy, and hydrometallurgy. The study demonstrates that a huge amount of smelting slag has been produced, with great variation and complexity, which represents a major potential resource for cobalt and copper metals (Contribution 2). The chemical and mineralogical composition of smelting slag varies from location to location, depending on the properties of the feed concentrate, type of fluxes, furnace type, and cooling rates employed during and after the smelting processes. The overview of the production trends and reprocessing techniques shows that while some notable effective options exist or are emerging, further research is needed into the reprocessing of smelting slag waste in order to create economic value, improve energy efficiency in metal production, increase critical metal supply, and reduce negative environmental impacts.

Municipal solid waste (MSW) is incinerated to reduce the volume and recover energy and materials. The generation of MSW has been increasing over the past few decades due to the increase in population and changing consumption habits. Rising environmental and economic concerns have increased the importance of waste treatment and recovery. Currently, MSW may take three alternate or parallel routes: direct recycling, incineration, or landfill, depending on the country and location. MSW incineration has three products in addition to energy: bottom ash, fly ash, and off-gas. After incineration, bottom ash usually still contains many materials to be recovered, such as glass, ceramics, and metals with a degree of oxidation. This study focuses on aluminum recovery from MSW incineration bottom ash from two different countries. The 2–30 mm fraction of aluminum particles was characterized in terms of its size, shape, and oxide thickness, and its effects on aluminum recovery were investigated. In addition, the ability of mechanical pre-treatment to remove

https://doi.org/10.3390/min16040386

oxides prior to melting was studied. The results were compared with the analytical modeling developed in this study. An increasing particle size and surface area resulted in an increase in aluminum recovery. Mechanical pre-treatment increased the yield for smaller particles to a larger extent than for larger particles due to the difference in the oxide/metal ratio (Contribution 3).

Red mud is a byproduct of alumina production, which is largely stored in landfills that can endanger the environment. Red mud, or bauxite residue, is a mixture of inorganic compounds of iron, aluminum, sodium, titanium, calcium, and silicon, mostly, as well as a large number of rare earth elements in small quantities. Although certain methods of using red mud already exist, none of them have been widely implemented on a large scale. This paper proposes a combination of two methods for the utilization of red mud, first by carbothermic reduction and then by leaching under high pressure in an autoclave, in order to extract useful components from it with a focus on titanium. In the first part of the work, the red mud was reduced with carbon at 1600 °C in an electric arc furnace, with the aim of removing as much iron as possible using magnetic separation (Contribution 4). After separation, the slag is leached in an autoclave at different parameters in order to obtain the highest possible yield of titanium, aiming for the formation of titanium oxysulfate and avoiding silica gel formation. A maximal leaching efficiency of titanium of 95% was reached at 150 °C using 5 mol/L sulfuric acid with 9 bar oxygen in 2 h. We found that high-pressure conditions enabled avoiding the formation of silica gel during the leaching of the slag using 5 mol/L sulfuric acid, which is a big problem at atmospheric pressure. Previously, silica gel formation was prevented using the dry digestion process with 12 mol/L sulfuric acid under atmospheric pressure (Contribution 4).

Lithium-ion batteries (LiBs) are utilized in numerous applications due to advancements in technology, and the recovery of end-of-life (EoL) LiBs is imperative for environmental and economic reasons. Pyrometallurgical and hydrometallurgical methods have been used in the recovery of metals such as Li, Co, and Ni in the EoL LiBs. Hydrometallurgical methods, which have been demonstrated to exhibit higher recovery efficiency and reduced energy consumption, have garnered increased attention in recent research. Inorganic acids, including HCl, HNO_3, and H_2SO_4, as well as organic acids such as acetic acid and citric acid, are employed in the hydrometallurgical recovery of these metals. It is imperative to acknowledge the environmental hazards posed by these acids. Consequently, solvometallurgical processes, which involve the use of organic solvents with minimal or no water, are gaining increasing attention as alternative or complementary techniques to conventional hydrometallurgical processes. In the context of solvent systems that have been examined for a range of solvometallurgical methods, deep eutectic solvents (DESs) have garnered particular interest due to their low toxicity, biodegradable nature, tunable properties, and efficient metal recovery potential. In this study, the leaching process of black mass containing graphite, LCO, NMC, and LMO was carried out in a short time using the ternary DES system. The ternary DES system consists of choline chloride (ChCl), glycolic acid (GLY), and ascorbic acid (AA). As a result of the leaching process of cathode powders in the black mass without any pre-enrichment process, Li, Co, Ni, and Mn elements passed into solution with an efficiency of over 95% at 60 °C and within 1 h. Moreover, the kinetics of the leaching process were investigated, and Density Functional Theory (DFT) calculations were used to explain the leaching mechanism (Contribution 5).

Significant chromite losses to tailings in gravity separation plants arise from both suboptimal separator design and inefficient beneficiation processes, posing major challenges to resource utilization, energy efficiency, and environmental sustainability. These losses are particularly critical because the material, already comminuted to liberation size, is discarded, leading to reduced concentrate yield, wasted energy input, and increased

https://doi.org/10.3390/min16040386

environmental pollution. To address this issue, an industrial-scale custom-designed shaking table was developed and tested to recover marketable-grade chromite concentrate ($\geq$42% Cr_2O_3) from processing plant tailings containing 3.25%–4.25% Cr_2O_3, which had accumulated over years of chromite beneficiation. Experimental results showed that, under optimized operating parameters (320 rpm stroke frequency, 13 mm stroke length, 1° deck slope, 1300 g/L pulp density, 800 kg/h feed rate, and 7 tph wash water flow rate), Cr_2O_3 recovery increased from 8% to 27% for the first and second floor operations and from approximately 17% to 41% for the third and fourth floor operations compared with existing plant performance (Contribution 6) The results revealed a strong interdependence between Cr_2O_3 recovery and concentrate grade, both of which are critical indicators of process efficiency. Intermediate particle sizes (−0.250 + 0.150 mm) provided the most favorable balance, yielding high recovery rates without substantially compromising the concentrated grade (Contribution 6).

Waste printed circuit boards (WPCBs) are one of the fastest-growing waste streams and pose a significant environmental challenge while also representing a valuable secondary resource due to their rich metal content, particularly copper (Cu). Since effective recovery of metals requires mechanical pre-treatment and advanced characterization, WPCBs were subjected to size reduction and then characterized through X-ray fluorescence (XRF), inductively coupled plasma optical emission spectroscopy (ICP-OES), scanning electron microscopy (SEM-EDS), and mineral liberation analysis (MLA). Results indicated that copper is predominantly found in coarser particle sizes due to its ductility, while glass fibers and ceramics dominate finer fractions. Liberation studies revealed that Cu is essentially free in fine particles (<100 μm) but tends to remain locked in coarser fractions. Based on these results, gravity separation methods were employed to concentrate the copper: coarse particles (>300 μm) were treated on a shaking table, achieving a Cu recovery of 95%, while fine particles (<300 μm) were processed using a multi-gravity separator (MGS), with recoveries of 94% for 100 × 300 μm and 81.5% for <100 μm size fractions. This study presents a gravity-based separation strategy that combines shaking tables and MGS to optimize Cu recovery from automotive WPCBs (Contribution 7). To the authors' knowledge, the MGS application for WPCBs has received little attention, despite its strong potential for separating this type of waste. The proposed methodology enhances the concentration and purity of the metallic fraction (in this case, Cu), especially in fine particles, which are challenging to work with, while reducing environmental impacts through minimal chemical use, thereby contributing to sustainable e-waste recycling.

Samples of flotation tailings generated during the exploitation and processing of Zn–Pb–Cu–Ag ore from the Rudnik mine (Serbia) were investigated for their mineralogical, geochemical, and magnetic susceptibility properties. The flotation tailings consist of a complex mineral assemblage, including silicates, carbonates, sulfides, phosphates, sulfates, oxides, hydroxides, and native elements. Quartz, calcite, and orthoclase dominate the coarse fraction (>400 μm), accompanied by epidote, Ca-garnet, and Ca-clinopyroxene. Sulfide minerals are concentrated in finer fractions (<400 μm), with pyrite and arsenopyrite being the most abundant, followed by pyrrhotite, sphalerite, galena, and chalcopyrite. These sulfides occur as dispersed grains within a silicate–carbonate matrix. Post-depositional oxidative alteration is moderately developed, with pyrite replaced by hematite, galena by cerussite, and chalcopyrite by malachite. Geochemical analyses reveal that SiO_2 (avg. 38.98 wt%), Fe_2O_3 (avg. 23.68 wt%), Al_2O_3 (avg. 8.95 wt%), CaO (avg. 9.03 wt%), and MgO (avg. 1.50 wt%) dominate the composition. Economically significant metals include Zn (avg. 0.47 wt%), Pb (avg. 0.20 wt%), Cu (avg. 0.11 wt%), Ag (max. 19 μg/g), and Bi (max. 130 μg/g). Mass magnetic susceptibility shows a strong correlation with S (r = 0.92), Co (r = 0.90), and Bi (r = 0.87); moderate correlation with Fe_2O_3, Al_2O_3, and As; and

https://doi.org/10.3390/min16040386

negative correlation with Mn, TiO_2, Zn, and Pb. The ferromagnetic phase most likely originates from pyrrhotite, as well as hematite formed during pyrite alteration, and goethite (Contribution 8).

3. Conclusions

Special Issue "Waste valorization: Recycling and Recovery of Critical and Strategic Metals" is a very important book that collected eight important papers based on copper, aluminum, titanium, lithium, chromium and other valuable metals, which offer new results needed for their recovery from bauxite residue from Bosnia and Herzegoviina, flotating tailings from preparation of Zn-Fe-Cu-Ag concentrates from Serbia, chromite tailings, spent lithium-ion batteries and waste printed circuit boards. Urban mining with metallurgical and mining activities in Brazil is mentioned in order to offer new possibilities for metal recovery. Unfortunately, the editors do not have high expectations regarding the implementation of the results, because all planned actions are always related to large costs and securing the necessary funding.

Conflicts of Interest: The authors declare no conflicts of interest.

List of Contributions:

1. Neto, J.M.M.; Leal, R.C.; Araújo, L.S.; da Silva, E.A. Challenges and Opportunities for the Development of Urban Mining in Brazil. *Minerals* **2025**, *15*, 593. https://doi.org/10.3390/min15060593.
2. Nikoloski, A.N.; Singh, P.; Phiri, T.C. From Waste to Resource: Critical Mineral Recovery and Environmental Impact Mitigation in Copper Smelting Slag. *Minerals* **2026**, *16*, 206. https://doi.org/10.3390/min16020206.
3. Gökelma, M.; Hatipoğlu, U.; Vallejo-Olivares, A.; Tüzgel, R.Ö.; Kivrak, O.; Bazoğlu, O.; Çizen, Z.S.; Trannel, G. Effects of Size and Mechanical Pre-Treatment on Aluminium Recovery from Municipal Solid Waste Incineration Bottom Ash. *Minerals* **2024**, *14*, 1006. https://doi.org/10.3390/min14101006.
4. Stopić, S.; Kostić, D.; Perušić, M.; Schneider, R.; Souza Filho, I.R.; Mitrašinović, A.; Friedrich, B. Comparative Analysis of Reduction Techniques Aiming for the Minimization of Contaminated Soil with Red Mud. *Minerals* **2025**, *15*, 470. https://doi.org/10.3390/min15050470.
5. Nazlı, F.; Hasdemir, I.; Uysal, E.; Dursun, H.N.; Gezici, U.O.; Özçelik, D.Y.; Burat, F.; Gürmen, S. Eco-Friendly Leaching of Spent Lithium-Ion Battery Black Mass Using a Ternary Deep Eutectic Solvent System Based on Choline Chloride, Glycolic Acid, and Ascorbic Acid. *Minerals* **2025**, *15*, 782.
6. Ozun, S.; Guraslan, A.K. Enhanced Chromite Recovery from Tailings via a Custom-Designed Shaking Table: Optimization and Performance. *Minerals* **2025**, *15*, 1100. https://doi.org/10.3390/min15111100.
7. Pourmohammad, M.; Oliva, J.; Anticoi, H.; Sampaio, C.H.; Alfonso, P.; César Valderrama, C.; Cortina, J.L.; Percy Escalante, P. Recycling Copper (Cu) from Waste Automotive Printed Circuit Boards (WPCBs) After Characterization and Liberation Study by Mineral Processing Techniques. *Minerals* **2025**, *15*, 1259. https://doi.org/10.3390/min15121259.
8. Petrović, S.; Nikolić, N.; Stojanović, J.; Cvetkov, V.; Simić, V.; Malbašić, J.; Obrenović, L.; Životić, D. Preliminary Study of Geochemical, Mineralogical and Magnetic Susceptibility Properties of Flotation Tailings from the Pb-Zn-Cu-Ag Rudnik Mine, Serbia. *Minerals* **2025**, *15*, 1287. https://doi.org/10.3390/min15121287.

Disclaimer/Publisher's Note: The statements, opinions and data contained in all publications are solely those of the individual author(s) and contributor(s) and not of MDPI and/or the editor(s). MDPI and/or the editor(s) disclaim responsibility for any injury to people or property resulting from any ideas, methods, instructions or products referred to in the content.

minerals

MDPI

Review

Challenges and Opportunities for the Development of Urban Mining in Brazil

José Machado Moita Neto [1], Régis Casimiro Leal [2,3], Nivianne Lima dos Santos Araújo [1] and Elaine Aparecida da Silva [3,4,*]

[1] Federal University of Parnaíba Delta, Ministro Reis Velloso Campus, Avenida São Sebastião, 2819, Nossa Senhora de Fátima, Parnaíba 64202-020, PI, Brazil; jose.machado.moita.neto@gmail.com (J.M.M.N.); niviannearaujo@ufdpar.edu.br (N.L.d.S.A.)
[2] Federal Institute of Education, Science and Technology of Rio Grande do Norte, Nova Cruz Campus, Avenida José Rodrigues de Aquino Filho, nº 640, RN-120, Alto de Santa Luzia, Nova Cruz 59215-000, RN, Brazil; regis.casimiro@ifrn.edu.br
[3] Postgraduate Program in Development and Environment, PRODEMA–TROPEN, Federal University of Piauí, Avenida Universitária, Teresina 64049-550, PI, Brazil
[4] Department of Water Resources, Geotechnics and Environmental Sanitation, Technology Center, Federal University of Piauí, Avenida Universitária, Teresina 64049-550, PI, Brazil
* Correspondence: elaine@ufpi.edu.br

Abstract: This article examines urban mining in Brazil, highlighting its unique context compared to other regions. While European Union focuses on critical metal supply and advanced Waste Electrical and Electronic Equipment (WEEE) legislation and circular economy, Brazil's urban mining is primarily driven by waste management and social inclusion. The current investigation was underpinned by the PRISMA extension for Scoping Reviews (PRISMA-ScR framework), using targeted searches on the Web of Science platform for technological processes and the Brazilian scenario, complemented by an analysis of legislative evolution and a Critical Discourse Analysis of national policies. The results indicate that, despite advanced legislation, significant gaps exist between discourse and practice, highlighting the need for technological appropriation, specific public policies that incentivize reverse logistics and the integration of the informal sector, and overcoming infrastructural challenges. It concludes that Brazil has a unique opportunity to develop an urban mining model that pioneeringly integrates environmental sustainability, technological innovation, and social inclusion, demanding coordinated efforts to overcome existing barriers.

Keywords: circular economy; e-waste; construction and demolition waste; urban solid waste; secondary raw materials; national solid waste policy; reverse logistics

1. Introduction

Urban mining, conceived as a circular economy strategy, encompasses various concepts that complement each other by aiming to transform waste into valuable secondary resources. Attention towards this type of mining has been growing in discussions about secondary raw materials, although its application in developing countries is often limited by local resources, technology, and ineffective legislation on electronic waste (e-waste) [1].

Kazançoglu et al. [2] describe urban mining as a management approach that aids the supply of secondary raw materials through the recycling of precious metals, contributing to improved consumption patterns and decreased resource use. Ghisellini et al. [3] expand on this idea, defining urban mining as a process (encompassing collection, separation, sorting, and processing) at the city level for waste streams such as Construction and Demolition

Waste (CDW) and Waste Electrical and Electronic Equipment (WEEE), aiming for their return to a new production cycle.

These concepts complement each other by highlighting that urban mining is an activity embedded within the context of the circular economy, with the main objective of recovering resources from waste, thereby decreasing the reliance on virgin raw materials. They differ, on the other hand, in the scope of the waste considered and the level of detail of the process. While some authors focus primarily on e-waste, others include a broader range of urban waste, such as CDW. Although considered for the development of urban mining, CDW is not included in the discussions in the discussions of this article.

In the context of the circular economy, urban mining operationalizes the principle of material circulation, transforming what would be discarded into a new source of resources. Fatimah et al. [4] state that efforts to overcome the e-waste problem exist, and urban mining is an essential component of these efforts. Ouro-Salim [5] also emphasizes the synergy between urban mining and the circular economy, highlighting that the former serves as a critical mechanism to realize the principles of the latter and minimize environmental impacts.

In the realm of sustainability, urban mining presents itself as a practice with the potential to generate positive impacts in various dimensions. Environmentally, it contributes to the reduction of pollution associated with the inadequate disposal of hazardous waste, such as those present in e-waste [1,5–8]. Economically, it can generate new business opportunities and green jobs, in addition to reducing costs for industries by providing secondary raw materials [1,9,10]. Socially, it can promote the formalization of the informal recycling sector and improve the working conditions of those involved [3,10].

Urban mining of e-waste is a new frontier to be explored in Brazil, with the potential for economic valorization and waste minimization [9]. Its successful implementation can play important roles in promoting several Sustainable Development Goals (SDGs), including sustainable cities and communities (SDG 11) and responsible consumption and production (SDG 12) [4].

When contrasting the approaches to urban mining in different global regions, such as Brazil and the European continent, it is noticeable that, although a common goal of sustainability may be shared, the urgency and motivators manifest in distinct ways. Specifically, the European Union (EU) presents a case of advanced regulatory development for WEEE and circular economy, though implementation and focus can vary.

The European Union (EU), in particular, driven by concerns over resource scarcity and a commitment to environmental leadership, has developed strong environmental regulations and ambitions to lead the transition to a circular economy. This positions urban mining as a central strategy to ensure access to essential materials and reduce import dependency. Baldé et al. [11] highlight that European countries, especially those within the EU, are often cited as examples in legislating and managing e-waste. The growing consumer awareness and the pressure for responsible business practices also drive this activity as a strategic priority for industrial competitiveness and security of supply within this bloc and other developed European nations.

On the other hand, Brazil, possessing vast mineral reserves, faces the challenge of reconciling economic development with the effective application of its environmental legislation, which often presents gaps and enforcement challenges. Although the country has abundant mineral resources, the uncontrolled exploitation and environmental impacts associated with conventional mining generate considerable social and environmental costs. In this context, urban mining in Brazil reveals itself as a necessity to promote sustainable development, reduce social inequalities, and protect its vast natural heritage.

A critical analysis reveals that the different socioeconomic and regulatory contexts shape the implementation of urban mining in Europe and Brazil. While Europe invests in advanced recycling technologies and the creation of value chains for recovered materials, aiming to strengthen its strategic autonomy and reduce its ecological footprint, Brazil still faces significant challenges. Among these challenges are the public's lack of knowledge about the correct destination of WEEE, the informality in the recycling chain, the lack of an official database on the generation and flows of WEEE, and the difficulties related to the traceability of this waste [10].

Additionally, Brazil's continental dimensions and the concentration of recyclers in the South and Southeast regions of the country, coupled with the scarcity of processing units for precious metals, increase logistical costs and may increase greenhouse gas emissions resulting from transportation, including for export. The lack of a specific and unified taxation policy for the sector also generates legal uncertainty and can discourage urban mining entrepreneurs. In contrast, the European Union, with its more developed infrastructure and cohesive policies regarding the circular economy and waste management, presents a more favorable scenario for the expansion of urban mining on a large scale. However, it is important to note that even within the EU, the effectiveness and implementation of these policies can vary, with challenges in meeting collection and recycling targets remaining [11].

Considering the presented panorama, this article proposes to analyze the challenges and opportunities for the development of urban mining in Brazil, focusing on the dimensions of knowledge production, technological appropriation, and the effectiveness of current and necessary legislation to drive this activity. Through the investigation of these pillars, this analysis seeks to contribute scientifically to a deeper understanding of Brazil's specific conditions, offering subsidies for future research and for the formulation of public policies that can effectively promote urban mining as a strategy for sustainability and the utilization of secondary resources in the country.

Despite growing global attention to urban mining, a comprehensive understanding of its development within the unique Brazilian context—marked by distinct socioeconomic drivers, technological capacities, and regulatory challenges compared to scenarios like the European one—remains limited. Specifically, while extensive research exists on urban mining in developed nations, there is a notable gap in the literature concerning its specific challenges and opportunities in developing countries such as Brazil, which possesses vast mineral reserves but faces significant hurdles in reconciling economic development with effective environmental legislation. This study addresses this critical research gap by systematically analyzing the dimensions of knowledge production, technological appropriation, and legislative effectiveness in Brazil, moving beyond the implied need for urban mining to a direct examination of its operationalization and support systems within a unique national context.

Therefore, this scoping review seeks to bridge this understanding gap by systematically investigating the current state and future perspectives of urban mining in Brazil through a multi-dimensional lens. Specifically, this study is guided by the following research questions:

1. What is the current state of knowledge production regarding urban mining in Brazil, and how does it compare with international trends?
2. What are the main technological routes being explored or required for urban mining in Brazil, and what are the challenges for their effective appropriation in the national context?
3. To what extent is the current Brazilian legislation effective in driving urban mining, and what are the main legal and regulatory obstacles that need to be overcome?

4. How do the challenges and opportunities for urban mining in Brazil compare with those observed in the European context, considering their distinct socioeconomic and environmental drivers?

2. Methodology

This study was conducted as a comprehensive scoping review to analyze the challenges and opportunities for the development of urban mining in Brazil, focusing on the dimensions of knowledge production, technological appropriation, and the effectiveness of legislation. The reporting of this review was guided by the principles outlined in the Preferred Reporting Items for Systematic reviews and Meta-Analyses (PRISMA) extension for Scoping Reviews (PRISMA-ScR) Checklist [12].

2.1. Eligibility Criteria (PRISMA Item 6)

Sources of evidence included original research articles and review articles. Priority was given to publications from the last five years (approximately 2020–2025), with consideration for seminal works up to 10 years old to ensure a robust overview of the current panorama while also identifying research gaps and avoiding duplications. Articles were primarily sought in English and Portuguese. The focus was on studies directly addressing urban mining concepts, processes, challenges, opportunities, and legislative aspects pertinent to Brazil or offering comparative insights. Studies that did not clearly align with these themes were excluded.

2.2. Information Sources and Search Strategy (PRISMA Items 7 and 8)

The primary information source for scientific literature was the Web of Science (WoS) platform. The most recent search was conducted in March 2025. The search strategy involved specific term combinations designed to capture different facets of urban mining relevant to the study objectives.

For the analysis of processes and technologies employed in urban mining (Section 4), combined searches were performed for the term "urban mining" with the main chemical recovery processes: "hydrometallurgy", "pyrometallurgy", and "biohydrometallurgy". To examine knowledge production and technological appropriation in Brazil (Section 6), the term "urban mining" was used, filtering the results by Countries/Regions: "Brazil". For all situations, we apply the filter by document type in order to obtain only original research articles and review articles. Table 1 summarizes the results for the main searches used:

Table 1. Quantification of searches versus keywords used.

Keywords	Records Obtained [1]
"urban mining" and "hydrometallurgy"	27
"urban mining" and "pyrometallurgy"	9
"urban mining" and "biohydrometallurgy"	10
"urban mining" and filtering the results by Countries/Regions: "Brazil"	41

[1] Search Period = the last search was conducted in March 2025.

Additionally, the methodological approach for the analysis of the legal dimension (Section 7) involved a review of legislative documents and policies pertinent to Brazil and the European Union. This analysis focused on providing an overview of the evolution of legislation on solid waste, with a comparison between Brazil [13–16] and the European Union [17–21], dedicating special attention to Waste Electrical and Electronic Equipment (WEEE) as a central raw material for urban mining. The National Solid Waste Policy [22]

and its subsequent decrees [23–26] were detailed, explaining concepts such as shared responsibility and reverse logistics.

Further relevant sources, in addition to those initially identified by the term combinations (Extra sources), were included whenever they were considered relevant to enrich the discussion and provide a more comprehensive understanding of the theme.

2.3. Selection of Sources of Evidence (PRISMA Item 9)

The selection process involved an initial screening of titles and abstracts of the articles retrieved from the database searches based on their relevance to the review's objectives and the eligibility criteria. Articles clearly outside the scope were excluded during this initial phase. Full-text articles deemed potentially relevant were then assessed for eligibility through a critical reading based on the criteria outlined above. This assessment focused on confirming the direct relevance and contribution to the specific analytical dimensions of this review (knowledge production, technological appropriation, legislative aspects, processes, and the Brazilian context). Articles that did not meet the inclusion criteria after full-text review were excluded, and the reasons for exclusion were noted.

To transparently illustrate the systematic selection of studies included in this review, a PRISMA flow diagram (Figure 1) has been rigorously adapted and presented. This diagram meticulously details the number of records identified from databases and other sources, the quantity screened, those assessed for eligibility, and ultimately, the total number of studies included. Furthermore, the diagram explicitly outlines the reasons for exclusion at each stage of the review process, thereby enhancing the reproducibility and clarity of our methodology in accordance with PRISMA-SCR guidelines. This comprehensive visual representation ensures a thorough understanding of the evidence selection process and addresses the need for adequate presentation and discussion of the flow of information through the different phases of this scoping review.

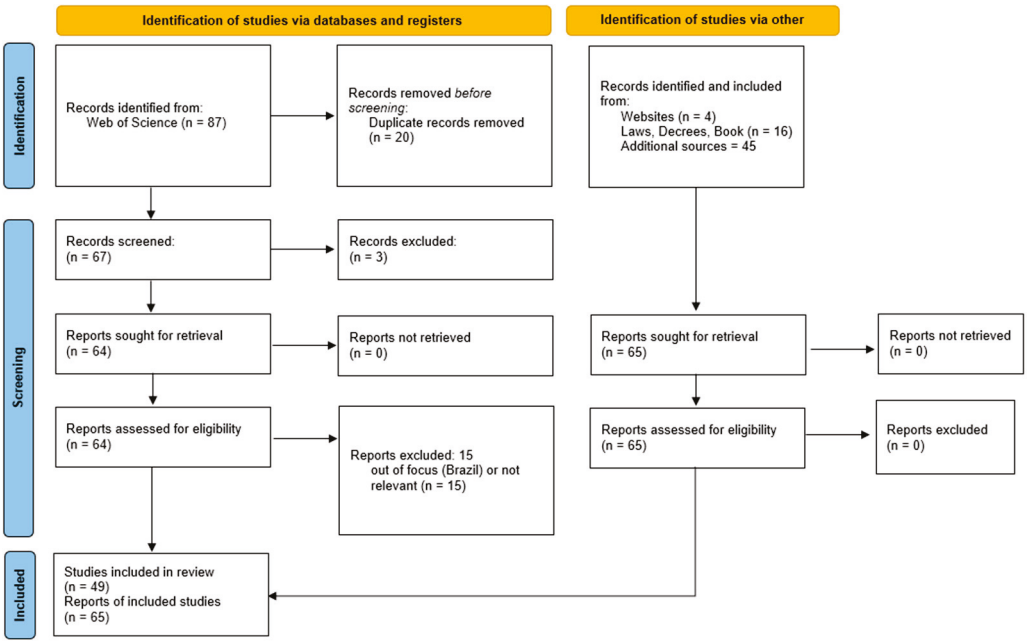


Figure 1. PRISMA flow diagram (adapted).

2.4. Data Charting and Synthesis of Results (PRISMA Items 10, 11, 13)

Data charting focused on identifying key information from the included studies relevant to the review questions and objectives. Variables for which data were sought included the study's focus (e.g., specific urban mining process, type of waste, geographical scope,

policy analysis), methodology of the primary study, key findings related to challenges and opportunities, technological approaches discussed, and legislative aspects analyzed.

The data were synthesized narratively and thematically, rather than through a quantitative meta-analysis, which is characteristic of scoping reviews. The findings were grouped and presented within the corresponding sections of this review, addressing the dimensions of knowledge production, technological appropriation, and the legal framework for urban mining in Brazil, often contrasting with the European context.

For the legal dimension (Section 7), a qualitative Critical Discourse Analysis (CDA), based mainly on the theoretical-methodological proposal of Norman Fairclough [27], was employed to analyze Brazilian policies related to WEEE. This analysis sought to identify the existing gaps between the official discourse and the operational reality, the lack of clarity and ambiguities in the definition of responsibilities, as well as the practical difficulties in the implementation of legal guidelines. The application of CDA allowed a more in-depth evaluation of the effectiveness of the current legislation, highlighting challenges such as the informality of the sector, the insufficient awareness of the population, and the need for investment in infrastructure, contributing directly to the analysis proposed in the article.

Extra sources, although not strictly part of a systematic database search, were included when they provided important context or complementary information not found in a systematic way within the search results. Information from these sources was integrated into the narrative synthesis where relevant.

3. Fundamentals of Urban Mining

Urban mining, which consists of the recovery of valuable materials and the coordination of materials, information, and services that enable the recovery of value from industrial and urban activities, can be understood as the set of processes and activities related to the production of secondary raw materials from Urban Solid Waste (USW) [28]. The term is applied exclusively to the recovery of secondary raw materials from waste under the concept of the 3Rs (reduce, reuse, and recycle), with the premise that valuable materials can be recovered from waste in a manner analogous to traditional mining, producing high-value and sustainable secondary raw materials [9].

The main components of urban mining (Figure 2) involve the collection and dismantling of waste; pre-treatment, which includes steps such as size reduction, grinding, and separation of metallic and non-metallic fractions; and processing for the recovery of valuable materials, using physical, chemical, or biological methods [29].

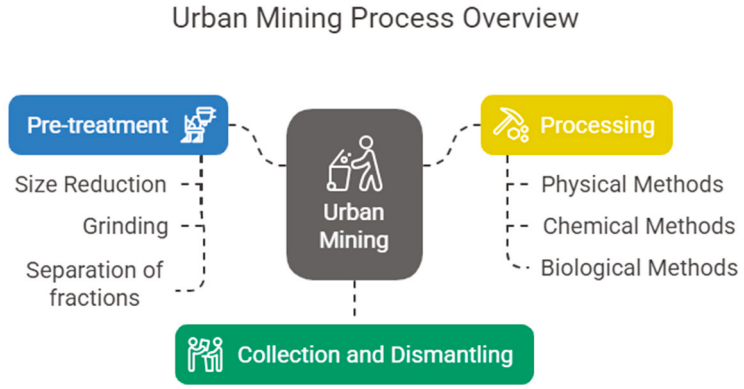


Figure 2. Main components of urban mining.

Various types of urban waste can be used as raw materials in urban mining, including: Waste Electrical and Electronic Equipment (WEEE) or e-waste, which has high potential due to its diversity and concentration of metals—this waste contains precious metals (Au,

Ag), base metals (Cu, Al), and critical metals (Li, Co); Construction and Demolition Waste (CDW), from which recycled aggregates and other materials can be recovered; Urban Solid Waste (USW), including plastics, metals, and even incineration ash; industrial waste, such as electrical and non-electrical equipment, and infrastructure waste, such as pavement, end-of-life vehicles (ELV), and landfill mining waste, with the potential for the recovery of plastics and metals [29].

Urban mining presents significant pros, encompassing the conservation of natural resources through the use of secondary sources [10], the mitigation of environmental impacts associated with traditional mining, such as lower energy and water consumption, and a reduction in waste generation and pollution [9,10]. This activity also promotes the economic valorization of waste, transforming discarded materials into valuable raw materials, and drives the circular economy, reintegrating materials into the production cycle and extending the lifespan of resources [9,10]. Other advantages include the reduction of dependence on primary raw materials and the risks in their supply chain, as well as the potential for job creation in the sectors of collection, processing, and material recovery [9,29].

However, there are challenges associated with urban mining that need to be recognized: the complexity of reverse logistics due to the variety of waste with different compositions, which hinders collection, transportation, and sorting; the costs involved in reverse logistics and recovery processes are also a challenge, which may question the economic viability of the activity in the context of the circular economy, with viability dependent on the quality and volume of the material; the need for specific technologies and technical knowledge for the processing and recovery of materials can be a barrier due to their limited availability or accessibility [10,29].

In addition, the presence of hazardous substances in some waste, such as in WEEE, requires special care in handling and processing to avoid contamination and health risks [29]. The informal recycling market, operating without adequate standards, hinders the formalization and control of the value chain [10]. The lack of specific regulations and economic incentives for the formal chain discourages urban mining compared to virgin raw materials, with the taxation of WEEE being a possible disincentive [10,29]. The need for correct waste disposal by consumers is essential to feed the chain, just as the scale of production and the diversity of electronic products impact the generation and treatment of WEEE [10].

4. Processes Used in Urban Mining

This section presents the main processes (Figure 3) employed in the recovery of valuable metals from urban waste: Hydrometallurgy (processing in aqueous solutions), Pyrometallurgy (processing at high temperatures), and Biometallurgy (use of microorganisms). Various technologies, both traditional and emerging such as electrochemistry and supercritical fluids, can be applied in the scenario of Rare and Precious Metal (RPM) recovery as presented by Wang et al. [30], while Xavier et al. [29] offer a comprehensive review on key concepts and treatment methods for materials in urban waste. Additionally, Firmansyah et al. [31] reviews technological advances focused on the recycling potential of electronic waste.

Recently, Kankanamge et al. [6] investigated the factors that influence the design and adoption of technologies to make urban mining of electronic waste more sustainable, proposing a taxonomy that groups these factors into four categories: the device cluster, referring to the intrinsic characteristics of the technologies; the process cluster, which encompasses variables such as efficiency and cost; the organizational cluster, relating to the structure and policies of the entities involved; and the macro cluster, which includes external influences such as data security and intellectual property. In the following subsections, we will assess the efficiency, environmental impact, and economic viability of each

process, conducting a comparative analysis of their advantages and disadvantages, aiming to identify future perspectives for metal recovery in the context of a circular economy.

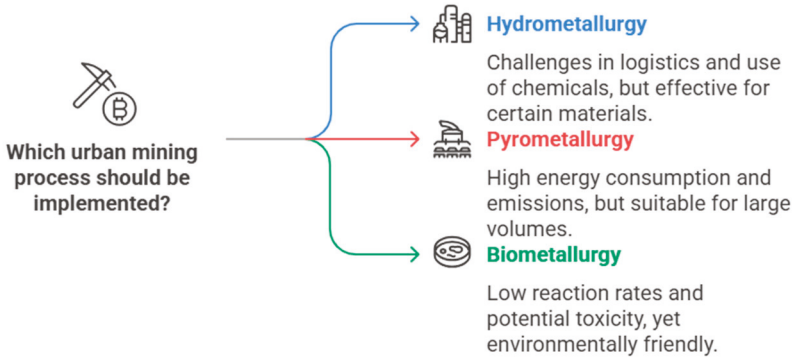


Figure 3. Main aspects of urban mining processes.

4.1. Hydrometallurgy

Hydrometallurgy, which extracts metals through chemical reactions with acidic or basic solutions, typically comprises steps such as leaching, precipitation, solvent extraction, and electrodeposition. According to Tunsu et al. [32], the advantages of applying hydrometallurgical methods for the urban mining of Rare Earth Elements (REEs) include the ability to process low-quality and complex materials, obtain products of higher purity, generate less gaseous pollution compared to pyrometallurgy, reduce dependence on primary mining, and enable the recycling of materials. However, it faces significant challenges such as the complex logistics of collection and sorting, the heterogeneity of materials that require flexible processes, the need for efficient separation methods for materials with low REE content, the intensive use of chemicals with the potential generation of secondary waste, and the costs of development and industrial implementation.

4.1.1. Leaching

Leaching consists of the selective dissolution of metals from solid waste using acidic or alkaline solutions, being applied in the recovery of valuable metals from electronic waste and spent catalysts. Gomes et al. [33] reviewed the acid leaching of REEs from WEEE, pointing to urban mining as a promising strategy. Anwer et al. [34] compared different acids in the extraction of metals from printed circuit boards (PCBs), highlighting organic acids (such as citric acid) as a more sustainable alternative. Alternatively to the traditional process, Prodius et al. [35] demonstrated a hydrometallurgical route using copper salts to recover REEs and cobalt from magnetic and electronic waste, with subsequent precipitation of the REEs for reuse as oxides.

Arya et al. [36] used chemical leaching to recover copper (Cu) and lead (Pb) from WPCBs (Waste Printed Circuit Boards), warning about the need for proper management of the waste generated. Acid leaching is also fundamental in the recovery of cobalt in lithium-ion batteries, using acids such as hydrochloric and sulfuric acid, to dissolve the components, followed by techniques such as solvent extraction, ion exchange, or precipitation to separate the cobalt, as highlighted by Botelho Júnior et al. [37]. Rocchetti et al. [38] proposed multi-stage countercurrent leaching as an innovative solution to recover indium from discarded Liquid Crystal Display (LCD) screens. This approach consists of using the same acid solution to treat several stages of LCD waste, concentrating the metal in the leaching solution. Oliveira et al. [39] suggested acid leaching as the most suitable method for recovering gallium and REEs from LEDs (Light Emitting Diodes).

Martins et al. [40] explored a three-stage sulfuric leaching to recover metals from WPCBs, especially in motherboard and memory board: the first stage focuses on the

recovery of iron (Fe), aluminum (Al), and tin (Sn); the second, in an oxidizing medium, selectively recovers copper (Cu), silver (Ag), nickel (Ni), and zinc (Zn); and the third, with nitric acid, solubilizes the remaining metals, with the extraction efficiency dependent on the metal/acid ratio. Agrawal et al. [41] developed an eco-friendly hydrometallurgical route to recover manganese (Mn) and nickel (Ni) from discarded tantalum capacitors, using selective leaching with hydrochloric acid that dissolves Mn (99.9%) and Ni (98.9%) while isolating tantalum (Ta), followed by solvent extraction. Finally, Tran et al. [42] reviewed leaching with thiosulfate as a benign alternative to cyanidation for recovering gold (Au) and silver (Ag) from WPCBs, addressing the specific challenges of its application in urban mining, such as reagent consumption and reaction complexity.

4.1.2. Precipitation

Precipitation separates dissolved metals by adding reagents that form poorly soluble compounds. In contrast to traditional and energy-intensive thermal treatments for dismantling PCBs, Yang et al. [43] proposed a green alternative that involves immersing PCBs in spent tin stripping solution (TSS) at room temperature, followed by the recovery of leached metals by chemical precipitation by adjusting the pH in different stages, achieving approximately 99% recovery of Sn, Pb, Fe, Cu, and Zn. This process offers advantages such as energy efficiency, waste reuse, and efficient metal recovery.

Caldas et al. [44] explored methods for selective silver recovery, proposing an effective route with two stages of sulfuric leaching, with 100% of the silver recovered, followed by silver purification by precipitation as AgCl with NaCl and the production of silver nanoparticles (AgNPs) by the Turkevich method. Lima et al. [45] used chemical precipitation as an initial step to recover aluminum from NCA (Nickel-Cobalt-Aluminum) batteries, a challenge due to the presence of aluminum in the cathode, then proceeding with the recovery of cobalt by solvent extraction and nickel/lithium by precipitation.

4.1.3. Solvent Extraction

This process involves the selective transfer of metals from an aqueous solution to an organic solvent, being applied in the recovery of precious metals and REEs from electronic waste. Tunsu et al. [46] tested different extractants (acidic, solvating and mixed extractant systems) for REEs in simulated acidic solutions and identified that the blended DEHPA–Cyanex 923 is effective in minimizing the co-extraction of iron. The use of Ionic Liquids (ILs) and Deep Eutectic Solvents (DESs) as alternatives to conventional REE recovery processes was explored by Quijada-Maldonado et al. [47] and Arrachart et al. [48], respectively. Alguacil e Robla [49] conducted a comprehensive review showing the potential of solvent extraction to recover various metals (rare earths, copper, lithium, gold, silver, palladium, platinum, etc.) from various sources using different types of extractants, discussing challenges and the future of the technique.

Zhang et al. [50] employed supercritical fluid extraction (SCFE) using supercritical carbon dioxide and a tributylphosphate–nitric acid adduct (TBP–HNO_3) to recover REEs, such as terbium (Tb), europium (Eu) and yttrium (Y), from fluorescent lamp waste, achieving extraction rates greater than 70% for yttrium and europium, and 50% for terbium. Castillo-Ramírez and Janssen [51] explored Pseudo-Protic Ionic Liquids (PPILs) for the extraction of metals relevant in urban mining. The authors tested four different PPILs for the extraction of indium, neodymium, yttrium, and lanthanum, with tri-hexylammonium octanoate showing high efficiency for all. And that indium was particularly well extracted by all PPILs tested. The authors reported the recyclability of most of the PPILs tested and the relative ease of yttrium and neodymium recovery.

4.1.4. Electrodeposition

Electrodeposition recovers metals in elemental form by applying electric current to an ionic solution, being used to obtain high-purity metals, such as copper, gold, and silver. Reyes-Valderrama et al. [52] combined acid leaching with selective electrochemical recovery, demonstrating the recovery of Cu by electrodeposition at pH 1.5 and of Zn at pH 5, although nickel did not show relevant deposition under the tested conditions. Recently, Son et al. [53] developed a gold electrodeposition process using a thiourea-based electrolyte, a less toxic alternative to cyanide, achieving 97% gold recovery with drastically reduced energy consumption (0.129 kWh/kg Au), attributed to the oxidation of thiourea at the anode. Although thiourea decomposes, electrodeposition slightly slows down this degradation compared to chemical deposition, possibly due to its regeneration at the cathode.

4.2. Pyrometallurgy

Pyrometallurgy [54–58] is a non-ferrous metal extraction process that uses high temperatures and consumes a lot of energy. It involves enrichment steps by smelting, conversion, and refining, being considered the most traditional and industrially used treatment. Its advantages include the ability to treat large volumes of waste, recover metals in high concentration, and process complex materials [59]. Application examples include the recovery of copper (Cu) [54], gold (Au) [60], zinc (Zn) and indium (In) [61], gallium (Ga) [62], among others. The key step is smelting (melting to separate metals by melting points), which can be performed by flash smelting processes, which use oxygenated gas for autogenous conditions, or by bath smelting, where the reaction occurs in a melt pool.

However, pyrometallurgy inevitably generates slag, soot, and toxic gases, requiring strict environmental controls, such as filters and gas treatment, to minimize pollution and ensure sustainability. The equipment is expensive, and energy consumption is high, making it unsuitable for small and medium-sized enterprises. Furthermore, it lacks selectivity for rare and precious metals and presents complexity in the recovery of pure metals [59]. The choice between hydrometallurgy and pyrometallurgy depends on the characteristics of the waste, the target metals, and environmental and economic factors, and in many cases, the combination of both may be the most efficient and sustainable solution. Therefore, future research is needed to optimize pyrometallurgical processes, reduce their impacts, and develop integrated technologies.

4.3. Biohydrometallurgy

Emerging as a promising, ecological, and economic alternative for the treatment of electronic waste, biohydrometallurgy uses microorganisms to extract and recover metals. Its main process, bioleaching, employs microorganisms such as bacteria (*Acidithiobacillus ferrooxidans* and *Thiooxidans*), fungi (*Penicillium*, *Aspergillus*, *Fusarium*, *Alternaria, Candida*), and their metabolites. Efficiency is demonstrated by works such as that of Madhavan et al. [63], who recovered copper (Cu) and gold (Au) from PCBs using *Alcaligenes aquatilis*; Rodrigues et al. [64] who demonstrated high efficiency of the fungus *Aspergillus niger* in the bioleaching of copper and gold and Thakur e Kumar [65] who used the bacterial strain *Bacillus sporothermodurans ISO1* for copper and silver recovery. Other biohydrometallurgical processes include bioaccumulation (adsorption of metals in microbial cells) [66] and bioreduction (reduction of metal ions to the elemental form) [67]. The biorecovery of critical metals, such as from lamp phosphor powder, exemplifies the transition to a biologically based circular economy [68].

The advantages of biohydrometallurgy include being a sustainable process (minimizes hazardous waste and emissions, reduces energy/chemical consumption), efficient

(selective recovery even at low concentrations), and flexible (adaptable and integrable with other technologies) [54]. Despite this, it has limitations such as low reaction rates, the possibility of metal precipitation, long process times, and potential toxicity of metals to microorganisms. Factors such as microorganism choice, surface area, pulp density, precursor, temperature, and pH are essential for success [54]. Although it still faces optimization and industrial scalability challenges, continuous development indicates a promising future for its application in waste recovery, contributing to sustainability and the circular economy.

4.4. Comparative Analysis Between the Processes

The economic viability of recovering metals from WEEE is multifaceted. Figure 4 presents an overview of the main aspects of each method, focusing on efficiency, scalability, economic viability, and environmental impact.

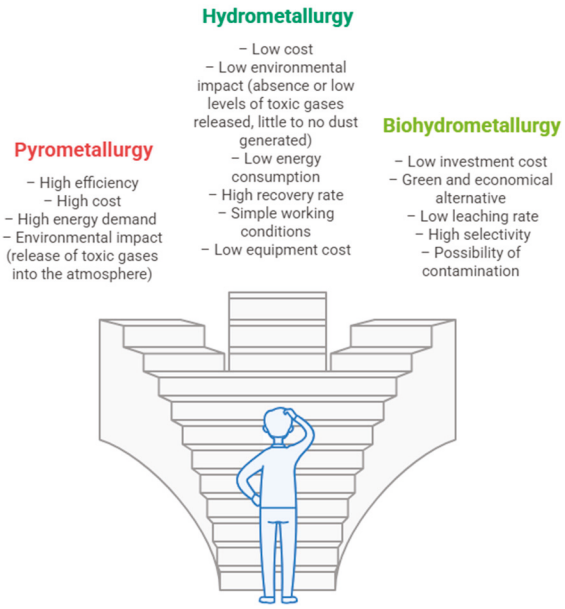


Figure 4. Comparative analysis (efficiency, scalability, economic viability, and environmental impact) of the main methods used in urban mining.

The purity of the recovered metals is generally high in formal processes (hydro and pyro), with pyrometallurgy being capable of achieving very high purity on a large scale, and hydrometallurgy proving effective for high purities in specific cases. Transportation costs and the absence of specific tax incentives in Brazil are significant economic barriers that negatively affect the viability of all formal methods. Furthermore, each method has its own cost/benefit factors: pyrometallurgy requires high capital investment and consumes a lot of energy, being mainly viable on an integrated large scale; hydrometallurgy has lower energy costs and is suitable for a smaller scale, but faces costs with chemical reagents and effluent disposal; biohydrometallurgy is promising due to its low cost and minimal use of chemicals, but still lacks economic feasibility studies on an industrial scale.

5. Perspectives of Urban Mining: A Comparison Between Brazil and the European Union Context

Since the main objective of urban mining is to extract precious metals, base metals, plastics, glass, and other reusable components, transforming what was previously considered waste into economic resources for some productive chain, the inputs produced compete with the extraction of virgin natural resources, and may, in principle, reduce the environmental impacts associated with conventional mining.

Many studies address the opportunities offered for the recycling of composite materials from different waste streams [69] and few contemplate the barriers and challenges faced by urban mining [1,2]. Its development faces challenges as complex as those of conventional mining, although of different natures.

While traditional mining deals with resource depletion, large-scale environmental impacts, and social conflicts related to land ownership [70], urban mining stumbles upon issues such as the complexity of waste composition, the presence of hazardous substances, the lack of adequate collection and processing infrastructure, the informality of the sector, the need for efficient and economically viable separation technologies, and the implementation of public policies that encourage recycling and extended producer responsibility. Table 2 presents a comparison between conventional and urban mining.

Table 2. Characteristics of Conventional and Urban Mining.

Characteristic	Conventional Mining	Urban Mining
Source of Resources	Mineral deposits (ores) located in the Earth's crust, generally in remote and specific areas.	Waste and discarded products in urban areas, including electronic waste, construction and demolition waste, end-of-life vehicles, and urban solid waste.
Environmental Impact	Destruction of ecosystems, deforestation, soil and water pollution, waste generation (tailings and sterile material), landscape alteration.	Reduced pressure on natural resources, decreased pollution, lower energy consumption, reduced volume of waste sent to landfills, recovery of degraded areas.
Location	Generally in rural or remote areas, often in regions of great biodiversity or environmental importance.	Predominantly in urban and peri-urban areas, close to consumption and waste generation centers.
Complexity	Complex extraction, beneficiation, and refining processes, which require large investments in infrastructure and technology.	Complex processes of collection, sorting, dismantling, separation, and refining, which require cutting-edge technologies and efficient logistics. The heterogeneous composition of waste is a major challenge.
Regulation	Rigorous environmental legislation, complex environmental licensing, requirements for the recovery of degraded areas, need for constant monitoring.	Legislation under development, need for specific regulation for the sector, definition of responsibilities, incentives for recycling and reverse logistics, combating informality.
Economy	Traditional sector, with a large impact on the global economy, job creation, and foreign exchange earnings, but also with negative externalities (environmental and social costs).	Growing sector, with the potential to generate green jobs, reduce dependence on imports, boost technological innovation, and promote the circular economy.
Challenges	Resource depletion, social conflicts, environmental impacts, increasing extraction costs, rigorous environmental regulations.	Efficient selective collection, separation technologies, reverse logistics, traceability of materials, economies of scale, public awareness, specific regulations, combating informality.
Perspectives	Development of more sustainable mining technologies, recovery of degraded areas, corporate social responsibility.	Expansion of selective collection, development of advanced recycling technologies, promotion of the circular economy, creation of markets for recycled materials, public awareness.

In the global scenario, Brazil and Europe contrast in their approaches to mining, both conventional and urban. Brazil, possessing vast mineral reserves and marked by social inequalities that have historically sustained the workforce in conventional mining, faces the challenge of reconciling economic development with the effective application of its environmental legislation, often permeated by gaps and enforcement challenges [70]. The European Union (EU), on the other hand, driven by resource scarcity and growing environ-

mental awareness, as evidenced by its policies on critical raw materials, directs its efforts toward urban mining as a central strategy to ensure access to essential materials, reduce dependence on imports, and promote a circular economy [11,71,72]. This is reflected in its comprehensive legislative framework for WEEE, such as the WEEE and RoHS Directives [11]. In addition, the mastery of specific technologies applicable in urban mining within developed European nations allows for the establishment of virtuous partnerships to the capital and geopolitics of selling technologies or services and acquiring products thus mined at a low price and without pollution in European countries.

In view of this, while Brazil seeks to optimize the management of its natural resources and mitigate the socio-environmental impacts of traditional mining, many European countries, particularly within the EU, invest in advanced recycling technologies and in the creation of value chains for recovered materials. This aims to strengthen their strategic autonomy and reduce their ecological footprint [1,5], although Baldé et al. [11] note that even EU Member States face challenges in meeting legally binding collection targets for e-waste.

The fundamental distinctions in urban mining approach and infrastructure between Brazil and the European context, particularly the European Union, are multifaceted and reflect their different socioeconomic, environmental and regulatory landscapes. Table 3 summarizes the main structural and focus differences that shape urban mining development in each region.

Table 3. Structural and approach differences in urban mining—Brazil vs. Europe/European Union.

Characteristic	Brazil	Europe/European Union
Main Drivers and Primary Focus	Reduction of waste volume in landfills; social inclusion of the informal workforce.	Resource scarcity; circular economy goals; security of critical metals supply.
Legislative Framework	National Solid Waste Policy (PNRS) and decrees: legal framework under development, with gaps in implementation, enforcement, and clarity of responsibilities.	More advanced and harmonized legislative framework (WEEE, RoHS Directives, Circular Economy Package), focusing on Extended Producer Responsibility; Variation in effectiveness among member states.
Infrastructure	Lack of adequate selective collection and processing infrastructure; logistics challenges (continental dimensions).	More developed and formalized collection and recycling infrastructure, despite challenges in meeting collection targets.
Technology and Innovation	Significant technological barriers; initial processing primarily local, export of noble-metal-rich components; growing research and development phase.	Investment in advanced recycling technologies and value chain creation; technological mastery and pursuit of strategic autonomy.
Informal Sector Integration	Prominent presence of informal collectors; need for inclusive approaches and formalization.	Predominantly formalized sector; challenges in uniform policy implementation.
Public Awareness	Low public awareness regarding correct WEEE disposal.	Growing consumer awareness and pressure for responsible practices.
Economic and Fiscal Incentives	Logistics costs and lack of specific fiscal incentives as barriers.	Pursuit of strengthening economic autonomy and reducing ecological footprint; creation of markets for recycled materials.

In contrast to the challenges observed in Brazil, European countries, guided by the WEEE Directive and national regulations, have developed relatively consolidated WEEE management systems, characterized by established collection schemes and formal recycling infrastructure [73]. Extended Producer Responsibility (EPR) plays a central role, assigning responsibility for end-of-life management to producers, who often operate or finance collective take-back schemes. These systems aim to maximize collection rates and channel WEEE towards appropriate treatment facilities to recover valuable materials and minimize environmental impacts [73,74].

Beyond basic recycling, there is a growing emphasis on higher tiers of the waste hierarchy, such as preparation for re-use. Experiences from several EU member states, including the UK, Belgium, France, Austria, and Spain, demonstrate that successful preparation for re-use is enabled by factors such as clear targets, adequate funding mechanisms, collaboration among stakeholders (including social enterprises), and infrastructure that facilitates collection and assessment of WEEE suitability for re-use [75]. Furthermore, analyses focusing on specific product streams, like small WEEE in Germany, highlight how manufacturer take-back systems and the implementation of tailored end-of-life strategies such as component reuse and remanufacturing can significantly improve resource recovery and potentially offer economic and environmental benefits compared to conventional recycling [76].

Despite these advancements and consolidated systems, challenges persist in Europe, including issues related to unreported WEEE flows through scavenging, mixing with other waste streams, and illegal exports [74]. Nevertheless, the European experience, particularly in developing formal collection networks, implementing EPR effectively, and promoting higher-value recovery strategies like re-use and remanufacturing, offers valuable insights and potential models for countries like Brazil seeking to enhance their urban mining capabilities within a framework of circular economy.

Therefore, the transposition of models observed in European countries, especially those from the European Union with advanced legislative frameworks, to Brazil requires a critical analysis, considering the distinct socioeconomic, environmental, technological, and regulatory specificities of the country. The rationale for focusing comparative legislative analysis on the EU lies in its harmonized and advanced directives on WEEE and circular economy, which serve as a significant international benchmark, despite variations in national implementation [11].

The direct application of European models to the Brazilian context ignores the profound existing differences. Brazil, although a country rich in mineral resources, faces complex challenges to ensure that conventional mining is conducted sustainably. Institutional fragility, precarious enforcement, and the prevalence of negligent practices have resulted in serious environmental and social disasters, such as the collapse of the Barragem do Fundão em Mariana (Minas Gerais) [77], a tragic landmark that exposed the flaws in the licensing system and the lack of socio-environmental responsibility of mining companies in this country.

The Mariana disaster, a tragic landmark of Brazilian conventional mining, serves as a stark warning: negligence and precarious enforcement cannot be repeated in the implementation of urban mining. Although promising, this modality, if conducted improperly, can replicate negative environmental and social impacts [78,79], such as soil and water contamination by heavy metals present in electronic waste, the exposure of workers to toxic substances during sorting and processing, and the creation of environmental liabilities resulting from the inadequate disposal of non-recoverable waste.

To avoid repeating the mistakes of conventional mining, urban mining must be guided by rigorous control and prevention measures. This includes conducting detailed and comprehensive environmental impact studies, adopting clean and innovative technologies

for the separation and processing of materials, and guaranteeing the active participation of civil society in the planning and oversight of activities. Furthermore, it is essential that mining companies assume extended responsibility [80–82] for the management of waste generated at all stages of the process, from selective collection to environmentally sound final disposal, prioritizing the traceability of materials and the implementation of circular economy practices.

Even so, the urgency of urban mining manifests itself differently in the Brazilian context compared to the European one, although they may share common sustainability goals. Within Europe, and particularly in the European Union, the perception of natural resource scarcity, the existence of strong environmental regulations (such as the EU WEEE Directive), and the ambition to lead the transition to a circular economy drive a pressing need to implement urban mining on a large scale [11]. Dependence on imports of critical raw materials, coupled with growing consumer awareness and pressure for responsible business practices, makes urban mining a strategic priority to ensure the competitiveness of European industry and security of supply.

From a geopolitical and economic point of view, security of supply for items that Europe does not produce can be achieved through diversified partnerships in Asia, Africa, and Latin America with contributions of technology and capital sufficient to transform their strategic needs into commodities. This strategy has been used by several economic and technological powers throughout recent history, marking a kind of neocolonialism.

Furthermore, while Europe stands out for its selective collection and recycling infrastructure, Brazil still faces significant challenges in the management of urban solid waste. Informality in collection, lack of adequate infrastructure, and low public awareness hinder the separation and routing of waste to urban mining. Also, some situations related to conventional mining demonstrate that Brazilian environmental legislation, although advanced in some aspects, lacks effective mechanisms to guarantee the accountability of companies and the reparation of damages caused by their activities [70,83,84]. Therefore, urban mining in Brazil cannot be presented as an environmental merit in itself without a set of guarantees of its efficacy, efficiency, and effectiveness.

Another point that deserves highlighting is the social issue. The experience of the city of Trento, in Italy, illustrates the implementation of a program coordinated by local recycling companies. Collaboration with entities specialized in waste management suggests a more formalized approach through selective collection [82,85,86]. In Brazil, informality and the presence of recyclable material collectors in situations of social vulnerability require a differentiated approach, which promotes social inclusion and income generation for this population.

In Brazil, the urgency of urban mining is revealed in a less immediate, but equally relevant way. Although the country has abundant mineral resources, conventional mining is only considered an effective social function at the beginning of the undertaking, after which it responds to the demands of the national and international market by lowering its costs, increasing its production without assuming all the environmental and social externalities it generates in the process and in the increase in the scale of production [70,83,84]. Therefore, unbridled conventional mining brings significant environmental impacts and social and environmental costs. Urban mining emerges as an alternative to diversify sources of raw materials, reduce pressure on fragile ecosystems, and promote social inclusion through the generation of green jobs and the formalization of the sector [87–89].

In addition, the increasing production of electronic waste and other complex waste streams requires urgent solutions to prevent soil and water contamination, protect public health, and recover valuable materials that can be reintroduced into the production chain. Thus, while Europe sees urban mining as a matter of economic security and environmental

leadership, Brazil needs to adopt it as a strategy to promote sustainable development, reduce social inequalities, and protect its vast natural heritage.

The news from the National Electric Energy Agency [90] about the expressive growth of 8.84 GW in micro- and mini-distributed generation of electricity, in 2024, highlights a critical point for the sustainability of the Brazilian energy sector: the urgent need to prepare the country for the management of the life cycle of the equipment used in these facilities. As in the case of large solar plants, the expansion of micro and mini-distributed generation, driven by photovoltaic solar panels installed in homes, businesses, and rural properties, will inevitably lead to a significant increase in the volume of electronic waste (e-waste) containing valuable and potentially hazardous materials [91].

In this scenario, urban mining becomes a key piece to ensure the environmental and economic sustainability of micro and mini-distributed generation. By recovering materials such as silicon, silver, copper, and aluminum present in end-of-life solar panels, urban mining can reduce the demand for virgin raw materials, reduce the environmental impacts of ore extraction and processing, and create new business opportunities and green jobs. However, the implementation of urban mining on a large scale in the context of micro and mini-distributed generation presents specific challenges. The geographical dispersion of facilities, the lack of adequate collection and sorting infrastructure, and the absence of specific regulations for the management of solar panel waste hinder reverse logistics and efficient material recovery.

To overcome these challenges, it is essential that the Brazilian government, in partnership with the private sector and civil society, develops public policies that encourage selective collection, the creation of specialized recycling centers, the promotion of extended producer responsibility, and the awareness of consumers about the importance of the correct disposal of end-of-life solar panels. In addition, it is necessary to invest in research and development of innovative recycling technologies, which allow the efficient recovery of materials present in solar panels, minimizing the costs and environmental impacts of the process.

By embracing urban mining as an integral part of the strategy to expand micro and mini-distributed generation, Brazil will be able to ensure that the energy sector becomes not only cleaner and more decentralized, but also more circular and sustainable. Thus, the role of the government is, first and foremost, to regulate the market so that it is virtuous by imposing on the private sector and, indirectly, on photovoltaic generators, the environmental costs of this technology. In this way, whoever profits and whoever benefits must internalize the environmental costs of the activity within a long-term vision that goes from production to decommissioning.

6. Knowledge Production and Technological Appropriation on Urban Mining in Brazil

The mapping of Brazilian scientific production on urban mining reveals a field of investigation that, although it demonstrates a recent growing interest, is still in a phase of development compared to other environmental areas or international production, especially European. A search carried out in March/2025 on the Web of Science resulted in 633 documents found for the term “urban mining” (all fields), of which 573 are articles, with 75 being reviews. Brazil ranks 6th among the countries that have produced the most articles on the topic, Figure 5.

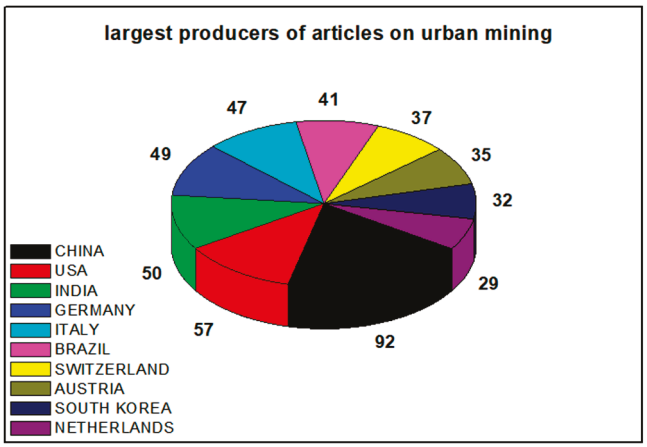


Figure 5. Top 10 producers of articles on urban mining.

The existing literature, dispersed in journals of various areas (engineering, chemistry, environmental sciences, management), conference proceedings, and, expressively, in theses and dissertations, tends to concentrate on specific thematic niches. Studies dedicated to the quantitative and qualitative characterization of flows such as Waste Electrical and Electronic Equipment (WEEE), in which it seeks to identify precious and critical metals, and Construction and Demolition Waste (CDW), whose focus lies on the potential for reuse of aggregates, predominate.

Investigations on technological routes for the processing of these wastes were also recovered, ranging from physical pre-treatments to metallurgical processes on a laboratory or pilot scale, often adapting technologies or seeking lower-cost alternatives. An analysis of this corpus suggests a preference for applied technical approaches, whose central objective seems to be the establishment of the technical–economic feasibility of material recovery, precluding discussions about the social, political contexts and the broader implications of urban mining in Brazil to a secondary plane.

Considering the growing challenge of managing WEEE in Brazil, whose generation exceeds population growth and which stand out for their complexity, potential hazard, and for containing valuable materials, the National Solid Waste Policy instituted Reverse Logistics Systems (RLS) as fundamental instruments for the transition to the circular economy [10,22]. In this context, urban mining emerges as a strategy fostered by RLS, although the effectiveness of both approaches faces significant paradoxes. High costs, logistical challenges, the informality of the recycling chain, public ignorance, the lack of adequate infrastructure and specific tax policies are bottlenecks that question the real contribution of these approaches to sustainability and emissions reduction, demanding the recognition of these obstacles to drive technological and regulatory solutions [10]. The lack of formal RLS, especially in metropolitan regions, contributes to a recycling rate estimated at only 2%, also influenced by the lack of reliable data, the significant role of the informal sector, and the continental dimensions of the country [92].

Aiming to improve urban mining, studies have focused on the detailed characterization of waste and the development of processing routes. Castro e Pereira-Filho [93], for example, carried out an exploratory study of the chemical composition of Printed Circuit Boards (PCBs) from hard drives, where it was possible to identify about twenty chemical elements through Inductively Coupled Plasma Optical Emission Spectrometry (ICP-OES) and Flame Atomic Absorption Spectrometry (FAAS). Using exploratory data analyses such as Principal Component Analysis (PCA) and correlation maps, it was also possible to make significant associations, demonstrating that the direct analysis of fragments combined with chemometrics is promising for the characterization and planning of recycling routes.

In a complementary way, Castro et al. [94] proposed the combined use of Laser-Induced Breakdown Spectroscopy (LIBS) and Parallel Factor Analysis (PARAFAC) to characterize PCBs, improving the identification of interferents and the accuracy in the classification of elements such as Au and Ag. The characterization of other WEEE, such as Light-Emitting Diodes (LEDs) and lithium-ion batteries, reveals not only the presence of valuable and critical materials (Cu, Ga, Y, In, Au, Ag in LEDs and Co, Ni, Li in lithium-ion batteries), but also toxic elements (such as Pb and As in LEDs) and a compositional heterogeneity that challenges recycling processes [95,96].

Overcoming technological barriers is identified as a critical factor in Brazil, which, despite being the largest generator of e-waste in South America, only performs the initial processing stage locally [97]. Using the DEMATEL (Decision Making Trial and Evaluation Laboratory) method based on expert opinion, the authors pointed out technology as the only primary and causal barrier, directly influencing others such as technical knowledge, pollution control, costs, and consumer. This lack of advanced technologies and specialized knowledge, added to the low collection flow (~2%), makes it impossible to install sophisticated recovery plants in the country, resulting in the export of components rich in noble materials [97]. In view of this, several processing approaches have been investigated. Hydrometallurgy is frequently cited as a promising route [29,45,55], with studies focusing on the optimization of parameters such as acid leaching (e.g., H_2SO_4, HNO_3, aqua regia), solid/liquid ratio, pH, and redox potential to recover metals such as Cu, Ag, Fe, Au, Ga and Rare Earth Elements (REE) from PCBs, LEDs, and other sources. Separation techniques such as selective precipitation, solvent extraction, ion exchange, and membrane separation (nanofiltration, reverse osmosis) are explored for the purification and concentration of metals and recovery of reactants [45,98].

Alternatives and emerging technologies are also highlighted in the search for sustainability. Bioleaching using fungi such as *Aspergillus niger* has proven efficient in the recovery of Cu and Au from PCBs, also enabling the synthesis of metallic nanoparticles [64]. Bio-hydrometallurgy in general is pointed out as a promising innovation, especially for critical raw materials [29,37,68]. Biphasic Aqueous Systems (BAS) emerge as a "green" alternative for the recovery of bismuth and gold, minimizing the use of organic solvents and operating under mild conditions [99,100]. Magnetic Nanohydrometallurgy (MNHM) is presented as an innovative nanotechnological approach for the selective separation of lanthanides [101].

Other techniques such as gravity concentration [102], hybrid (mechanical-thermal) approaches for photovoltaic panels [103] and supercritical water (SCW) technology for simultaneous recycling of solar panels and effluent treatment [104] are also investigated. The recovery of REE, given their technological importance and supply risk, is a particular focus, although acid leaching still predominates and recovery from PCBs remains a challenge [33,105]. Similarly, the recovery of indium from LCDs faces analytical and market challenges in Brazil [106].

As already mentioned, urban mining is not restricted to WEEE, also covering CDW, where the concept of buildings as material banks proposes to treat buildings as recoverable sources [107]. Although Brazil has research in the area, it contrasts with European countries due to the lack of robust public policies, with systematized data and incentive policies being necessary to overcome the competitiveness of virgin materials. The incorporation of waste such as milled asphalt pavement [108] and polyethylene [109] in asphalt mixtures also demonstrates potential, although the environmental benefits depend on the technologies and energy matrices employed and more Life Cycle Assessment (LCA) studies are needed. The recovery of lead from motorcycle batteries also presents economic and environmental

relevance, with significant forecasts of obtaining it via urban mining, but faces capacity and illegal recycling challenges [110].

The spatial and social perspective of urban mining reveals additional complexities. A study in the Metropolitan Region of Rio de Janeiro (MRRJ) identified significant potential, but also a concentration of recyclers that leaves areas of high generation isolated, reinforcing the need to optimize routes and improve data management and collection [81]. Universities emerge as promising sources of WEEE ("urban mines"), however, even in higher education communities, there is ignorance about proper disposal and reverse logistics, with the lack of infrastructure and information being significant barriers [111]. Urban mining is strongly connected to Sustainable Development Goals (SDGs) such as industry/innovation (SDG 9) and responsible consumption/production (SDG 12), but presents social trade-offs, especially linked to informality and precarious working conditions of waste pickers, demanding ethical and inclusive approaches [28].

The geography of urban mining is uneven, shaped by the local political economy, resulting in disparities in practices and technologies between different urban contexts. For example, while the London Larger Urban Zone (LLUZ) and Sao Paulo Macrometropolis (SPMM) stand out for the predominance of formal companies and advanced recycling technologies, the Greater Accra Region (GAR) faces significant challenges with informal collection and rudimentary techniques that generate environmental and health impacts [82]. In addition, the mining activity itself, even urban, can entail socio-environmental risks, such as subsidence in Maceió, requiring tools such as Geographic Information System (GIS) and Multi-Criteria Decision Aid (MCDA) for mapping vulnerabilities and supporting urban planning [112]. The lack of standardization in sustainability reports on waste management also hinders a complete view of flows and the advancement of the circular economy [113].

In summary, urban mining, aligned with the principles of the circular economy, is presented as an important strategy in the face of pressure on primary resources and the increase in waste generation in Brazil. Although it represents an opportunity to recover valuable and critical materials from various anthropogenic sources, such as WEEE and CDW, its consolidation depends on overcoming technological, logistical, economic, informational, and socio-political barriers. The development and implementation of characterization and processing technologies, combined with effective public policies, functional reverse logistics systems, greater public awareness, and socially inclusive approaches, are fundamental for urban mining to reach its potential to contribute to sustainability and the efficient management of resources in the country.

7. Legal Dimension of Urban Mining: Effectiveness of Brazilian Legislation and Obstacles to Overcome

Regarding the legal dimension, urban mining, particularly with regard to the utilization of WEEE, is intrinsically linked to the normative framework that regulates the management of solid waste in the country. The evolution of this legislation, from the establishment of the National Solid Waste Policy (NSWP) [22], in 2010 to the most recent decrees [23–26] that improve the regulation of WEEE management, demonstrates a normative progress towards shared responsibility and reverse logistics. However, the mere existence of a set of laws and regulations does not guarantee its effectiveness.

This section proposes to deepen the critical analysis of Brazilian legislation applicable to urban mining, examining to what extent the current legal framework is effective in driving this activity, as well as the main persistent challenges in its practical implementation and enforcement. From an assessment of the normative scenario and the obstacles encountered in its application, it will be possible to identify the gaps and the needs for legislative

improvement for the full development of urban mining as a strategy for sustainability and the utilization of secondary resources in Brazil.

The trajectory of waste management in the European Union [17–21], with its progressive legislative sophistication guided by the search for sustainable practices and the principles of the circular economy, serves as an important benchmark for the analysis of policies in other regions. Although Brazil has its particularities and challenges inherent to international experiences, such as the European one, often influence the adoption of models and the normative evolution in developing countries. In this context, the understanding of international approaches and the principles that govern the management of WEEE helps to examine the effectiveness of Brazilian legislation applicable to urban mining.

The evolution of waste management in the European Union (Table 2) demonstrates a progressive legislative sophistication, guided by the search for sustainable practices. The Table 4 shows that, in the 1970s, Europe adopted Directive 75/442/CEE [17], which prioritized the elimination of waste, with the aim of mitigating the environmental impacts associated with final disposal. Although this approach was fundamental, it focused on solving the problem in a reactive way, that is, after the generation of waste.

Table 4. Waste legislation in Europe.

Year	Approach
1970	Europe: Directive 75/442/CEE—prioritization of waste elimination
1990	Directive 91/156/CEE—introduction of the paradigm of integrated management and prevention at the source
2006–2008	Directive 94/62/CE—specific directives for packaging Consolidation and improvement of the legal framework (Directive 2006/12/CE and Waste Framework Directive 2008/98/CE)
2008	Incorporation of the principles of the circular economy

Directive 91/156/CEE [18], in the 1990s, introduced the paradigm of integrated management, shifting the focus to prevention at the source and the valorization of waste. This change represented a significant conceptual advance, promoting the hierarchization of management strategies. Concomitantly, specific directives for waste streams, such as 94/62/CE for packaging, were promulgated, complementing the framework legislation and establishing specific requirements for each type of waste.

The period between 2006 and 2008 was characterized by the consolidation and improvement of the legal framework. Directive 2006/12/CE [19] codified the pre-existing legislation, while the Waste Framework Directive (2008/98/CE) [20] consolidated the management hierarchy, with emphasis on prevention, reuse, recycling, and valorization, and strengthened producer responsibility.

From 2008 onwards, the legislation incorporated the principles of the circular economy. The 2018 Circular Economy Package, for example, established ambitious targets for recycling and reducing final disposal, aiming for a transition to a more sustainable production and consumption model. This trajectory demonstrates the EU's commitment to sustainability in waste management, continuously seeking to optimize policies and internalize the principles of circularity.

The European directives on WEEE are well formulated, with a focus on Extended Producer Responsibility, which seeks to involve manufacturers in the product life cycle. The EU WEEE Directive, for example, sets criteria for collection, treatment, and recovery [11]. However, its effectiveness across Member States varies; efficient enforcement, public

awareness, and adequate infrastructure for collection and recycling are crucial. Baldé et al. [11] report that while Europe (as a region) documents a formal collection and recycling rate of 42.8% for e-waste, many EU Member States struggle to meet their specific, legally binding collection targets, with only a few achieving them by 2022. For WEEE policies to be successful, it is necessary to invest in these areas and ensure coordination between legislation, companies, consumers, and government agencies.

Although Brazil is independent, some practices of European companies (and those of other countries) influence the use of some models already adopted by other countries. The search for sustainable practices in waste management has driven legislative evolution in various regions of the world, Brazil has demonstrated a progressive development of its normative structure for the governance of WEEE, consolidating a comprehensive legal framework that encompasses laws, decrees, normative instructions, and technical standards. This normative set aims not only to minimize the negative impacts of improper disposal but also to promote the transition to a circular economy model, promoting the use of resources present in WEEE.

The National Solid Waste Policy (Law nº 12.305/2010) [22] bases the management of Waste Electrical and Electronic Equipment (WEEE) on shared responsibility and reverse logistics. Distributing responsibilities among manufacturers, importers, distributors, merchants, consumers, and the government, the NSWP integrates management, aiming at proper disposal. The policy aims to assign manufacturers the responsibility for the environmental costs of the production, use, and disposal of WEEE (such as pollution and resource depletion), encouraging these costs to be reflected in the final price of the products. This encourages the prevention of waste generation, through the development of more durable and less polluting products.

In addition, the NSWP prioritizes the reuse of equipment, the recycling of its components, and the recovery of valuable materials, thus minimizing the amount of waste that reaches landfills and the associated environmental impact. Co-responsibility encourages sustainable practices, from product design to its disposal, closing the life cycle and promoting the circular economy. The aforementioned Policy thus seeks to mitigate waste generation, conserve natural resources, and reduce pollution, contributing to sustainable development. Reverse logistics operationalizes the manufacturer's responsibility, ensuring the collection and proper processing of WEEE, while consumer participation is fundamental for the success of the system.

Complementing the NSWP, recent decrees have improved the regulation of WEEE management, with emphasis on Decree nº 10.240/2020 [23], which establishes goals and deadlines for the implementation of reverse logistics; Decree nº 10.657/2021 [24], which, by promoting the Pro-minerals Policy and defining criteria for strategic minerals, indirectly drives urban mining of WEEE; and Decrees nº 10.936/2022 [25] and nº 11.413/2023 [26], which promote improvements in the regulation of the PNRS and institute the Reverse Logistics Recycling Credit Certificate, the Structuring and Recycling Certificate of General Packaging, and the Future Mass Credit Certificate, within the scope of reverse logistics systems, respectively. The convergence of these legal instruments strengthens the regulatory structure and creates an environment conducive to the development of urban mining, a practice that aims at the recovery of metals and other valuable materials from WEEE, aligning with the principles of the circular economy.

The standardization of processes and the guarantee of safety and efficiency in the management of WEEE are ensured by technical standards of the Brazilian Association of Technical Standards. Brazilian Standard—NBR 10.004:2004 [13] establishes the classification of solid waste according to its risks, providing guidelines for the proper handling of WEEE. Standards NBR 16.156:2013 [14] and NBR 15.833:2018 [15] specify the requirements for

the reverse manufacturing of electro-electronics and refrigeration appliances, respectively, promoting recycling and material recovery. Additionally, NBR IEC 63.000:2019 [16], harmonized with the European RoHS (Restriction of Hazardous Substances) Directive, regulates the restriction of hazardous substances in electrical and electronic equipment, contributing to the protection of human health and the environment.

Although the normative advance is remarkable, the full implementation of WEEE management in Brazil still faces significant challenges. The complexity of the production chain, the high informality in the recycling sector, the insufficient awareness of the population about the correct disposal, and the need for greater investments in collection and processing infrastructure represent obstacles to be overcome.

To achieve the sustainability objectives outlined in the NSWP, the intensification of enforcement of compliance with the legislation, the stimulation of technological innovation in recycling processes, the strengthening of articulation between the different levels of government (municipal, state, and federal), and the promotion of environmental education campaigns become essential. Future research should prioritize the evaluation of the impact of current legislation, the identification of bottlenecks in the implementation, and the proposition of solutions for the improvement of the system, aiming at a more efficient and fully aligned WEEE management with the principles of the circular economy.

In Brazil, many practices are still in initial stages or are adopted incompletely. This difference can be explained by the variation in environmental regulations and the level of social and economic pressure that motivates companies to adopt more sustainable practices. In developed countries, stricter environmental legislation and the growing consumer demand for sustainable practices contribute to greater adherence to these initiatives.

Critical Discourse Analysis

Critical Discourse Analysis (CDA) is a valuable theoretical-methodological approach for critical organizational studies, as it contributes to the reflection on contemporary social issues and seeks to denaturalize beliefs that sustain structures of domination. Although the use of CDA in Administration is not recent, its application is still limited, and the analysis of the textual dimension is not always explored in depth. Our article relies on the theoretical and methodological assumptions of CDA, as proposed by Norman Fairclough (2010) [27], and we offer subsidies for the analysis of the representational dimension, illustrating its operationalization. Our objective is to clarify aspects related to the linguistic analysis of normative texts between Brazil and Europe.

The analysis of the National Solid Waste Policy (NSWP) from the perspective of Critical Discourse Analysis (CDA) reveals a discrepancy between its normative discourse and practical application. Textually, the technical language present in Law nº. 12.305/2010 [22], such as in Article 9 when defining the waste management hierarchy, hinders comprehension by the lay public and limits citizen participation in social control and guideline implementation. Furthermore, the legislation presents ambiguities in the definition of responsibilities. Article 18 attributes waste management to municipalities, while Articles 16 and 17 stipulate that states complement the guidelines, leading to an overlap of competencies and hindering the efficient execution of actions.

Another critical aspect is the emphasis on sanctions rather than incentives. Article 3 of Decree nº. 12.189, enacted in 2024, prescribes penalties for non-compliance with regulations, which may generate resistance among the involved stakeholders. To foster voluntary adherence to sustainable practices, it is imperative to combine punitive mechanisms with incentive and engagement strategies.

Discursively, the adoption of the formal and impersonal language characteristic of legal norms can distance official discourse from the needs of the population. The legal language

of the NSWP, specifically in Article 3, paragraph XVII, defines "shared responsibility for the life cycle of products", but without clarifying practical means of implementation. This lack of clarity impedes effective application of the norm. The interconnection between laws also complicates understanding of the policy. Article 51 of Law nº. 12.305/2010 [22] refers to Law nº. 9.605/1998 [114], which addresses environmental sanctions, thereby requiring knowledge of various norms for a comprehensive interpretation.

Waste generators are depicted solely as passive agents, subject to legal obligations without incentives for active participation. Article 33 of Law nº. 12.305/2010 [22] imposes upon manufacturers, distributors, and retailers the creation of reverse logistics systems, yet lacks clear guidelines for engagement and awareness, thereby limiting their effectiveness in promoting sustainable practices.

Socio-historically, the NSWP reflects the ideology of ecological modernization, which seeks to balance economic development and sustainability. Article 7, item II, stipulates that waste management should "stimulate sustainable development through the use of environmentally sound technologies". This modernization is further underscored by Article 44, which provides for incentives for sustainable practices, thus combining regulation with economic stimuli.

However, this ideology can justify greenwashing practices, masking unsustainable production and consumption models. Article 33 of Law nº. 12.305/2010 [22] mandates reverse logistics systems, but without efficient oversight, this allows for merely formal compliance. Power dynamics in the formulation and implementation of public policies frequently result in the marginalization of vulnerable groups. Although Decree nº. 10.936/2022 [24] recognizes the participation of recyclable and reusable waste pickers, legitimizing their inclusion in the production chain through Article 36, the normative text does not specifically detail their rights and duties. This lack of detailed specification can limit their effective integration and protection within the formal waste management system.

Despite its robust structure, the legislation often fails in practice, rendering shared responsibility fragile and leading to problems in waste disposal. Consequently, the lack of planning adapted to the reality of each municipality exacerbates environmental challenges. Article 54 of Law nº. 12.305/2010 [22] mandates the elimination of open dumps and the implementation of sanitary landfills, but without considering local specificities, which hinders its application. For cities with fewer than 50,000 inhabitants, the deadline for compliance was set for 2 August 2024, however, many municipalities have yet to meet this requirement, highlighting implementation difficulties and the need for solutions more tailored to regional conditions.

The effective adoption of circular business models, the strategic use of technology, and the strengthening of Extended Producer Responsibility are fundamental elements for a more efficient and equitable waste management system. In this context, CDA is an essential tool for highlighting hegemonic discourses and revealing the power relations underlying environmental policies, thereby contributing to the improvement of regulatory frameworks and the inclusion of historically marginalized actors.

8. Conclusions

Urban mining in Brazil is distinct from models in other regions, like the EU, primarily focusing on waste reduction and integrating the informal workforce rather than critical metal scarcity. Significant gaps exist in Brazil regarding knowledge production and technological appropriation for critical metal recovery from WEEE, which requires sophisticated technologies and greater incentives for research and development. The Brazilian legal framework, despite evolving, faces challenges in practical implementation due to a lack of clarity, ambiguities, and enforcement difficulties. The informal recycling sector and

low public awareness further contrast with the more consolidated infrastructure in many European countries.

To advance this sector, policy recommendations include implementing fiscal incentives such as tax exemptions and credits for companies investing in advanced recycling technologies and formalizing informal workers. Crucially, technical and professional training programs are needed to empower workers for efficient and safer recycling technologies, fostering better working conditions and integration into industrial processes. Establishing quality standards for recovered metals is also vital to encourage their reinsertion into the productive chain.

Future research should prioritize developing efficient and sustainable recycling technologies adapted to Brazil's heterogeneous waste. Detailed analyses of the social and environmental impacts of urban mining in various national contexts are necessary, alongside evaluating the economic viability of different business models. Further investigations should focus on technological solutions tailored to the Brazilian reality, identifying bottlenecks in reverse logistics, and exploring social inclusion models that ensure fair working conditions. Assessing the real impact of current legislation and identifying obstacles to its practical application are also critical research areas.

9. On the Use of Artificial Intelligence

In accordance with the guidelines for the ethical and responsible use of Generative Artificial Intelligence (AI), the production of this article was aided by AI tools at various stages of the research, writing and image production process. It is essential to emphasize that all outputs generated by AI tools were subjected to rigorous curation and validation by the authors, ensuring the scientific accuracy and integrity of the final content.

Author Contributions: Writing—original draft preparation, J.M.M.N., R.C.L., N.L.d.S.A. and E.A.d.S.; writing—review and editing, J.M.M.N., R.C.L., N.L.d.S.A. and E.A.d.S. All authors have read and agreed to the published version of the manuscript.

Funding: This research received no external funding.

Data Availability Statement: The original contributions presented in this study are included in the article. Further inquiries can be directed at the corresponding author.

Acknowledgments: One of the authors (JMMN) acknowledges CNPq and FAPEPI for research support (PDCTR—Process 301246/2022-0).

Conflicts of Interest: The authors declare no conflicts of interest.

Abbreviations

The following abbreviations are used in this manuscript:

AgNPs	Silver Nanoparticles
ATPS	Aqueous Two-Phase Systems
CDA	Critical Discourse Analysis
CDW	Construction and Demolition Waste
CE	European Conformity
DEMATEL	Decision Making Trial and Evaluation Laboratory
DESs	Deep Eutectic Solvents
EEC	European Economic Community
ELV	End-of-Life Vehicles
EU	European Union
FAAS	Flame Atomic Absorption Spectroscopy
GIS	Geographic Information System
ICP-OES	Inductively Coupled Plasma-Optical Emission Spectroscopy

IEC	International Electrotechnical Commission
ILs	Ionic Liquids
LCA	Life Cycle Assessment
LCD	Liquid Crystal Display
LEDs	Light Emitting Diodes
LIBS	Laser-Induced Breakdown Spectroscopy
MCDA	Multi-Criteria Decision Aid
MNHM	Magnetic Nanohydrometallurgy
MRRJ	Metropolitan Region of Rio de Janeiro
NCA	Nickel-Cobalt-Aluminum
PARAFAC	Parallel Factor Analysis
PCBs	Printed Circuit Boards
NSWP	National Solid Waste Policy
PPILs	Pseudo-Protic Ionic Liquids
REEs	Rare Earth Elements
RLSs	Reverse Logistics Systems
RoHS	Restriction of Hazardous Substances
RPMs	Rare and Precious Metals
SCFE	Supercritical Fluid Extraction
SDGs	Sustainable Development Goals
SWT	Supercritical Water Technology
TSS	Tin Stripping Solution
USW	Urban Solid Waste
WEEE	Waste Electrical and Electronic Equipment
WPCBs	Waste Printed Circuit Boards

References

1. Erdiaw-Kwasie, M.O.; Abunyewah, M.; Baah, C. A systematic review of the factors—Barriers, drivers, and technologies—Affecting e-waste urban mining: On the circular economy future of developing countries. *J. Clean. Prod.* **2024**, *436*, 140645. [CrossRef]
2. Kazançoglu, Y.; Ada, E.; Ozturkoglu, Y.; Ozbiltekin, M. Analysis of the barriers to urban mining for resource melioration in emerging economies. *Resour. Pol.* **2020**, *68*, 101768. [CrossRef]
3. Ghisellini, P.; Ncube, A.; Casazza, M.; Passaro, R. Toward circular and socially just urban mining in global societies and cities: Present state and future perspectives. *Front. Sustain. Cities* **2022**, *4*, 930061. [CrossRef]
4. Fatimah, Y.A.; Govindan, K.; Sasongko, N.A.; Hasibuan, Z.A. The critical success factors for sustainable resource management in circular economy: Assessment of urban mining maturity level. *J. Clean. Prod.* **2024**, *469*, 143084. [CrossRef]
5. Ouro-Salim, O. Urban mining of e-waste management globally: Literature review. *Clean. Waste Syst.* **2024**, *9*, 100162. [CrossRef]
6. Udage Kankanamge, A.K.S.; Erdiaw-Kwasie, M.O.; Abunyewah, M. Towards a Taxonomy of E-Waste Urban Mining Technology Design and Adoption: A Systematic Literature Review. *Sustainability* **2024**, *16*, 6389. [CrossRef]
7. Ogunseitan, O.A.; Schoenung, J.M.; Saphores, J.D.M.; Shapiro, A.A. The electronics revolution: From e-wonderland to e-wasteland. *Science* **2009**, *326*, 670–671. [CrossRef]
8. Arora, R.; Paterok, K.; Banerjee, A.; Saluja, M.S. Potential and relevance of urban mining in the context of sustainable cities. *IIMB Manag. Rev.* **2017**, *29*, 210–224. [CrossRef]
9. Xavier, L.H.; Giese, E.C.; Ribeiro-Duthie, A.C.; Lins, F.A.F. Sustainability and the circular economy: A theoretical approach focused on e-waste urban mining. *Resour. Policy* **2021**, *74*, 101467. [CrossRef]
10. Contador, L.S.; Freire, L.S.; Xavier, L.H. Paradoxes of electronic waste reverse logistics and urban mining in Brazil. *Rev. Tecnol. Soc.* **2022**, *18*, 141–153. [CrossRef]
11. Baldé, C.P.; Kuehr, R.; Yamamoto, T.; McDonald, R.; D'Angelo, E.; Althaf, S.; Bel, G.; Deubzer, O.; Fernandez-Cubillo, E.; Forti, V.; et al. International Telecommunication Union (ITU) and United Nations Institute for Training and Research (UNITAR). Global E-waste Monitor. 2024. Available online: https://ewastemonitor.info/the-global-e-waste-monitor-2024/ (accessed on 18 May 2025).
12. Tricco, A.C.; Lillie, E.; Zarin, W.; O'Brien, K.K.; Colquhoun, H.; Levac, D.; Moher, D.; Peters, M.D.J.; Horsley, T.; Weeks, L.; et al. PRISMA Extension for Scoping Reviews (PRISMA-ScR): Checklist and Explanation. *Ann. Intern. Med.* **2018**, *169*, 467–473. [CrossRef] [PubMed]
13. *ABNT NBR 10004*; Resíduos Sólidos—Classificação. ABNT: Rio de Janeiro, Brazil, 2004.

14. *ABNT NBR 16156*; Resíduos de Equipamentos Eletroeletrônicos—Requisitos Para Atividade de Manufatura Reversa. ABNT: Rio de Janeiro, Brazil, 2013.
15. *ABNT NBR 15833*; Manufatura Reversa—Aparelhos de Refrigeração. ABNT: Rio de Janeiro, Brazil, 2018.
16. *ABNT NBR IEC 63000*; Documentação Técnica Para a Avaliação de Produtos Elétricos e Eletrônicos Com Relação à Restrição de Substâncias Perigosas (RoHS). ABNT: Rio de Janeiro, Brazil, 2019.
17. União Europeia. Conselho. Diretiva 75/442/CEE, de 15 de Julho de 1975, Relativa aos resíduos. In *Jornal Oficial das Comunidades Europeias, L 194*; European Union: Geneva, Switzerland, 1975.
18. União Europeia. Conselho. Diretiva 91/156/CEE, de 18 de Março de 1991, Que Altera a Diretiva 75/442/CEE relativa aos resíduos. In *Jornal Oficial das Comunidades Europeias, L 78*; European Union: Geneva, Switzerland, 1991.
19. União Europeia. Parlamento Europeu. Conselho. Diretiva 2006/12/CE, de 5 de abril de 2006, relativa aos resíduos. In *Jornal Oficial da União Europeia, L 114*; European Union: Geneva, Switzerland, 2006.
20. União Europeia. Parlamento Europeu. Conselho. Diretiva 2008/98/CE, de 19 de novembro de 2008, relativa aos resíduos e que revoga certas Diretivas. In *Jornal Oficial da União Europeia, L 312*; European Union: Geneva, Switzerland, 2008.
21. União Europeia. Parlamento Europeu. Conselho. Diretiva 2012/19/UE, de 4 de julho de 2012, relativa a resíduos de equipamentos elétricos e eletrónicos (REEE). In *Jornal Oficial da União Europeia, L 197*; European Union: Geneva, Switzerland, 2012.
22. Brasil. Lei nº 12.305, de 2 de Agosto de 2010. Institui a Política Nacional de Resíduos Sólidos; Altera a Lei no 9.605, de 12 de Fevereiro de 1998; e Dá Outras Providências. Diário Oficial da União, Brasília, DF, 03 Ago. 2010. Available online: https://www.planalto.gov.br/ccivil_03/_ato2007-2010/2010/lei/l12305.htm (accessed on 20 April 2025).
23. Brasil. Decreto nº 10.240, de 12 de Fevereiro de 2020. Acordo Setorial Para Implementação de Sistema de Logística Reversa de Produtos Eletroeletrônicos e Seus Componentes de Uso Doméstico. Available online: http://www.planalto.gov.br/ccivil_03/_ato2019-2022/2020/decreto/D10240.htm (accessed on 6 April 2025).
24. Brasil. Decreto nº 10.657, de 24 de março de 2021. Institui a Política de Apoio ao Licenciamento Ambiental de Projetos de Investimentos Para a Produção de Minerais Estratégicos—Pró-Minerais Estratégicos, Dispõe Sobre Sua Qualificação no Âmbito do Programa de Parcerias de Investimentos da Presidência da República e Institui o Comitê Interministerial de Análise de Projetos de Minerais Estratégicos. Available online: https://www.planalto.gov.br/ccivil_03/_Ato2019-2022/2021/Decreto/D10657.htm (accessed on 20 April 2025).
25. Brasil. Decreto nº 10.936, de 12 de Janeiro de 2022. Regulamenta Dispositivos da Lei nº 12.305, de 2 de Agosto de 2010, Que Institui a Política Nacional de Resíduos Sólidos. Available online: https://www.planalto.gov.br/ccivil_03/_ato2019-2022/2022/decreto/d10936.htm (accessed on 20 April 2025).
26. Brasil. Decreto nº 11.413, de 13 de Fevereiro de 2023. Institui o Certificado de Crédito de Reciclagem de Logística Reversa, o Certificado de Estruturação e Reciclagem de Embalagens em Geral e o Certificado de Crédito de Massa Futura, no Âmbito dos Sistemas de Logística Reversa de Que Trata o Art. 33 da Lei nº 12.305, de 2 de Agosto de 2010. Available online: https://www.planalto.gov.br/ccivil_03/_Ato2023-2026/2023/Decreto/D11413.htm (accessed on 20 April 2025).
27. Fairclough, N. *Critical Discourse Analysis: The Critical Study of Language*; Longman: London, UK, 2010.
28. Botelho, A.B., Jr.; Martins, F.P.; Cezarino, L.O.; Liboni, L.B.; Tenório, J.A.S.; Espinosa, D.C.R. The sustainable development goals, urban mining, and the circular economy. *Extr. Ind. Soc.* **2023**, *16*, 101367. [CrossRef]
29. Xavier, L.H.; Ottoni, M.; Abreu, L.P.P. A comprehensive review of urban mining and the value recovery from e-waste materials. *Resour. Conserv. Recycl.* **2023**, *190*, 106840. [CrossRef]
30. Wang, M.; Tan, Q.; Chiang, J.F.; Li, J. Recovery of rare and precious metals from urban mines—A review. *Front. Environ. Sci. Eng.* **2017**, *11*, 1. [CrossRef]
31. Firmansyah, M.L.; Rizki, I.N.; Ullah, N. Recent advances in urban mining technology: A focus on electronic waste recycling potential in Indonesia. *Clean. Waste Syst.* **2025**, *10*, 100239. [CrossRef]
32. Tunsu, C.; Petranikova, M.; Gergorić, M.; Ekberg, C.; Retegan, T. Reclaiming rare earth elements from end-of-life products: A review of the perspectives for urban mining using hydrometallurgical unit operations. *Hydrometallurgy* **2015**, *156*, 239–258. [CrossRef]
33. Gomes, R.F.; Pereira, M.M.; Leão, V.A. Acid Leaching of Rare Earth Elements Present in Waste Electrical and Electronic Equipment: A Brief Review. *Rev. Virtual Quim.* **2022**, *14*, 319–328. [CrossRef]
34. Anwer, S.; Panghal, A.; Majid, I.; Mallick, S. Urban mining: Recovery of metals from printed circuit boards. *Int. J. Environ. Sci. Technol.* **2022**, *19*, 9731–9740. [CrossRef]
35. Prodius, D.; Gandha, K.; Mudring, A.V.; Nlebedim, I.C. Sustainable Urban Mining of Critical Elements from Magnet and Electronic Wastes. *ACS Sustain. Chem. Eng.* **2020**, *8*, 1455–1463. [CrossRef]
36. Arya, S.; Patel, A.; Kumar, S.; Pau-Loke, S. Urban mining of obsolete computers by manual dismantling and waste printed circuit boards by chemical leaching and toxicity assessment of its waste residues. *Environ. Pollut.* **2021**, *283*, 117033. [CrossRef]
37. Botelho, A.B., Jr.; Stopic, S.; Friedrich, B.; Tenório, J.A.S.; Espinosa, D.C.R. Cobalt Recovery from Li-Ion Battery Recycling: A Critical Review. *Metals* **2021**, *11*, 1999. [CrossRef]

38. Rocchetti, L.; Amato, A.; Fonti, V.; Ubaldini, S.; De Michelis, I.; Kopacek, B.; Vegliò, F.; Beolchini, F. Cross-current leaching of indium from end-of-life LCD panels. *Waste Manag.* **2015**, *42*, 180–187. [CrossRef]
39. Oliveira, R.P.; Benvenuti, J.; Espinosa, D.C.R. A review of the current progress in recycling technologies for gallium and rare earth elements from light-emitting diodes. *Renew. Sustain. Energy Rev.* **2021**, *145*, 111090. [CrossRef]
40. Martins, T.A.G.; Caldas, M.P.K.; Moraes, V.T.; Tenório, J.A.S.; Espinosa, D.C.R. Recovering metals from motherboard and memory board waste through sulfuric leaching. *J. Environ. Chem. Eng.* **2021**, *9*, 106789. [CrossRef]
41. Agrawal, M.; Singh, K.K.; Singh, R. Hydrometallurgical recovery of manganese and nickel and isolation of tantalum from obsolete tantalum capacitor. *J. Environ. Chem. Eng.* **2022**, *10*, 108887. [CrossRef]
42. Tran, D.T.; Tran, N.T.T.; Song, M.H.; Pham, T.P.T.; Yun, Y.S. Thiosulfate-based leaching for eco-friendly urban mining: Recent developments and challenges. *Sep. Purif. Technol.* **2025**, *359*, 130775. [CrossRef]
43. Yang, C.; Li, J.; Tan, Q.; Liu, L.; Dong, Q. Green Process of Metal Recycling: Coprocessing Waste Printed Circuit Boards and Spent Tin Stripping Solution. *ACS Sustain. Chem. Eng.* **2017**, *5*, 3524–3531. [CrossRef]
44. Caldas, M.P.K.; Martins, T.A.G.; Moraes, V.T.; Tenório, J.A.S.; Espinosa, D.C.R. Synthesis of Ag nanoparticles from waste printed circuit board. *J. Environ. Chem. Eng.* **2021**, *9*, 106845. [CrossRef]
45. Lima, A.M.N.O.; Espinosa, D.C.R.; Botelho Júnior, A.B.; Tenório, J.A.S. NCA Type Lithium Ion Battery: A Review of Separation and Purification Technologies for Recycling Metals. *J. Sustain. Metall.* **2024**, *10*, 1036–1050. [CrossRef]
46. Tunsu, C.; Menard, Y.; Eriksen, D.Ø.; Ekberg, C.; Petranikova, M. Recovery of critical materials from mine tailings: A comparative study of the solvent extraction of rare earths using acidic, solvating and mixed extractant systems. *J. Clean. Prod.* **2019**, *218*, 425–437. [CrossRef]
47. Quijada-Maldonado, E.; Olea, F.; Sepúlveda, R.; Castillo, J.; Cabezas, R.; Merlet, G.; Romero, J. Possibilities and challenges for ionic liquids in hydrometallurgy. *Sep. Purif. Technol.* **2020**, *251*, 117289. [CrossRef]
48. Arrachart, G.; Couturier, J.; Dourdain, S.; Levard, C.; Pellet-Rostaing, S. Recovery of Rare Earth Elements (REEs) Using Ionic Solvents. *Processes* **2021**, *9*, 1202. [CrossRef]
49. Alguacil, F.J.; Robla, J.I. Solvent extraction in the recovery of metals from solutions: Entering the third decade of XXI century. *Desalin. Water Treat.* **2022**, *265*, 71–93. [CrossRef]
50. Zhang, J.; Anawati, J.; Azimi, G. Urban mining of terbium, europium, and yttrium from real fluorescent lamp waste using supercritical fluid extraction: Process development and mechanistic investigation. *Waste Manag.* **2022**, *139*, 168–178. [CrossRef]
51. Castillo-Ramírez, C.; Janssen, C.H.C. Pseudo-Protic Ionic Liquids for the Extraction of Metals Relevant for Urban Mining. *Ind. Eng. Chem. Res.* **2023**, *62*, 627–636. [CrossRef]
52. Reyes-Valderrama, M.I.; Salinas-Rodríguez, E.; Montiel-Hernández, J.F.; Rivera-Landero, I.; Cerecedo-Sáenz, E.; Hernández-Ávila, J.; Arenas-Flores, A. Urban Mining and Electrochemistry: Cyclic Voltammetry Study of Acidic Solutions from Electronic Wastes (Printed Circuit Boards) for Recovery of Cu, Zn, and Ni. *Metals* **2017**, *7*, 55. [CrossRef]
53. Son, J.; Han, J.I.; Hong, Y.; Yavuz, C.T. Energy-efficient electrochemical recovery of gold enabled by a thiourea-based electrolyte system. *J. Environ. Chem. Eng.* **2023**, *11*, 111120. [CrossRef]
54. Pinto, C.F.; Malpass, A.C.G.; Malpass, G.R.P. Recycling of Printed Circuit Boards for Cooper Extraction: A Review of the Methods Employed. *Rev. Virtual Quim.* **2024**, *16*, 456–471.
55. Nithya, R.; Sivasankari, C.; Thirunavukkarasu, A. Electronic waste generation, regulation and metal recovery: A review. *Environ. Chem. Lett.* **2021**, *19*, 1347–1368. [CrossRef]
56. Zhang, L.; Xu, Z. A review of current progress of recycling technologies for metals from waste electrical and electronic equipment. *J. Clean. Prod.* **2016**, *127*, 19–36. [CrossRef]
57. Hsu, E.; Barmak, K.; West, A.C.; Park, A.H.A. Advancements in the treatment and processing of electronic waste with sustainability: A review of metal extraction and recovery technologies. *Green Chem.* **2019**, *21*, 919–936. [CrossRef]
58. Thakur, P.; Kumar, S. Metallurgical processes unveil the unexplored "sleeping mines" e- waste: A review. *Environ. Sci. Pollut. Res.* **2020**, *27*, 32359–32370. [CrossRef] [PubMed]
59. Kaya, M. Recovery of metals and nonmetals from electronic waste by physical and chemical recycling processes. *Waste Manag.* **2016**, *57*, 64–90. [CrossRef] [PubMed]
60. Schwartz, E.; He, H.; Frost, K.; Nauyen, B.H.; Ogunseitan, O.A.; Schoenung, J.M. Comparative life cycle assessment of copper and gold recovery from waste printed circuit boards: Pyrometallurgy, chemical leaching and bioleaching. *J. Hazard. Mater.* **2024**, *473*, 134545. [CrossRef]
61. Lee, T.H.; Joo, S.H.; Nersisyan, H.H.; Kong, M.S.; Lee, J.W.; Park, K.W.; Lee, J.H. Reduction Kinetics of Zinc Powder from Brass Converter Slag by Pyrometallurgical Method Using Hydrogen Gas. *KONA Powder Part. J.* **2016**, *33*, 278–286. [CrossRef]
62. Li, X.; Ma, B.; Wang, C.; Chen, Y. Recycling and recovery of spent copper–indium–gallium–diselenide (CIGS) solar cells: A review. *Int. J. Miner., Metall. Mater.* **2023**, *30*, 989–1002. [CrossRef]
63. Madhavan, M.; Shetty Kodialbail, V.; Saidutta, M.B. Performance of Fluidized-Bed Bioreactor in Copper Bioleaching from Printed Circuit Boards using Alcaligenes aquatilis. *Waste Biomass Valor.* **2024**, *15*, 1213–1224. [CrossRef]

64. Rodrigues, É.F.; Cesa Rovaris, B.; Valerio, A.; de Oliveira, D.; Hotza, D. Bioleaching of Printed Circuit Board Waste to Obtain Metallic Nanoparticles. *Sustainability* **2024**, *16*, 9837. [CrossRef]
65. Thakur, P.; Kumar, S. Exploring bioleaching potential of indigenous Bacillus sporothermodurans ISO1 for metals recovery from PCBs through sequential leaching process. *Waste Manag. Res.* **2023**, *41*, 1255–1268. [CrossRef]
66. Jones, M.P.; Bismarck, A. Mycomining: Perspective on fungi as scavengers of scattered metal, mineral, and rare earth element resources. *RSC Sustain.* **2024**, *2*, 1350–1357. [CrossRef]
67. Maes, S.; Props, R.; Fitts, J.P.; Smet, R.; Vilchez-Vargas, R.; Vital, M.; Pieper, D.H.; Vanhaecke, F.; Boon, N.; Hennebel, T. Platinum Recovery from Synthetic Extreme Environments by Halophilic Bacteria. *Environ. Sci. Technol.* **2016**, *50*, 2619–2626. [CrossRef] [PubMed]
68. Giese, E.C. E-waste mining and the transition toward a bio-based economy: The case of lamp phosphor powder. *MRS Energy Sustain.* **2022**, *9*, 494–500. [CrossRef] [PubMed]
69. Kumar, A.; Holuszko, M.; Espinosa, D.C.R. E-waste: An Overview on Generation, Collection, Legislation and Recycling Practices. *Resour. Conserv. Recycl.* **2017**, *122*, 32–42. [CrossRef]
70. Monteiro, N.B.R.; Bezerra, A.K.L.; Moita Neto, J.M.; Silva, E.A. Mining Law: In Search of Sustainable Mining. *Sustainability* **2021**, *13*, 867. [CrossRef]
71. Christmann, P. Mineral Resource Governance in the 21st Century and a Sustainable European Union. *Miner. Econ.* **2021**, *34*, 187–208. [CrossRef]
72. Gedam, V.V.; Raut, R.D.; Jabbour, A.B.L.S.; Agrawal, N. Moving the Circular Economy Forward in the Mining Industry: Challenges to closed-loop in an emerging economy. *Resour. Policy* **2021**, *74*, 102279. [CrossRef]
73. Salhofer, S.; Steuer, B.; Ramusch, R.; Beigl, P. WEEE management in Europe and China—A comparison. *Waste Manag.* **2016**, *57*, 27–35. [CrossRef]
74. Habib, H.; Wagner, M.; Baldé, C.P.; Martínez, L.H.; Huisman, J.; Dewulf, J. What gets measured gets managed—Does it? Uncovering the waste electrical and electronic equipment flows in the European Union. *Resour. Conserv. Recycl.* **2022**, *181*, 106222. [CrossRef]
75. McMahon, K.; Johnson, M.; Fitzpatrick, C. Enabling preparation for re-use of waste electrical and electronic equipment in Ireland: Lessons from other EU member states. *J. Clean. Prod.* **2019**, *232*, 1005–1017. [CrossRef]
76. Nikolic, M.; Bergmann, G.; Schelte, N.; Severengiz, S. Closing the loop of small WEEE—Life cycle based approach for the evaluation of end-of-life strategies on the example of coffee machines. *Resour. Conserv. Recycl. Adv.* **2024**, *23*, 200220. [CrossRef]
77. Brasil. Conheça a Linha do Tempo da Tragédia de Mariana (MG). Publicado em 25/10/2024. Available online: https://www.gov.br/planalto/pt-br/repactuacao-do-acordo-do-rio-doce/conheca-a-linha-do-tempo-da-tragedia-de-mariana-mg (accessed on 17 April 2025).
78. Ferronato, N.; Torretta, V. Waste Mismanagement in Developing Countries: A Review of Global Issues. *Int. J. Environ. Res. Public Health* **2019**, *16*, 1060. [CrossRef] [PubMed]
79. Ballesteros, F., Jr.; de Sales, L.; Yoshida, A.; Terazono, A.; Tembresa, J. Urban Mining from a Circularity Perspective. *E3S Web Conf.* **2023**, *468*, 10013. [CrossRef]
80. Patil, R.A.; Ramakrishna, S. A Comprehensive Analysis of E-waste Legislation Worldwide. *Environ. Sci. Pollut. Res.* **2020**, *27*, 14412–14431. [CrossRef]
81. Ottoni, M.; Dias, P.; Xavier, L.H. A Circular Approach to the E-waste Valorization Through Urban Mining in Rio de Janeiro, Brazil. *J. Clean. Prod.* **2020**, *261*, 120990. [CrossRef]
82. Santos, K.L. Unequal Geographies of Urban Mining: E-waste Management in London, Sao Paulo and Accra. *Environ. Plann. E Nat. Space* **2022**, *6*, 1874–1888. [CrossRef]
83. Monteiro, N.B.R.; da Silva, E.A. Environmental Licensing in Brazilian's Crushed Stone Industries. *Environ. Impact Assess. Rev.* **2018**, *71*, 49–59. [CrossRef]
84. Monteiro, N.B.R.; Silva, E.A.; Moita Neto, J.M. Sustainable Development Goals in Mining. *J. Clean. Prod.* **2019**, *228*, 509–520. [CrossRef]
85. Funari, V.; Gomes, H.I.; Santos, R.; Toller, S.; Vitale, L. Urban Mining of Municipal Solid Waste Incineration (MSWI) Residues with Emphasis on Bioleaching Technologies. *Environ. Sci. Pollut. Res.* **2022**, *29*, 59128–59150. [CrossRef] [PubMed]
86. Ragazzi, M.; Fedrizzi, S.; Rada, E.C.; Ionescu, G.; Ciudin, R.; Cioca, L.I. Experiencing Urban Mining in an Italian Municipality Towards a Circular Economy Vision. *Energy Procedia* **2017**, *119*, 192–200. [CrossRef]
87. Arora, M.; Raspall, F.; Fearnley, L.; Silva, A. Urban Mining in Buildings for a Circular Economy: Planning, Process and Feasibility Prospects. *Resour. Conserv. Recycl.* **2021**, *174*, 105754. [CrossRef]
88. Tejaswini, M.; Pathak, P.; Gupta, D.K. Sustainable Approach for Valorization of Solid Wastes as a Secondary Resource Through Urban Mining. *J. Environ. Manag.* **2022**, *319*, 115727. [CrossRef] [PubMed]
89. Schlezak, S.L.; Styer, J.E. Inclusive Urban Mining: An Opportunity for Engineering Education. *Mining* **2023**, *3*, 284–303. [CrossRef]

90. Agência Nacional de Energia Elétrica—ANEEL. Micro e Minigeração Distribuída de Energia Elétrica Cresceu 8,85 GW Em 2024, 2025. Available online: https://www.gov.br/aneel/pt-br/assuntos/noticias/2025/micro-e-minigeracao-distribuida-de-energia-eletrica-cresceu-8-84-gw-em-2024 (accessed on 6 April 2025).
91. Green Eletron. Resíduos Eletrônicos no Brasil—2023. 2023. Available online: https://greeneletron.org.br/download/RELATORIO_DADOS_2023.pdf (accessed on 6 April 2025).
92. Xavier, L.H.; Ottoni, M.; Lepawsky, J. Circular economy and e-waste management in the Americas: Brazilian and Canadian frameworks. *J. Clean. Prod.* **2021**, *297*, 126570. [CrossRef]
93. Castro, J.P.; Pereira-Filho, E.R. Chemical Exploratory Analysis of Printed Circuit Board (PCB) Using Inductively Coupled Plasma Optical Emission Spectrometry (Icp Oes): Data Treatment and Elements Correlation. *Detritus* **2020**, *13*, 131–139. [CrossRef]
94. Castro, J.P.; Pereira-Filho, E.R.; Bro, R. Laser-induced breakdown spectroscopy (LIBS) spectra interpretation and characterization using parallel factor analysis (PARAFAC): A new procedure for data and spectral interference processing fostering the waste electrical and electronic equipment (WEEE) recycling process. *J. Anal. At. Spectrom.* **2020**, *35*, 1115–1124.
95. Vinhal, J.T.; Oliveira, R.P.; Coleti, J.L.; Espinosa, D.C.R. Characterization of end-of-life LEDs: Mapping critical, valuable and hazardous elements in different devices. *Waste Manag.* **2022**, *151*, 113–122. [CrossRef]
96. Guimarães, L.F.; Tenório, J.A.S.; Vaccari, M.; Espinosa, D.C.R.; Botelho Junior, A.B. Characterization of Lithium-Ion Batteries from Recycling Perspective towards Circular Economy. *Minerals* **2024**, *14*, 878. [CrossRef]
97. Oliveira Neto, J.F.; Souza, A.P.S.; Silva, M.M.; Santos, S.M.; Florencio, L. Critical barriers to material recovery from e-waste in Brazil. *J. Hazard. Mater. Adv.* **2025**, *17*, 100562. [CrossRef]
98. Annoni, R.; Lange, L.C.; Amaral, M.C.S.; Silva, A.M.; Assunção, M.C.; Franco, M.B.; Souza, W. Light emitting diode waste: Potential of metals concentration and acid reuse via the integration of leaching and membrane processes. *J. Clean. Prod.* **2020**, *246*, 119057. [CrossRef]
99. Hespanhol, M.C.; Patrício, P.R.; Silva, L.H.M.; Vargas, S.J.R.; Rezende, T.C.S.; Campos, R.A. A Sustainable Methodology to Extract Bismuth from Secondary Sources. *J. Braz. Chem. Soc.* **2019**, *30*, 2376–2385. [CrossRef]
100. Hespanhol, M.C.; Fontoura, B.M.; Quintão, J.C.; Silva, L.H.M. Extraction and purification of gold from raw acidic electronic leachate using an aqueous biphasic system. *J. Taiwan Inst. Chem. Eng.* **2020**, *115*, 218–222. [CrossRef]
101. Melo, F.M.; Almeida, S.N.; Toma, H.E. Magnetic Nanohydrometallurgy Applied to Lanthanide Separation. *Minerals* **2020**, *10*, 530. [CrossRef]
102. Ambrós, W.M. Gravity Concentration in Urban Mining Applications—A Review. *Recycling* **2023**, *8*, 85. [CrossRef]
103. Camargo, P.S.S.; Domingues, A.S.; Palomero, J.P.G.; Cenci, M.P.; Kasper, A.C.; Dias, P.R.; Veit, H.M. c-Si PV module recycling: Analysis of the use of a mechanical pre-treatment to reduce the environmental impact of thermal treatment and enhance materials recovery. *Waste Manag. Res.* **2023**, *41*, 1661–1673. [CrossRef]
104. Pereira, M.B.; Souza, G.B.M.; Espinosa, D.C.R.; Pavão, L.V.; Alonso, C.G.; Cabral, V.F.; Cardozo-Filho, L. Simultaneous recycling of waste solar panels and treatment of persistent organic compounds via supercritical water technology. *Environ. Pollut.* **2023**, *335*, 122331. [CrossRef]
105. Pimassoni, Y.S.; Lima, M.T.W.D.C.; Yamane, L.H.; Siman, R.R. The recovery of rare earth elements from waste electrical and electronic equipment: A review. *Hydrometallurgy* **2023**, *222*, 106156. [CrossRef]
106. Castro, J.P.; Garcia, J.A.; Souza, R.G.; Pereira-Filho, E.R. Indium Recovery from End-of-Life E-Waste: Important Details Related to Spectroanalytical Determination and Recycling Viability. *J. Braz. Chem. Soc.* **2024**, *35*, e-20230201. [CrossRef]
107. Oliveira, J.D.; Schreiber, D.; Jahno, V.D. Circular Economy and Buildings as Material Banks in Mitigation of Environmental Impacts from Construction and Demolition Waste. *Sustainability* **2024**, *16*, 5022. [CrossRef]
108. Mascarenhas, Z.M.G.; Piao, Z.; Vasconcelos, K.L.; Poulikakos, L.D.; Bernucci, L.L.B. Comparative environmental performance of pavement structures considering recycled materials and regional differences. *Sci. Total Environ.* **2023**, *858*, 159862. [CrossRef]
109. Poulikakos, L.D.; Pasquini, E.; Tusar, M.; Hernando, D.; Wang, D.; Mikhailenko, P.; Pasetto, M.; Baliello, A.; Falchetto, A.C.; Miljković, M.; et al. RILEM interlaboratory study on the mechanical properties of asphalt mixtures modified with polyethylene waste. *J. Clean. Prod.* **2022**, *375*, 134124. [CrossRef]
110. Bezerra, M.L.M.; Silva, M.M.; Santos, S.M. Forecasting of secondary lead recovery from motorcycle batteries in Brazil: A contribution to waste management. *Environ. Sci. Pollut. Res.* **2023**, *30*, 106260–106275. [CrossRef] [PubMed]
111. D'Almeida, F.S.; Carvalho, R.B.; Santos, F.S.; Souza, R.F.M. On the Hibernating Electronic Waste in Rio de Janeiro Higher Education Community: An Assessment of Population Behavior Analysis and Economic Potential. *Sustainability* **2021**, *13*, 9181. [CrossRef]
112. Rosa, A.G.F.; Silva, W.D.O.; Fontana, M.E.; Levino, N.; Guarnieri, P. A GIS-based multi-criteria approach for identifying areas vulnerable to subsidence in the world's largest ongoing urban socio-environmental mining disaster. *Extr. Ind. Soc.* **2024**, *19*, 101500. [CrossRef]

113. Maia, R.; Ottoni, M.; Barros, J.; Santos, M.A. Assessment of the waste management reporting in the electricity sector. *Clean. Responsible Consum.* **2021**, *3*, 100031. [CrossRef]
114. BRASIL. Lei nº 9.605, de 12 de Fevereiro de 1998. Dispõe sobre as sanções penais e administrativas derivadas de condutas e atividades lesivas ao meio ambiente, e dá outras providências. Diário Oficial da União, Brasília, DF, 13 Fev. 1998. Available online: https://www.planalto.gov.br/ccivil_03/LEIS/L9605.htm (accessed on 30 May 2025).

Disclaimer/Publisher's Note: The statements, opinions and data contained in all publications are solely those of the individual author(s) and contributor(s) and not of MDPI and/or the editor(s). MDPI and/or the editor(s) disclaim responsibility for any injury to people or property resulting from any ideas, methods, instructions or products referred to in the content.

minerals

MDPI

Review

From Waste to Resource: Critical Mineral Recovery and Environmental Impact Mitigation in Copper Smelting Slag †

Aleksandar N. Nikoloski [1,*], Pritam Singh [1] and Tina Chanda Phiri [2]

[1] Extractive Metallurgy Hub, Harry Butler Institute (Centre for Water Energy and Waste), Murdoch University, Perth, WA 6168, Australia; p.singh@murdoch.edu.au
[2] School of Mines and Mineral Sciences, Copperbelt University, Kitwe P.O. Box 21962, Zambia; tina.phiri@cbu.ac.zm
* Correspondence: a.nikoloski@murdoch.edu.au; Tel.: +61-8-9360-2835
† This article is a revised and expanded version of a paper entitled "An overview of global copper smelting slag production and reprocessing approaches" in Nikoloski, A.N.; Singh, P.; Phiri, T. An overview of global copper smelting slag production and reprocessing approaches. In Proceedings of the XVI International Mineral Processing and Recycling Conference (IMPRC 2025), Belgrade, Serbia, 28–30 May 2025.

Abstract

Copper and cobalt are critically important metals for the transition to renewable energy and various aspects of modern life. Their production from primary sources, ores, necessitates metallurgical separation from the unwanted host materials, resulting in the generation of a huge amount of waste. Copper smelting slag is one of these metallurgical wastes, with 39 million tonnes of slag generated and discarded globally each year. These massive amounts of slag occupy a considerable and growing land footprint, often close to residential areas, and present a hazard that potentially releases contaminants into the environment. On the other hand, they also represent a material that often contains a significant residual amount of valuable copper and cobalt. To better understand and address the challenge of reducing the adverse impacts of the waste, as well as the possible commercial opportunity the contained critical metals present, this study reviews global smelting slag production over the last 25 years, its composition, and technical reprocessing options. A summary of the chemical and mineralogical characterization of the copper slag from diverse research is thus provided, as well as a comprehensive overview of the processing strategies for metal recovery from copper slag, such as flotation, pyrometallurgy, and hydrometallurgy. The study demonstrates that a huge amount of smelting slag has been produced, with great variation and complexity, which represents a major potential resource for cobalt and copper metals. The chemical and mineralogical composition of smelting slag varies from location to location, depending on the properties of the feed concentrate, type of fluxes, furnace type, and cooling rates employed during and after the smelting processes. The overview of the production trends and reprocessing techniques shows that while some notable effective options exist or are emerging, further research is needed into the reprocessing of smelting slag waste in order to create economic value, improve energy efficiency in metal production, increase critical metal supply, and reduce negative environmental impacts.

Keywords: copper; cobalt; waste valorisation; smelting slag; environmental impact; sustainability

1. Introduction

Copper smelting slag is a waste product generated during the pyrometallurgical processing of copper concentrates. Global production of smelting slag is estimated at

37.7 million tons per year [1]. A considerable amount of smelting slag containing hazardous elements is often dumped in a slag disposal pit, and most of it is not fully utilized [1–6]. These hazardous substances are toxic and can accumulate in organisms, causing serious health risks to all organisms [7,8]. With fewer available sites for dumping smelting slag and stricter environmental regulations, the copper smelting industry faces an enormous challenge in managing the slag waste. As a result, it is becoming increasingly important to reduce waste disposal by making better use of copper slag as a valuable resource of critical minerals.

Copper slag contains significant amounts of essential metals such as (Cu), cobalt (Co), silver (Ag), nickel (Ni), zinc (Zn), lead (Pb), cadmium (Cd), and iron (Fe) in oxide, sulphide, and/or metallic forms [1]. This has sparked increased interest in recovering these valuable metals from copper slag using various techniques, including flotation, hydrometallurgy, pyrometallurgy, and a combination of pyrometallurgy and hydrometallurgy. The flotation process employs various collectors, modifiers, frothers, and depressants to extract entrained metal compounds from copper slag [9–12]. The hydrometallurgy technique for leaching copper slag with various lixiviants has been widely exploited [12–18]. The pyrometallurgical approach includes calcination, carbothermic reduction/smelting reduction, and reduction roasting, followed by magnetic separation. This technique has mostly been used to extract metals from copper slag via carbothermic reduction at temperatures ranging from 1400 to 1800 °C [19]. An integration of pyrometallurgy and hydrometallurgy for processing copper smelter slag that involves roasting the smelting slag followed by water or acid leaching has also been suggested [16,20–22]. However, no commercial application has been found for the extraction of valuable metals from smelting slag using these techniques.

Copper slag exhibits pronounced chemical and mineralogical heterogeneity, resulting in wide compositional variability. Consequently, comprehensive characterisation of copper slag is essential for selecting appropriate metal recovery techniques, conducting robust environmental impact assessments, and developing effective utilisation strategies. Gorai et al. [2] presented a comprehensive review of copper slag characterisation, with particular emphasis on metal recovery and utilisation technologies. Piatak et al. [23] examined the properties of ferrous and non-ferrous slags, highlighting their environmental impacts and potential as valuable secondary resources for reuse and recycling. Potysz et al. [6] synthesised existing knowledge on metallurgical slags, focusing on chemical and phase compositions, metal recovery potential, environmental risks, and long-term fate. More recently, Phiri et al. [24] provided an in-depth review of the chemical and mineralogical characteristics of copper slag, together with processing methodologies and utilisation pathways for copper smelting slags. Tian et al. [25] systematically evaluated metallurgical techniques for recycling and further purification of copper slag. Additionally, Phiri et al. [1] assessed global copper smelting slag generation as a potential secondary source of copper and cobalt within a circular economy framework. Collectively, these studies establish a comprehensive understanding of copper slag as both a metallurgical by-product and a valuable secondary resource. Early reviews by Gorai et al. [2] and Piatak et al. [23] provided foundational insights into slag characterization, environmental implications, and reuse potential, while Potysz et al. [6] deepened this knowledge by integrating chemical, mineralogical, and ecological aspects. More recent works by Phiri et al. [1,24] and Tian et al. [25] extend this framework by highlighting modern recovery techniques, circular-economy perspectives, and the emerging strategic importance of copper and cobalt in green-energy transitions. Together, these contributions underscore copper slag's dual role as an environmental liability and a critical resource reservoir, emphasizing the need for innovative, sustainable recovery technologies to transform it into a viable resource for future metal supply chains.

https://doi.org/10.3390/min16020206

Metallurgical recycling and processing solutions for copper smelting slag are still at the development stage, despite intensive research over the last several decades. Therefore, a review of current knowledge is required to guide the further development of techniques capable of leveraging the resource potential of copper smelting slag for the extraction of critical metals. The primary objective of this study is to present a comprehensive review of global copper smelting slag generation, as well as the various proposed approaches tested to date for extracting critical metals from copper smelting slag. Finally, the technical challenges and development bottlenecks of copper slag metallurgical processes, as well as potential measures to overcome these barriers, are summarized in order to provide useful and significant guidance for efficient copper slag processing and utilization.

2. World Overview of Copper Smelting Slag

The global copper slag production is estimated at 966 million tons for the period between 2000 and 2024 from the 13 main producing countries (Figure 1). Copper smelting slag is considered a potential world resource owing to the huge amounts being produced worldwide, which contain substantial amounts of valuable metals [24]. The production figures for the period between 2000 and 2024 serve as evidence that huge amounts of copper slag waste are generated every year, and the upward trend in these figures is expected to continue in the coming decade due to the increase in global population, economic growth, and technological advancement. The average annual production is estimated at 38.6 million tons (Figure 1).

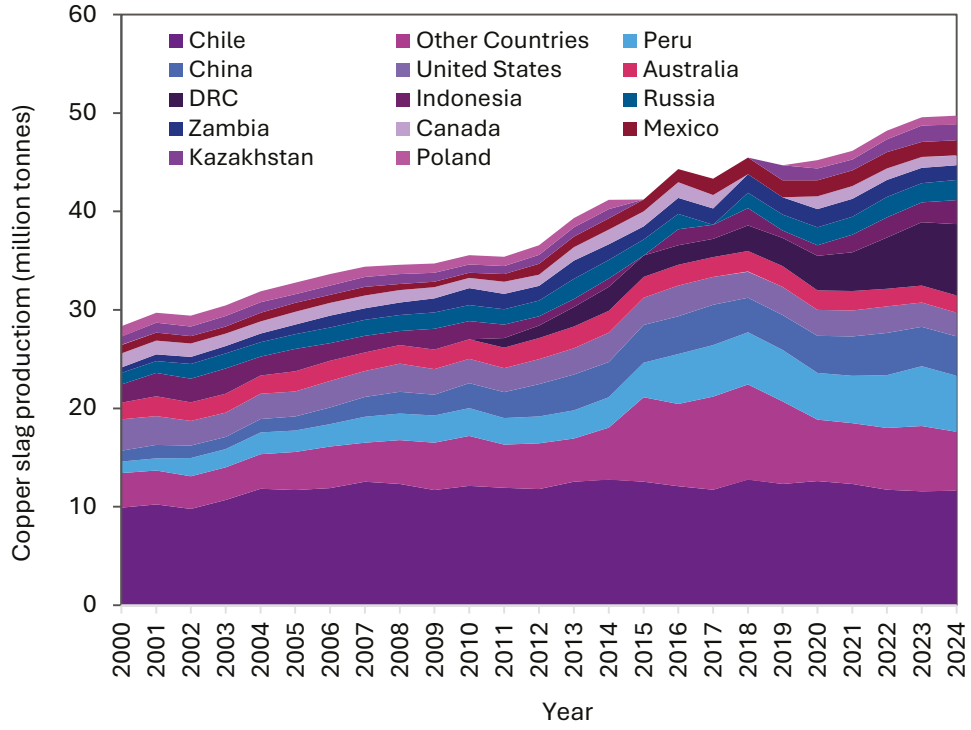


Figure 1. Global copper smelting slag production for the period 2000 to 2024 from the 13 main producing countries. Approximately 966 million tons of copper slag waste has been produced in the last 25 years. Data Source: [26].

3. Furnace Technologies Producing Copper Slag

Copper slag generation is inherently linked to the type of furnace and the thermochemical processing route used in pyrometallurgical copper production. Each furnace design exhibits unique operational characteristics, reaction environments, and matte–slag separation efficiencies, resulting in significant variation in slag composition and copper

losses. The following section reviews the principal furnace types, including reverberatory, electric, flash smelting, top-submerged lance (TSL), Peirce–Smith converter, and Teniente converter systems, and synthesizes key findings from the metallurgical literature.

3.1. Reverberatory Furnace

Reverberatory furnaces once formed the backbone of global copper smelting, operating at temperatures of approximately 1100–1300 °C. Their broad, pool-type bath geometry provides limited turbulence and slow matte–slag separation, conditions that inherently promote high copper losses to slag. Resulting slags typically contain 1.5–4.5 wt.% Cu, with levels reaching ~6 wt.% under sub-optimal operating conditions [27]. Copper reporting to the slag is predominantly associated with mechanically entrained matte droplets, dissolved Cu_2O, and Cu–Fe–O spinel phases. Although central to early industrial copper production, reverberatory furnaces have been largely phased out due to their low thermal efficiency, high fuel consumption, and the large slag volumes they generate, which diminish overall metal recovery [28].

3.2. Electric Furnace (Electric Settling Furnaces)

Electric furnaces play a critical role in modern copper smelting flowsheets, primarily as slag-cleaning units that enhance matte–slag separation through high-intensity resistive heating. Operating at temperatures typically exceeding 1200–1500 °C [29], these furnaces generate strong convective currents and provide extended residence times, both of which promote the reduction and settling of entrained matte droplets. As a result, electric furnace slags usually contain only 0.5–1.5 wt.% Cu, ranking among the cleanest slags produced in pyrometallurgical copper processing [30]. Their ability to recover copper and other valuable metals from both primary smelting slags and converter slags makes electric furnaces indispensable components of contemporary, high-efficiency smelting operations.

3.3. Flash Smelting Furnace Slags (Outokumpu/INCO)

Flash smelting is the leading primary copper smelting technology worldwide and accounts for over half of global matte production [27]. In this process, finely ground copper concentrate is oxidized in suspension using oxygen-enriched air, enabling extremely rapid reaction kinetics, high heat generation, and autogenous smelting. Sulfide minerals such as chalcopyrite ($CuFeS_2$) react almost instantaneously with the oxidant stream, producing sufficient exothermic heat to melt the feed and yielding a stable operating environment characterized by automatic temperature and composition control. Flash smelting has been widely adopted due to its high energy efficiency, effective sulfur capture, and elevated copper throughput [27,31]. The process typically produces a Cu–Fe–S matte containing 60–75% Cu alongside an iron–silicate slag with 0.8–2 wt.% Cu, depending on furnace conditions and feed characteristics [27]. Copper losses mainly arise from fine matte droplet entrainment and the formation of magnetite-rich slag phases [31] Importantly, flash furnaces generate significantly lower slag volumes than reverberatory furnaces due to reduced flux demand and more complete oxidation. Overall, flash smelting is considered the most economical and environmentally favorable industrial route for copper concentrate smelting and is central to achieving more sustainable metallurgical operations.

3.4. Top-Submerged Lance (TSL) Furnaces (Isasmelt/Ausmelt)

The Top-Submerged Lance (TSL) reactor is a highly adaptable, intensively mixed smelting technology whose efficiency is largely dictated by lance configuration and operation. The lance serves as the central functional element of the system, delivering oxidant gas, auxiliary fuels, and fine or dried concentrates directly into the molten bath, while additional feed can be supplied through overhead ports. Through the controlled delivery

https://doi.org/10.3390/min16020206

of these streams, the lance effectively regulates the oxygen partial pressure (pO_2) within the furnace,a key variable influencing reaction pathways, matte and slag formation, and overall process thermodynamics [32]. Slags produced in TSL operations typically contain 0.8–1.5 wt.% Cu, with further reductions commonly achieved via electric furnace settling downstream of the main reactor [27,28]. Although the intrinsic turbulence of TSL operation can increase matte entrainment, modern monitoring and process control strategies significantly limit this effect. Owing to its compact design, lower operating and capital requirements, and strong environmental performance, TSL technology has become an increasingly preferred alternative to traditional smelting methods in both primary and secondary copper processing.

3.5. Peirce–Smith Converter

The Peirce–Smith Converter (PSC) is a batch oxidative smelting vessel widely used in copper production to convert copper matte (typically 65–75% Cu) into blister copper (98–99% Cu). Air or oxygen-enriched air is blown through tuyeres located along the converter barrel, oxidizing iron sulfide to form an FeO–SiO_2 slag and driving the evolution of SO_2 gas. The process proceeds in two main stages: the slag-forming (iron blow) stage, during which FeS is preferentially oxidized and removed as slag, followed by the copper blow, where remaining copper sulfide is oxidized to blister copper. Peirce–Smith Converter operation is influenced by high magnetite (Fe_3O_4) formation, which increases slag viscosity and contributes to copper losses through matte entrainment and Cu–Fe–O spinel formation [33]. Typical converter slags contain 1–2 wt.% Cu [34,35]. Despite drawbacks such as noise, high energy use, and discontinuous operation, PSCs remain dominant globally due to their robustness, operational simplicity, and compatibility with existing smelting flowsheets.

3.6. Teniente Converter

The Teniente converter is a continuous conversion reactor widely used in Chile and the United States. It uses a large cylindrical furnace with submerged tuyeres (35 to 50 tuyeres) of approximately 4 to 5 m and blows oxygen-enriched air through the tuyeres into molten matte. The dried concentrate, flux, reverts, coal/coke, recycle materials, and scrap are blown into the furnace through 3 or 4 dedicated tuyeres. The concentrate oxidation is achieved by blowing oxygen-enriched air through tuyeres into the furnace. Teniente converter typically contains 1–2 wt.% Cu, with losses influenced by blowing intensity, slag viscosity, and magnetite formation [27,30]. Thermodynamic studies have clarified the behavior of Cu–Fe–O–SiO_2 phases in this system, highlighting the importance of oxygen potential control [27]. Teniente converters allow smoother operation and reduced fugitive emissions relative to Peirce–Smith Converters.

The variation in copper content among slags reflects the efficiency and operating philosophy of different furnaces. Reverberatory systems exhibit the highest copper losses due to slow settling, while electric furnaces provide the cleanest slags. Flash smelting and TSL furnaces represent modern high-efficiency technologies that balance productivity with low copper losses. Converter slags, particularly from PSC and Teniente systems, remain important targets for secondary recovery. Understanding these furnace-dependent slag characteristics is essential for optimizing copper extraction, minimizing losses, and designing effective slag treatment strategies.

4. Characterization of Smelting Slag

4.1. Chemical Composition

The bulk chemical composition of copper smelting slags is largely governed by the metallurgical conditions under which they are generated, including the mineralogy of

https://doi.org/10.3390/min16020206

the feed concentrate, furnace type, flux addition, and cooling regime [2,6,23,36]. Major constituents of copper smelter slags typically include silica (SiO_2), ferrous oxide (FeO), ferric oxide (Fe_2O_3), calcium oxide (CaO), and alumina (Al_2O_3), which together define the physicochemical behavior of the slag during solidification and subsequent weathering. Copper smelter slags exhibit pronounced chemical and mineralogical heterogeneity, as reflected in the wide compositional ranges reported in Table 1. This variability is strongly influenced by cooling mechanisms, with air-cooled and water-quenched slags displaying markedly different phase assemblages. Cooling rate plays a critical role in controlling crystallization processes and phase diversity within the slag matrix. Ravindra et al. [37]) reported that fayalite (Fe_2SiO_4) is the dominant mineral phase in copper slags, constituting up to 57% of air-cooled slags compared to approximately 15% in quenched slags. Consistent with these observations, Potysz et al. [6] found that rapidly quenched slags are characterized by reduced crystalline phase diversity relative to slowly cooled slags. During slow cooling, crystallization occurs under conditions closer to thermodynamic equilibrium, promoting the development of multiple, well-defined mineral phases [38]. In contrast, rapid quenching suppresses extensive crystallization, resulting in a predominantly glassy matrix with limited crystalline content. These differences in cooling history have important implications for the physicochemical properties, environmental behavior, and potential secondary utilization of copper smelting slags.

Table 1. Average chemical composition of copper smelter slag for minor elements from over 80 studies globally [24].

Component	Ca	Al	Zn	Ag	Mg	Cu	Pb	Co	As	Ti	Ni	Mn	Sb	Mo
Content (wt.%)	3.05	2.59	1.83	1.67	1.36	1.19	0.94	0.48	0.38	0.28	0.24	0.22	0.10	0.06

These findings are consistent with previous observations that rapid cooling causes the formation of amorphous phases and metal oxide segregation, whereas slow cooling leads to the formation of vitreous and crystalline components [2,6,23,37]. This demonstrates that the cooling rate of the slag has a significant impact on phase composition. Table 1 summarises the average chemical composition of copper smelter slags derived from over 80 studies across 21 different countries. The average chemical composition of copper slag was calculated by considering studies conducted in each country at various copper smelting locations. The studies demonstrate substantial amounts of metals and metalloids, with an average of 3.05 wt.% Ca and 2.59 wt.% Al, 1.83 wt.% Zn, 1.67 wt.% Ag, 1.36 wt.% Mg, 1.19 wt.% Cu, 0.94 wt.% Pb, and 0.48 wt.% Co (Table 1). Other metals and metalloids such as As, Ti, Ni, Mn, Sb, and Mo were also detected but in much lesser amounts (lower than 0.4 wt.%).

The grade of Co and Cu in the slag exceeds the average ore grade for most mines due to the depletion of high- grade deposits in recent years. These minor elements exist in the slag as entrained sulfides, oxides, and metallic elements. Under high-temperature conditions, elements such as Cu, Co, and Ni preferentially form sulfide droplets that may become mechanically trapped within the silicate melt. Simultaneously, more oxidized conditions promote the formation of oxide and spinel phases (Fe_3O_4, Fe_2SiO_4) that incorporate trace metals through solid solution. During cooling, varying redox potentials and melt viscosities prevent full phase segregation, causing metallic copper and sulfide particles to remain dispersed within the glassy matrix. Consequently, the coexistence of these phases reflects non-equilibrium solidification, variable oxidation states, and mechanical entrapment of metal-rich phases, which together govern the mineralogical complexity and metal recoverability of copper slags.

https://doi.org/10.3390/min16020206

4.2. Mineralogy of Copper Slag

Copper slag is primarily composed of fayalite (Fe_2SiO_4) and silicate glassy matrices, with crystalline oxides, sulfides, metallic elements, alloys, and intermetallic compounds as minor constituents [16,23,39–42]. The fayalite structure in copper slags is formed when pyrite is oxidized to iron oxide in the presence of silica and may contain minor amorphous silica phases [24,43]. In our recent study, the silicate phase was described as principally fayalite and kirschsteinite from the olivine group, while the copper phase was made up of copper matte and metallic copper [42]. Meanwhile, the magnetite phase was primarily found interbedded with the fayalite and kirschsteinite phases, forming a coherent structure with iron and other metallic components. Other research discovered certain common silicates with compositions equivalent to Melilite ($(Ca, Na)_2(Al, Mg, Fe^{2+})(Si, Al)_2O_7$) and willemite ($Zn_2SiO_4$) [7,36,44]. Granulated slags were discovered to contain a significant amount of calcium and chloride, as well as iron in the form of magnetite, fayalite, and ferrosilite. The other sulfide phases that have been found to be present within the copper slags are pyrite (FeS_2), galena (PbS), sphalerite ((Zn,Fe)S), pyrrhotite (Fe(1-X)S) and wurtzite ((Zn,Fe)S) whereas covellite (CuS), cubanite ($CuFe_2S_3$), digenite (Cu_9S_5), troilite (FeS), and pentlandite ($(Fe,Ni)_9S_8$) are rarely observed [23,36,45].

Potysz et al. [6] discovered that copper slags comprised several synthetic forms of naturally occurring mineral phases. Copper slags commonly contain sulfide minerals such as bornite (Cu_5FeS_4), chalcocite (Cu_2S), and chalcopyrite ($CuFeS_2$) [21,46,47]. The principal iron oxide minerals found in copper slag are fayalite (Fe_2SiO_4), spinels ($MgAl_2O_4$), hematite (Fe_2O_3), magnetite (Fe_3O_4) and wustite (FeO) 1 [23,36,37]. Copper slags can contain trace amounts of oxides, including leucite ($K(AlSi_2O_6)$), hercynite ($FeAl_2O_4$) [38,48,49]. Pyroxene group minerals like diopside ($FeCaSi_2O_6$) and hedenbergite ($CaFeSi_2O_6$), as well as the olivine group minerals like kirschsteinite ($CaFe^{2+}SiO_4$) and forsterite (Mg_2SiO_4) are also found in copper slags 1 [23,42,44,46].

5. Embedment of Critical Metals in the Smelting Slag

To show the embedment of critical metals in copper slag, backscattered electron (BSE) imaging was used to examine the polished surface of the smelting slag sample [42]. Figure 2 depicts the BSE images and mapping results for all the detectable metals in the smelting slag.

The distribution of copper in the mapped area (Figure 2b) is not uniform, and a significant concentration of copper can only be observed in Area 1 (Figure 2c). The considerable overlap between copper and sulfur at point 1 in the mapping area shows that this region is made up of CuS or Cu_2S [42]. The principal types of copper metal were copper matte and metallic copper, which were interbedded with the silicate matrix. Also embedded were relatively small amounts of Co, Fe, Si, O, Ca, Al, and K, which were evenly distributed throughout the copper slag. This is consistent with earlier research findings that show copper is lost to the slag in the form of copper matte [2,23,46]. Highly oxidized slags from converting and/or direct-to-blister smelting methods contain copper in the form of iron and copper-bearing oxides such as delafossite [50].

In the study by Phiri et al. [42], the area labelled 2 in Figure 2a exhibited a perfect euhedral structure typical of iron oxide spinels. This area showed Co overlapping with other metallic elements, including Fe, Ti, and O as depicted in Figure 2f–h. Si was not detected in this area, suggesting the presence of magnetite containing embedded Co and Ti metals. The mapping area labelled 3 revealed identical features for Co, Fe, Si, Ti, K, Mg, Ca, and O, suggesting the presence of a complex silicate matrix with multiple metal encapsulations. The distribution of Co in the copper slag in the area labelled 4 matched the distribution of Fe and Ti, implying the presence of a Co-Ti-Fe alloy. The images also

https://doi.org/10.3390/min16020206

showed that copper was primarily dispersed as copper sulfide, but it was also found in an alloy with Fe. Overall, the mapping results show that substantial amounts of cobalt and other valuable metals (such as Cu, Ti, Fe, Si, K, Mg, and Ca) were embedded in the complex silicate matrix and magnetite phase, making extraction challenging.

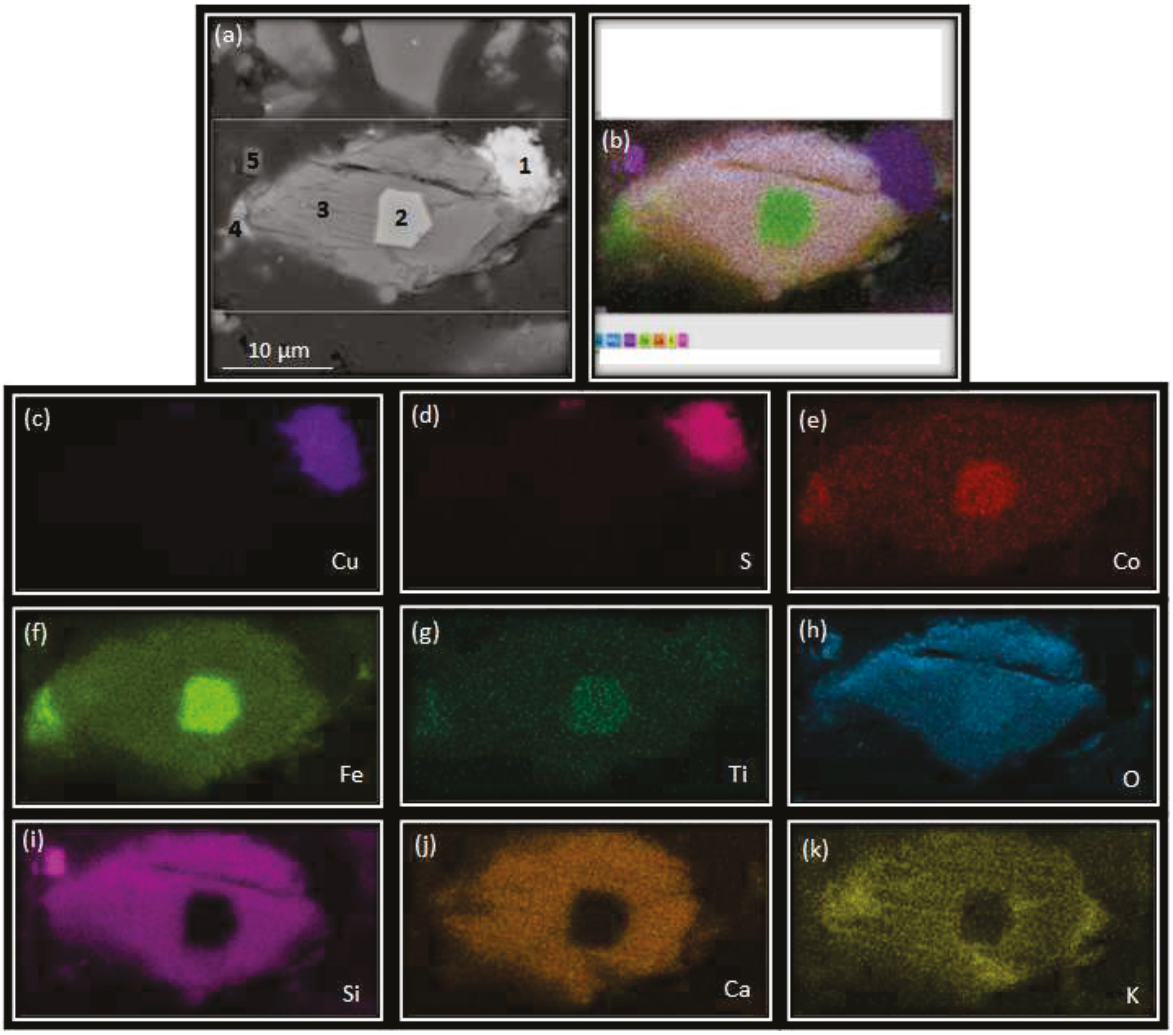


Figure 2. Backscattered electron images of the polished surface of copper slag (**a**), mapping images overview (**b**), and mapping images for Cu (**c**), S (**d**), Co (**e**), Fe (**f**), Ti (**g**), O (**h**), Si (**i**), Ca (**j**), K (**k**) [42]. Numbers 1–5 in (**a**) indicate distinct Areas of the sample discussed in the text.

5.1. Copper Embedment in the Smelting Slag

To further illustrate mineral embedment in the smelting slag, Figure 3a presents an additional BSE image showing multiple interconnected mineral phases within the copper slag. To get comprehensive BSE microstructure information, the highlighted areas X, Y, and Z in Figure 3a were deconvoluted, and the results are presented in Figure 3b, c, and d, respectively. Tables 2 and 3 display the corresponding compositions at various points in Figure 3b, c, respectively.

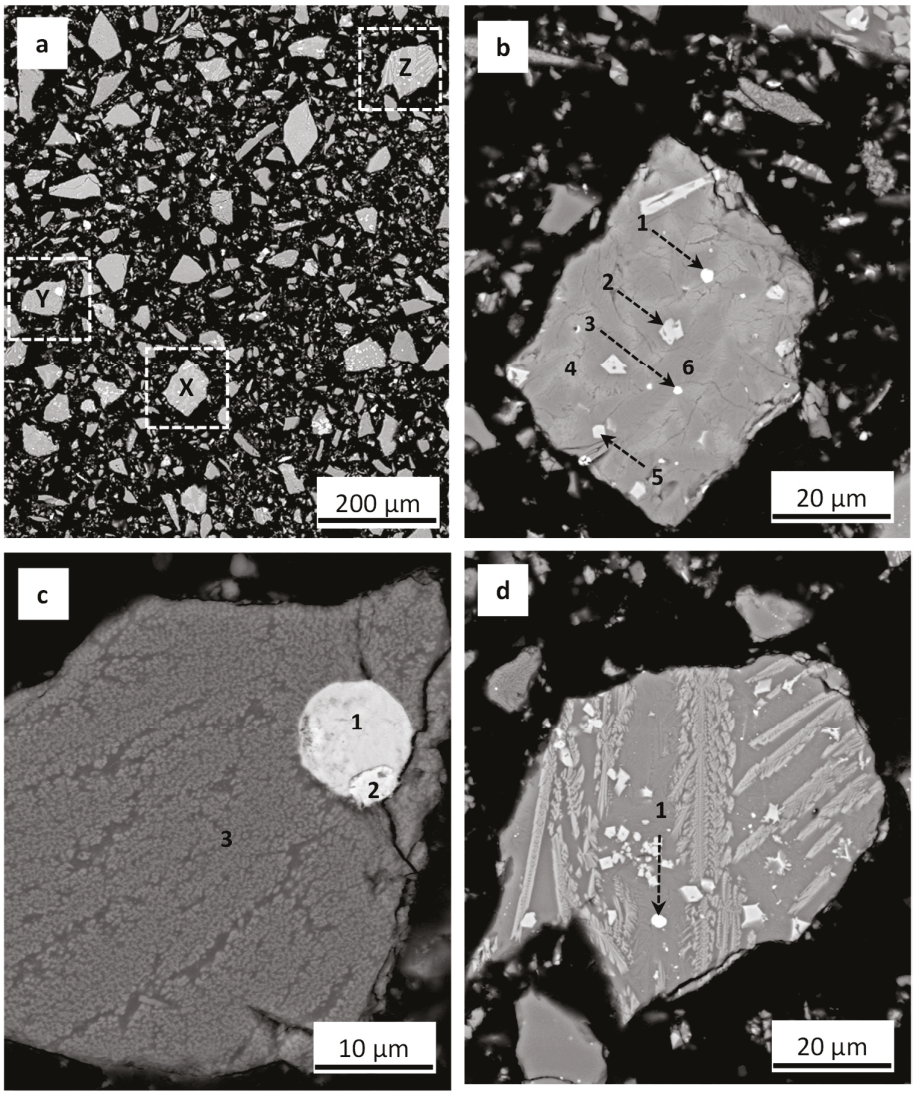


Figure 3. Backscattered electron micrograph of the polished surface in copper slag (**a**) and deconvoluted images of areas marked X (**b**), Y (**c**), and Z (**d**) [42]. The numbers in Figure 3b and c correspond to the points in Tables 2 and 3, respectively.

Table 2. Elemental composition (wt.%) of the main phases in the copper slag in Figure 3b [42].

Mineral Phase	Point	Co	Cu	S	Fe	Si	O	Ca	Al	Mg	Ti	K
Copper matte	1	0.38	57.56	20.8	11.01	2.34	4.76	0.6	0.64			0.46
Magnetite	2	1.85			51.33	3.94	24.87	1.43	2.49	0.34	1.14	1.08
Silicate	3	1.3	5.08	2.04	24.91	14.07	24.81	4.71	2.29	0.76	0.12	1.49
Silicate	4	1.25			31.11	16.29	28.37	2.51	3.9	0.39	0.14	3.52
Silicate	5	1.44			25.24	12.26	25.9	6	2.07	1.8	0.43	0.91
Silicate	6	1.32			20.9	19.44	31.46	7.98	3.43	2.41	0.16	1.18

Table 3. Elemental composition (wt.%) of the main phases in the copper slag in Figure 3c [42].

Mineral Phase	Point	Co	Cu	S	Fe	Si	O	Ca	Al	Mg	Ti	K
Copper matte	1	0.11	73.52	18.36	2.5	0.08	0.67					
Copper metallic	2	0.14	89.62	0.12	3.17	0.37	1.38	0.08				
Silicate	3	1.05	0.54		22.4	23.25	40.9	1.73	5.17	2.25	0.45	2.82

https://doi.org/10.3390/min16020206

Backscattered electron (BSE) imaging (Figure 3b,c), together with the quantitative data presented in Tables 2 and 3, indicates that copper is predominantly distributed among silicate phases, copper matte, and metallic copper phases. The corresponding Cu contents reach up to 5.08 wt.% in silicate phases, 73.52 wt.% in copper matte, and 89.62 wt.% in metallic copper. Consistent with these observations, Zhang et al. [51] reported that although copper metal occurs at higher weight percentages within iron-bearing phases compared to fayalite (Fe_2SiO_4) and magnetite (Fe_3O_4), fayalite exhibits a stronger affinity for heavy metal incorporation. The study demonstrated that 89.7% of As, 85.0% of Pb, and 76.9% of Cu were preferentially embedded within the fayalite phase [51]. Previous studies have similarly shown that Cu can be structurally incorporated into fayalite through substitution at Fe lattice sites [43,51,52]. Furthermore, Zhou et al. [53], through analysis of Cu–Fe binary phase diagrams, demonstrated that Cu and Fe exhibit extensive mutual solid solubility, a behaviour attributed to their comparable chemical characteristics and crystal chemistry. This miscibility provides a mechanistic explanation for the observed incorporation of Cu into Fe-bearing silicate phases.

5.2. Cobalt Embedment in Mineral Phases of the Copper Slag

In the study by Phiri et al. [42], cobalt in copper smelting slag was mostly discovered embedded in the silicate and magnetite phases (Tables 2 and 3). Cobalt was also consistently found in various phases of copper slag, interspersed with other metals such as Cu, Fe, Ca, K, Al, Ti, and S. According to the backscattered electron (BSE) images in Figure 3b and Table 2, the Co content was uniformly distributed in the magnetite, silicate, and copper matte phases, with up to 1.85 wt.%, 1.44 wt.%, and 0.38 wt.%, respectively. This finding is consistent with the research undertaken by Yang et al. [17], who found that Co predominantly occurs in the fayalite phase, specifically in the form of silicate and ferrite. Vítková, et al. [46] report that Co substitutes for Fe in olivine-group silicates (such as fayalite) up to 7.15 wt.% CoO, and also occurs in oxide/spinel phases. This aligns with the idea that Co is stabilized in silicate phases due to substitution for iron.

6. Critical Metal Processing Strategies for Smelting Slag

6.1. Recovery of Copper from Smelting Slag Using Flotation

The froth flotation technique has been found to be an essential operation in the recovery of copper from smelting slag [5,9–11,54,55]. The copper values in the smelting slag that are present either as independent metallic particles or in the form of sulfides can be floated effectively. Flotation has been studied for the recovery of metals from copper slag employing various collectors, frothers, modifiers, and depressants. Froth flotation uses the differences in surface characteristics of minerals to separate valuable minerals from unwanted gangue minerals. The process produces an enriched concentrate, and the gangue or unwanted material reports to the tailings. Middlings are a third product composed of valuable and gangue minerals that have remained locked together. This material is typically reground to liberate the valuable mineral particles. Copper slag flotation resembles sulfide ore flotation [20]. The main parameters investigated for the flotation technique are particle size, collector dosage, and pH. The copper slag is fed into the flotation unit, where the sulfide minerals (Cu_2S, Cu_5FeS_4) are floated using collector and frother reagents to produce a concentrate.

6.1.1. Recovery of Copper from Smelting Slag Using Xanthate Collectors

Xanthates are one of the most common commercial collectors used in copper sulfide flotation and are known to be strongly chemisorbed on the surfaces of many valuable minerals [56]. Sarrafi et al. [9] explored copper recovery from reverberatory furnace slag

using flotation. The following parameters were investigated: cooling rate, particle size, collector dosage, pH, and flotation time. The results demonstrated that for an air-cooled slag at optimum conditions of pH 11.5, R407 collector dosage of 30 g/t., solid in pulp of 30% and flotation time of 12.5 min, a copper recovery of 72% was obtained in one-stage flotation with a copper concentrate grade of 12.6%. In a similar work, Das et al. [10] investigated the recovery of copper values from an Indian smelter slag through flotation using conventional sodium isopropyl xanthate (SIPX) as the collector. The effects of flotation parameters like pH and collector concentration were studied. The results under optimum flotation conditions showed a copper grade of approximately 21% with copper recovery of more than 80% at xanthate concentration of 600 g/ton and slightly alkaline pH of 9. Copper recovery from smelting slag employing butyl xanthate as the collector was investigated [11]. The copper slag sample was primarily composed of bornite (Cu_5FeS_4) as the major Cu-bearing mineral. The sample was ground to a particle size of 80% passing 74 μm and floated at pH 10 with sodium carbonate as a pH modifier and 50 g/t butyl xanthate [11]. The results showed a 14.47% concentrate copper grade with copper recovery of around 79.66%. The authors reported that reagent type, reagent dosage, particle size, and pH were the significant operating parameters governing the flotation process. Similarly, Li et al. [57] investigated the recovery of metals from copper slag waste using butyl xanthate collectors. The results indicated that using flotation butyl xanthate as the collector and terpene oil as the frother resulted in a flotation concentrate copper grade of 21.50% with a recovery rate of 77.78%. Meanwhile, Roy et al. [5] examined the flotation of copper sulfide from copper smelter slag using mixtures of several collectors containing sodium isopropyl xanthate (SIPX), sodium di-ethyl dithiophosphate (DTP), and alkyl hydroxamate at different dosages. The results demonstrated that using a 40:160 g/t mixture of sodium isopropyl xanthate and di-ethyl dithiophosphate resulted in a greater copper recovery of 84.82%, compared to 78.11% when using the best performing single collector at pH 9 [5]. Similarly, a 160:40 g/t mixture of sodium isopropyl xanthate and alkyl hydroxamate resulted in a relatively high copper recovery of 83.07%. The influence of grinding duration on flotation recovery of copper smelter slags in the Bardaskan district of Iran was studied by Shamsi et al. [55]. After grinding the material for 85 min to a particle size of 80% passing 48 μm, copper recovery of 79.89% was achieved.

6.1.2. Recovery of Copper from Smelting Slag Using Thionocarbamate Collectors

Several attempts have been made to identify alternatives to xanthates. to improve metal recovery. Thionocarbamate collectors, for example, have been reported in the literature primarily for the flotation of copper-bearing minerals such as chalcocite, covellite, chalcopyrite, and bornite, either in combination with xanthates or alone [58–60]. Thionocarbamates can form stable chelating complexes with metal ions on the surface of particles containing copper by using C=S and N-H bonds [60]. Štirbanovič et al. [61] examined the use of thionocarbamates in copper slag flotation. The results showed a 22.34% enrichment in copper content at a recovery of 83–87% from a 3.56% feed at pH 9. Thionocarbamates' selective nature, which makes them suitable for adsorption on copper-bearing sulfide minerals, aids in their separation from other sulfides, such as pyrite, arsenopyrite, galena, and sphalerite.

6.1.3. Recovery of Copper from Smelting Slag Using Xanthate with Secondary Collectors

Several research studies have shown that combining xanthates with some secondary collectors can improve Cu recovery [13,55,62]. Mixed collectors appear to have a synergistic effect, which reduces reagent usage, improves selectivity, and increases coarse particle recovery [63]. Roy et al. [5] evaluated the efficacy of a mixed collector system using sodium

https://doi.org/10.3390/min16020206

isopropyl xanthate (SIPX) and di-ethyl dithiophosphate (DTP) for recovering copper values from smelting slag, versus SIPX alone. The copper in the smelting slag took the form of Cu_5FeS_4. The combination of collectors, when used in the ratio of 40:160 g/t, resulted in a greater copper recovery of 84.82%, compared to the best recovery values of a single collector system (78.11% Cu). The research also investigated a combination of SIPX and alkyl hydroxamate at a ratio of 160:40 g/t, which resulted in an 83.07% copper recovery. The primary collector SIPX was effective at adsorbing fines, while DTP and alkyl hydroxamates interacted with SIPX to efficiently recover unliberated coarse copper-bearing particles. These findings were consistent with the experimental results reported by Shamsi et al. [55] who conducted flotation experiments using a single collector system of potassium amyl xanthate (PAX), resulting in a copper recovery of 62.23%, then repeated the experiments in a mixed collector system containing PAX and sodium isopropyl xanthate (SIPX), resulting in a substantially increased recovery of 80.27% at pH of 11.

6.1.4. Disadvantages of the Flotation Method on the Recovery of Copper and Cobalt from Smelting Slag

Studies have indicated that the majority of the copper and cobalt in the slag are in the oxide phase, which cannot be treated directly using the flotation process [21]. Conversely, Hara and Jha [64] made similar observations, stating that most of the copper in the slag is in the oxide phase, and virtually all the cobalt is chemically bound with silica, iron, calcium, and/or aluminum oxides, making flotation extremely difficult. A study on the surface modification of oxide minerals using ethanediamine [65] found that oxide minerals are more difficult to float than sulfide minerals due to their higher solubility and extensive hydration. The direct flotation of copper oxides using collectors such as fatty acids, hydroxamates, and petroleum sulfonates has been extensively studied. Despite promising performance at a laboratory scale, these collectors have so far not been successful in plant-scale trials. Moreover, these collectors have been used for copper oxide minerals only. Their application for Cu slag flotation has not been reported.

A more recent study found that difficulties using the flotation technique for the recovery of copper oxides may be ascribed to the presence of dangling ionic bonds, which enable water molecule adsorption on oxide surfaces via polarization [63]. As a result of electrostatic attraction, a thick and stable layer of hydrophilic hydration film forms on the oxide mineral surface, preventing the collector from penetrating and then adsorbing onto it. Kundu et al. [63] suggested investigating the possibility of improving the flotation performance of copper-bearing oxides by employing sulphidation reagents, such as sodium sulfide. Sulphidation treatment alters the surface of Cu bearing oxides by adsorbing S^{2-} and HS^{-} ions, resulting in a metal sulfide coating that promotes collector adsorption [66]. Extensive study on the flotation of Cu slag, using xanthates with sulphidation reagents, has been conducted.

6.1.5. Economic Viability of the Flotation Approach for Reprocessing of Copper Slag

The froth flotation process remains one of the most economically viable and operationally established techniques for the recovery of copper from smelting slags. Its economic appeal lies in its low energy requirement, moderate reagent cost, and compatibility with existing flotation circuits used in sulfide ore processing. The technique effectively recovers metallic and sulphidic copper species, which commonly occur in slag as discrete metallic particles or as sulfide minerals such as bornite (Cu_5FeS_4) and chalcocite (Cu_2S). Numerous studies [5,9–11,48,54,55] have demonstrated that flotation under optimized conditions can achieve 70–85% Cu recovery with concentrate grades ranging between 12% and 23% Cu, depending on slag mineralogy, particle size, and reagent system.

https://doi.org/10.3390/min16020206

Economically, flotation benefits from low operating and reagent costs compared with hydrometallurgical approaches. Collectors such as xanthates (sodium isopropyl xanthate, butyl xanthate) are inexpensive and widely available, while mixed collector systems—combining xanthates with diethyl dithiophosphate (DTP) or alkyl hydroxamates—have exhibited synergistic improvements in selectivity and coarse particle recovery, yielding 84–86% copper recovery with limited reagent dosages [5]. Moreover, the process can be readily implemented within existing concentrator infrastructure, thereby reducing capital investment and promoting near-plant slag valorization.

Nevertheless, the economic feasibility of flotation diminishes when copper is predominantly present in oxide or silicate-bound phases. As reported by Dimitrijevic et al. [21] and Hara and Jha [64], the flotation of oxidized slags is challenging due to the hydrophilic nature of oxide minerals and the strong bonding of copper with iron and silica matrices, which leads to poor recovery and high reagent consumption. To address this, sulphidation pretreatment using sodium sulfide (Na_2S) has been proposed to convert oxides into sulfides, enhancing collector adsorption and improving overall flotation performance [63,66]. Although this additional step increases reagent costs, the corresponding rise in copper recovery can restore process profitability and enhance overall metal yield.

In summary, the flotation approach is economically viable for slags containing significant sulphidic or metallic copper, offering low-cost, high-throughput recovery with rapid payback potential. Its advantages—namely, scalability, operational simplicity, and low energy input—make it a preferred first-stage beneficiation process. However, for highly oxidized slags, the integration of flotation with sulphidation or subsequent hydrometallurgical treatment is essential to maintain economic efficiency and ensure comprehensive metal recovery. When combined with mechanical activation or selective acid leaching, flotation can serve as a cost-effective and sustainable component of an integrated copper slag valorization strategy.

6.2. Copper and Cobalt Recovery from Smelting Slag Using Hydrometallurgy

The hydrometallurgical route via leaching is the most common approach for recovering metals from low-grade materials like smelting slag. Because of its economic benefits and relatively minimal environmental impact, the hydrometallurgical technique offers a high potential for effective metal extraction. The hydrometallurgical technique for metal extraction from smelting slag has been examined using various parameters such as leaching system, extractant concentration, temperature, solid/liquid ratio, and leaching period. The emphasis has been on atmospheric leaching using lixiviants such as acids, bases, and salts. Many of these lixiviants form aqueous solutions that can dissolve metals from ores, concentrates, and slag.

6.2.1. Recovery of Copper and Cobalt Using Sulfuric Acid

Sulfuric acid (H_2SO_4) is the most widely employed lixiviant for metal recovery from copper slags due to its low cost, high reactivity, and widespread availability. It is particularly effective for the leaching of metal oxides and is one of the strongest inorganic acids, being completely miscible with water at all concentrations. Sulfuric acid may be applied in dilute or concentrated form, or in combination with oxidising agents such as oxygen to enhance leaching kinetics. Its suitability for on-site application is further supported by its availability as a common by-product of copper smelting operations. Numerous studies have demonstrated the effectiveness of sulfuric acid as a leaching agent for copper slags, reporting high metal extraction efficiencies [13,16,17,67–71]. For example, Yang et al. [17] achieved metal recoveries of 98% for cobalt, 97% for zinc, and 89% for copper using sulfuric acid leaching. In addition to high extraction efficiencies, the process enabled faster solid–liquid

https://doi.org/10.3390/min16020206

separation and significantly mitigated the adverse effects of silica and ferric oxides on target metal recovery. Despite these advantages, challenges remain, particularly the high consumption of acid and neutralising agents such as lime. Further research is therefore required to optimise reagent usage, improve process economics, and enhance the overall sustainability of sulfuric acid leaching for copper slag treatment.

Mussapyrova et al. [72] investigate how mechanical activation (high-energy milling) alters the structure of copper smelter slag and enables selective, high-efficiency copper leaching at room temperature, without the need for high-temperature or aggressive chemical conditions. Mechanical activation produces dramatic changes in reactivity, allowing copper to be leached using dilute sulfuric acid (0.1 M H_2SO_4) at 25 °C, which is normally ineffective for untreated slag. Subsequent Taguchi-designed leaching tests identified distinctly different optimal leaching conditions for maximizing copper recovery depending on the milling device. For attritor-activated slag, the optimum was 0.15 M $K_2Cr_2O_7$, 0.5 M H_2SO_4, 120 min, L:S = 75:1, yielding a copper recovery of 87.31% and Cu selectivity of 95.44%. Planetary-activated slag achieved optimum recovery under 0.03 M $K_2Cr_2O_7$, 0.1 M H_2SO_4, 120 min, L:S = 200:1, producing 84.63% Cu recovery and 97.87% selectivity [72]. These results show that planetary milling induces higher amorphization and requires lower oxidant concentrations for similar or improved performance.

Autoclaves have been employed to examine oxidative high-pressure sulfuric acid leaching by Baghalha et al. [71]. Leaching with sulfuric acid at increased pressure resulted in improved leaching extraction and solid-liquid separation [67]. Bese [70] explored how ultrasonic energy affects the solubility of copper from copper converter slag during sulfuric acid leaching. The effects of temperature, acid concentration, ferric sulphate concentration, and time were investigated. The results showed that copper, zinc, cobalt, and iron extraction efficiencies were 89.28%, 51.32%, 69.87%, and 13.73%, respectively, whereas in the absence of ultrasound, the efficiencies were lower, 80.41%, 48.28%, 64.52%, and 12.16%, respectively [70]. The amorphous structure of copper slags has a variety of negative effects on sulfuric acid leaching, increasing the viscosity of the leach liquor by forming silica gel, as illustrated in Equation (1).

$$2FeO{\cdot}SiO_2 + 2H_2SO_4 \rightarrow 2FeSO_4 + H_4SiO_4 \quad (1)$$

Overall, acid leaching studies have consistently demonstrated a positive correlation between acid concentration and metal extraction efficiency across a range of leaching conditions [14,16,17,49,67,69,71]. However, several investigations have reported that, despite high extraction efficiencies, the treatment of slags with elevated silica contents is associated with excessive sulfuric acid consumption and the formation of silica gel [16,17,49,64,67]. This behaviour arises from the occurrence of metals such as cobalt and copper within spinel oxides, ferrites, and silicate phases, which require aggressive leaching conditions for dissolution. The resulting high consumption of sulfuric acid and neutralising agents (e.g., lime), together with poor solid–liquid separation caused by the formation of iron hydroxide precipitates and silica gel, significantly constrains the practical applicability of conventional acid leaching processes [17,64]. In response to these limitations, alternative approaches have been explored, including the use of combined acid–oxidant systems to enhance metal recovery from copper slags while mitigating reagent consumption and process inefficiencies [24].

6.2.2. Recovery of Copper and Cobalt Using Citric Acid

Citric acid, an r-hydroxyl tricarboxylic acid, is widely known for its chemical adaptability in leaching transition metal ions. Citric acid leaching of Cu, Co, Ni, and Fe from copper granulated slag was investigated by Meshram et al. [41]. The process involves

leaching the copper slag with 2 N citric acid to extract Co, Ni, and Fe, followed by leaching the residual with a high copper content with 2 M sulfuric acid. The study found that the first stage of leaching with citric acid at room temperature and 10% pulp density resulted in maximum extractions of 4.47% Cu, 88.3% Co, 95% Ni, and 93.8% Fe, whereas the second stage extracted 66–72% of the copper from the leach residue.

6.2.3. Recovery of Copper and Cobalt Using Nitric Acid

Nitric acid (HNO_3) is a strong oxidizing agent that reacts aggressively with many metallic compounds during leaching. Tshiongo et al. [73] compared the use of nitric acid and ammonia solution as leaching agents for copper slags formed under different cooling conditions, including water quenching, air cooling, and furnace cooling. They discovered that the slag cooling rate affected base metal leaching by altering the phase distribution in the slag as well as the base metal distribution within the phases. Tshiongo et al. [73] discovered that quick cooling of the slag inhibited crystallization and resulted in an amorphous phase containing the base metals. However, they discovered that the amorphous slags were more leachable in nitric acid than in basic medium (NH_4OH), with best resulting extractions of 46% Cu, 95% Co, 85% Zn, 92% Pb and 79% Fe.

These studies demonstrate that nitric acid is a highly effective leachant for copper smelting slags, particularly when applied to amorphous or finely comminuted materials and when adequate acid strength is maintained. High nitric acid concentrations can achieve near-quantitative recoveries of Cu, Pb, Zn, Co, and Fe, depending on slag composition and mineralogy. However, structural characteristics—most notably cooling history and degree of crystallinity, exert a strong influence on leaching behaviour and ultimately constrain achievable extraction efficiencies. Consequently, nitric acid leaching represents a potent and versatile approach for copper slag processing, with its performance governed by the interplay between slag structure, acid concentration, and redox conditions.

6.2.4. Recovery of Copper and Cobalt Using Amino Acids

Amino acids have received a lot of interest in hydrometallurgy over the last decade as a highly selective and environmentally benign way to extract metals from various sources [74]. Glycine is the most common amino acid tested and is distinguished by the presence of a carboxyl group and an amino group [75,76]. Glycine is widely used for effectively extracting critical metals from various natural resources [74–77]. Our recent study demonstrated that substantially higher amount of copper can be extracted from the copper smelting slag, suggesting that glycine is effective for leaching copper. Oraby et al. [77] investigated the extraction of nickel and cobalt from a flotation tailings material using an alkaline glycine-based lixiviant system. The findings indicate that the highest extractions of 90% Co and 88% Ni were achieved at a fine particle size of 15 μm. Guo et al. [78] revealed that copper exhibits superior coordination ability to glycine compared to other transition metals in the first series. Huang et al. [76] observed a significant drop in the NH_2CH_2COOH fraction in the species distribution of glycine as the pH value increased from 8 to 10. Thus, by increasing the pH of the solution to an alkaline level, NH_2CH_2COOH undergoes dehydrogenation to produce $NH_2CH_2COO^-$ and form a stable complexation with Cu^{2+} and Co^{2+}, resulting in the formation of $Cu(NH_2CH_2COO)_2$ and $Co(NH_2CH_2COO)_2$, respectively.

6.2.5. Recovery of Copper and Cobalt Using Oxidants or Acid/Oxidant Combinations

Oxidants are excellent leaching agents for naturally occurring minerals that are vulnerable to oxidation reactions. Liquids such as oxygen, hydrogen peroxide, sodium chlorate, and Fe(II)/Fe(III) are thought to be effective oxidants for leaching of copper slag [13,67,69,71]. The use of oxidants as leaching agents can be an effective option for

solving the problem of silica gel formation while also removing iron from solution via the oxidation process. Banza et al. [13] investigated hydrogen peroxide (H_2O_2) as an oxidant for the extraction of metals from copper slag while preventing the problem of silica gel formation. The study achieved extraction efficiencies of 80% of Cu, 90% of Co, 90% of Zn, and Fe extraction was reduced to 5%. A similar study revealed that the use of oxidants such as sodium chlorate ($NaClO_3$) combined with using calcium hydroxide ($Ca(OH)_2$) as a neutralizing agent reduced silica gel formation, and facilitated filtration of the solution [17]. The results achieved metal extractions of 89%, 98%, 97% for Cu, Co, and Zn, respectively, while the iron extraction was as low as 0.02%. Sodium chlorate ($NaClO_3$) was found to prevent the formation of silica gel due to the oxidation of Fe^{2+} to Fe^{3+}. Acid leaching using sulfuric acid in the presence of hydrogen peroxide was found to overcome the issue of silica gel formation by the simultaneous oxidation of iron and sulfide, followed by the removal of iron-bearing impurities [63]. The iron dissolution from copper slag is illustrated in the following Equations (2)–(4) [63]:

$$CuS + 2H_2SO_4 + 2H_2O_2 = CuSO_4 + 2H_2SO_3 + 2H_2O \quad (2)$$

$$FeO + H_2SO_4 = FeSO_4 + H_2O \quad (3)$$

$$2Fe_SO_4 + H_2O_2 + 2H_2O = 2FeOOH + 2H_2SO_4 \quad (4)$$

The leaching investigations produced silica gel-free solutions containing dissolved metal values, which could be readily filtered. An alternative strategy for recovering metals from copper slag while suppressing silica gel formation was reported by Yang et al. [17]. This approach involved sulfuric acid leaching in the presence of sodium chlorate as an oxidising agent, followed by neutralisation with lime to enhance precipitate filtration. The combined use of an oxidant and controlled neutralisation effectively mitigated the adverse effects associated with silica gel precipitation. The effects of key operating parameters, including acid and oxidant consumption, reaction temperature, and leaching duration, were systematically evaluated. Lime addition was identified as a critical step for the selective precipitation of silica and ferric oxides prior to filtration. Under optimised conditions, an overall copper extraction efficiency of 89% was achieved.

Anand et al. [67] conducted research on the leaching of copper slag using high oxygen pressure, and the results showed improved metal extraction efficiencies of 90% of Cu and 98% of Co. It was observed that oxygen availability was an important factor for the oxidation of $Fe^{2+,}$ which minimized the extraction of iron. For example, at lower oxygen pressure, the extraction efficiency of Fe was 1.2%, whereas at higher oxygen pressure, it was 0.81% Fe. These findings were consistent with the study conducted by Basir and Rabah [69], who found that oxygenated conditions can improve copper and cobalt extraction efficiencies while simultaneously achieving a low iron extraction.

The influence of sulfuric acid and potassium dichromate concentrations on the extraction of metals from copper slag has been extensively investigated [14,15,18]. In particular, Altundoğan et al. (2004) [14] studied the leaching of copper converter slag using sulfuric acid (H_2SO_4) in the presence of potassium dichromate ($K_2Cr_2O_7$). The optimal lixiviant composition was identified as 0.25 M H_2SO_4 and 0.1 M $K_2Cr_2O_7$, with a solid-to-liquid ratio of 10 g/L, a temperature of 25 °C, and a contact time of 120 min. Under these conditions, the presence of $K_2Cr_2O_7$ facilitated a copper extraction efficiency of 81.15%, while significantly limiting the extraction of other metals, with Co, Zn, and Fe recoveries of 12.0%, 10.27%, and 3.15%, respectively. In contrast, using 1.0 M H_2SO_4 without potassium dichromate under the same operating conditions (contact time of 120 min, slag-to-solution ratio of 10 g/L, and 298 K), the extraction efficiencies for Cu, Co, Fe, and Zn were 20.5%, 66.6%, 62.1%, and 65.7%, respectively. These results highlight the critical role of oxidants such as

https://doi.org/10.3390/min16020206

$K_2Cr_2O_7$ in selectively enhancing copper recovery, while also illustrating the trade-offs in the extraction of other metals.

In a related study, Boyrazli et al. [15] investigated the effects of temperature (25–70 °C), leaching time (5–240 min), and solid-to-liquid ratio (5–400 g/L) on metal extraction from copper slag. The highest copper extraction efficiency of 99.6% was achieved at 0.25 M H_2SO_4, 0.1 M $K_2Cr_2O_7$, 70 °C, and 120 min of leaching. In contrast, the extraction efficiencies for Co, Zn, and Fe under these conditions were substantially lower, at 42.09%, 49.86%, and 27.59%, respectively. The study noted that the extraction of Co, Zn, and Fe improved only at elevated temperatures, likely due to the reduced adsorption of dichromate ions, which are responsible for passivation effects on these metals. These findings are consistent with more recent investigations of the H_2SO_4–$K_2Cr_2O_7$ system for leaching copper, Zn, and Fe from copper smelter slag [18]. The study reported that dichromate presence enhanced copper recovery, achieving 68% Cu extraction, while significantly suppressing Zn and Fe recovery to 4% and 5%, respectively, under the same conditions. The authors attributed the decreased extraction of non-copper metals to precipitation and surface passivation effects induced by dichromate ions, while noting that copper extraction improved with increasing dichromate concentration [18].

6.2.6. Recovery of Copper and Cobalt Using Bases and Salts

Several studies have investigated the leaching of copper slag using bases and salts such as ferric chloride [79], ferric sulphate [39,48,70], ammonium sulphate [68], ammonium chloride [47,80], chlorine solution [62,70] and ammonium hydroxide [81,82]. Hydrochloric acid with ammonium hydroxide has also been investigated [69]

A number of studies have shown that using hydrochloric acid with ammonium hydroxide has several advantages and can eliminate problems associated with leaching using common acids [6,81,82]. For example, ammonium hydroxide (NH_4OH), which is also known as aqua ammonia in aqueous solutions, can dissolve various metal oxides and hydroxides, such as copper (II) hydroxide, to form ammine complexes. Ammonium chloride is a safe, non-volatile agent and an environmentally friendly crystalline substance at room temperature. The physico-chemical principles for metal recovery using ammonia and ammonium are based on the behavior of the H_2O–NH_3–NH_4Cl system containing metal amines, and the phase equilibria for liquid and solid, and liquid and vapor [81]. The following Equations (5) and (6) show the dissolution of metals in an aqueous solution of NH_4OH [81].

Several studies have demonstrated that the use of hydrochloric acid in combination with ammonium hydroxide (NH_4OH) offers distinct advantages and can overcome limitations associated with conventional acid leaching [6,81,82]. Ammonium hydroxide, also referred to as aqua ammonia in aqueous solution, can dissolve various metal oxides and hydroxides, such as copper(II) hydroxide, by forming stable ammine complexes. Ammonium chloride, a non-volatile and environmentally benign crystalline compound at room temperature, is commonly used as a supporting agent in these systems. The physicochemical principles underlying metal recovery with ammonia and ammonium are based on the behaviour of the H_2O–NH_3–NH_4Cl system, which governs the formation of metal–amine complexes as well as the phase equilibria between liquid–solid and liquid–vapor states [81]. The dissolution of metals in aqueous NH_4OH solutions can be represented by the following reactions (Equations (5) and (6)) [81].

$$MO + 4NH_{3(sol)} + nH_2O \rightarrow [M(NH_3)_4](OH)_2 + (n-1)H_2O \quad (5)$$

$$O + xNH_{3(sol)} + 2NH_4Cl_{(sol)} \rightarrow [M(NH_3)_n]_2 + 2Cl^- + H_2O \quad (6)$$

https://doi.org/10.3390/min16020206

where M = metals, e.g., Cu; n = x + 2

Equation (5) shows the dissolution of metals in the absence of Cl^- ions, and Equation (6) in the presence of Cl^- ions.

Overall, the reviewed studies demonstrate that oxidative and complexing leaching systems are most effective for copper recovery from smelting slags. Ferric-based oxidants ($FeCl_3$, $Fe_2(SO_4)_3$) consistently achieve the highest copper dissolution rates, often exceeding 70–85% recovery by oxidizing metallic and sulfide copper phases. Ammonium salts and hydroxides, on the other hand, offer greater selectivity by forming stable copper–ammonia complexes while minimizing iron dissolution. Chloride- and chlorine-based systems further enhance solubility but pose environmental and corrosion challenges. Collectively, these findings confirm that the choice of leaching reagent, redox potential, and pH control are critical for optimizing copper extraction efficiency and selectivity from copper smelting slags.

6.2.7. Recovery of Copper and Cobalt Using Chlorination Roast-Water Leach

Chlorination roasting followed by water leaching relies on the formation of stable, water-soluble metal chlorides during a roast, which can then be readily leached out in water to recover the metallic values. Anand et al. [79] investigated the leaching of copper slag using ferric chloride and observed that the extraction of copper increased with an increase in ferric ions. The chlorination reactions are summarized in the following Equations (7) and (8).

$$Cu_2S + 2FeCl_3 \rightarrow 2CuCl + 2FeCl_2 + S \quad (7)$$

$$Cu + FeCl_3 \rightarrow CuCl + FeCl_2 \quad (8)$$

The study demonstrated that ferric chloride is the most effective chloride for direct leaching of copper minerals, achieving copper extraction of 92%. Herreros et al. [62] investigated the leaching of copper from reverberatory slag using a chlorine solution. In this slag, most copper was present as metallic copper, chalcocite (Cu_2S), bornite (Cu_5FeS_4), and other complex sulphides, with mineral liberation occurring at particle sizes below 20 μm. The study evaluated the effects of stirring speed, particle size, initial chlorine and chloride concentrations, and temperature on the leachability of the copper. Maximum copper extraction reached 80%, while iron solubilisation remained low at approximately 5%. In a similar investigation, Bese et al. [70] examined the treatment of converter slag using chlorine-saturated water. The study identified optimum conditions for copper dissolution that minimized iron dissolution, achieving a copper extraction efficiency of 98.35%.

Borisov et al. [80] observed that the reaction of chloride with oxides and sulfides of some metal-bearing compounds, such as CaO, ZnO, CuS, FeS, ZnS, and Fe_2O_3, leads to the formation of chloro–metallate complexes such as $(NH_4)2ZnCl_4$ and $(NH)_4CuCl_3$. These complexes could be further decomposed into chlorides. The results revealed that oxides of Si and Al did not react with ammonium chloride, which makes it a good leaching agent for silicate materials. Ammonia solutions containing ammonium chloride were found to be effective for the extraction of Cu and Zn from copper smelter slag [81]. The study used the central composite rotatable design and approximation method to determine the optimum conditions for the recovery of copper and zinc. The model successfully predicted the responses, and maximum copper and zinc recoveries of 81.16% and 56.48%, respectively, were obtained. In a recent study by Aracena et al. [82] a high copper recovery of 87.7% has been reported using an ammonia column system for the leaching of copper converter slag.

https://doi.org/10.3390/min16020206

6.2.8. Recovery of Copper and Cobalt Using Ultraviolet Radiation

The application of ultraviolet (UV) radiation in hydrometallurgical leaching has emerged as an innovative approach for enhancing the dissolution of valuable metals from refractory mineral residues. Recent investigations, including Sari and Turan [83] and [84], provide complementary insights into the role of UV-induced photochemical processes in improving the recovery of metals, such as copper and cobalt, from complex slag matrices.

Sari and Turan [83] evaluated the direct photooxidative leaching of copper slag under UV irradiation and demonstrated that high-energy UV wavelengths, specifically vacuum ultraviolet (VUV, 185 nm) and UVC (254 nm), significantly enhance copper dissolution compared with conventional acid leaching. Under optimal conditions (1.5 mol/L H_2SO_4, 55 °C, 180 min), copper extraction increased from 70.7% in non-UV conditions to 85.1% under 185 nm irradiation. Iron dissolution exceeded 90% in both conditions. The authors attributed these improvements to the in-situ generation of potent oxidative radicals arising from the photolysis of water and sulfate species under high-energy UV irradiation. These radicals promote the oxidation of both oxide and sulfide copper phases, accelerating their dissolution into Cu^{2+}.

Complementary mechanistic understanding is provided by Deng et al. [84], whose work demonstrates the fundamental ability of UV radiation to drive rapid redox transformations in aqueous metal–ligand complexes. Under 254 nm irradiation, Fe(III)-oxalate complexes were photochemically reduced and precipitated as Fe(II)-oxalate with efficiencies exceeding 97% within 30 min. This redox behavior parallels the photooxidative and photoreductive mechanisms observed in UV-enhanced leaching of copper slag, emphasizing UV's capacity to manipulate metal oxidation states and promote dissolution of complex phases [84]. For copper slag, where copper and cobalt are commonly hosted in fayalite, magnetite, and complex silicate matrices, UV-generated radicals accelerate decomposition of the silicate network, promote oxidation of Cu(I) and Co(II) species, and enhance the dissolution kinetics of Fe-bearing phases.

6.2.9. Economic Viability of the Hydrometallurgy Approach for Reprocessing of Copper Slag

These findings underscore the broader potential of UV-based photochemical recovery of metals from copper slag. By leveraging photon-driven radical chemistry, UV irradiation offers a pathway toward higher metal recovery efficiencies, reduced chemical consumption, and improved processing of refractory waste materials. Hydrometallurgical processing has emerged as a technically efficient and economically feasible method for recovering valuable metals, particularly copper and cobalt, from copper smelting slags. Among the various lixiviants examined, sulfuric acid (H_2SO_4) remains the most widely applied due to its low cost, strong leaching capability, and ready availability as a smelter byproduct, allowing on-site integration without significant reagent import or waste disposal costs. Numerous investigations [13,14,17,67,70] have demonstrated high metal extraction efficiencies up to 98% Co, 97% Zn, and 89% Cu, under optimized temperature, pressure, and acid concentration conditions.

However, conventional acid leaching suffers from high acid and lime consumption, excessive silica gel formation, and poor filtration characteristics caused by iron hydroxide precipitation. To overcome these economic and operational constraints, researchers have introduced mechanochemical activation and acid–oxidant hybrid systems. Mussapyrova et al. [72] demonstrated that mechanical activation via high-energy milling substantially increases slag reactivity, enabling selective copper leaching (84–87%) using dilute acid (0.1–0.5 M H_2SO_4) at room temperature a major reduction in both reagent and energy costs.

https://doi.org/10.3390/min16020206

Similarly, oxidant-assisted leaching systems (e.g., H_2SO_4–H_2O_2 or H_2SO_4–$NaClO_3$) have achieved high metal recoveries (>90%) while minimizing silica gel formation and iron dissolution [13,17,63].

Complementary work using alternative organic lixiviants such as citric acid [41], nitric acid [73], and amino acids like glycine [74–76] demonstrates growing interest in eco-efficient and recyclable leaching systems. Although these reagents are more expensive, they provide cleaner solutions, reduced waste generation, and greater metal selectivity, aligning with circular-economy and low-carbon processing goals. Overall, the reviewed studies confirm that hydrometallurgical leaching, particularly sulfuric-acid-based and oxidant-enhanced processes, offers a commercially viable pathway for valorizing copper slags. The combination of mechanical activation, controlled oxidation, and reagent recycling significantly reduces energy intensity and reagent costs, transforming slag from a metallurgical residue into a sustainable secondary resource for critical metals essential to the global clean-energy transition.

6.3. Pyrometallurgical Approaches for Processing of Copper Slag

Pyrometallurgy involves chemical reactions of solids, gases, or molten materials at elevated temperatures in a furnace.

Recovery of Copper and Cobalt Using Carbothermal Reduction

In carbothermic reduction, carbon serves as a reductant to convert minerals in the slag into metallic phases at elevated temperatures. Yucel et al. [19] investigated the treatment of ancient Kure copper slag using a carbothermal reduction method in a DC arc furnace at 1430–1480 °C, achieving maximum recoveries of 95.7% for cobalt and 90% for copper in a closed system. Hara and Jha [64] developed an alternative approach involving the reduction and sulphurisation of copper slag with activated charcoal, attaining a copper recovery of 90% at 1323 K. Zhang et al. [85] reported that gas-phase diffusion, with an activation energy of 118.06 kJ mol^{-1}, was the rate-limiting step during isothermal reduction of carbon-bearing copper slag pellets. Despite these successes, pyrometallurgical reduction requires substantial energy input, with operating temperatures exceeding 1200 °C, largely due to the high melting point of fayalite in copper slag [57,85]. The presence of significant amounts of fayalite further complicates the reduction process [86]. Moreover, this approach has the potential to generate considerable environmental contamination, as it produces multiple types of solid waste.

6.4. Pyro-Hydrometallurgical Approach for Processing Copper Slag

The most common method for pyro-hydrometallurgical processing of copper smelting slag is roasting, followed by water or acid leaching. The pyro-hydrometallurgy involves the study of the effects of roasting time, acid/slag ratio, and roasting temperature, and the effect of thermal decomposition prior to leaching on metal dissolution was examined. The roasting of copper sulfide produces a calcine, which is then treated using the hydrometallurgical technique. Extensive studies have been done on the roasting of copper slag using roasting agents such as sulfuric acid (H_2SO_4) [16,20,21,68], pyrite (FeS_2) [87], ferric sulphate ($Fe_2(SO_4)_2$) [39], graphite [48] and ammonium sulphate ($(NH_4)_2SO_4$) [68] to yield metal sulphates.

6.4.1. Recovery of Copper and Cobalt Using Sulphation Roasting-Water Leach

Sulphation roasting involves the addition of sulphate salts, sulfuric acid, or SO_3 gas during roasting, producing stable and water-soluble metal sulphate complexes. It is among several low-temperature methods reported for recovering metals from copper slag. Tümen and Bailey [86] investigated the sulphation roasting of primary and secondary slags with

https://doi.org/10.3390/min16020206

pyrite, followed by hot water leaching of the calcines. The addition of pyrite enhanced copper recovery from primary converter slag to 95%, with minimal iron contamination of approximately 2%. However, this approach was less effective for other metals, achieving only 58%, 35%, and 29% extraction efficiencies for Co, Ni, and Zn, respectively. Mututubanya [88] applied solid-state carbothermic reduction in an inert nitrogen atmosphere using charcoal as a reductant at 600–1000 °C, followed by sulfuric acid leaching. This process selectively reduced Co, Ni, and Cu oxides while retaining the majority of Fe in the slag. Cobalt extraction reached 52% at 950 °C. Subsequent experiments incorporating pyrite and cobalt sulphide concentrates as sulphating agents improved cobalt recovery to 72% at a 1:1 slag-to-pyrite ratio. Altundoğan and Tümen [39] proposed an alternative approach involving roasting with ferric sulphate at 500 °C followed by water leaching. Ferric sulphate promoted sulphation of copper slag constituents, yielding extraction efficiencies of 93% for Cu, 38% for Co, 13% for Ni, and 59% for Zn.

The recovery of Cu, Co and Zn from copper smelter and converter slags by roasting with sulfuric acid was conducted by Arslan and Arslan [20]. The study investigated the effects of roasting time, roasting temperature, and acid/slag ratio. Metal extractions of 88% of Cu, 87% of Co, 93% of Zn and 83% of Fe were achieved after two hours of roasting at 150 °C and with a 3:1 acid/slag ratio. The authors observed that increasing the roasting time to four hours further increased the extraction of copper to 95%. However, high iron content would make further treatment of the leach liquor difficult. In a similar study, Sukla et al. [68] studied roasting of copper converter slag using sulfuric acid and achieved recoveries for Cu, Ni and Co of 95%, 90% and 99%, respectively. It was observed that the Fe contamination was 60–80% and removal of most of the Fe from the leach liquors was achieved with ammonia liquor and lime as precipitants, bringing the Fe level to about 3%. A recent study has shown that increasing the sulphation temperature could reduce the iron content in the leach liquor [21]. The method involved roasting the slag in the presence of sulfuric acid at an initial temperature of 250 °C, achieving maximum copper extraction efficiency of about 94% with iron dissolution of 55%. When further experiments were carried out by roasting at a much higher temperature of 600 °C, the iron extraction efficiency was reduced to about 6%; however, the copper recovery was also reduced to 79%.

The use of ammonium sulphate in the roasting was found to be effective and maximum copper recovery levels of over 80% were obtained. Rudnik et al. (2009) [89] explored the roasting of slag in reducing conditions to produce Cu–Co–Fe–Pb alloy, and thereafter electrolytic dissolution of the alloy in an ammonium chloride solution was conducted. The results indicated that 99.9% high purity copper was deposited, while cobalt recovery of 92.0% was obtained during the selective electrowinning process. Other roast-leach approaches have involved roasting the copper slag with a combination of sulfuric acid and ammonium sulphate (Sukla et al.,1986 [68]). This study was carried out by roasting the slag at 150 °C, leading to the sulphation of the metals of interest. The leaching was conducted in water in an agitated system using a particle size of −150 μm. Similar investigations were conducted by Hamamci and Ziyadanogullari [90] on the influence of roasting with ammonium sulphate on the extraction of copper. Copper extraction of up to 88% was achieved at particle sizes of less than 100 mesh at a roasting temperature of 400 °C for 60 min. The preliminary conversion of Cu and Co in copper slag to Cu_2S and CoS using H_2S gas has been shown to attain high extraction efficiencies for copper and cobalt metals [91]. The recoveries after roasting and leaching with agitation in water at a particle size of 149 μm were 100% of the Cu and 70.7% of the Co. Deng and Ling [16] demonstrated that thermal acid aging followed by water leaching was an effective method for recovery of metal values from copper slag, giving an extraction efficiency of 93% of the Cu. Grudinsky et al. [92]

https://doi.org/10.3390/min16020206

investigated the efficacy of sulphatising roasting using iron sulphates, followed by water leaching, to extract copper values from discarded slags rich in silica content. The copper slag sample was ground to a particle size of 100% passing 100 μm and mixed with pure iron sulphates for 24 h. The recovery of copper was up to 79% at a roasting temperature of 625 °C for 6 h.

6.4.2. Recovery of Copper and Cobalt Using Carbothermal Reduction-Sulfuric Acid Leach

The carbothermal reduction of copper slag in a submerged DC arc furnace was investigated by Acma [93]. The study demonstrated that copper slag could be carbothermally smelted with partial reduction of iron oxide (FeO) to a metallic phase containing copper and other metals at temperatures of 1400–1800 °C. The reduced material was subsequently leached with H_2SO_4, and copper was recovered as CuS following purification with H_2S, while iron precipitated as goethite. Bulut [48] studied the reduction of copper slag using graphite in a DC arc furnace, followed by hot sulfuric acid leaching at 60 °C with an acid concentration of 120 g L^{-1} for 2 h. The process achieved extraction efficiencies of 71.5% for Fe, 78% for Cu, and 90% for Co. More recently, Phiri et al. [22] investigated low-temperature carbothermic reduction of copper slag using charcoal in the presence of borax, followed by H_2SO_4 leaching. Thermochemical calculations, phase characterisation, and experimental results demonstrated that borax addition lowered the temperature required for fayalite reduction and promoted the transformation of copper slag microstructures into amorphous and metallic phases. Subsequent leaching yielded high extraction efficiencies for Cu, Co, and Fe, reaching 83.8%, 84.8%, and 85.7% at 850 °C, respectively.

6.4.3. Economic Viability of the Pyrometallurgy Approach for Reprocessing of Copper Slag

Pyrometallurgical processing remains an established but energy-intensive and capital-demanding route for the recovery of copper and cobalt from smelting slags. The process relies on high-temperature reactions between molten, solid, and gaseous phases to reduce oxides and form metallic or sulphidic products suitable for further refining. Although pyrometallurgy offers rapid reaction kinetics and high metal recoveries, its economic viability is constrained by high energy consumption, complex furnace operation, and environmental control costs associated with off-gas and solid waste management.

Among pyrometallurgical methods, carbothermal reduction has been widely studied for its capacity to recover over 90% Cu and 95% Co at temperatures above 1400 °C [19,64]. However, the requirement for sustained high-temperature operation increases both operating and maintenance costs, making the process economically feasible only when integrated into existing smelter infrastructure. Moreover, the high melting point of fayalite (Fe_2SiO_4) in the slag [85] necessitates additional fluxing or reductant additives to lower melting temperatures, further increasing reagent expenditure. The process also generates substantial solid waste residues and CO_2 emissions, which add to environmental compliance costs and reduce the net economic margin.

To improve efficiency, hybrid pyro-hydrometallurgical routes have been developed, wherein roasting precedes acid or water leaching to enhance metal solubility. Studies on sulphation roasting followed by leaching have achieved copper recoveries of 88–95%, cobalt recoveries of 70–87%, and zinc recoveries above 90% under moderate roasting temperatures (150–600 °C) and acid-to-slag ratios of 3:1 [20,39,68,88]. These hybrid systems operate at significantly lower energy inputs than direct reduction smelting, improving their economic outlook. However, they still require thermal energy for roasting, acid neutralization reagents, and multi-step solid–liquid separation systems, which increase processing costs compared to purely hydrometallurgical options.

https://doi.org/10.3390/min16020206

Recent innovations, such as borax-assisted carbothermal reduction [22], have shown promise in lowering operational temperatures to below 900 °C while maintaining high extraction efficiencies (Cu: 83.8%, Co: 84.75%, Fe: 85.69%). These modifications improve the energy-to-yield ratio, thereby enhancing process economics and sustainability. Similarly, sulphation roasting with ferric sulphate or ammonium sulphate provides a cost advantage by achieving metal recoveries exceeding 90% at 500 °C, compared to >1200 °C in conventional smelting [39,90].

Economically, pyrometallurgical routes are most viable when implemented in conjunction with existing copper smelter operations, utilizing available heat, gas-handling systems, and byproduct acid streams. However, as stand-alone processes, they are generally less competitive than hydrometallurgical or flotation methods due to higher energy input, infrastructure costs, and environmental constraints. The pyro-hydrometallurgical hybrid approach, especially sulphation roasting followed by leaching, represents a balanced compromise between metallurgical efficiency and operational cost, achieving high recovery yields with reduced energy demand.

Overall, while pyrometallurgical and pyro-hydrometallurgical methods can deliver high copper and cobalt recoveries, their economic viability depends heavily on process integration, waste minimization, and thermal efficiency improvements. Emerging low-temperature reduction and sulphation roasting technologies, combined with selective leaching, offer a pathway toward cost-effective and environmentally responsible valorization of copper smelting slags.

7. Conclusions

This study reviewed global smelting slag production over the last 25 years, and the results demonstrate that huge amounts of smelting slag have been produced. This represents a significant potential resource for cobalt and copper metals. The chemical and mineralogical characterization of smelting slag has shown that it is highly heterogeneous and chemically diverse. However, the high metal content in smelting slag has attracted extensive research in finding innovative processing strategies to reprocess the critical metals. The recovery of copper and cobalt from copper slag could significantly augment the supply of these metals, which are essential to facilitating the transition to green energy, while simultaneously addressing environmental concerns regarding slag disposal. The important aspects of various processing techniques for recovering copper and cobalt from the smelting slag have been discussed. Froth flotation using xanthates is a well-known beneficiation technique for the recovery of copper from copper slags worldwide. A mixed collector system, with xanthates as one of the collectors, works better than any single collector. The mixed collectors have higher adsorption and selectivity on the slag surface, thereby inducing higher separation efficiency. However, froth flotation is ineffective for the recovery of copper from oxides. Therefore, sulphidation treatment of copper oxide-containing slags is essential for slag flotation. Although some collectors, such as hydroxamates, have been employed in the flotation of copper oxide minerals without sulfidation treatments, their efficacy at large scale or for Cu slags is yet to be studied. However, cobalt cannot be recovered by the flotation technique because it is embedded in silicate and magnetite structures.

The traditional hydrometallurgical approach by leaching is the most common method used for extracting critical metals from smelting slag. However, the high consumption of sulfuric acid and lime, as well as poor settling and filtration characteristics caused by the formation of iron hydroxide precipitates and silica gel, limit the application of the process. The use of oxidants is promising in overcoming these challenges. The pyrometallurgical methods for the recovery of copper and cobalt from slag at high temperatures are the most

https://doi.org/10.3390/min16020206

effective approaches. However, they necessitate considerable energy consumption with temperatures over 1200 °C and cause considerable environmental contamination. The combustion of carbonaceous reductants and oxidation of sulfide minerals release large quantities of sulfur dioxide, carbon monoxide, and carbon dioxide, contributing to air pollution and greenhouse gas accumulation. Trace volatile metals such as As, Pb, Zn, and Cd may also vaporize and condense as fine particulates, posing health and environmental risks. Research has shown that the use of basicity flux can lower the temperature for fayalite disaggregation. A pyro-hydrometallurgical process involves the transformation of the smelting slag using roasting and reduction. The products after roasting and reduction are subsequently leached in water or acid to recover the critical metals of interest. However, pilot-scale studies need to be conducted to ascertain the economic viability of this processing route.

Author Contributions: Conceptualization, A.N.N. and T.C.P.; methodology, A.N.N. and T.C.P.; software, T.C.P.; validation, A.N.N., T.C.P. and P.S.; formal analysis, T.C.P.; investigation, A.N.N. and T.C.P.; resources, A.N.N. and T.C.P.; data curation, T.C.P.; writing—original draft preparation, T.C.P.; writing—review and editing, A.N.N. and T.C.P.; visualization, T.C.P.; supervision, A.N.N. and P.S.; project administration, A.N.N.; funding acquisition, A.N.N. and T.C.P. All authors have read and agreed to the published version of the manuscript.

Funding: The research was supported by the Schlumberger Foundation.

Data Availability Statement: The raw data supporting the conclusions of this article will be made available by the authors on request.

Conflicts of Interest: The authors declare no conflict of interest.

References

1. Phiri, T.C.; Singh, P.; Nikoloski, A.N. The potential for copper slag waste as a resource for a circular economy: A review—Part II. *Miner. Eng.* **2022**, *180*, 107474. [CrossRef]
2. Gorai, B.; Jana, R.K. Characteristics and utilisation of copper slag—A review. *Resour. Conserv. Recycl.* **2003**, *39*, 299–313. [CrossRef]
3. Alp, I.; Deveci, H.; Süngün, H. Utilisation of flotation wastes of copper slag as raw material in cement production. *J. Hazard. Mater.* **2008**, *159*, 390–395. [CrossRef] [PubMed]
4. Chen, W.L.; Liu, Z.H.; Ding, Y.G. Study on comprehensive recovery of copper and iron from a copper smelting slag. *Nonferrous Met. (Miner. Process. Sect.)* **2019**, *4*, 58–62.
5. Roy, S.; Datta, A.; Rehani, S. Flotation of copper sulphide from copper smelter slag using multiple collectors and their mixtures. *Int. J. Miner. Process.* **2015**, *143*, 43–49. [CrossRef]
6. Potysz, A.; Hullebusch, E.D.V.; Kierczak, J.; Grybos, M.; Lens, P.N.L.; Guibaud, G. Copper Metallurgical Slags—Current Knowledge and Fate: A Review. *Crit. Rev. Environ. Sci. Technol.* **2015**, *45*, 2424–2488. [CrossRef]
7. Ettler, V.; Piantone, P.; Touray, J.C. Mineralogical control on inorganic contaminant mobility in leachate from lead-zinc metallurgical slag: Experimental approach and long-term assessment. *Mineral. Mag.* **2003**, *67*, 1269–1283. [CrossRef]
8. Kambole, C.; Paige-Green, P.; Kupolati, W.K.; Ndambuki, J.M.; Adeboje, A. Comparison of technical and short-term environmental characteristics of weathered and fresh blast furnace slag aggregates for road base applications in South Africa. *Case Stud. Constr. Mater.* **2019**, *11*, e00239. [CrossRef]
9. Sarrafi, A.; Rahmati, B.; Hassani, H.R.; Shirazi, H.H. Recovery of copper from reverberatory furnace slag by flotation. *Miner. Eng.* **2004**, *17*, 457–459. [CrossRef]
10. Das, B.; Mishra, B.K.; Angadi, S.; Pradhan, S.K.; Prakash, S.; Mohanty, J.K. Characterisation and recovery of copper values from discarded slag. *Waste Manage. Res.* **2010**, *28*, 561–567. [CrossRef]
11. Fan, J.; Li, H.; Wei, L.; Li, C.; Sun, S. *The Recovery of Copper from Smelting Slag by Flotation Process*; The Minerals, Metals & Materials Society: Pittsburgh, PA, USA, 2017.
12. Sanchez, R.M.I.; Rivera, J.; Frias, M.; Esteban, J.L.; Olaya, M. Leaching characteristics of blended mortars containing copper slag. *ACI Spec. Publ.* **2004**, *221*, 925–940.
13. Banza, A.N.; Gock, E.; Kongolo, K. Base metals recovery from copper smelter slag by oxidizing leaching and solvent extraction. *Hydrometallurgy* **2002**, *67*, 63–69. [CrossRef]

14. Altundoğan, H.S.; Boyrazli, M.; Tümen, F. A study on the sulphuric acid leaching of copper converter slag in the presence of dichromate. *Miner. Eng.* **2004**, *17*, 465–467. [CrossRef]
15. Boyrazli, M.; Altundoğan, H.S.; Tümen, F. Recovery of Metals from Copper Converter Slag by Leaching with $K_2Cr_2O_7$-H_2SO_4. *Can. Metall. Q.* **2006**, *45*, 145–152. [CrossRef]
16. Deng, T.; Ling, Y. Processing of copper converter slag for metal reclamation. Part I: Extraction and recovery of copper and cobalt. *Waste Manage. Res.* **2007**, *25*, 440–448. [CrossRef]
17. Yang, Z.; Rui-lin, M.; Wang-dong, N.; Hui, W. Selective leaching of base metals from copper smelter slag. *Hydrometallurgy* **2010**, *103*, 25–29. [CrossRef]
18. Nadirov, R.K.; Mussapyrova, L.A. Copper Smelter Slag Leaching by using H2SO4 in the presence of Dichromate. *J. Chem. Technol. Metall.* **2019**, *54*, 657–662.
19. Yucel, O.; Addemir, O.; Tekin, A.; Nizamoglu, S. Recovery of Cobalt from Copper Slags. *Mineral Process. Extr. Metall. Rev.* **1992**, *10*, 99–107. [CrossRef]
20. Arslan, C.; Arslan, F. Recovery of copper, cobalt and zinc from copper smelter and converter slags. *Hydrometallurgy* **2002**, *67*, 1–7. [CrossRef]
21. Dimitrijević, M.D.; Urošević, D.M.; Janković, Z.D.; Milić, S.M. Recovery of Copper from Smelting Slag by Sulphation Roasting and Water Leaching. *Physicochem. Probl. Miner. Process.* **2016**, *52*, 409–421.
22. Phiri, T.C.; Singh, P.; Hara, Y.S.; Siame, J.; Nikoloski, A.N. Carbothermic Reduction of Copper Slag in the Presence of Borax. *Mineral Process. Extr. Metall. Rev.* **2023**, *46*, 165–176. [CrossRef]
23. Piatak, N.M.; Parsons, M.B.; Seal, R.R., II. Characteristics and environmental aspects of slags: A review. *Appl. Geochem.* **2014**, *57*, 236–266. [CrossRef]
24. Phiri, T.C.; Singh, P.; Nikoloski, A.N. The potential for copper slag waste as a resource for a circular economy: A review—Part I. *Miner. Eng.* **2021**, *172*, 107150. [CrossRef]
25. Tian, H.; Guo, Z.; Wang, D.; Pan, J.; Zhu, D.; Yang, C.; Xue, Y.; Li, S. Comprehensive review on metallurgical recycling and cleaning of copper slag. *Resour. Conserv. Recycl.* **2021**, *168*, 105366. [CrossRef]
26. U.S. Geological Survey. *USGS Mineral Commodity Summaries (2001–2025)*; U.S. Geological Survey: Reston, VA, USA, 2025.
27. Davenport, W.G.; King, M.; Schlesinger, M.; Biswas, A.K. *Extractive Metallurgy of Copper*, 4th ed.; Elsevier: Amsterdam, The Netherlands, 2002; pp. 1–452.
28. Jones, R.T. Pyrometallurgy of copper. *J. S. Afr. Inst. Min. Metall.* **2014**, *114*, 239–248.
29. Warczok, A.; Riveros, G.; Echeverría, P.; Díaz, C.M.; Schwarze, H.; Sánchez, G. Factors Governing Slag Cleaning in an Electric Furnace. *Can. Metall. Q.* **2002**, *41*, 465–473. [CrossRef]
30. Shen, H.; Forssberg, E. An overview of recovery of metals from slags. *Waste Manag.* **2003**, *23*, 933–949. [CrossRef]
31. Davenport, W.G.; Partelpoeg, E.H. *Flash Smelting: Analysis, Control and Optimization*; Pergamon Press: Oxford, UK, 2015.
32. Kandalam, A.; Reuter, M.A.; Stelter, M.; Reinmöller, M.; Gräbner, M.; Richter, A.; Charitos, A. A Review of Top-Submerged Lance (TSL) Processing—Part I: Plant and Reactor Engineering. *Metals* **2023**, *13*, 1728. [CrossRef]
33. Jak, E.; Hayes, P. Slag phase equilibria and viscosities in ferronickel smelting slags. In Proceedings of the 12th International Ferroalloys Congress, Sustainable Future, Helsinki, Finland, 6–9 June 2010.
34. Gupta, C.K.; Krishnamurthy, N. Extractive metallurgy of rare earths. *Int. Mater. Rev.* **1992**, *37*, 197–248. [CrossRef]
35. Mackey, P. Evolution of the Large Copper Smelter—1800s to 2013. In *Celebrating the Megascale: Proceedings of the Extraction and Processing Division Symposium on Pyrometallurgy in Honor of David G.C. Robertson*; Wiley: Hoboken, NJ, USA, 2014.
36. Lottermoser, B.G. Mobilisation of heavy metals from historical smelting slag dumps, north Queensland, Australia. *Mineral. Mag.* **2002**, *66*, 475–490. [CrossRef]
37. Ravindra, K.; OBE, D.; Brito, J.D.; Mangabhai, R.; Lye, C.Q. *Sustainable Construction Materials: Copper Slag*; Woodhead Publishing: Sawston, UK, 2017; pp. 28–86.
38. Kierczak, J.; Pietranik, A. Mineralogy and composition of historical Cu Slags from the Rudawy Janowickie Mountains. Southwestern Poland. *Can. Mineral.* **2011**, *49*, 1281–1296. [CrossRef]
39. Altundoğan, H.S.; Tümen, F. Metal recovery from copper converter slag by roasting with ferric sulphate. *Hydrometallurgy* **1997**, *44*, 261–267. [CrossRef]
40. Kaksonen, A.H.; Särkijärvi, S.; Puhakka, J.A.; Peuraniemi, E.; Junnikkala, S.; Tuovinen, O.H. Chemical and bacterial leaching of metals from a smelter slag in acid solutions. *Hydrometallurgy* **2016**, *159*, 46–53. [CrossRef]
41. Meshram, P.; Bhagat, L.; Prakash, U.; Pandey, B.D.; Abhilash. Organic acid leaching of base metals from copper granulated slag and evaluation of mechanism. *Can. Metall. Q.* **2017**, *56*, 168–178. [CrossRef]
42. Phiri, T.C.; Singh, P.; Elsayed, O.; Nikoloski, A.N. Mineralogical characterisation of copper slag and phase transformation after carbocatalytic reduction for hydrometallurgical extraction of copper and cobalt. *Metals* **2024**, *14*, 1119. [CrossRef]
43. Li, Y.; Perederiy, I.; Papangelakis, V.G. Cleaning of waste smelter slag and recovery of valuable metals by pressure oxidative leaching. *J. Hazard. Mater.* **2008**, *152*, 607–615. [CrossRef]

44. Manasse, A.; Mellini, M. Chemical and textural characterisation of medieval slags from the Massa Marittima smelting sites (Tuscany, Italy). *J. Cult. Herit.* **2002**, *3*, 187–198. [CrossRef]
45. Ettler, V.; Johan, Z.; Kříbek, B.; Šebek, O.; Michaljevič, M. Mineralogy and environmental stability of slags from Tsumeb smelter, Namibia. *Appl. Geochem.* **2009**, *24*, 1–15. [CrossRef]
46. Vítková, M.; Ettler, V.; Johan, Z.; Kříbek, B.; Šebek, O.; Mihaljevič, M. Primary and secondary phases in copper-cobalt smelting slags from the Copperbelt Province. Zambia. *Mineral. Mag.* **2010**, *74*, 581–600. [CrossRef]
47. Nadirov, R.K.; Syzdykova, L.I.; Zhussupova, A.K.; Usserbaev, M.T. Recovery of value metals from copper smelter slag by ammonium chloride treatment. *Int. J. Miner. Process.* **2013**, *124*, 145–149. [CrossRef]
48. Bulut, G. Recovery of copper and cobalt from ancient slag. *Waste Manage. Res.* **2006**, *24*, 118–124. [CrossRef] [PubMed]
49. Potysz, A.; Kierczak, J.; Fuchs, Y.; Grybos, M.; Guibaud, G.; Lens, P.N.L.; Hullebusch, E.D.V. Characterisation and pH-dependent leaching behaviour of historical and modern copper slags. *J. Geochem. Explor.* **2016**, *160*, 1–15. [CrossRef]
50. Gargul, K. Ammonia leaching of slag from direct-to-blister copper smelting technology. *AIMS Mater. Sci.* **2020**, *7*, 565–580. [CrossRef]
51. Zhang, S.; Zhu, N.; Shen, W.; Wei, X.; Li, F.; Ma, W.; Mao, F.; Wu, P. Relationship between mineralogical phase and bound heavy metals in copper smelting slags. *Resour. Conserv. Recycl.* **2022**, *178*, 106098. [CrossRef]
52. Zhao, Z.; Wang, Z.; Peng, N.; Peng, B.; Liang, Y.; Qu, S.; Dong, Z.; Zeng, W. Copper behavior and fayalite microstructure changes influenced by Cu2O dissolution. *JOM* **2019**, *71*, 2891–2898. [CrossRef]
53. Zhou, S.; Wei, Y.; Li, B.; Wang, H. Effect of Iron Phase Evolution on Copper Separation from Slag Via Coal-Based Reduction. *Metall. Mater. Trans. B* **2018**, *49*, 3086–3096. [CrossRef]
54. Kim, B.S.; Jo, S.K.; Shin, D.; Lee, J.C.; Jeong, S.B. A physico-chemical separation process for upgrading iron from waste copper slag. *Int. J. Miner. Process.* **2013**, *124*, 124–127. [CrossRef]
55. Shamsi, M.; Noparast, M.; Shafaie, S.Z.; Gharabaghi, M.; Aslani, S. Effect of grinding time on flotation recovery of copper smelting slags in Bardaskan district. *J. Min. Environ.* **2015**, *6*, 237–249.
56. Andreev, G.N.; Barzev, A. Raman spectroscopic study of some chalcopyrite–xanthate flotation products. *J. Mol. Struct.* **2003**, *661–662*, 325–332. [CrossRef]
57. Li, H.; Oraby, E.; Eksteen, J. Cyanide consumption minimisation and concomitant toxic effluent minimisation during precious metals extraction from waste printed circuit boards. *Waste Manag.* **2021**, *125*, 87–97. [CrossRef]
58. Liu, G.; Zhong, H.; Dai, T.-G. The separation of Cu/Fe sulfide minerals at slightly alkaline conditions by using ethoxycarbonyl thionocarbamates as collectors: Theory and practice. *Miner. Eng.* **2006**, *19*, 1380–1384. [CrossRef]
59. Buckley, G.A.; Hope, G.; Lee, K.C.; Petrovic, E.A.; Woods, R. Adsorption of O-isopropyl-N-ethyl thionocarbamate on cu sulfide ore minerals. *Miner. Eng.* **2014**, *69*, 120–132. [CrossRef]
60. Wills, B.A.; Finch, J.A. *Wills' Mineral Processing Technology—An Introduction to the Practical Aspects of Ore Treatment and Mineral Recovery*, 8th ed.; Elsevier Science & Technology Books; Elsevier: Amsterdam, The Netherlands, 2016.
61. Štirbanović, Z.; Urošević, D.; Đorđević, M.; Sokolović, J.; Aksič, N.; Živadinović, N.; Milutinović, S. Application of thionocarbamates in copper slag flotation. *Metals* **2022**, *12*, 832. [CrossRef]
62. Herreros, O.; Quiroz, R.; Manzano, E.; Bou, C.; Viñals, J. Copper extraction from reverberatory and flash furnace slags by chlorine leaching. *Hydrometallurgy* **1998**, *49*, 87–101. [CrossRef]
63. Kundu, T.; Senapati, S.; Das, S.K.; Angadi, S.I.; Rath, S.S. A comprehensive review on the recovery of copper values from copper slag. *Powder Technol.* **2023**, *426*, 118693. [CrossRef]
64. Hara, Y.; Jha, A. Carbothermic Processing of Copper–Cobalt Mineral Sulphide Concentrates and Slag Waste for the Extraction of Metallic Values. In *Sustainability in the Mineral and Energy Sectors*; CRC Press: Boca Raton, FL, USA, 2016; Chapter 7; pp. 105–124.
65. Feng, Q.; Zhao, W.; Wen, S. Surface modification of malachite with ethanediamine and its effect on sulphidisation flotation. *Appl. Surf. Sci.* **2018**, *436*, 823–831. [CrossRef]
66. Wu, D.D.; Mao, Y.B.; Deng, J.S.; Wen, S.M. Activation mechanism of ammonium ions on sulfidation of malachite surface by DFT study. *Appl. Surf. Sci.* **2017**, *410*, 126–133. [CrossRef]
67. Anand, S.; Rao, K.S.; Jena, P.K. Pressure leaching of copper converter slag using dilute sulphuric acid for the extraction of cobalt, nickel and copper values. *Hydrometallurgy* **1983**, *10*, 305–312. [CrossRef]
68. Sukla, L.B.; Panda, S.C.; Jena, P.K. Recovery of cobalt, nickel and copper from converter slag through roasting with ammonium sulphate and sulphuric acid. *Hydrometallurgy* **1986**, *16*, 153–165. [CrossRef]
69. Basir, S.M.A.; Rabah, M.A. Hydrometallurgical recovery of metal values from brass melting slag. *Hydrometallurgy* **1999**, *53*, 31–44. [CrossRef]
70. Bese, A.V. Effect of ultrasound on the dissolution of copper from copper converter slag by acid leaching. *Ultrason. Sonochem.* **2007**, *14*, 790–796. [CrossRef] [PubMed]
71. Baghalha, M.; Papangelakis, V.G.; Curlook, W. Factors affecting the leachability of Ni/Co/Cu slags at high temperature. *Hydrometallurgy* **2007**, *85*, 42–52. [CrossRef]

72. Mussapyrova, L.; Nadirov, R.; Bal, P.; Raj, M.; Bure, R.; Bal, M. Selective room-temperature leaching of copper from mechanically activated copper smelter slag. *J. Mater. Res. Technol.* **2021**, *12*, 2011–2025. [CrossRef]
73. Tshiongo, N.; Mbaya, R.K.K.; Maweja, K.; Tshabalala, L.C. Effect of Cooling Rate on base Metals Recovery from Copper Matte Smelting Slags. *World Acad. Sci. Eng. Technol.* **2010**, *4*, 236–240.
74. Li, H.; Deng, Z.; Oraby, E.; Eksteen, J. Amino acids as lixiviants for metals extraction from natural and secondary resources with emphasis on glycine: A literature review. *Hydrometallurgy* **2023**, *216*, 106008. [CrossRef]
75. Eksteen, J.J.; Oraby, E.A.; Nguyen, V. Leaching and ion exchange based recovery of nickel and cobalt from a low grade, serpentine-rich sulphide ore using an alkaline glycine lixiviant system. *Miner. Eng.* **2020**, *145*, 106072. [CrossRef]
76. Huang, Y.; Wang, D.; Liu, H.; Fan, G.; Peng, W.; Cao, Y. Selective complexation leaching of copper from copper smelting slag with the alkaline glycine solution: An effective recovery method of copper from secondary resource. *Sep. Purif. Technol.* **2023**, *326*, 124619. [CrossRef]
77. Oraby, E.A.; Li, H.; Eksteen, J.J. An Alkaline Glycine-Based Leach Process of Base and Precious Metals from Powdered Waste Printed Circuit Boards. *Waste Biomass Valorization* **2019**, *11*, 3897–3909. [CrossRef]
78. Guo, H.Z.X.; Jia, J.; Yang, J.; Meng, X. Density functional theory study on coordination ability of glycine and the first series transition metals. *J. Nanjing Univ. Nat. Sci.* **2019**, *55*, 1040–1046. [CrossRef]
79. Anand, S.; Rao, P.K.; Jena, P.K. Recovery of metal values from copper converter and smelter slags by ferric chloride leaching. *Hydrometallurgy* **1980**, *5*, 355–365. [CrossRef]
80. Borisov, V.A.; D'yachenko, A.N.; Kraidenko, R.I. Reaction of ammonium chloride with the copper (II) sulfide and oxide, and identification of the reaction products. *Russ. J. Gen. Chem.* **2011**, *81*, 1430–1433. [CrossRef]
81. Nadirov, R.K.; Syzdykova, L.; Zhussupova, A. Copper smelter slag treatment by ammonia solution: Leaching process optimisation. *J. Cent. South Univ.* **2017**, *24*, 2799–2804. [CrossRef]
82. Aracena, A.; Fern´andez, F.; Jerez, O.; Jaques, A. Converter slag leaching in ammonia medium/column system with subsequent crystallisation with NaSH. *Hydrometallurgy* **2019**, *188*, 31–37. [CrossRef]
83. Sari, Z.A.; Turan, M.D. Leaching of copper slags by direct photooxidation mechanism using ultraviolet light. *J. Cent. South Univ.* **2024**, *31*, 1476−1493. [CrossRef]
84. Deng, B.; Li, X.; Zhang, Y. Photochemical redox transformation of iron–oxalate complexes under UV irradiation and its implications for aqueous metal systems. *J. Photochem. Photobiol. A Chem.* **2018**, *364*, 617–625. [CrossRef]
85. Zhang, H.; Wang, G.; Zhang, S. Direct reduction kinetics of copper slag. *Nonferrous Met. Sci. Eng.* **2019**, *10*, 28–33.
86. Lan, C.; Zhang, S.; Liu, R.; Lyu, Q.; Yan, G.; Wang, B. Thermodynamic and kinetic behaviours of copper slag carbothermal reduction process. *Ironmak. Steelmak. Process. Prod. Appl.* **2023**, *50*, 123–133. [CrossRef]
87. Tümen, F.; Bailey, N. Recovery of metal values from copper smelter slags by roasting with pyrite. *Hydrometallurgy* **1990**, *25*, 317–328. [CrossRef]
88. Mututubanya, A. Cobalt Recovery from Old Nkana Copper Slag via Solid State Carbothermic Reduction and Sulphation. Master's Thesis, University of Zambia, Lusaka, Zambia, 2013.
89. Rudnik, E.; Burzyńska, L.; Gumowska, W. Hydrometallurgical recovery of copper and cobalt from reduction-roasted copper converter slag. *Miner. Eng.* **2009**, *22*, 88–95. [CrossRef]
90. Hamamci, C.; Ziyadanoğullari, B. Effect of roasting with ammonium sulfate and sulfuric acid on the extraction of copper and cobalt from copper converter slag. *Sep. Sci. Technol.* **1991**, *26*, 1147–1154. [CrossRef]
91. Ziyadanoğullari, R. A new method for recovering Fe(II) sulphate, copper, and cobalt from converter slag. *Sep. Sci. Technol.* **1992**, *27*, 389–398. [CrossRef]
92. Grudinsky, P.I.; Podjelnikova, E.S.; Dyubanov, V.G. Research on the process of sulphatizing roasting of copper slag flotation tailings using iron sulphates. *IOP Conf. Ser. Earth Environ. Sci.* **2020**, *459*, 042004. [CrossRef]
93. Acma, E.; Sesigur, H.; Addemir, O.; Tekin, A. Processing of Kure (Turkey) copper slag for the recovery of copper and cobalt and the production of gamma Fe_2O_3. *Trans. Indian Inst. Met.* **1997**, *50*, 147–151.

Disclaimer/Publisher's Note: The statements, opinions and data contained in all publications are solely those of the individual author(s) and contributor(s) and not of MDPI and/or the editor(s). MDPI and/or the editor(s) disclaim responsibility for any injury to people or property resulting from any ideas, methods, instructions or products referred to in the content.

minerals

MDPI

Article

Effects of Size and Mechanical Pre-Treatment on Aluminium Recovery from Municipal Solid Waste Incineration Bottom Ash

Mertol Gökelma [1,*], Utku Hatipoğlu [1], Alicia Vallejo-Olivares [2], Rabia Önen Tüzgel [1], Olcay Kıvrak [1], Elif Bazoğlu [1], Zeynep Su Çizen [1] and Gabriella Tranell [2]

[1] Department of Materials Science and Engineering, Izmir Institute of Technology, 35430 Izmir, Türkiye; utkuhatipoglu@iyte.edu.tr (U.H.); olcaykivrakk@gmail.com (O.K.)
[2] Department of Materials Science and Engineering, Norwegian University of Science and Technology, 7491 Trondheim, Norway; gabriella.tranell@ntnu.no (G.T.)
* Correspondence: mertolgokelma@iyte.edu.tr

Abstract: Municipal solid waste (MSW) is incinerated to reduce the volume and recover energy and materials. The generation of MSW has been increasing over the past few decades due to the increase in population and changing consumption habits. Rising environmental and economic concerns have increased the importance of waste treatment and recovery. Currently, MSW may take three alternate or parallel routes: direct recycling, incineration, or landfill, depending on the country and location. MSW incineration has three products in addition to energy: bottom ash, fly ash, and off-gas. After incineration, bottom ash usually still contains many materials to be recovered, such as glass, ceramics, and metals with a degree of oxidation. This study focuses on aluminium recovery from MSW incineration bottom ash from two different countries. The 2–30 mm fraction of aluminium particles was characterized in terms of its size, shape, and oxide thickness, and its effects on aluminium recovery were investigated. In addition, the ability of mechanical pre-treatment to remove oxides prior to melting was studied. The results were compared with the analytical modeling developed in this study. An increasing particle size and surface area resulted in an increase in aluminium recovery. Mechanical pre-treatment increased the yield for smaller particles to a larger extent than larger particles due to the difference in the oxide/metal ratio.

Keywords: incineration; oxidation; solid waste; recycling; compaction

1. Introduction

The increasing population and changing consumption habits have resulted in a growing volume of municipal solid waste (MSW). The amount of MSW generated in the world annually is estimated to be 3.4 billion tonnes by 2050 [1]. MSW contains metal, ceramic, glass, plastic, and organic fractions. The widespread utilization of incineration applications for MSW in the solid waste management industry ensures an up to 90% reduction in volume and at least 70% reduction in mass compared to initial values due to the burning of organics [2].

End-of-life products are recycled, landfilled, and/or incinerated to various extents, depending on the country. Globally, around 19% of waste generated is recycled, and 11% is incinerated [3]. Direct recycling is the most effective process for material recovery. However, social behavior and governmental regulations directly affect the amount and type of metals being recycled. Metallic fractions oxidize and are contaminated by the surrounding materials, which reduces the recoverable amount of the metal. The rest of the waste is landfilled, which is the worst scenario for the environment due to soil acidification and contamination as well as the economic impact.

Figure 1 presents the recycling and incineration ratios of European countries in 2021. It can be observed that Norway, Finland, and Sweden incinerate more than 50% of their MSW.

On the other hand, Switzerland, Belgium, Luxembourg, Denmark, the Netherlands, Austria, Germany, Slovenia, and Italy recycle more than 50% of their MSW. These two groups of countries landfill less than 10% (except Italy ≈19%) of their total MSW. From the 32 countries given in Figure 1, 9 countries (Cyprus, Greece, Malta, Romania, Montenegro, North Macedonia, Albania, Türkiye, and Kosovo) landfill more than 70% of their MSW which corresponds to approximately 40 million tons of MSW landfilled.

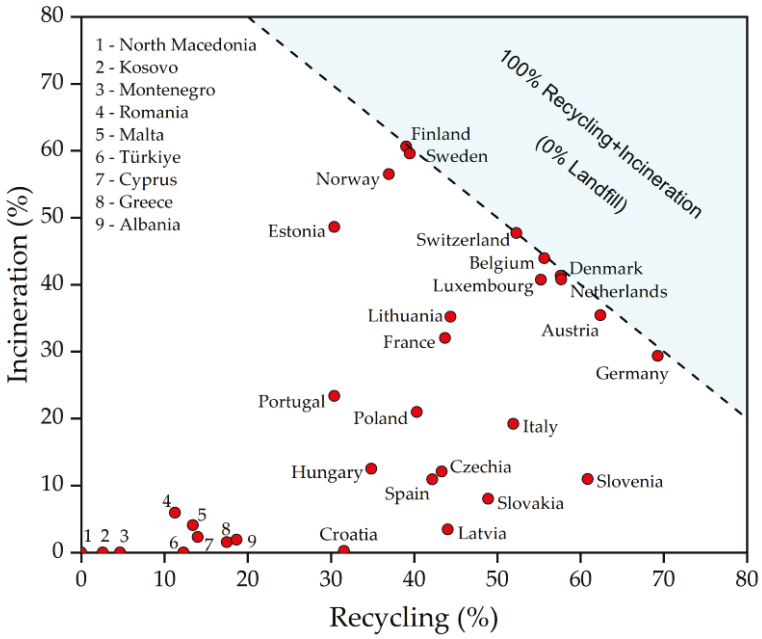


Figure 1. Incineration and recycling ratios of MSW in 2021 (data: Eurostat) [4].

Figure 2 presents the annual municipal waste generation per country as a function of their gross domestic product (GDP). Although a linear correlation cannot be seen, it can be stated that countries generate more waste with increasing GDP. Only Sweden and the Netherlands are among the countries with a higher GDP than the EU (European Union) and generate less waste than the EU on average.

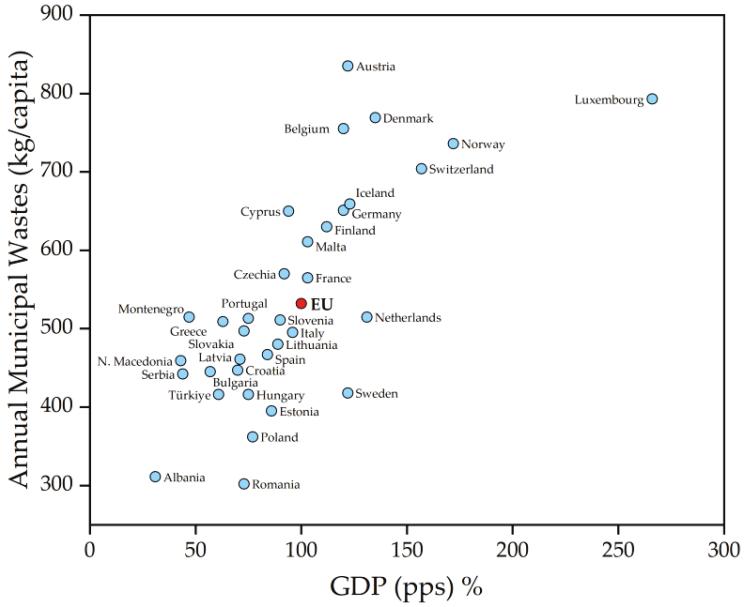


Figure 2. Annual MSW production per capita in comparison with the GDP of different European countries in 2021 (Data: Eurostat) [4].

Municipal solid waste incineration (MSWI) can be converted using three different types of combustion devices: rotary furnaces, fluidized beds, and grate incinerators. European MSWI is predominantly performed in grate-firing-type incinerators. The waste is introduced into the furnace and is carried by the moving grate through the incineration zone and discharged after the incineration is completed. The average temperature on the bed surface is approximately 900 °C; however, the temperature distribution in such furnaces is heterogeneous [5]. Bunge reported that 80% of materials during incineration are subjected to temperatures between 700 °C and 1100 °C [6].

The outputs of a MSW incineration process are heat, off-gas, bottom ash, and fly ash [7]. Both ashes represent the unburned fractions of the waste. Fly ash is mainly fine oxidic particles collected on the way to the chimney [8]. Bottom ash consists of larger particles, including ceramic, glass, and metals [9]. The bottom ash is sorted by the type of materials, such as glass, ceramic, aluminium, iron, and copper [10]. In addition, due to the wide range of particle size, the ash is also sorted according to size. While the size fraction below 2 mm can be used in construction materials, fractions over 2 mm contain a significant number of metals to be recovered [11].

Warrings and Fellner reported that approximately 11 wt.% of the aluminium is lost due to oxidation in incineration plants [12]. Chen et al. [13] investigated the metallic aluminium content of the aluminium fraction in bottom ash for sizes between 0.5 and 1.6 mm, and an aluminium content of 6 to 71 wt.% was reported. Gökelma et al. reported that the oxide thickness of the aluminium fraction in bottom ash was 68 μm on average, but no correlation was found between the oxide thickness and particle size or origin [14]. Vallejo Olivares et al. reported a life cycle assessment of the recycling of waste streams, including bottom ash in rotary furnaces. The study concluded that recycling 1 tonne of waste streams with a metal yield of 72% saves 13.2 t CO_2 eq [15]. Syvertsen et al. studied the yield and composition of aluminium bottom ash particle ranging from 5 to 50 mm (mostly in the range of 5–25 mm). Heavy elements such as Pb, Hg, Bi, Cd, and Sb were detected from one to several hundred ppm, and a 90% to 96% metal yield was reported [16]. Marthinsen et al. assessed the possibility of AlSi10Mg alloy production from bottom ash. Salt treatment and arc remelting were both applied, and with Si and Mg additions the AlSi10Mg alloy was obtained. Studies regarding economic feasibility and impurity issues are still ongoing [17]. MSW and its fractions in bottom ash are very heterogeneous in terms of composition and size, which makes characterization very difficult and limits the modeling of expected efficiencies. Therefore, more measurements and characterization studies are needed to better understand the recyclability of these types of materials.

This study investigates the effects of size, shape, and the mechanical pre-treatment of the MSWI aluminium fraction on the formed oxide thickness during the incineration procedure and metal yield. Aluminium fractions from two countries (the United Kingdom and the United States of America) were remelted before and after compaction as a form of pre-treatment to assess the metal yield. The samples were analyzed under computed tomography (CT) analysis and Scanning Electron Microscope (SEM), and their oxide thicknesses were measured using ImageJ (version 1.54g) software. EDS and XRF analysis were performed to measure the composition of the oxide layer. An analytical model was developed to approximate the metal yield results, and a model was proposed that is independent of the bottom ash source. Predicted aluminium yield values for particles that are 1 to 30 mm with an oxide layer of up to 500 μm are shown.

2. Materials and Methods

2.1. Materials

The bottom ash samples used in this study were received from a European recycling company. Samples were collected from incinerators in the USA and the UK and dry-sorted. Industrial sorting was achieved in three size groups, which were 2–6, 6–12, and 12–30 mm. However, due to industrial sorting techniques and the heterogeneity of the material, further separation of glass, dust, ferrous, and non-ferrous fractions in the bottom

ash was performed manually as part of the current study. Compaction was applied for some bottom ash samples under 100 kN for 5 s to observe the effects of compaction.

2.2. Remelting

The sample size groups from different sources were remelted in a laboratory-scale resistance chamber furnace at 800 °C. In addition, 2–6 and 6–12 mm fractions were compacted into cylindrical briquettes using uniaxial pressure to see the effect of compaction on the metal yield. A clay-bonded graphite crucible with a volume of 0.3 lt was used for remelting. The remelting was carried out under a salt flux to remove the thick oxide layer and prevent further metal losses during melting. The salt flux consisted of chlorides NaCl-KCl (70:30 wt.%) and 2 wt.% CaF_2 was added to promote coagulation. After melting, the melt in the crucible was stirred with a graphite rod and the crucible was allowed to cool in the furnace. After cooling to room temperature, the salt dross was washed out, and the metal fraction was collected.

2.3. Characterization

The samples in all size ranges were analyzed using the image analysis program ImageJ to calculate their 2D surface area, perimeter, and circularity. Three samples were randomly selected from each size range and origin and mounted in epoxy. After sanding and polishing, the cross-section of samples was analyzed under SEM, and oxide layer thicknesses were measured from at least 40 positions from each sample. EDS and XRF analysis were used to assess the composition of the oxide layer of the samples. In addition, compacted bottom ash samples were analyzed using CT to observe the compaction degree and internal porosity.

2.4. Analytical Modeling

An analytical model was developed, which is valid for a broad size range of particles and oxide layers. This model covers most of the oxide/metal ratios possible during incineration. The results were obtained by calculating the oxide mass of bottom ash samples by changing the diameter of the sample and the thickness of the oxide. Particles as shown in Figure 3 with a radius of "r" with an oxide thickness of "x" were used for the model, where r ranges from 1 to 30 mm and x is 10 to 500 μm. The assumptions made for the model are shown below:

- Bottom ash particles are spherical;
- Oxide and metal phases have the same porosity value;
- Oxide thickness is the same throughout the entire surface;
- The density of the metal alloy is 2.7 g/cm^3;
- The density of the oxide layer is 3.99 g/cm^3.

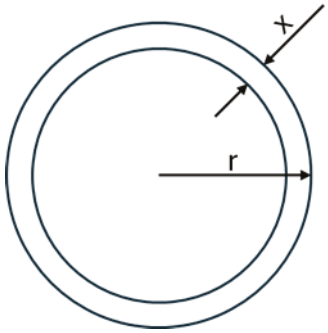


Figure 3. Schematic of a spherical bottom ash particle with an oxide layer.

The mass of the outer oxide layer and the metal core were calculated by multiplying the volume and density of each. The metal yield was calculated by the ratio of metal to the entire sample, as shown in Equation (1). ρ_{Al} is the density of aluminium, ρ_{oxide} is the

density of the oxide layer, π is the number of pi, r is the radius of the sample, and x is the thickness of the oxide layer.

$$\text{Predicted Metal Yield} = \frac{\rho_{Al} \cdot {}^{4}/_{3}\pi(r-x)^{3}}{\rho_{Al} \cdot {}^{4}/_{3}\pi(r-x)^{3} + \rho_{oxide} \cdot {}^{4}/_{3}\pi\left(r^{3} - (r-x)^{3}\right)} \quad (1)$$

3. Results and Discussion

The length and surface area of samples from the aluminium fraction were characterized using ImageJ image analysis software, and samples were sorted into four groups for each country. Figure 4 presents the picture of three samples from the USA, which was used for image analysis. The same process was conducted for every particle group, and, in total, 1150 samples were analyzed.

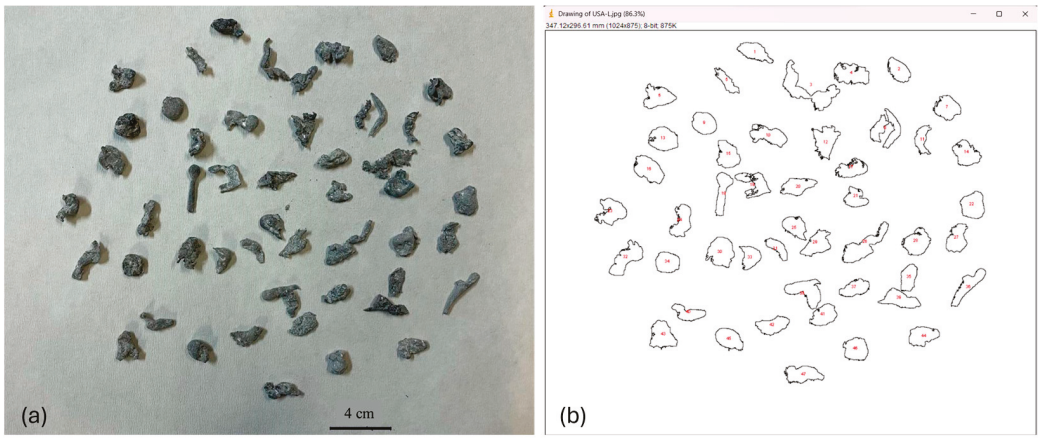


Figure 4. (**a**) A representative picture of the USA 3-sample group; (**b**) image analysis screen shot of the samples.

Figure 5 shows the computed tomography analysis picture of compacted bottom ash samples. It can be observed from the picture that the direct contact of samples was achieved. Also, glass contamination could be observed in the structure, which is common due to the inefficient sorting of fractions. The internal porosity was measured as 22%, which is acceptable due to the high content of hard oxides on the surface. Due to the high hardness of oxides, cracked oxides were observed in powder form during compaction. In total, 1.4 ± 0.4 wt.% weight loss was observed in 18 compaction tests. The collected powder was analyzed by XRF. XRF results showed that the powder consisted of 31% Al_2O_3, 27% SiO_2, 16% CaO, 3% Fe_2O_3, and 3% Na_2O (in wt.%), which are typical oxides found on aluminium scraps and incinerated waste.

Table 1 shows the length and surface area of the samples as well as their metal yield values after remelting under salt flux. The length was measured by taking the longest axis of the sample, which is an area that represents the two-dimensional area of the samples, as seen in Figure 4b. The aluminium yield after remelting the bottom ash samples was calculated using Equation (2).

$$\text{Metal Yield} = \frac{m_{\text{recovered Al}}}{m_{\text{input Al}-\text{fraction}}} \times 100\% \quad (2)$$

where $m_{\text{input Al-fraction}}$ is the total mass of charged bottom ash samples and $m_{\text{recovered Al}}$ is the mass of all aluminium droplets recovered via salt remelting. The metal yield was found to be between 71.9 and 95.7 wt.% depending on the size, which is in line with previous studies, which showed yields of 76–93 [14] and 83–92 wt.% [18].



Figure 5. CT analysis of bottom ash samples compacted by uniaxial pressure.

Table 1. Maximum length and surface area measurements of aluminium fraction samples.

	Av. Axis Length (mm)	Std of Length (%)	Av. 2D Area (mm^2)	Std of Area (%)	Al Yield (%)	Al Yield after Compaction (%)
USA 1	5	2.82	77	58.31	71.91	77.6
UK 1	5.6	2.29	76	62.37	77.15	80.1
USA 2	8.6	2.57	164	43.60	81.30	83.8
UK 2	9.3	2.66	155	44.32	82.96	83.2
USA 3	14.3	1.68	277	32.56	86.59	-
UK 3	15.9	1.55	217	26.04	83.53	-
USA 4	27.9	2.93	357	35.57	95.67	-
UK 4	28	2.76	353	29.18	91.84	-

Figure 6 shows the metal yield of the four fractions from the two countries shown in Table 1 as a function of size. Each particle was measured as mentioned above, and the average of their longest length (with a standard deviation of 1.55% to 2.93%) used is shown in Figure 6. A clear trend can be observed with an R^2 value of 0.88, which indicated that increasing the size of the aluminium fraction in bottom ash results in a higher metal yield. An almost 25% yield difference was observed between a 5 and 28 mm particle length. For the mentioned size range, a linear yield difference is expressed, as shown below:

$$\text{Metal yield} = 0.0775\text{L} + 0.7278 \quad (3)$$

where, metal yield is calculated via Equation (2) and L is the max length of the sample calculated via ImageJ.

Further investigation was conducted to determine the effect of surface area on the metal yield. Figure 7 shows an increase in metal yield with an increase in surface area similar to the trend seen between metal yield and length; however, a deviation in surface area measurements was observed between 26% and 62% due to for the irregular shape of the bottom ash particles. Due to high deviation in surface area measurements, it is recommended to use the length instead of the area to define the relation. The linear trend with an R^2 value of 0.8668 can be expressed as follows:

$$\text{Metal yield} = 0.0635\text{L} + 0.7058 \quad (4)$$

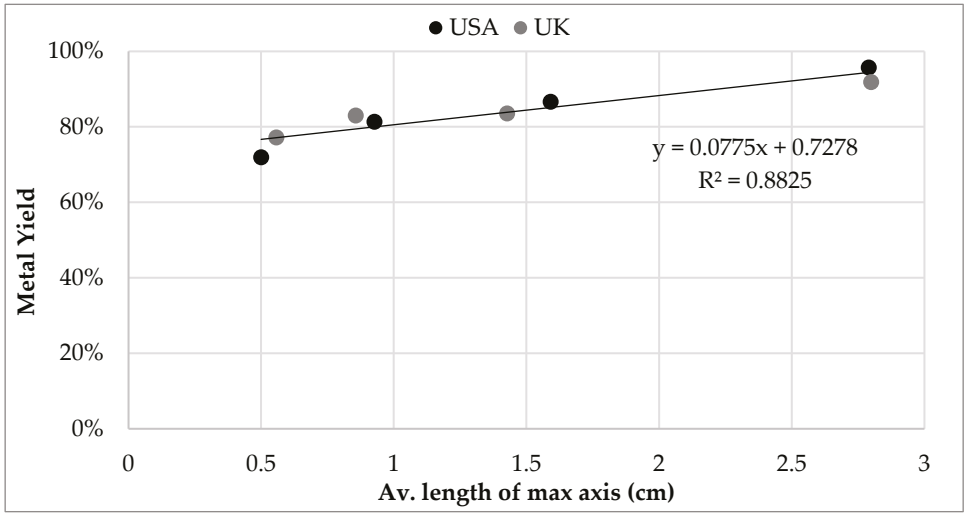


Figure 6. Metal yield of each size fraction as a function of the average max axis of samples.

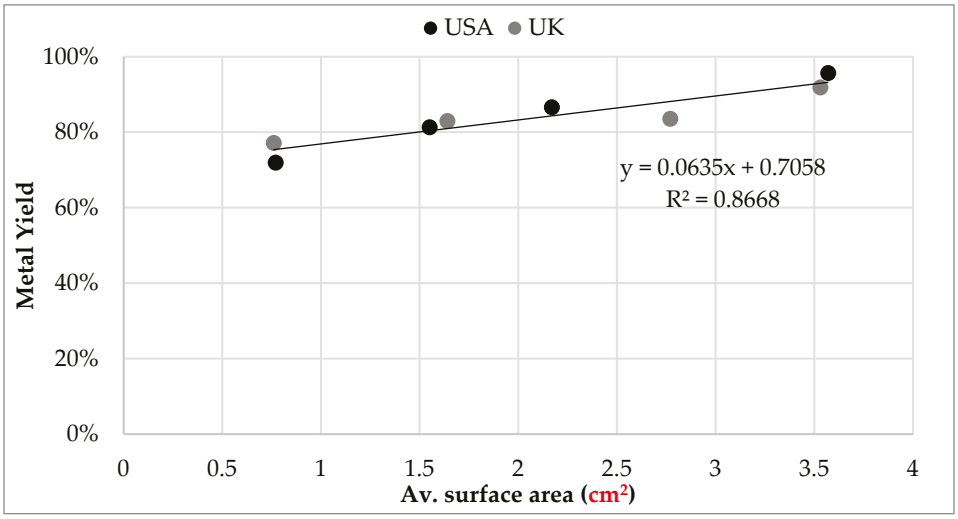


Figure 7. Metal yield of each size fraction as a function of the average surface area of samples.

Figure 8 presents each oxide thickness measurement under SEM for bottom ash samples from UK and USA. Multiple SEM pictures were taken from each sample, and random locations were measured.

Table 2 summarizes the 906 measurements performed using ImageJ in terms of the oxide thickness fractions. The thickness results were grouped as <40, <50, 50–100, and >100 µm. In total, 63.5% of all measurements were below 50 µm, 25.9% were between 50 and 100 µm, and 10.6% were thicker than 100 µm. The mean thickness value of all 906 measurements was 70 µm. A significant difference between UK and USA samples were not observed in terms of oxide thickness distribution.

Table 2. Oxide thickness distribution in all samples.

Oxide Thickness (µm)	UK (% of Samples)	USA (% of Samples)	Average, All Samples (%)
<40	53.6	51.9	52.1
<50	64.6	62.3	63.5
50–100	23.4	28.7	25.9
>100	12.0	9.0	10.6

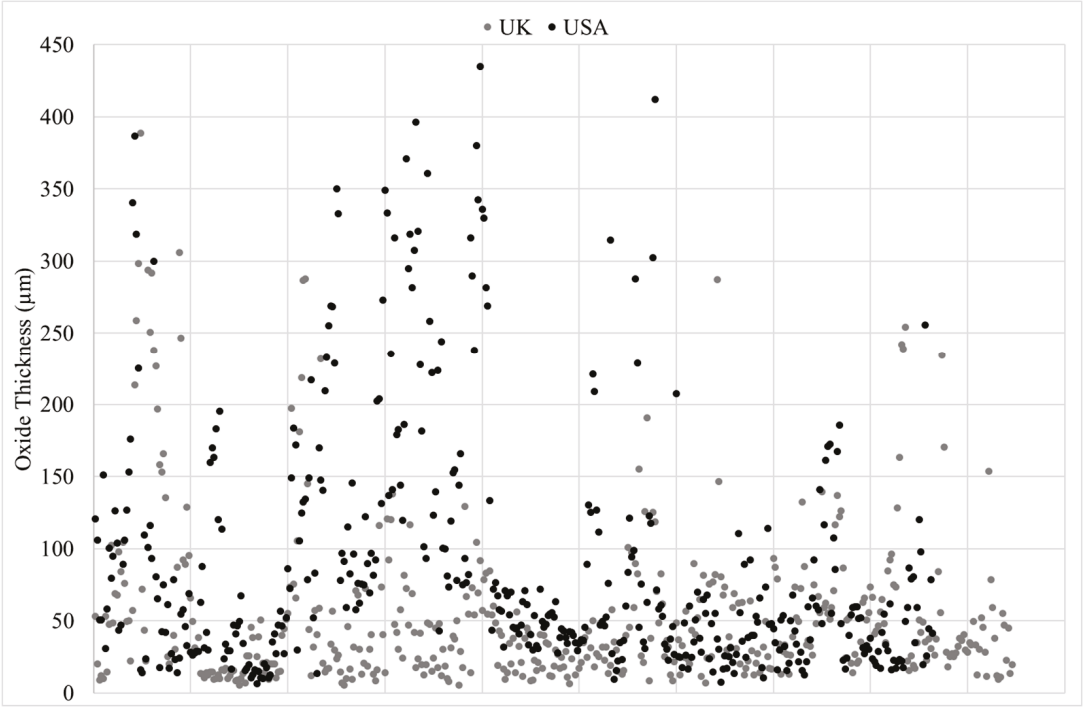


Figure 8. Oxide thickness measurement for 906 measurement points of samples from the UK and USA.

Figure 9 shows a typical cross-section of an aluminium sample in bottom ash. The oxide layer can be clearly seen in a darker color. The layer is not homogeneous, and the thickness varies throughout the surface.

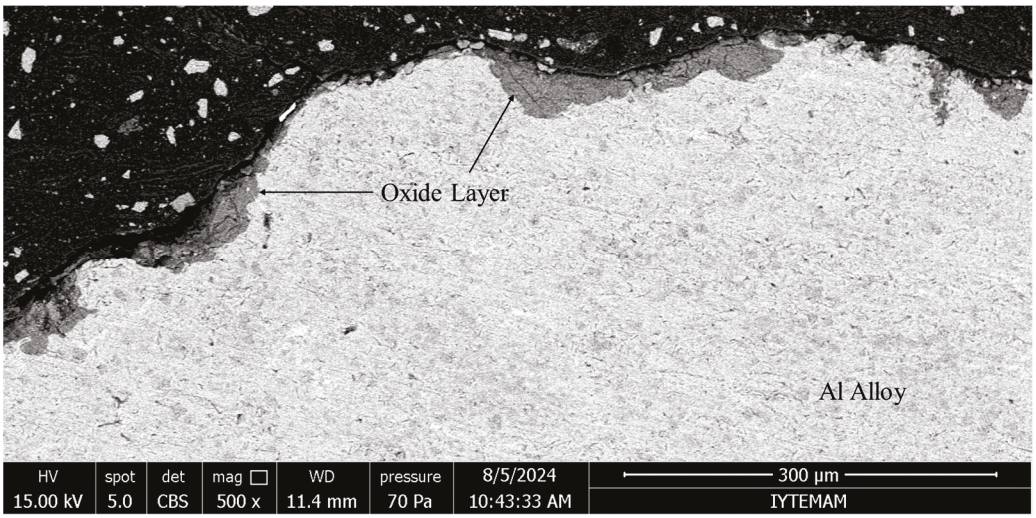


Figure 9. SEM image of the cross-section of a representative bottom ash sample.

The oxide layer of the samples was analyzed by EDS. A high oxygen and aluminium content were observed in all samples, as expected, due to the heavy oxidation of aluminium during incineration. Na, K, and Cl were found in all samples. Cl content mainly originates from PVC, food waste, and batteries [19]. This can lead to HCl formation during the remelting of the aluminium fraction, and thermal decomposition up to 600 °C can lead to molecular Cl_2 [20]. In addition, bottom ash materials, especially fine fractions, can be used in secondary building materials, but the Cl content becomes a challenge due to strict regulations for building materials [21]. Chloride content can be found at up to 5 wt.% depending on the fraction and size of the sample [22]. Sulphur content in the samples can

also lead to the formation of harmful gasses, which should be taken into account during recycling/remelting processes.

Analytical Modeling

Figure 10 presents the modeling results for bottom ash particles from 1 to 30 mm in diameter with an oxide layer of up to 500 µm. Increasing the sample size and decreasing oxide thickness increases the metal yield due to the decreasing oxide/metal mass ratio. The predicted yields for 70 µm (mean value of measured samples) oxide thickness are 55% for 1 mm, 74% for 2 mm, 89% for 5 mm, 94% for 10 mm, 97% for 20 mm, and 98% for 30 mm aluminium samples. The degree of oxidation becomes more important with the decreasing sample size and effects the metal yield significantly.

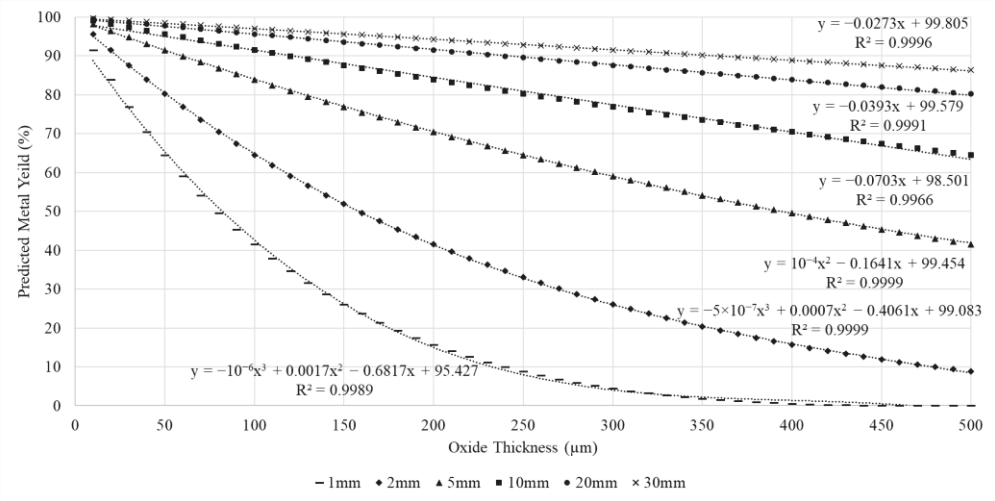


Figure 10. Metal yield predictions of changing particle size and oxide thickness.

In order to compare the modeling results with experimental results, calculations were also conducted for the average particle sizes used in the remelting experiments. Table 3 presents the modelling results where x is oxide thickness (mm) and y represents the predicted metal losses.

Table 3. Trendlines calculated by the analytical model for the average particle sizes used in remelting experiments.

Average Particle Size (mm)	Formula	R^2	Equation
9	$y = -2 \times 10^{-8} \times 3 + 5 \times 10^{-5}x^2 - 0.0982x + 99.992$	1	(5)
15	$y = -0.0505x + 99.281$	0.9984	(6)
28	$y = -0.029x + 99.778$	0.9995	(7)

Figure 11 shows the metal yield results calculated by the model for particles with a homogenous oxide thickness of 70 µm and the results from the remelting experiments. The predicted yield is higher than the experimental results for all sizes. The main reason for this difference is the effect of particle shape. Particles are assumed to be spherical in the modeling, and a spherical shape has a lower specific surface area than the real shape of bottom ash particles. The lower specific surface area results in a lower mass of oxides in comparison with the metal. However, the difference between the model and experiments decreases with increasing particle sizes. This is due to the decreasing oxide/metal mass ratio with increasing particle size. It can also be observed that the yield after compaction increases up to 5% due to the loss of the oxide layer during compaction. Compaction works like mechanical pre-treatment, decreasing the non-metal content. However, this

effect decreases with increasing size due to the decreasing oxide/metal ratio. The rafination of the recovered aluminium alloy melt must be improved in further studies since the composition of the recovered alloy may change depending on the season, location, and treatment. The mechanical pre-treatment of bottom ash must be further studied to increase the yield and decrease the usage of salt flux for more sustainable recycling processes.

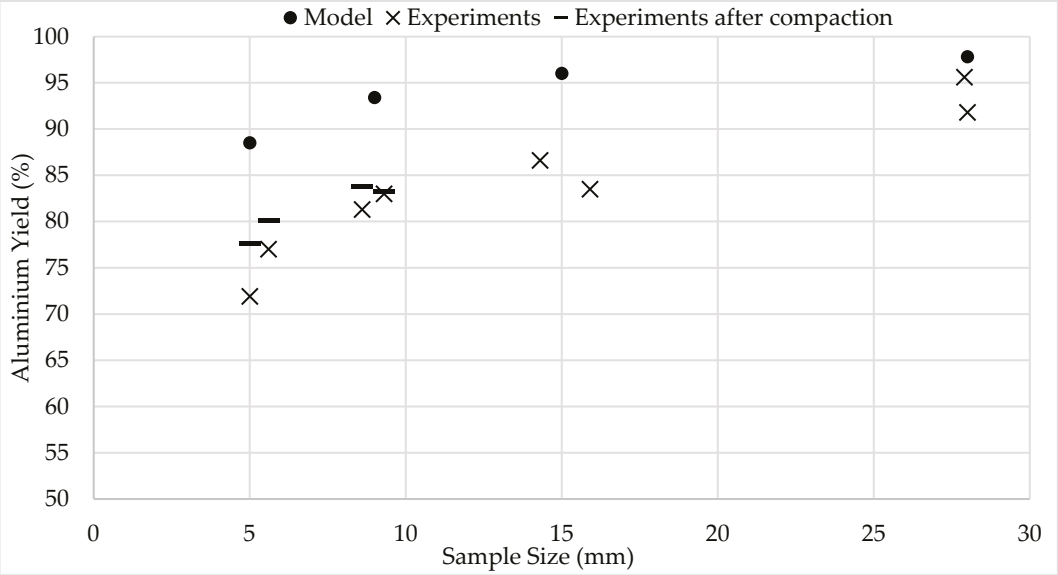


Figure 11. Comparison of the metal yield results calculated by the analytical model and measured by experiments.

4. Conclusions

The effect of particle size, shape, and mechanical pre-treatment has been experimentally studied, and an analytical model has been developed. The following conclusions can be drawn as a result of the research:

- The particle length and surface area have a linear correlation with recoverable aluminium content for bottom ash particles between a 2 and 30 mm fraction.
- Mechanical pre-treatment decreased the oxide content by cracking the oxides, which increased the aluminium yield. However, this effect became less significant with increasing particle size due to a decrease in oxide/metal ratio.
- The analytical model showed a 5% to 15% higher yield for particles with an average size of 28 to 5 mm, respectively. The difference between the model and experiments originated due to the specific surface area difference in spherical to irregular particles.

Author Contributions: M.G.: conceptualization, data curation, formal analysis, methodology, project management, validation, and writing—original draft; M.G. and G.T.: conceptualization, methodology, supervision, validation, and writing—review and editing; A.V.-O. and U.H.: data curation, investigation, methodology, visualization, and writing—review and editing; R.Ö.T., O.K., E.B. and Z.S.Ç.: investigation, methodology, and validation. All authors have read and agreed to the published version of the manuscript.

Funding: This research received no external funding.

Data Availability Statement: The data are contained within the article.

Acknowledgments: The Center for Materials Research at İzmir Institute of Technology is gratefully acknowledged for the sample analyses. The Environmental Research Center at İzmir Institute of Technology is gratefully acknowledged for metal analyses.

Conflicts of Interest: The authors declare there are no conflicts of interests.

References

1. Kaza, S.; Yao, L.; Bhada-Tata, P.; Van Woerden, F. *What a Waste 2.0: A Global Snapshot of Solid Waste Management to 2050*; World Bank Publications: Washington, DC, USA, 2018.
2. Kumar, S.; Singh, D. Municipal solid waste incineration bottom ash: A competent raw material with new possibilities. *Innov. Infrastruct. Solut.* **2021**, *6*, 201. [CrossRef]
3. Joseph, A.M.; Snellings, R.; Nielsen, P.; Matthys, S.; De Belie, N. Pre-treatment and utilisation of municipal solid waste incineration bottom ashes towards a circular economy. *Constr. Build. Mater.* **2020**, *260*, 120485. [CrossRef]
4. Eurostat. Municipal Waste by Waste Management Operations. Available online: https://ec.europa.eu/eurostat/databrowser/view/env_wasmun/default/table?lang=en (accessed on 16 August 2024).
5. Leckner, B.; Lind, F. Combustion of municipal solid waste in fluidized bed or on grate—A comparison. *Waste Manag.* **2020**, *109*, 94–108. [CrossRef] [PubMed]
6. Bunge, R. Recovery of Metals from Waste Incinerator Bottom Ash. 2016. Available online: www.vbsa.ch (accessed on 4 October 2024).
7. Chimenos, J.M.; Segarra, M.; Fernandez, M.A.; Espiell, F. Characterization of the bottom ash in municipal solid waste incinerator. *J. Hazard. Mater. A* **1999**, *64*, 211–222. [CrossRef]
8. Wu, H.Y.; Ting, Y.P. Metal extraction from municipal solid waste (MSW) incinerator fly ash—Chemical leaching and fungal bioleaching. *Enzyme Microb. Technol.* **2006**, *38*, 839–847. [CrossRef]
9. Stabile, P.; Bello, M.; Petrelli, M.; Paris, E.; Carroll, M.R. Vitrification treatment of municipal solid waste bottom ash. *Waste Manag.* **2019**, *95*, 250–258. [CrossRef] [PubMed]
10. Verbinnen, B.; Billen, P.; Van Caneghem, J.; Vandecasteele, C. Recycling of MSWI Bottom Ash: A Review of Chemical Barriers, Engineering Applications and Treatment Technologies. *Waste Biomass Valorization* **2017**, *8*, 1453–1466. [CrossRef]
11. Muchová, L. Wet Physical Separation of MSWI Bottom Ash. Ph.D. Thesis, TU Delft, Delft, The Netherlands, 2010.
12. Warrings, R.; Fellner, J. Current status of circularity for aluminum from household waste in Austria. *Waste Manag.* **2018**, *76*, 217–224. [CrossRef] [PubMed]
13. Chen, B.; Chen, J.; de Mendonça Filho, F.F.; Sun, Y.; van Zijl, M.B.; Copuroglu, O.; Ye, G. Characterization and mechanical removal of metallic aluminum (Al) embedded in weathered municipal solid waste incineration (MSWI) bottom ash for application as supplementary cementitious material. *Waste Manag.* **2024**, *176*, 128–139. [CrossRef] [PubMed]
14. Gökelma, M.; Vallejo-Olivares, A.; Tranell, G. Characteristic properties and recyclability of the aluminium fraction of MSWI bottom ash. *Waste Manag.* **2021**, *130*, 65–73. [CrossRef] [PubMed]
15. Olivares, A.V.; Pastor-Vallés, E.; Pettersen, J.B.; Tranell, G. LCA of recycling aluminium incineration bottom ash, dross and shavings in a rotary furnace and environmental benefits of salt-slag valorisation. *Waste Manag.* **2024**, *182*, 11–20. [CrossRef] [PubMed]
16. Syvertsen, M.; Ludwig, T.; Rist, S.; Ellingsen, K. Use of Incinerator Bottom Ash (IBA) in Aluminium Recycling. In *Light Metals 2022*; Eskin, D., Ed.; Springer International Publishing: Cham, Switzerland, 2022; pp. 1051–1055.
17. Marthinsen, A.; Graff, J.S.; Syvertsen, M.; Ellingsen, K.; M'Hamdi, M. Towards Formulation of AlSi10Mg Alloy from Incinerator Bottom Ash. In *Light Metals 2022*; Eskin, D., Ed.; Springer International Publishing: Cham, Switzerland, 2022; pp. 1056–1065.
18. Gökelma, M.; Meling, I.; Soylu, E.; Kvithyld, A.; Tranell, G. A method for assessment of recyclability of aluminum from incinerated household waste. In *Light Metals 2019*; Minerals, Metals and Materials Series; Springer International Publishing: Cham, Switzerland, 2019; pp. 1359–1365. [CrossRef]
19. Ma, W.; Wenga, T.; Frandsen, F.J.; Yan, B.; Chen, G. The Fate of Chlorine during MSW Incineration: Vaporization, Transformation, Deposition, Corrosion and Remedies. *Prog. Energy Combust. Sci.* **2020**, *76*, 100789. [CrossRef]
20. Frandsen, F.J.; Frandsen, F.J.; van Lith, S.C.; Korbee, R.; Yrjas, P.; Backman, R.; Obernberger, I.; Brunner, T.; Jöller, M. Quantification of the release of inorganic elements from biofuels. *Fuel Process. Technol.* **2007**, *88*, 1118–1128. [CrossRef]
21. Chandler, A.J.; Eighmy, T.T.; Hjelmar, O.; Kosson, D.S.; Sawell, S.E.; Vehlow, J.; van der Sloot, H.A.; Hartlén, J. *Municipal Solid Waste Incinerator Residues*; Elsevier: Amsterdam, The Netherlands, 1997.
22. Yang, S.; Saffarzadeh, A.; Shimaoka, T.; Kawano, T. Existence of Cl in municipal solid waste incineration bottom ash and dechlorination effect of thermal treatment. *J. Hazard. Mater.* **2014**, *267*, 214–220. [CrossRef] [PubMed]

Disclaimer/Publisher's Note: The statements, opinions and data contained in all publications are solely those of the individual author(s) and contributor(s) and not of MDPI and/or the editor(s). MDPI and/or the editor(s) disclaim responsibility for any injury to people or property resulting from any ideas, methods, instructions or products referred to in the content.

minerals

MDPI

Article

Recovery of Titanium from Red Mud Using Carbothermic Reduction and High Pressure Leaching of the Slag in an Autoclave

Srecko Stopic [1,*], Duško Kostić [1,2], Richard Schneider [1], Magnus Sievers [1], Florian Wegmann [1], Elif Emil Kaya [3], Mitar Perušić [2] and Bernd Friedrich [1]

[1] IME Process Metallurgy and Metal Recycling, RWTH Aachen University, 52056 Aachen, Germany; dkostic@metallurgie.rwth-aachen.de (D.K.); msievers@metallurgie.rwth-aachen.de (M.S.); fwegmann@metallurgie.rwth-aachen.de (F.W.); bfriedrich@metallurgie.rwth-aachen.de (B.F.)
[2] Faculty of Technology Zvornik, University of East Sarajevo, Karakaj 34A, 75400 Zvornik, Republic of Srpska, Bosnia and Herzegovina; mitar.perusic@tfzv.ues.rs.ba
[3] Department of Materials Science and Engineering, Norwegian University of Science and Technology, Høgskoleringen 1, 7034 Trondheim, Norway; elif.e.kaya@ntnu.no
* Correspondence: sstopic@metallurgie.rwth-aachen.de; Tel.: +49-17678261674

Abstract: Red mud is a by-product of alumina production, which is largely stored in landfills that can endanger the environment. Red mud, or bauxite residue, is a mixture of inorganic compounds of iron, aluminum, sodium, titanium, calcium and silicon mostly, as well as a large number of rare earth elements in small quantities. Although certain methods of using red mud already exist, none of them have been widely implemented on a large scale. This paper proposes a combination of two methods for the utilization of red mud, first by carbothermic reduction and then, by leaching under high pressure in an autoclave in order to extract useful components from it with a focus on titanium. In the first part of the work, the red mud was reduced with carbon at 1600 °C in an electric arc furnace, with the aim of removing as much iron as possible using magnetic separation. After separation, the slag is leached in an autoclave at different parameters in order to obtain the highest possible yield of titanium, aiming for the formation of titanium oxysulfate and avoiding silica gel formation. A maximal leaching efficiency of titanium of 95% was reached at 150 °C using 5 mol/L sulfuric acid with 9 bar oxygen in 2 h. We found that high-pressure conditions enabled avoiding the formation of silica gel during leaching of the slag using 5 mol/L sulfuric acid, which is a big problem at atmospheric pressure. Previously silica gel formation was prevented using the dry digestion process with 12 mol/L sulfuric acid under atmospheric pressure.

Keywords: direct reduction; leaching; titanium; slag

1. Introduction

Red mud (RM), also known as bauxite residue, is the sludge produced during the Bayer process of alumina production from bauxite ore. This sludge is a very complex mixture of compounds. With approximately 180 million tons produced annually, red mud has become one of the largest environmentally hazardous waste products, accumulating to a staggering 4 billion tons worldwide [1,2].

RM contains a high concentration of iron compounds, which can be significantly reduced through chemical reduction processes. Additionally, it has a notable amount of titanium compounds that can be utilized for titanium production. Furthermore, red mud contains rare earth elements and a significant amount of sodium oxide (Na_2O), the latter varying based on the washing efficiency in the Bayer process [3].

Due to its alkalinity and its chemical and mineralogical properties, red mud is classified as a toxic industrial waste that must be treated before discharge. Its environmental and

health impacts include land use (conventional disposal of red mud occupies large areas of potentially productive land), groundwater contamination, soil and plant properties (it impacts soil's physical properties and has ecotoxicological effects on plants), dust generation and health risks [4].

Over the years, researchers worldwide have extensively explored various economical methods for utilizing red mud. Investigated applications include [5–9]: stabilization material, adsorbents, catalyst preparation, metal recovery (such as iron, aluminum and titanium), radiopaque materials, ceramics, construction bricks, pigments and paints and cements.

However, large quantities of red mud are never treated due to high costs and transport difficulties. For instance, it is challenging to neutralize red mud if the refinery is far from seawater or mines experiencing Acid Mine Drainage (AMD) issues. Additionally, red mud produced by refineries is unsuitable for long-distance transport, and many proposed methods for its treatment are not economical. One of the sustainable ways to utilize red mud is the recovery of titanium using reduction and leaching techniques [1,10,11].

Reduction of metallic oxides is a crucial process in metallurgy, involving the conversion of metal oxides into their respective metals. This process is vital for extracting pure metals from their ores and is achieved through various methods, primarily involving chemical reduction. The general principle of reduction involves a reducing agent that reacts with the oxygen in the metal oxide, removing the oxygen and leaving behind the pure metal [12–14].

Carbothermic reduction and hydrogen reduction are both important methods for reducing metal oxides to metals, each with distinct processes and environmental impacts.

Carbothermic reduction uses carbon as a reducing agent, typically in the form of coke, charcoal or coal. The process involves heating the metal oxide with carbon at high temperatures in a furnace. The carbon reacts with the oxygen in the metal oxide to form carbon dioxide or carbon monoxide, resulting in the extraction of pure metal. This method is widely used in the production of metals like iron, lead and zinc, and is fundamental to the steel-making industry. The advantages of carbothermic reduction include its well-established technology and efficiency for large-scale production. However, it has significant drawbacks such as high energy consumption due to the need for very high temperatures and substantial CO_2 emissions, which contribute to environmental pollution and climate change [12,15–17].

The carbothermic reduction process of RM may be represented as the following reactions [18]:

$$3Fe_2O_3 + CO \rightarrow 2Fe_3O_4 + CO_2 \quad (1)$$

$$Fe_3O_4 + CO \rightarrow 3FeO + CO_2 \quad (2)$$

$$FeO + CO \rightarrow Fe + CO_2 \quad (3)$$

In contrast, hydrogen reduction uses hydrogen gas as the reducing agent. This method has potential applications in producing metals such as iron, copper and nickel, and is considered promising for green metallurgy and clean energy technologies. The key advantage of hydrogen reduction is its lower environmental impact, as the by-product is water instead of CO_2. It also aligns with sustainable and environmentally friendly practices. However, hydrogen reduction faces challenges such as the high cost of hydrogen gas production, which often relies on non-renewable energy sources, and the need for careful handling due to the flammability and explosiveness of hydrogen gas. Additionally, it is still in the development and optimization stage for large-scale industrial applications [19–23].

Overall, while carbothermic reduction remains the dominant method due to its established use and efficiency, hydrogen reduction offers a promising alternative that could significantly reduce environmental impacts and support sustainable development in the metallurgical industry.

Leaching is a crucial process in extractive metallurgy which is used to extract valuable metals from ores. It involves treating the ore with specific chemicals that react with the metal compounds to form soluble salts, while the impurities remain insoluble. These soluble salts can then be washed out from the ore and further processed to obtain pure

metal. The residual materials left behind after the valuable metals have been extracted are known as tailings [16,24–26].

However, leaching also has significant drawbacks, often resulting in large volumes of waste effluent and tailings. These waste products are frequently highly acidic or alkaline and can contain toxic substances, posing environmental and health risks [27,28].

Leaching processes can be applied in various ways, such as pressure leaching, atmospheric leaching and ultrasound-assisted leaching. Leaching is often performed at high temperatures to obtain better leaching efficiency. Despite its challenges, leaching remains a vital technique in the mining industry, providing a method to extract metals that might be otherwise economically or technically unfeasible to obtain through other means. Proper management and treatment of leaching effluents and tailings are essential to minimize the environmental impact and ensure the sustainability of this extraction method [28].

Several studies have explored methods for recovering valuable metals from red mud. One approach achieved high titanium (91%) and scandium (93%) recoveries through a multi-stage process involving leaching, hydrolysis and solvent extraction [29].

Another study utilized diluted sulfuric acid under atmospheric conditions, achieving a 64.5% recovery of titanium [30].

Additionally, a multi-step process involving pre-reducing-smelting and leaching achieved high recovery rates for iron (98.15%) and titanium dioxide (95.53%) with hydrochloric acid [14].

This paper presents a novel approach (Figure 1) for the utilization of red mud through the combination of carbothermic reduction and high-pressure autoclave leaching to recover valuable components, particularly titanium. By reducing red mud at 1600 °C and using magnetic separation to remove the iron, followed by optimized leaching under high-pressure conditions, the study addresses a key challenge in avoiding silica gel formation, which often hinders titanium recovery.

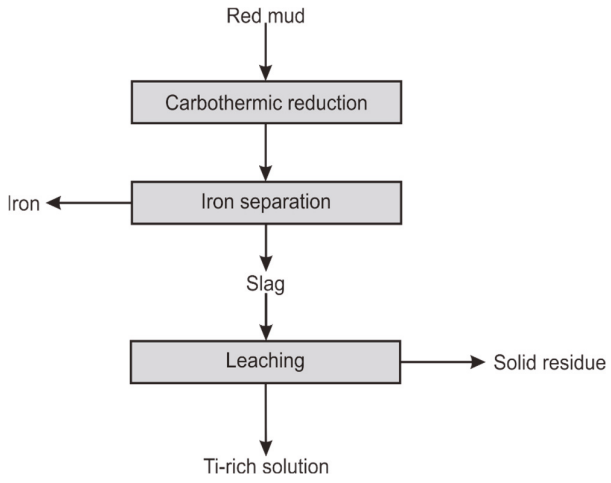


Figure 1. Design of research methodology.

Furthermore, the sustainability of this process lies in its ability to transform industrial waste into valuable raw materials. The reduction step not only removes the majority of the iron, which can be reused in the steel industry but also enriches other components like titanium, making them more accessible for further hydrometallurgical processing. Although carbothermic reduction uses high temperatures and carbon, it provides a means of significantly reducing red mud waste.

The main aim of this work is to treat our research strategy by combining the hydrometallurgical and pyrometallurgical treatment of red mud. The first step is the thermochemical modeling of carbothermic reduction in order to predict the chemical composition of produced slag, gases and metals.

2. Thermochemical Modeling

As it was already stated in the introduction part, thermodynamical modeling of the reduction of red mud is performed by the FactSage^{TM} 8.0 software, GTT Technologies, Kohlscheid, Germany. The thermochemical modeling is performed for different temperatures and different amounts of reducing agents. All parameters of the simulations are shown in Table 1. All simulations are performed for 100 g of red mud input.

Table 1. Design of the experiments for thermochemical modeling.

Calculation No.	Temperature (°C)	Mass of C (g)	Calculation No.	Temperature (°C)	Mass of C (g)
1	1600	0	12	1700	0
2	1600	5	13	1700	5
3	1600	10	14	1700	10
4	1600	15	15	1700	15
5	1600	20	16	1700	20
6	1600	25	17	1700	25
7	1600	30	18	1700	30
8	1600	35	19	1700	35
9	1600	40	20	1700	40
10	1600	45	21	1700	45
11	1600	50	22	1700	50

As seen in Figure 2, during the reduction process, Fe_2O_3 is firstly reduced to FeO and, with the increase of reducing the agent's mass, it is further reduced to metal Fe. So, after the reduction process, there are two phases: a slag phase which is low in Fe, and the metal Fe phase. This iron metal phase can then be easily separated from the slag phase.

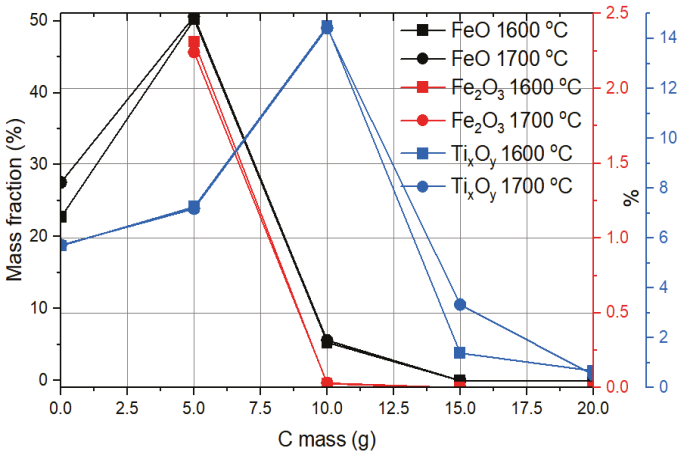


Figure 2. Dependence of the compound mass fractions on carbon content in slag.

Thermochemical modeling was essential for optimizing the carbothermic reduction of red mud. The model indicated that carbon is highly effective at reducing iron oxides, nearly to completion, as illustrated in Figure 2. However, increasing the carbon amount beyond a certain threshold leads to the reduction of titanium oxides to titanium carbide (TiC), which complicates the subsequent leaching process. Figure 2 shows that with 10 g of carbon per 100 g of red mud, the titanium oxide concentration in the slag reaches a maximum of 14.4%. Beyond this point, the concentration of titanium oxides dramatically decreases, indicating that excessive carbon leads to the formation of TiC rather than the desired titanium oxides. According to the thermochemical simulation, a carbon mass of 10 g per 100 g of red mud is optimal for the reduction process.

Figure 3 shows the different compositions of the metal phase in dependency on the mass of C. The concentration of Fe is almost 100% at a lower mass of carbon, but if the

carbon mass is increased, the Fe content decreases while other components, such as C, Si or titanium, are incorporated in the metal phase. So, the composition of the metal phase also shows that a quantity of 10 g C is suitable for the experimental trials of red mud reduction.

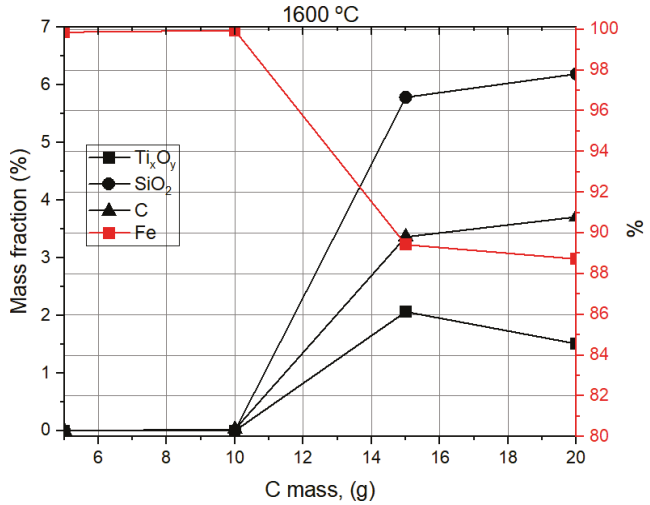


Figure 3. Composition of the metal phase depending on the reducing agent's mass.

Depending on the concentration of the reducing agent, it can be seen (Figure 4) that slag mass decreases as the mass of the reducing agent increases. The decrease can be explained because carbon is reducing the iron oxides in the red mud. The decrease is higher when the carbon mass is higher than 10 g because it also reduces the Ti oxides to TiC, which is an unwanted side product.

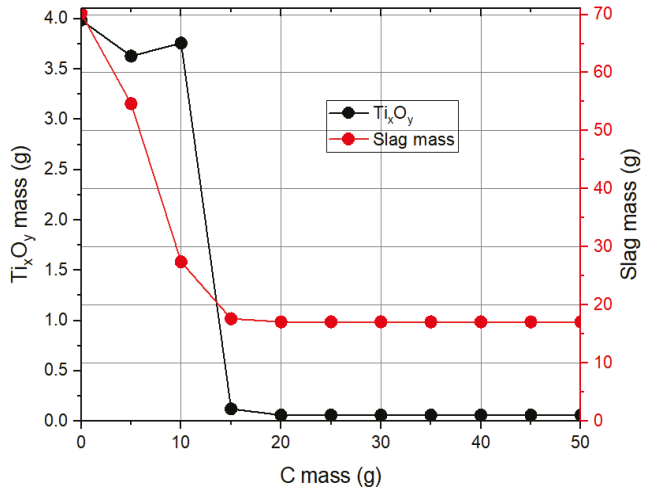


Figure 4. Dependence of slag and titanium oxide masses in the slag from reducing agent's mass.

3. Experimental Part

3.1. Material and Methods

In this work, red mud from the factory "alumina" d.o.o. was used as a raw material from Zvornik. The red mud was previously dried, ground and prepared for the reduction process. Red mud characterization was performed using an XRD analysis. The XRD analysis of red mud is shown in Figure 5.

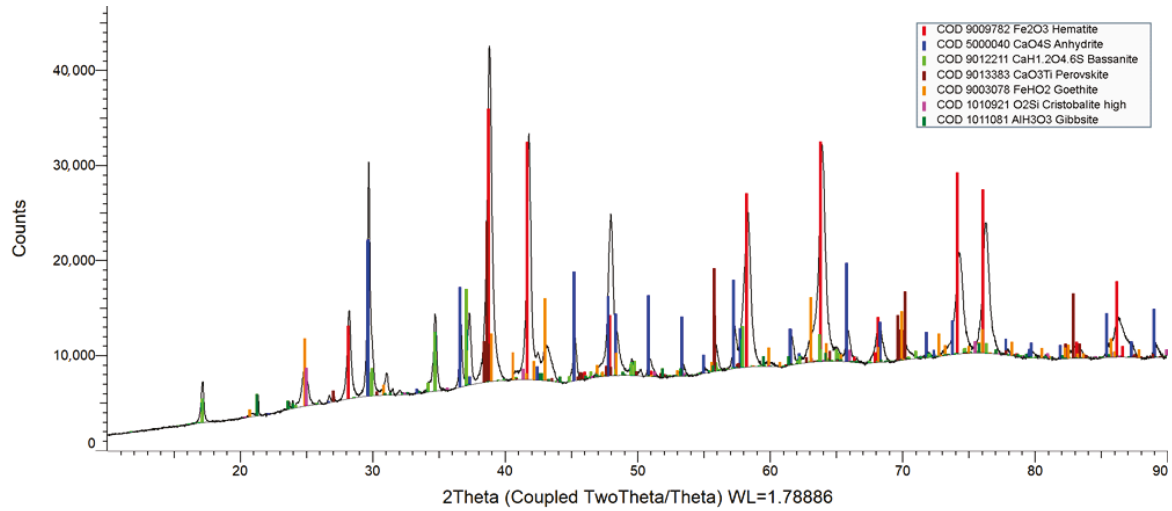


Figure 5. XRD Analysis of red mud.

As shown in Figure 5, the XRD analysis of red mud revealed the following phases: hematite, perovskite, cancrinite, ilmenite, calcite, diaspore, gibbsite and hydrogarnet. Iron is present in the structures of hematite and ilmenite. Titanium is found in the structures of perovskite and ilmenite, while aluminum is present in the structures of cancrinite, diaspore, boehmite, gibbsite and hydrogarnet. The composition of red mud is detailed in Table 2.

Table 2. Red mud composition.

Compounds	%	Compounds	%
Ignition loss at 1000 °C	8.32	Ga_2O_3	0.225
SiO_2	10.52	CuO	0.007
Fe_2O_3	49.29	K_2O	0.159
Na_2O	2.45	Tl_2O_3	0.088
TiO_2	4.59	MnO	0.145
CaO	8.23	MgO	0.627
Al_2O_3	12.03	NiO	0.034
Ag_2O	0.001	PbO	0.019
BaO	0.014	P_2O_5	0.930
Cr_2O_3	0.133	ZnO	0.016
Sc_2O_3	0.011	V_2O_5	0.135
Co_2O_3	0.012	SrO	0.075

The reduction process took place in a DC electric arc furnace. Three kilograms of red mud and 10 g graphite per 100 g of red mud as the carbon-reducing agent are mixed and charged into the furnace. Because of the high viscosity of the slag after reducing the iron-oxides, the slag creates a foam. To lower the viscosity, CaO was added as a fluxing agent. The positive side effect of CaO is that the possible FeO from Fe_2SiO_4 is dissolved back into the slag with a positive change of activity of FeO. After charging, a holding time of 45 min was started to let the C react with the slag. After the holding time, the furnace was tapped to win the Fe metal phase, while the slag phase was left in the crucible.

The samples were separated mechanically using magnetic separation. The obtained products were analyzed by XRD. In Figure 6, the electric arc furnace's reduction of red mud (a) and the products of reduction (b) are shown.

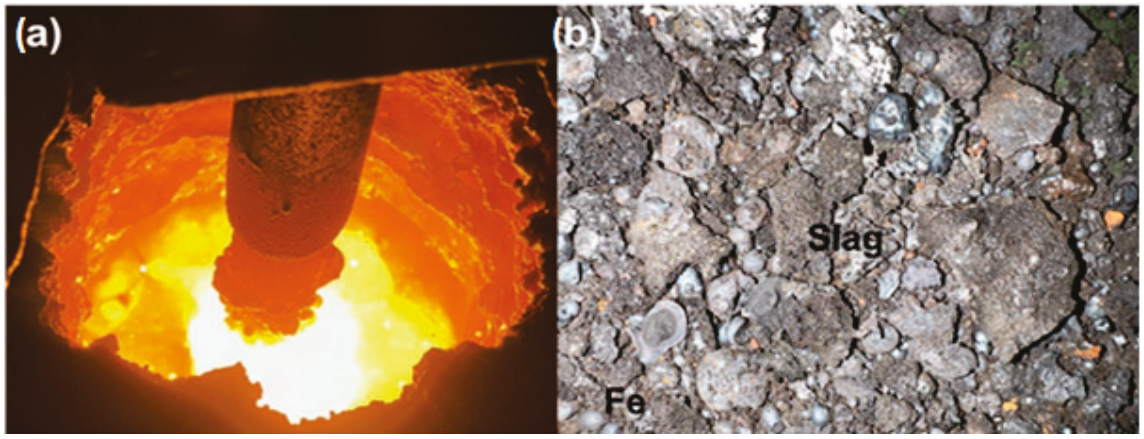


Figure 6. Electric arc furnace (**a**) and carbon-reduced red mud (**b**).

As can be clearly seen in Figure 6b, the reduction products are separated very easily, and the difference between slag and metallic iron droplets is clearly visible.

Leaching of the slag is performed in an autoclave in Buchi, Switzerland, which was designed for acid leaching (1.53 L, max pressure 200 bar, max. Temperature 270 °C) [31], as shown in Figure 7. This experimental set contains a heat exchanger with a thermostat, a mixer and probes for increasing and decreasing the pressure and also the possibility of taking a sample during the operation. The autoclave is connected to a computer and can be fully controlled by software that records all data during operation, which can later be used to process the results. Pressure in this autoclave was monitored using a manometer and digital sensors. The pressure in the system was formed from oxygen pressure (6, 9 bars) and water vapor pressure (total of 12–15 bar). The cooling of the autoclave was performed using a special system for cooling. The heating rate was 10 °C/min. The autoclave must be manually sealed with screws, and a pressure test must be performed before each operation.

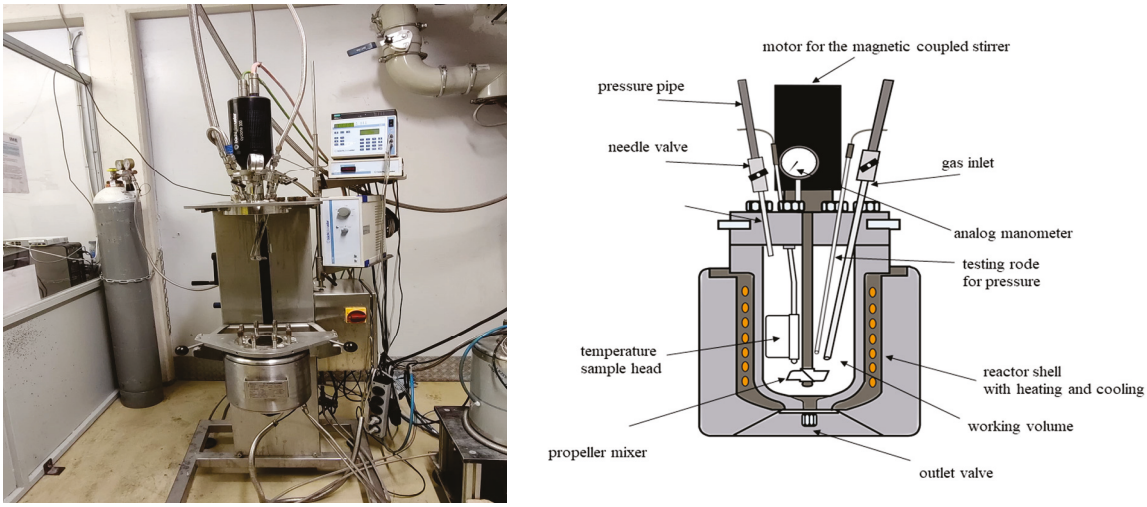


Figure 7. Experimental setup for leaching and schematic diagram of the autoclave.

The leaching process took place in an autoclave at elevated pressure and temperature. Sulfuric acid was used for leaching. The leaching process is followed by filtration, i.e., the separation of tailings from the solution. The solution was analyzed by ICP, and the solid residue with an XRD analysis. The design of the leaching is shown in Table 3.

Table 3. Design of leaching experiments.

Exp. No.	Temperature (°C)	Initial Pressure of O_2 (bar)	Concentration of Acid (mol/dm^3)	Liquid:Solid Ratio (mL/g)	Time (min)
1	150	0 bar	0.5	10:1	30
2	150	6 bar	0.5	10:1	30
3	150	6 bar	2.5	10:1	60
4	150	6 bar	5	10:1	120
5	180	6 bar	5	10:1	120
6	150	9 bar	5	10:1	120

All experiments have been carried out in the laboratories of the IME RWTH.

In this paper, leaching is used to extract titanium from the earlier reduced slag and represents a combination of pyrometallurgical and hydrometallurgical methods of red mud processing in order to optimize and find the optimal processing process.

Pure oxygen was needed to react with titanium from the slag in order to form a dissolved form of titanium oxysulfate.

The reduced red mud powder samples were analyzed at room temperature with an X-ray powder diffraction technique using the Ultima IV Rigaku diffractometer (Rigaku, Tokyo, Japan), equipped with CuK$\alpha_{1,2}$ radiation, using a generator voltage of 40 kV and a generator current of 40 mA. The range of 10–100° 2θ was used for all powder samples in a continuous scan mode with a scanning step size of 0.02° and at a scan rate of 1°/min, using a D/TeX Ultra-high speed detector (Rigaku, Tokyo, Japan). A glass sample carrier for sample preparation was used. The PDXL2 (Ver. 2.8.4.0) software was used to evaluate the phase composition and identification. All obtained powders were identified using the ICDD database.

An Energy-Dispersive X-Ray Spectroscopy (EDX) analysis was conducted using an Octane Plus-A system from Ametek-EDAX (2015 model, AMETEK Inc., Berwyn, PA, USA), with data analyzed through the Genesis V 6.53 software by Ametek-EDAX.

The chemical composition of the elements dissolved in the solution was determined using high-resolution inductively coupled plasma optical emission spectroscopy (ICP-OES). This technique enables the detection of elements with atomic mass numbers ranging from 7 to 250 (Li to U). The analysis was performed using a Spectro Genesis spectrometer (SPECTRO Analytical Instruments GmbH, Kleve, Germany).

3.2. Results and Discussion

3.2.1. Carbothermic Reduction of Red Mud in an Electric Arc Furnace

As can be seen in Figure 8, thermodynamic calculations show that the experiment does not always confirm the theory. The experimentally obtained results show that less metal is obtained during reduction and that there is a greater loss of mass compared to the theory with the slag. The theoretically calculated and experimentally obtained results are close, and the differences can be because the thermodynamic calculations provide an idealized outcome based on equilibrium conditions and do not always account for kinetic factors. In reality, the reaction kinetics, including activation energy and reaction rates, could be slower, resulting in the incomplete reduction of the metallic oxide. Also, the presence of impurities in the raw materials or the reactants can lead to side reactions that are not accounted for in thermodynamic models.

In comparison to the red mud, slag shows fewer phases (Figure 9), reflecting a reduction of hematite due to the carbothermal reduction process. While perovskite and magnetite are still present, the absence of phases like hematite and gibbsite, replaced by gehlenite and more concentrated magnetite, suggests a significant transformation in the mineral composition. The slag appears more crystallized and less heterogeneous than the untreated red mud. The reduction process simplifies the mineral composition, concentrating titanium and other elements while iron-based phases are reduced or transformed.

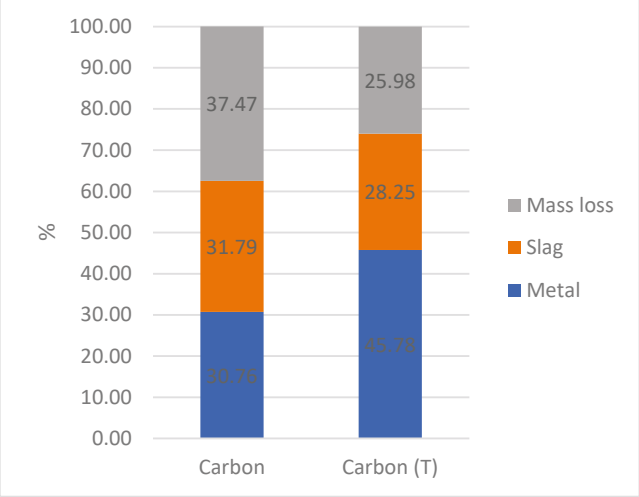


Figure 8. Thermodynamic calculation reduction of red mud (T) and experimentally obtained results.

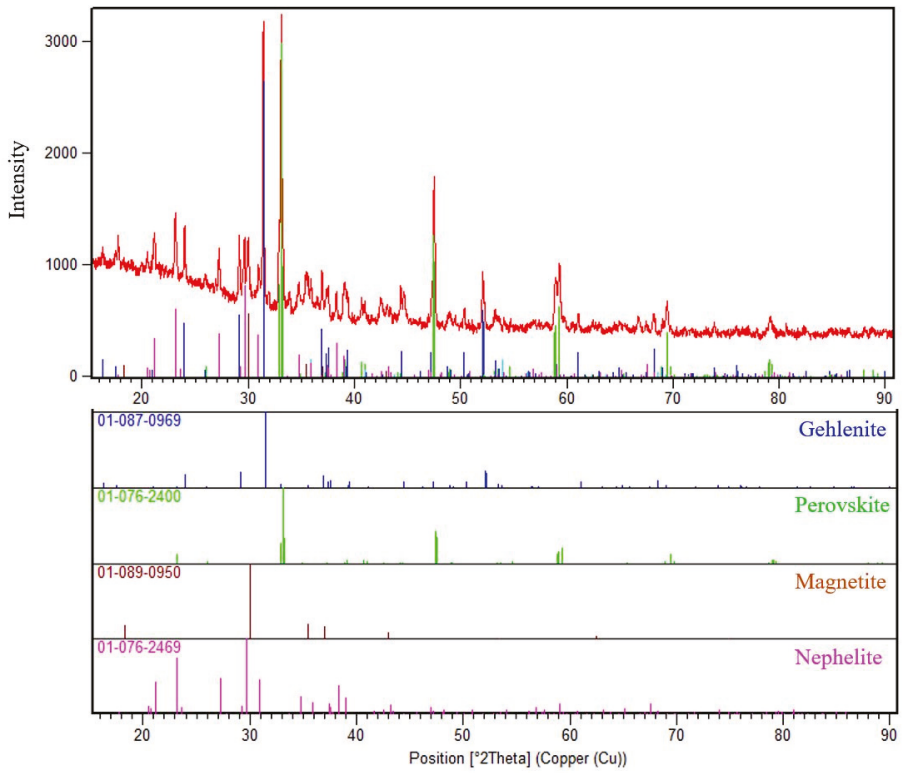


Figure 9. Diffractograms for slag reduced at 1600 °C. Identified minerals (gehlenite, perovskite and magnetite) with positions of diffraction maxima are shown in the lower part. The position of intensive diffraction maxima which do not overlap with the other maxima of the other minerals are shown in colored bands and used for comparison in mineral abundance.

3.2.2. Leaching

Leaching of slag containing mostly iron oxide is a very complex process, and its mechanism is very complicated. However, the reactions that can take place in the leaching process can be assumed as:

$$Fe_2O_{3_{(s)}} + 3\,H_2SO_{4_{(aq)}} \rightarrow Fe_2(SO_4)_{3_{(aq)}} + 3\,H_2O \quad (4)$$

$$TiO_2 + H_2SO_4 \rightarrow [TiO]SO_4 + H_2O \quad (5)$$

$$TiO[SO_4] + \frac{1}{2} O_2 \rightarrow [TiO\text{-}O]SO_4 \quad (6)$$

$$Al_2O_3 + 3\,H_2SO_4 \rightarrow Al_2(SO_4)_3 + H_2O \quad (7)$$

$$CaO + H_2SO_4 \rightarrow CaSO_{4(s)} + H_2O \quad (8)$$

$$CaTiO_3 + H_2SO_4 + 1.5O_2 = TiOSO_4 + H_2O + CaSO_4 \quad (9)$$

In Figure 10, leaching efficiency is shown for the different parameters.

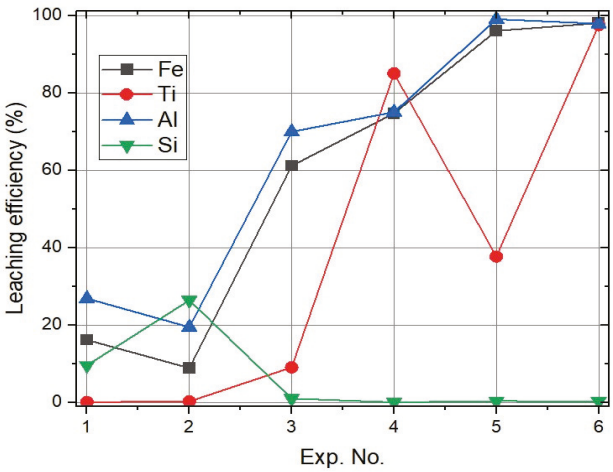


Figure 10. Leaching efficiency for different parameters (150 °C, 6–9 bar O_2, 0.5–5 mol/L H_2SO_4).

In the first three experiments, the selected parameters, such as temperature, oxygen pressure and sulfuric acid concentration, are not sufficient for the efficient leaching of titanium compounds. As the temperature increases, there is a noticeable rise in the concentrations of aluminum (Al) and iron (Fe) in the leachate, indicating enhanced leaching of these metals. However, the concentration of titanium (Ti) decreases significantly with the rise in temperature, which suggests that higher temperatures (180 °C) negatively affect the leaching efficiency of titanium under the given conditions. This indicates a possible inhibitory effect of temperature on titanium dissolution or a change in titanium's phase, making it less soluble.

On the other hand, the oxygen pressure plays a crucial role in the leaching efficiency of titanium. When the oxygen pressure is increased from 6 to 9 bars, there is a substantial improvement in titanium leaching efficiency. At an oxygen pressure of 9 bars, the leaching efficiency for titanium reaches 97.5%, demonstrating that oxygen pressure is a key parameter for optimizing the dissolution of titanium compounds. The presence of oxygen likely enhances the oxidative dissolution of titanium, making it more reactive and easier to leach in the acidic solution. Experiment number six enables the formation of titanium oxysulfate, using an increased oxygen partial pressure of 9 bar at 150 °C, using 5 mol/L of sulfuric acid, which is not present in the other mentioned experiments. The formation of titanium oxysulfate is favorable for industrial companies and the best way to recover titanium from a slag.

In addition to titanium, the leaching efficiencies for iron and aluminum are also high at increased oxygen pressures. This suggests that higher oxygen pressures not only promote the leaching of titanium but also support the dissolution of other metals like iron and aluminum, which are commonly found in similar phases within the mineral matrix.

As for silica (SiO_2), under conditions of high temperature, increased acid concentration and high oxygen pressure, the amount of leached silica is very low. This is a positive outcome because it prevents the problem of silica gelation, which can occur when too much silica is dissolved and precipitates out as a gel, causing processing difficulties. The low silica leaching under these conditions suggests that the process parameters are well-optimized to minimize silica dissolution while maximizing the leaching of target metals.

Table 4 provides the elemental analysis of the slag and solid residue from leaching experiment three (conducted at 1 h, 2.5 M H_2SO_4, 6 bar O_2, and a solid-to-liquid ratio of 10:1). It is evident from the data that the leaching efficiencies of all elements, especially titanium, are very low under these conditions. The low oxygen pressure (6 bars) appears to be the limiting factor, as evidenced by the much higher titanium leaching efficiency observed at 9 bars of oxygen pressure. The experiment also highlights that the other parameters, such as temperature and acid concentration, are not sufficient to achieve effective leaching without adequate oxygen pressure. This suggests that, while temperature and acid concentration play a role, oxygen pressure is the dominant factor influencing the dissolution of titanium in these experiments.

Table 4. Elemental analysis of slag and solid residue (experiment three).

Sample	Fe, %	Al, %	Si, %	Ti, %
Slag	5.27	4.14	2.72	5.59
Solid residue	4.49	3.82	2.48	5.18

Figure 11 shows the diffractogram of the solid residue after the leaching process, while Figure 5 illustrates the slag prior to leaching. A significant change in the mineralogical structure of the solid residue compared to the original slag is evident under the specified conditions (temperature of 150 °C, duration of 2 h, pressure 9 bar O_2 and 5 mol/L sulfuric acid concentration). As confirmed in Figure 11, the leaching process effectively dissolves elements such as titanium, iron and aluminum, leaving calcium, which remains in the form of calcium sulfate.

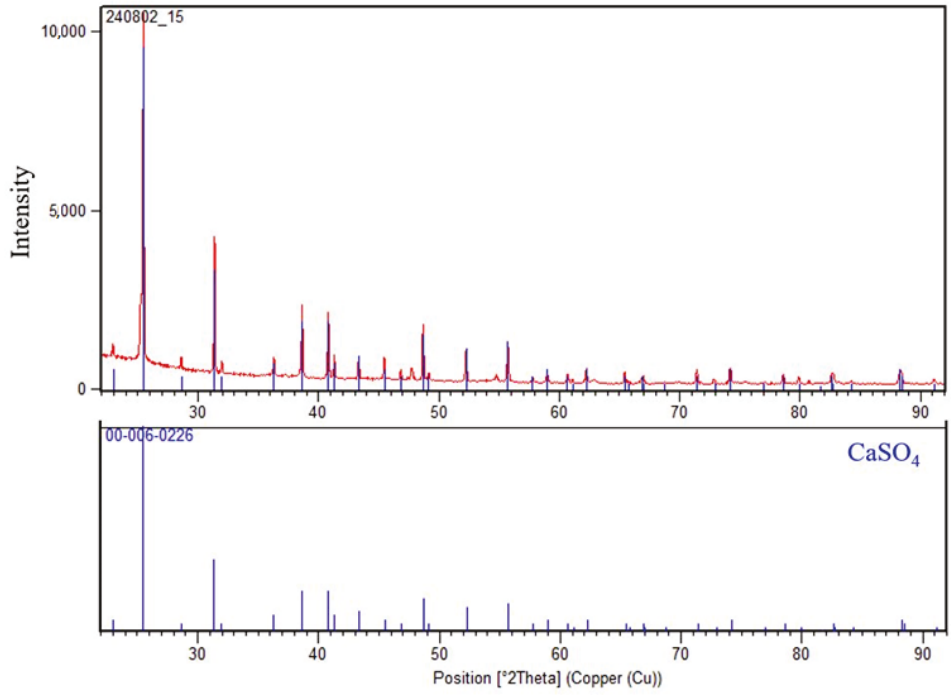


Figure 11. XRD diffractogram for solid residue after the leaching process at 150 °C, 9 bar O_2, 2 h (experiment nine).

Figure 12 further supports the extraction of titanium from the slag, with the EDS analysis showing that only a trace amount of titanium (0.4%) remains in the residue. This confirms the effective dissolution of titanium during the leaching process. Additionally, the EDS analysis identifies elements such as aluminum, silicon and other minor components, in addition to calcium, sulfur and oxygen, suggesting the presence of an amorphous phase. Since this amorphous phase cannot be detected by XRD, it indicates

that a portion of the solid residue exists in a non-crystalline form, adding complexity to the post-leaching material and further explaining the material composition that XRD alone could not fully characterize.

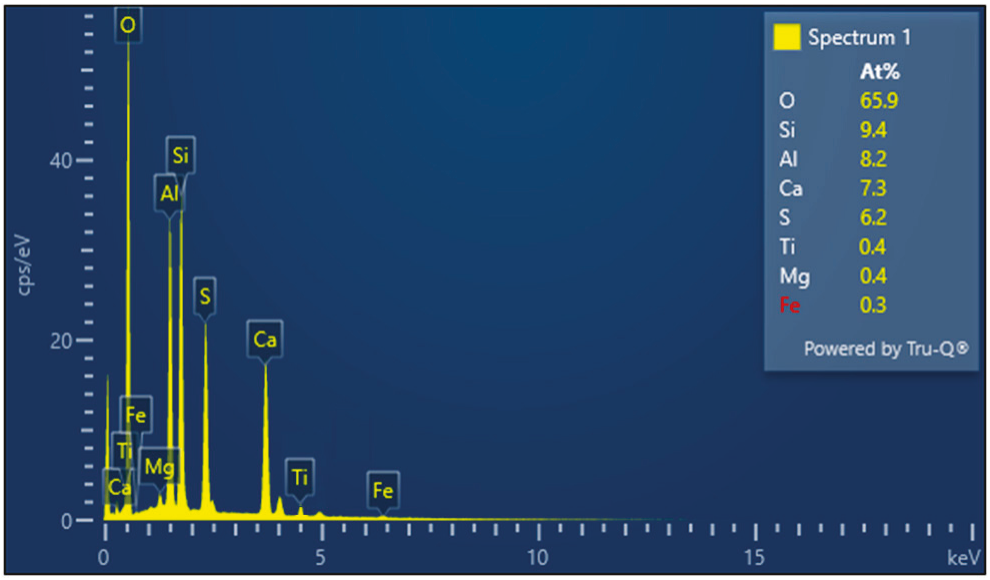


Figure 12. EDS analysis of solid residue (experiment nine).

4. Conclusions

This study successfully utilized red mud from the alumina d.o.o. factory in Zvornik as a raw material for the reduction and leaching processes. The reduction yielded easily separable products, with a clear distinction between slag and metallic iron, as evidenced in Figure 6b. Despite thermodynamic calculations predicting a certain yield, the experimental results indicated a lower metal recovery and greater mass loss during reduction, although the slag's theoretical and actual results were comparable (Figure 8).

In this study, we employ a method that first removes iron through reduction, effectively enriching the remaining components and making them easier to dissolve during subsequent leaching. The thermal treatment applied also disrupts the structural integrity of the red mud, facilitating the dissolution process. Furthermore, our approach addresses the common issue of silica gelation encountered in many other studies, ensuring a more efficient and effective leaching process.

The leaching phase, optimized for titanium recovery, revealed that increasing the oxygen pressure was crucial. At 9 bars of oxygen pressure, titanium leaching efficiency reached 97.5%. While higher temperatures improved aluminum and iron recovery, they decreased titanium extraction. This research underscores the importance of process optimization, particularly regarding oxygen pressure, to enhance the recovery of valuable metals such as titanium from red mud. The EDS and XRD analyses have confirmed the efficiency of titanium leaching. The novelty of this research lies in the innovative approach of leaching titanium in the form of oxysulfate using oxygen pressure, which significantly contributed to the high titanium recovery observed. Future investigations will explore the leaching efficiency of titanium from slag produced by plasma hydrogen reduction, aiming to compare different reduction methodologies in order to reach a maximal recovery of iron from red mud forming new slag without iron.

Author Contributions: Conceptualization, S.S. and D.K.; methodology, S.S.; software, E.E.K.; validation, S.S., D.K. and R.S.; formal analysis, M.S.; investigation, F.W., M.S. and D.K.; resources, S.S.; data curation, S.S.; writing—original draft preparation, D.K. and S.S.; writing—review and editing, R.S.; M.P. and E.E.K.; visualization, D.K.; supervision, B.F. and M.P.; project administration, S.S.;

funding acquisition, S.S. and M.P. All authors have read and agreed to the published version of the manuscript.

Funding: This research was funded by the European Commission, grant number 101135077 (EURO-TITAN).

Data Availability Statement: Data are contained within the article.

Acknowledgments: We would like to thank Nenad Nikolic, Milena Rosic and Dragana Zivotic for performing the XRD analysis and for the continuous support on the study of reduction of red mud.

Conflicts of Interest: The authors declare no conflicts of interest.

References

1. Tang, W.; Khavarian, M.; Yousefi, A. Red Mud. In *Sustainable Concrete Made with Ashes and Dust from Different Sources: Materials, Properties and Applications*; Woodhead Publishing: Sawston, UK, 2022; pp. 577–606. [CrossRef]
2. Verma, A.S.; Suri, N.M.; Kant, S. Applications of Bauxite Residue: A Mini-Review. *Waste Manag. Res.* **2017**, *35*, 999–1012. [CrossRef] [PubMed]
3. Sutar, H.; Mishra, S.C.; Sahoo, S.K.; Chakraverty, A.P.; Maharana, H.S. Progress of Red Mud Utilization: An Overview. *Chem. Sci. Int. J.* **2014**, *4*, 255–279. [CrossRef]
4. Morsali, S.; Yildirim, F. Environmental Impact Assessment of Red Mud Utilization in Concrete Production: A Life Cycle Assessment Study. *Environ. Dev. Sustain.* **2024**, *26*, 12219–12238. [CrossRef]
5. Mi, H.; Yi, L.; Wu, Q.; Xia, J.; Zhang, B. A Review of Comprehensive Utilization of Red Mud. *Waste Manag. Res.* **2022**, *40*, 1594–1607. [CrossRef]
6. Pan, X.; Wu, H.; Lv, Z.; Yu, H.; Tu, G. Recovery of Valuable Metals from Red Mud: A Comprehensive Review. *Sci. Total Environ.* **2023**, *904*, 166686. [CrossRef] [PubMed]
7. Archambo, M.S.; Kawatra, S.K. Utilization of Bauxite Residue: Recovering Iron Values Using the Iron Nugget Process. *Miner. Process. Extr. Metall. Rev.* **2021**, *42*, 222–230. [CrossRef]
8. Liu, Y.; Naidu, R.; Ming, H. Red Mud as an Amendment for Pollutants in Solid and Liquid Phases. *Geoderma* **2011**, *163*, 1–12. [CrossRef]
9. Amritphale, S.S.; Anshul, A.; Chandra, N.; Ramakrishnan, N. A Novel Process for Making Radiopaque Materials Using Bauxite—Red Mud. *J. Eur. Ceram. Soc.* **2007**, *27*, 1945–1951. [CrossRef]
10. Kumar, S.; Kumar, R.; Bandopadhyay, A. Innovative Methodologies for the Utilisation of Wastes from Metallurgical and Allied Industries. *Resour. Conserv. Recycl.* **2006**, *48*, 301–314. [CrossRef]
11. Kalkan, E. Utilization of Red Mud as a Stabilization Material for the Preparation of Clay Liners. *Eng. Geol.* **2006**, *87*, 220–229. [CrossRef]
12. Agrawal, S.; Rayapudi, V.; Dhawan, N. Extraction of Iron Values from Red Mud. *Mater. Today Proc.* **2018**, *5*, 17064–17072. [CrossRef]
13. Tokumitsu, K. Reduction of Metal Oxides by Mechanical Alloying Method. *Solid State Ion.* **1997**, *101–103*, 25–31. [CrossRef]
14. Li, S.; Pan, J.; Zhu, D.; Guo, Z.; Shi, Y.; Dong, T.; Lu, S.; Tian, H. A New Route for Separation and Recovery of Fe, Al and Ti from Red Mud. *Resour. Conserv. Recycl.* **2021**, *168*, 105314. [CrossRef]
15. Habibi, H.; Piruzian, D.; Shakibania, S.; Pourkarimi, Z.; Mokmeli, M. The Effect of Carbothermal Reduction on the Physical and Chemical Separation of the Red Mud Components. *Min. Eng.* **2021**, *173*, 107216. [CrossRef]
16. Cheema, H.A.; Ilyas, S.; Farhan, M.; Yang, J.H.; Kim, H. Extraction of Fe and Al from Red Mud Using Carbothermic Reduction Followed by Water Leaching. *J. Ind. Eng. Chem.* **2024**, *136*, 201–210. [CrossRef]
17. Rukini, A.; Rhamdhani, M.A.; Brooks, G.A.; van den Bulck, A. Metals Production and Metal Oxides Reduction Using Hydrogen: A Review. *J. Sustain. Metall.* **2022**, *8*, 1–24. [CrossRef]
18. Zinoveev, D.; Pasechnik, L.; Grudinsky, P.; Yurtaeva, A.; Dyubanov, V. Kinetics and Mechanism of Red Mud Carbothermic Reduction and Reduced Iron Grain Growth: An Influence of Sodium Sulfate. *Crystals* **2022**, *13*, 1. [CrossRef]
19. Stopić, S.; Nikolić, N.; Životić, D.; Krstić, J.; Rosić, M.; Friedrich, B.; Damjanović, V. Hydrogen Metallurgy for a Treatment of Bauxite Residues-First Results on the EURO-TITAN Project. In Proceedings of the XXV YuCorr, Divčibare, Serbia, 28 May 2024.
20. Liu, X.; Han, Y.; He, F.; Gao, P.; Yuan, S. Characteristic, Hazard and Iron Recovery Technology of Red Mud—A Critical Review. *J. Hazard. Mater.* **2021**, *420*, 126542. [CrossRef]
21. Spreitzer, D.; Schenk, J. Reduction of Iron Oxides with Hydrogen—A Review. *Steel Res. Int.* **2019**, *90*, 1900108. [CrossRef]
22. Agrawal, S.; Dhawan, N. Hydrogen Reduction of Red Mud for Extraction of Metallic Values. *J. Sustain. Metall.* **2023**, *9*, 386–397. [CrossRef]
23. Zarei-Jelyani, F.; Salahi, F.; Rahimpour, M.R. Introduction to Hydrogen as a Clean Source of Energy. *Encycl. Renew. Energy Sustain. Environ.* **2023**, *4*, 95–104. [CrossRef]
24. Free, M.L. *Hydrometallurgy: Fundamentals and Applications*; Springer: Cham, Switzerland, 2013; 432p. [CrossRef]
25. Othusitse, N.; Muzenda, D. Predictive Models of Leaching Processes: A Critical Review. In Proceedings of the 7th International Conference on Latest Trends in Engineering & Technology (ICLTET'2015), Irene, South Africa, 26–27 November 2015. [CrossRef]

26. Zhou, K.; Teng, C.; Zhang, X.; Peng, C.; Chen, W. Enhanced Selective Leaching of Scandium from Red Mud. *Hydrometallurgy* **2018**, *182*, 57–63. [CrossRef]
27. Borra, C.R.; Mermans, J.; Blanpain, B.; Pontikes, Y.; Binnemans, K.; van Gerven, T. Selective Recovery of Rare Earths from Bauxite Residue by Combination of Sulfation, Roasting and Leaching. *Min. Eng* **2016**, *92*, 151–159. [CrossRef]
28. Faraji, F.; Alizadeh, A.; Rashchi, F.; Mostoufi, N. Kinetics of Leaching: A Review. *Rev. Chem. Eng.* **2022**, *38*, 113–148. [CrossRef]
29. Habibi, H.; Mokmeli, M.; Shakibania, S.; Pirouzan, D.; Pourkarimi, Z. Separation and Recovery of Titanium and Scandium from the Red Mud. *Sep. Purif. Technol.* **2023**, *317*, 123882. [CrossRef]
30. Agatzini-Leonardou, S.; Oustadakis, P.; Tsakiridis, P.E.; Markopoulos, C. Titanium Leaching from Red Mud by Diluted Sulfuric Acid at Atmospheric Pressure. *J. Hazard. Mater.* **2008**, *157*, 579–586. [CrossRef]
31. Emil-Kaya, E.; Polat, B.; Stopic, S.; Gürmen, S.; Friedrich, B. Recycling of NdFeB magnets employing oxidation, selective leaching, and iron precipitation in an autoclave. *RSC Adv.* **2023**, *13*, 1320–1332. [CrossRef]

Disclaimer/Publisher's Note: The statements, opinions and data contained in all publications are solely those of the individual author(s) and contributor(s) and not of MDPI and/or the editor(s). MDPI and/or the editor(s) disclaim responsibility for any injury to people or property resulting from any ideas, methods, instructions or products referred to in the content.

minerals

MDPI

Article

Eco-Friendly Leaching of Spent Lithium-Ion Battery Black Mass Using a Ternary Deep Eutectic Solvent System Based on Choline Chloride, Glycolic Acid, and Ascorbic Acid

Furkan Nazlı [1], Işıl Hasdemir [1], Emircan Uysal [2,*], Halide Nur Dursun [1,3], Utku Orçun Gezici [1], Duygu Yesiltepe Özçelik [1], Fırat Burat [3] and Sebahattin Gürmen [1]

[1] Department of Metallurgical and Materials Engineering, Istanbul Technical University, 34469 Istanbul, Türkiye; nazli20@itu.edu.tr (F.N.); hasdemiri20@itu.edu.tr (I.H.); dursunh17@itu.edu.tr (H.N.D.); geziciu@itu.edu.tr (U.O.G.); yesiltepe15@itu.edu.tr (D.Y.Ö.); gurmen@itu.edu.tr (S.G.)
[2] Department of Chemical Engineering, KTH Royal Institute of Technology, Teknikringen 42, 11428 Stockholm, Sweden
[3] Department of Mineral Processing Engineering, Istanbul Technical University, 34469 Istanbul, Türkiye; buratf@itu.edu.tr
* Correspondence: emircanu@kth.se

Abstract: Lithium-ion batteries (LiBs) are utilized in numerous applications due to advancements in technology, and the recovery of end-of-life (EoL) LiBs is imperative for environmental and economic reasons. Pyrometallurgical and hydrometallurgical methods have been used in the recovery of metals such as Li, Co, and Ni in the EoL LiBs. Hydrometallurgical methods, which have been demonstrated to exhibit higher recovery efficiency and reduced energy consumption, have garnered increased attention in recent research. Inorganic acids, including HCl, HNO_3 , and H_2SO_4 , as well as organic acids such as acetic acid and citric acid, are employed in the hydrometallurgical recovery of these metals. It is imperative to acknowledge the environmental hazards posed by these acids. Consequently, solvometallurgical processes, which involve the use of organic solvents with minimal or no water, are gaining increasing attention as alternative or complementary techniques to conventional hydrometallurgical processes. In the context of solvent systems that have been examined for a range of solvometallurgical methods, deep eutectic solvents (DESs) have garnered particular interest due to their low toxicity, biodegradable nature, tunable properties, and efficient metal recovery potential. In this study, the leaching process of black mass containing graphite, LCO, NMC, and LMO was carried out in a short time using the ternary DES system. The ternary DES system consists of choline chloride (ChCl), glycolic acid (GLY), and ascorbic acid (AA). As a result of the leaching process of cathode powders in the black mass without any pre-enrichment process, Li, Co, Ni, and Mn elements passed into solution with an efficiency of over 95% at 60 °C and within 1 h. Moreover, the kinetics of the leaching process was investigated, and Density Functional Theory (DFT) calculations were used to explain the leaching mechanism.

Keywords: ternary DES; Solvometallurgy; Recycling of LiBs

1. Introduction

Lithium-ion batteries (LIBs) are advanced energy storage devices characterized by a wide operational temperature range, high voltage, and elevated energy and power density. These advantages have led to the widespread adoption of LIBs in electric vehicles (EVs),

hybrid electric vehicles (HEVs), laptops, mobile phones, hard drives, solar panels, and wind turbines [1]. In smaller electronic devices (e.g., smartphones, laptops, cameras), the average lifespan of LIBs ranges from 3 to 5 years, whereas in larger systems such as EVs, their operational lifetime is estimated to be around 10 years [2]. With increasing demand each year and the growing number of applications, end-of-life LIBs are accumulating as millions of tons of waste [3]. By 2030, it is projected that approximately 2 million EVs will reach end-of-life annually, and this number is expected to increase exponentially over the following decade [4]. Furthermore, the rising demand for LIBs has led to significant price increases in critical elements such as lithium (Li), nickel (Ni), and cobalt (Co). Additionally, the large-scale accumulation of metals like Co and Li poses environmental and biological hazards due to their toxic nature. In particular, the fact that LIB cathodes typically consist of approximately 20% Co and 7% Li by weight highlights the critical importance of battery recycling. The presence of toxic and flammable electrolytes, such as lithium hexafluorophosphate ($LiPF_6$), further intensifies these risks. Therefore, it is crucial to recover raw materials from used LIBs in an environmentally friendly and sustainable manner [5,6].

Two of the most widely adopted techniques for recycling LIBs are pyrometallurgy and hydrometallurgy [7]. However, hydrometallurgical methods are often chosen as an alternative because of variables including high energy consumption, high prices, and the release of hazardous gases during the pyrometallurgical process [8,9]. Hydrometallurgical methods are notable for their lower energy needs, higher purity of recovered materials, and reduced gas emissions when compared to pyrometallurgical methods [10]. Moreover, the cumulative energy demand value of hydrometallurgical recycling processes was reported as 198.2 MJ kWh^{-1} , while that of pyro- + hydro- processes was reported as 228.2 MJ kWh^{-1} , and it was observed that hydrometallurgical processes exhibited less energy consumption than pyro- + hydro- combinations [11]. Nevertheless, the use of strong and toxic mineral acids, such as HNO_3 , HCl, and H_2SO_4 , during hydrometallurgical recycling presents a significant threat to environmental safety [12].

To address these environmental concerns and improve metal recovery rates, deep eutectic solvents (DESs) were introduced in 2003 by Abbott et al. as a combination of quaternary ammonium salts and hydrogen bond donors, resulting in low-melting, biodegradable, and environmentally friendly solvents [13,14]. Although the environmental and economic impacts associated with the production of raw materials for DES synthesis require further investigation, the use of biodegradable and less corrosive organic compounds in DES-based leaching processes may offer a more environmentally friendly alternative compared to commercial mineral acids. A number of studies in the literature have investigated the use of DESs with different solvent compositions for metal recovery from batteries. For instance, Peeters et al. formulated several DESs in varying ratios and reported the Co leaching efficiencies [15]. One of these investigations achieved a recovery rate of over 98% by leaching Co from lithium cobalt oxide (LCO) batteries using a DES made of ChCl and citric acid in a 2:1 molar ratio. The leaching procedure was carried out at 40 °C for 60 min. However, the study noted that citric acid exhibited high viscosity and therefore had to be diluted with 35% water to reduce the solvent's resistance to mass transfer.

Ma et al. investigated a DES system made of ChCl and L-tartaric acid for the removal of metals from the cathodes of NMC and LCO batteries [16]. The DES was prepared in a 1:1 molar ratio, and varying amounts of water were added to the mixture. The optimal leaching temperature was found to be 70 °C, resulting in a metal recovery efficiency of 98.5%. Furthermore, it was observed that increasing the water content improved the leaching performance. However, higher water content was also found to reduce the rate of lithium recovery. Additionally, excessive water can disrupt the hydrogen bonding network of the DES, which may change the coordination and behavior of metal ions, ultimately

decreasing leaching efficiency [17]. For this reason, water-free DES systems have also been explored.

Ternary DES systems have recently gained significant attention as an alternative to the binary systems frequently used in the literature. These systems offer several advantages over binary ones in the recovery of LCO from spent LIBs. Jafari et al. investigated the influence of a ternary DES system composed of ChCl:urea: ethylene glycol (EG) on the leaching process [18]. Multiple DES systems, such as the ternary ChCl:urea: EG system, ChCl: urea, and ChCl: EG system, were prepared in different mole ratios. Following preparation, 5 mL of DES and 0.1 g of battery powder were used in the leaching experiments. For every DES system, leaching tests were carried out at 50 °C, 75 °C, and 100 °C. When combined with urea and ChCl, the EG structure in the ternary DES remained chemically stable and unaltered, according to FT-IR measurements. By increasing its efficacy throughout the procedure, EG's stability in the ternary system made a substantial contribution to the leaching performance. The findings of the characterization showed that metal recovery rose in direct proportion to temperature. With a high Li recovery rate of 97%, it was found that 100 °C was the ideal temperature for DES-based recovery. Furthermore, recovery efficiencies for Mn, Ni, and Co were 34%, 40%, and 41%, respectively. The ternary DES exhibited better selectivity for Co and Ni, whereas the binary DES system made of ChCl and urea showed great selectivity for Li and Mn. The literature also identifies important challenges in DES-based metal recovery procedures, such as high viscosity, the requirement for high temperatures, and extended leaching times.

This study aims to design and optimize novel DES systems to address persistent challenges. One major issue with DESs is their inherently high viscosity, which frequently requires water dilution, which runs counter to their ecologically friendly nature. To overcome this limitation, the present work focuses on developing water-free DES systems composed solely of organic acids and ammonium salts. In many DES formulations, glycolic acid (GLY) is a favored HBD, which makes it very useful for metal recovery operations. Van der Waals forces and electrostatic interactions, in addition to the strong hydrogen bonding interactions between HBDs and HBAs, are responsible for the high viscosity characteristic of DESs [19]. This type of viscosity hinders mass transport, which creates obstacles to effective leaching kinetics [20]. GLY is used as a viscosity-reducing HBD in anhydrous DES formulations to lessen these disadvantages. GLY ($C_2H_4O_3$), a member of the alpha-hydroxy acid (AHA) family [21] , has a molecular weight of 76.05 g/mol, a melting point of 75–80 °C, and a decomposition temperature of 100 °C. Glycolic acid was selected in this study due to its carboxylic functional group, ability to reduce viscosity, and favorable coordination with transition metal ions, all of which contribute to enhanced leaching kinetics in DES systems. Moreover, it has no color or smell, is a weak acid, and is very water soluble [21]. Due to its diverse chemical characteristics, it is widely used in the food industry, textiles, dermatology, cosmetics, and metal extraction [22].

In the study by Kaur et al., ChCl was used as the HBA and GLY as the HBD. The GLY content was adjusted at molar ratios of 1:1, 1:2, and 1:3. Results indicated that increasing GLY content reduced viscosity [23]. However, a higher GLY proportion led to decreased dye extraction efficiency. At lower mole ratios, DESs with a 1:1 GLY: ChCl ratio exhibited the highest performance, followed by 2:1 and 3:1 ratios, while at higher DES dosages, extraction efficiencies among all ratios were comparable.

Ascorbic acid (AA), commonly known as vitamin C, has the chemical formula $C_6H_8O_6$ [24]. Its density is around 1.65 g/cm^3 , its melting and decomposition points are between 190 and 192 °C, and its molecular weight is 176.12 g/mol. It is highly soluble in both water and ethanol [24,25]. Owing to its carbon groups, AA exhibits strong reducing properties, and the proximity of its hydroxyl and carbonyl groups enables it to act as a

hydrogen donor [26]. In DES systems, cobalt is reported to dissolve in its +2 oxidation state. Accordingly, Peeters et al. achieved successful Co recovery from $LiCoO_2$ cathodes by employing reductants such as Cu and Al to reduce Co^{3+} ions to Co^{2+} [15]. Similarly, Dixon et al. utilized L-ascorbic acid to reduce a pentaamine chromate cobalt (III) complex through a two-step process: first, Cr was reduced, and then Co^{3+} was reduced to Co^{2+} [27]. To minimize the introduction of additional metals into the system, we propose the use of AA as an alternative to conventional reductants such as Cu and Al.

One of the innovative aspects of this study is the use of a three-component DES system (ChCl:GLY:AA) instead of a conventional binary system. The high solubility of GLY, combined with the reduction potential of AA under +2 oxidation state conditions during the leaching process, contributes to the uniqueness of the system. Furthermore, this study aims to address existing gaps in the battery recycling sector by optimizing novel DES systems and providing solutions to the challenges identified in the current literature.

2. Materials and Methods

2.1. Materials

Choline chloride (ChCl, ≥98%, Sigma Aldrich, Shanghai, China), glycolic acid (GLY, ≥98% , Sigma-Aldrich, St. Louis, MO, USA), and L (+)-ascorbic acid (AA, ≥99%, Merck Ltd. Beijing, China) were used to prepare DESs. Moreover, HNO_3 (65%, Tekkim Kimya San. ve Tic. A.Ş. Istanbul, Türkiye) was used for sample preparation. Ethanol (Merck KGaA Darmstadt, Germany), acetone (99.5%, Tekkim Kimya San. ve Tic. A.Ş. Istanbul, Türkiye), and de-ionized water (produced by Milli-Q) were utilized at various stages.

2.2. Characterization of Black Mass

The black mass used in this study was obtained as industrial waste from a lithium-ion battery recycling facility located in Türkiye. It consisted primarily of shredded cathode materials and residual graphite collected from spent LIBs. The characterization of black mass was conducted in our previous study [28]. Briefly, the presence of $LiCoO_2$, $LiNi_{0.33}Mn_{0.33}Co_{0.33}O_2$, $LiMn_2O_4$, and graphite phases was observed in the black mass. Additionally, the composition of the black mass was ascertained to be 35.38% graphite by weight, 29.62 ppm Li, 195.86 ppm Co, 79.55 ppm Ni, and 59.48 ppm Mn. Furthermore, the particle morphology of the black mass was found to exhibit a heterogeneous structure, with an average particle size of 70 μm.

2.3. Preparation of DES Solutions

To prepare homogeneous binary and ternary DESs, ChCl was used as the HBA at a constant concentration of 1 mole, while GLY and AA served as HBDs in varying mole ratios. The mole ratios of the prepared solutions are given in Table 1. The components were mixed and stirred at 700 rpm at 60 °C, via a magnetic heating stirrer (model: MS300HS-MTOPS), until a uniform, homogeneous solution was obtained. A 5 mL sample of the prepared DES was transferred to a glass container.

Table 1. Binary and ternary DES compositions.

DES Codes	Choline Chloride Ratio (Mole)	Glycolic Acid Ratio (Mole)	Ascorbic Acid Ratio (Mole)
1:2 ChCl:GLY	1	2	-
1:1.9:0.1 ChCl:GLY:AA	1	1.9	0.1

Table 1. *Cont.*

DES Codes	Choline Chloride Ratio (Mole)	Glycolic Acid Ratio (Mole)	Ascorbic Acid Ratio (Mole)
1:1.8:0.2 ChCl:GLY:AA	1	1.8	0.2
1:1.7:0.3 ChCl:GLY:AA	1	1.7	0.3
1:3 ChCl:GLY	1	3	-
1:2.9:0.1 ChCl:GLY:AA	1	2.9	0.1
1:2.8:0.2 ChCl:GLY:AA	1	2.8	0.2
1:2.7:0.3 ChCl:GLY:AA	1	2.7	0.3
1:4 ChCl:GLY	1	4	-
1:3.9:0.1 ChCl:GLY:AA	1	3.9	0.1
1:3.8:0.2 ChCl:GLY:AA	1	3.8	0.2
1:3.7:0.3 ChCl:GLY:AA	1	3.7	0.3

2.4. Leaching Experiments

Black mass containing graphite, lithium nickel-manganese-cobalt oxide (NMC), lithium cobalt oxide (LCO), and lithium manganese oxide (LMO) was accurately weighed and added to the 5 mL of DES system at different solid-to-liquid ratios. The leaching process was conducted on a magnetic stirrer at 700 rpm and 60 °C for 1 h. Experimental parameters, including leaching temperature and time, DES composition, solid-to-liquid ratio, and stirring rate, were systematically varied to optimize the leaching efficiencies. After the leaching process, the solution was subjected to filtration using a syringe filter with a pore size of 0.22 μm to facilitate the separation of solid and liquid phases.

2.5. Characterization

FTIR analysis was conducted in the wavenumber range of 400–4000 cm^{-1} using a Bruker FTIR spectrometer. The DES samples were analyzed after complete homogenization in the liquid phase to ensure uniform hydrogen bonding interaction across the ternary system. After leaching, the samples were filtered using a 0.22 μm syringe filter. The resulting filtrates were diluted to appropriate levels depending on metal concentration—typically 50×, 100×, 250×, 500×, or 1000× dilutions were prepared with a 2% HNO_3 solution (v/v). The Atomic Absorption Spectroscopy (AAS) instrument (Agilent Technologies, Santa Clara, CA, USA) was calibrated using certified standard solutions of Li, Co, Ni, and Mn. The metal ion concentrations in the leachates were calculated based on the corresponding calibration curves. Leaching efficiency was calculated with Equation (1) [29].

$$\begin{aligned} &\textit{The leaching efficiencies } (\%) \\ &= \frac{\textit{Metal ion concentration } \left(\frac{g}{L}\right) * \textit{Leach volume}(L)}{\textit{Metal amount of specific metal } (\%) * \textit{Initial metal amount } (g)} * 100 \end{aligned} \quad (1)$$

The complex formation energies between Co^{2+} and selected ligands—ascorbic acid, glycolic acid, and choline chloride—were calculated using the ORCA 6.0.1 quantum chemistry package [30]. All calculations were carried out using the density functional theory (DFT) hybrid functional B3LYP, in conjunction with Grimme's D3BJ dispersion correction to improve the accuracy of non-covalent interactions. The def2-TZVP basis set was employed for all atoms, providing a balance between computational cost and chemical accuracy. Geometry optimizations were performed using tight self-consistent field (SCF) convergence criteria and without imposing any symmetry constraints. To simulate solvation

conditions more realistically, the conductor-like polarizable continuum model (CPCM) was applied during all geometry optimizations and energy evaluations. Binding energies (ΔE) were computed to evaluate the relative stability of the complexes, using the following Equation (2)

$$\Delta E = E_{complex} - \left(E_{Co^{2+}} + \sum E_{ligand}\right) \quad (2)$$

In this equation $E_{complex}$ refers to the total energy of the optimized Co–ligand complex, while $E_{Co^{2+}}$ and E_{ligand} denote the energies of the isolated cobalt ion and individual ligands, respectively. All computed energies are expressed in Hartree units. This methodology enables a theoretical assessment of the coordination behavior and binding preferences of cobalt in the presence of environmentally benign ligands under solvated conditions.

3. Results and Discussion

3.1. Characterization of DES

Figure 1A illustrates the chemical structures of GLY, AA, and ChCl. Both GLY and AA act as HBD owing to the presence of hydroxyl (-OH) groups in their molecular structures. In contrast, ChCl behaves as an HBA, primarily due to its Cl^- anion [31]. These compounds can form a DES through hydrogen bonding interactions between the HBD and HBA components. Moreover, this interaction ensures that the binary and ternary DESs prepared at different molar ratios remain in liquid form at room temperature, lowering their eutectic points below room temperature. Figure 1B shows the FTIR pattern of ChCl:GLY binary DESs prepared at 1:2 and 1:3 molar ratios. Strong absorption peaks were observed at 1085 cm^{-1} , 1422 cm^{-1} , 1732 cm^{-1} , and 3290 cm^{-1} in the 1:2 ChCl:GLY DES spectra. These peaks correspond to the stretching of the C-O, the stretching of the $–COO^-$, the stretching of the C=O, and the stretching of the O-H group from pure GLY, respectively [32]. Moreover, the ChCl presence led to the appearance of N–H stretching peaks at 2918 and 3032 cm^{-1} [33]. Furthermore, the characteristic peak derived from the ChCl $(CH_3)_3N^+$ group was observed at 1477 cm^{-1} [33]. Increasing the GLY ratio from 2 to 3 does not significantly alter the FTIR pattern; however, a decrease in the intensity of the characteristic ChCl peak at 1477 cm^{-1} is observed, which can be attributed to the reduced ChCl mole ratio. The FTIR pattern of the DESs containing AA is presented in Figure 1C. Upon the addition of AA, a vibration band corresponding to the C=C bond in its structure appears at around 1600 cm^{-1} [34] , and the intensity of this peak increases with higher amounts of AA. The peak observed in the 3000–3600 cm^{-1} range for all DESs appears broad, with no distinct sharp peak in this region, indicating that the OH groups are involved in hydrogen bonding interactions with ChCl [33,34]. The addition of ascorbic acid to the DES system led to a notable increase in the absorbance intensity within the 1000–1100 cm^{-1} region, as highlighted in Figure 1C. This spectral region is primarily associated with C–O stretching vibrations, which are characteristic of the multiple hydroxyl groups present in ascorbic acid molecules. The emergence and intensification of these peaks upon ascorbic acid incorporation indicate its successful integration into the DES matrix. This observation suggests the formation of additional hydrogen bonding interactions between ascorbic acid and other DES components, potentially enhancing the overall hydrogen bond network density. Consequently, the presence of ascorbic acid is expected to influence the physicochemical properties of the DES, such as polarity, viscosity, and its capacity for metal chelation or redox reactions.

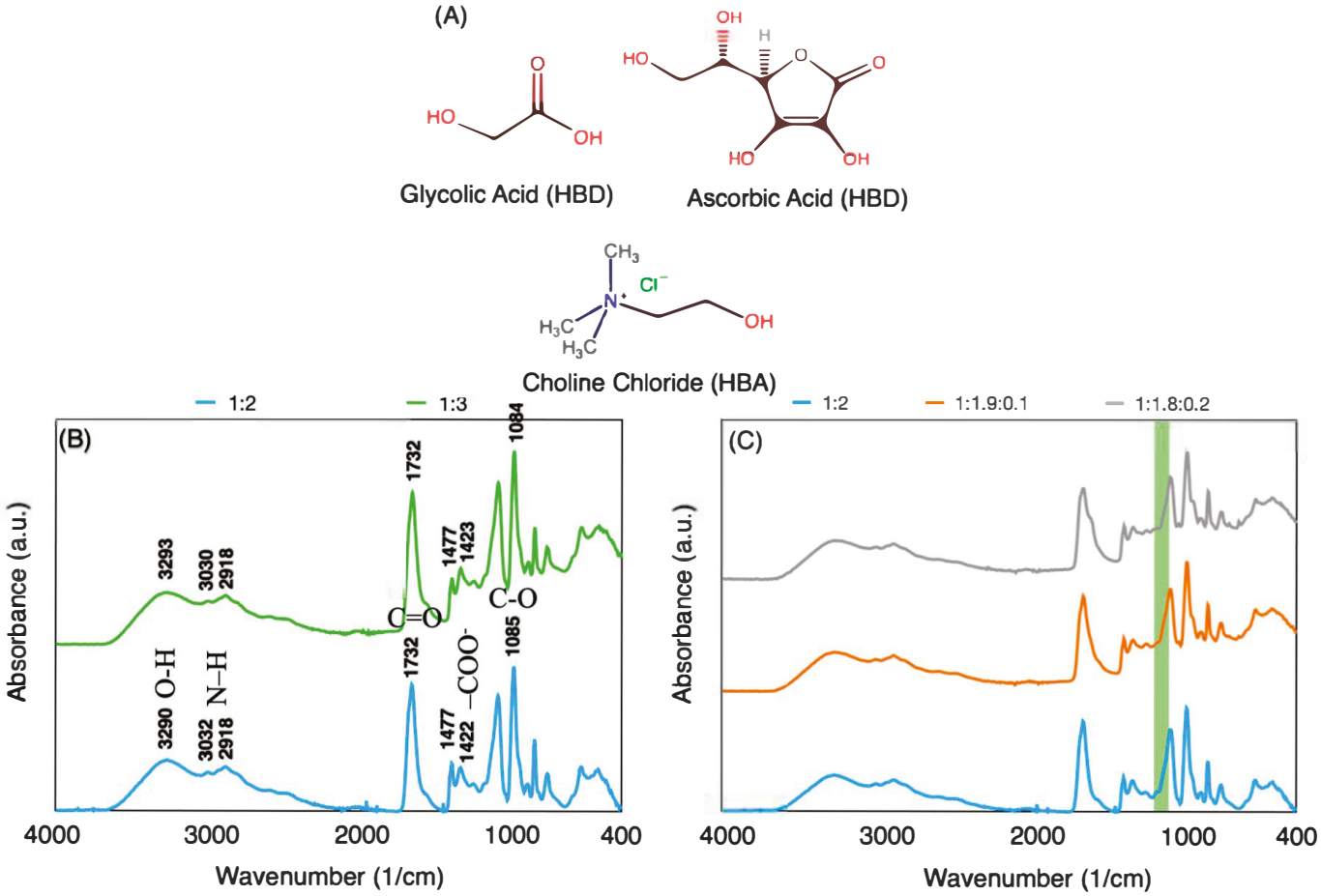


Figure 1. Chemical structures of ChCl, GLY, and AA (**A**), FTIR pattern of binary (**B**), and ternary DES (**C**).

3.2. Leaching of Black Mass

3.2.1. Effect of GLY Mole Ratio on Leaching Efficiency

To investigate the effect of the amount of carboxylic groups on the leaching efficiency, three different Na-DES with different mole ratios were prepared. ChCl and GLY solutions were prepared at a molar ratio of 1:2, 1:3, and 1:4, and leaching experiments were carried out at a solid-liquid ratio of 10 g/L for 1 h at 60 °C. Leaching efficiencies obtained for the three different Na-DES are presented in Figure 2. Increasing the GLY molar ratio from 2 to 4 resulted in an enhancement of leaching efficiency, with increases observed from 20.24% to 47.47%, from 4.31% to 12.07%, from 17.50% to 43.92%, and from 19.28% to 28.48%, respectively, for Li, Co, Ni, and Mn. Lu et al. (2022) reported that the leaching efficiency of Malonic acid (MA) (containing a carboxyl group) with ChCl was higher than EG: ChCl and EG: urea [35]. DESs containing carboxyl groups provide higher leaching efficiency than other DESs due to the large number of free protons and the strong coordination ability between the carboxylate and metals [36]. Consequently, the increase in the GLY molar ratio exhibited a significant effect on the leaching efficiency.

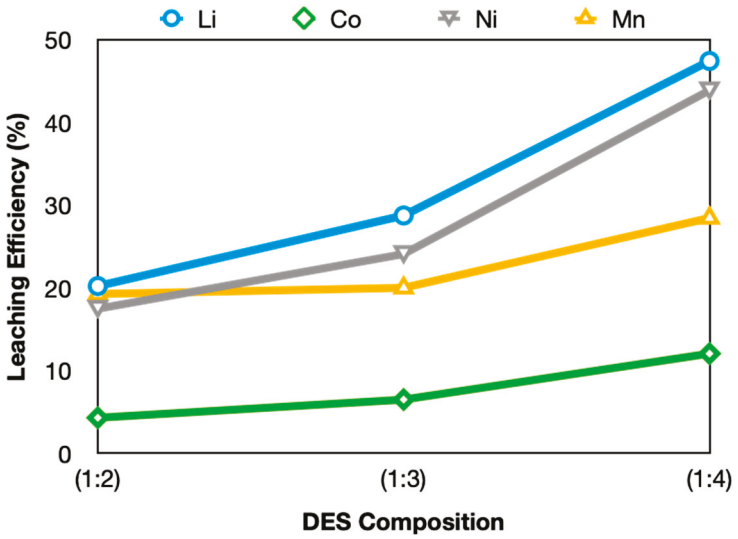


Figure 2. Leaching efficiencies obtained with ChCl:GLY Na-DES prepared at three different mole ratios (60 °C, 10 g/L, 1 h).

3.2.2. Effect of Ternary System Mole Ratios on Leaching Efficiency

The leaching efficiency could not be increased above 48% for four metals by the use of ChCl and GLY. Leaching studies with DESs prepared with oxalic acid (OxA) or MA (containing a carboxyl group): ChCl have been conducted in the literature, and leaching efficiencies are high [35,37]. Among the three acids (oxalic, malonic, and glycolic), oxalic acid demonstrates the highest degree of acidity due to its pronounced resonance and inductive effects. MA exhibits weaker interactions due to the presence of a leaving methylene group. GLY demonstrates the least acidic properties due to the absence of multiple carboxylic groups and the reliance on weaker inductive effects from its hydroxyl group. Nevertheless, the viscosity order of the DESs prepared separately with these three acids and ChCl is as follows: ChCl:GLY < ChCl: MA < ChCl:OxA [38]. The high viscosity values of DES pose a significant challenge in the utilization of these solvents in industrial recycling processes [39]. Therefore, the leaching efficiency of the mixture of GLY (containing a carboxyl group) and ChCl was tried to be increased by adding a third organic substance in DES. AA was added to the system to maintain the ChCl:acid ratio due to its reducing and solvent properties. As seen in Figure 3A, the addition of AA into the ChCl:GLY system significantly improved the leaching efficiencies of Li, Co, Ni, and Mn. In the reaction where 1:2 ChCl:GLY DES solution was used, 20.24%, 4.31%, 17.50%, and 19.28% leaching efficiency was obtained for Li, Co, Ni, and Mn, respectively. Moreover, in the reaction where 1:1.9:0.1 ChCl:GLY:AA was used, 99.68%, 98.95%, 98.58%, and 95.56% leaching efficiency was obtained for Li, Co, Ni, and Mn, respectively. However, increasing the amount of AA (1:1.8:0.2 and 1:1.7:0.3 ChCl:Gly:AA) caused a significant decrease in leaching efficiency. In their study, Liu et al. (2018) reported that an increase in the amount of AA in the ChCl:AA DES solution increased solution viscosity [40]. Additionally, Kaur et al. (2018) reported in their study that increasing the GLY ratio in the ChCl:GLY system decreased the viscosity [23]. It is thought that the decrease in the amount of GLY and the increase in the amount of AA in the ternary DES system increased viscosity. It has been demonstrated that elevated viscosity leads to increased solvent flow, as well as greater resistance to heat and mass transfer [41]. Consequently, this results in a reduction in leaching efficiency.

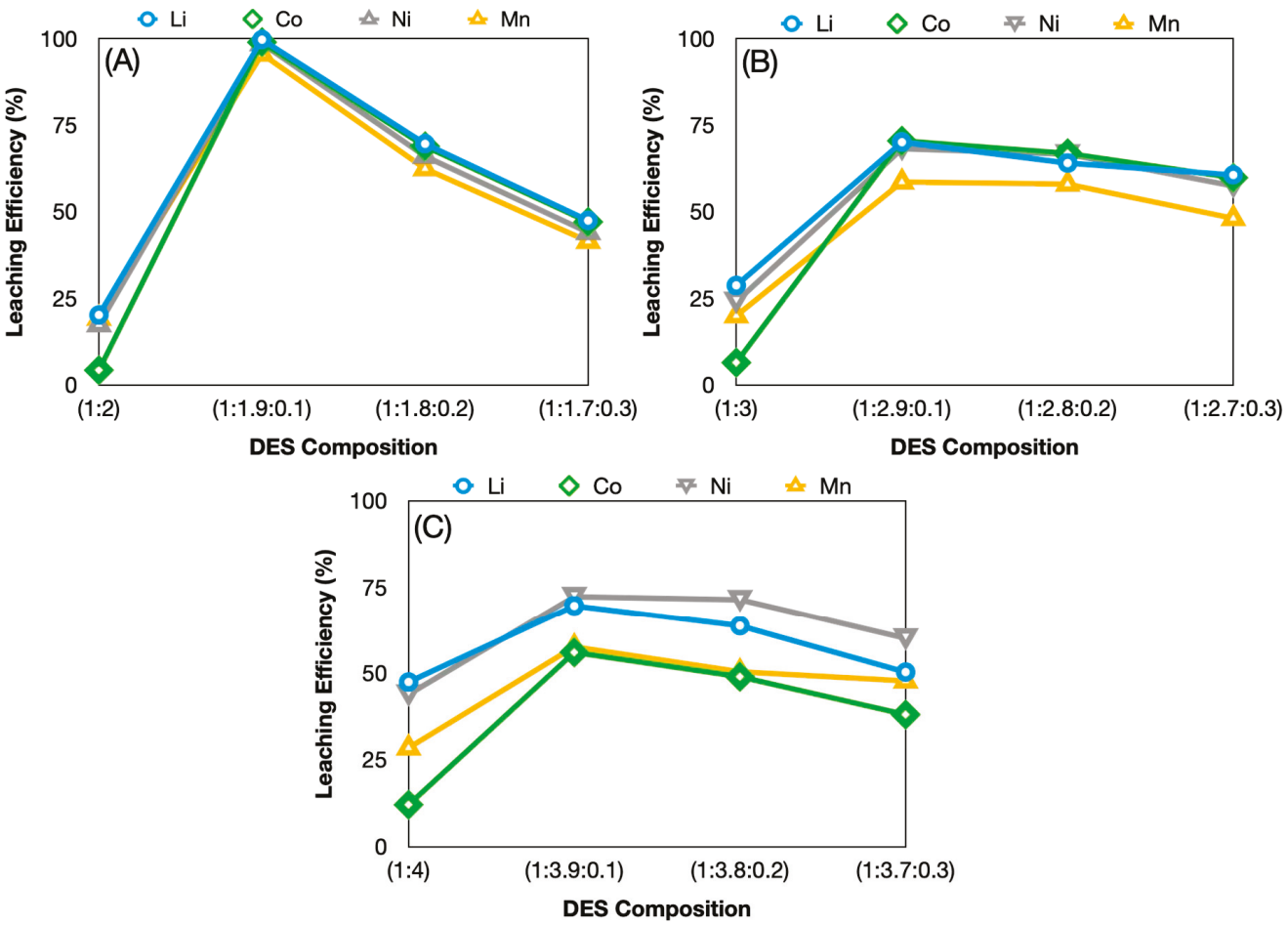


Figure 3. Leaching efficiencies obtained with ChCl:GLY:AA ternary Na-DES prepared at different mole ratios; 1:2 ChCl:Acid (**A**), 1:3 ChCl:Acid (**B**), and 1:4 ChCl:Acid (**C**) (60 °C, 10 g/L, 1 h).

In the leaching reactions where 1:3 ChCl:Acid and 1:4 ChCl:Acid systems were used, it was observed that the leaching efficiency did not exceed 70% (see Figure 3B,C). While 70.52% Co leaching efficiency was obtained in the leaching reaction using 1:2.9:0.1 ChCl:GLY:AA system, 56.01% Co leaching efficiency was obtained in the leaching reaction using 1:3.9:0.1 ChCl:GLY:AA system. The dissolution mechanism of LCO powders in DESs prepared with MA containing a carboxyl group and ChCl was explained [35]. It was shown that after the reduction from Co^{3+} to Co^{2+} by HBD, Cl^- anions in HBA formed complexes with Co^{2+} , and the formed complexes were tetrachloro complexes ($[Co(II)Cl_4]^{2-}$). This study observed that the leaching efficiency decreased with increasing acid-mole ratio in DES systems. The reason for this was thought to be the decrease in the amount of Cl^- anions that complex with metal ions. Due to the reducing nature of AA in ternary DES in this study, it easily reduces metal cations and then forms a complex with Cl^- in ChCl. It was thought that the decrease in the amount of ChCl decreased the leaching efficiency. Furthermore, an increase in AA content was observed in 1:3 and 1:4 ChCl:Acid systems, which exhibited a decrease in leaching efficiency, which was hypothesized to be attributable to an increase in viscosity. Additionally, leaching efficiencies varying with DES composition are summarized in Table 2.

Table 2. Summarized leaching efficiencies obtained with varying DES composition (60 °C, 10 g/L, 1 h).

DES Compositions	Leaching Efficiencies (%)			
	Li	Co	Ni	Mn
(1:2)	20.24	4.31	17.50	19.28
(1:1.9:0.1)	99.68	98.95	98.59	95.56
(1:1.8:0.2)	69.62	68.92	66.05	62.45
(1:1.7:0.3)	47.47	47.09	44.09	41.49
(1:3)	28.78	6.51	24.12	20.03
(1:2.9:0.1)	70.09	70.52	68.25	58.63
(1:2.8:0.2)	64.08	66.88	66.67	58.01
(1:2.7:0.3)	60.63	59.85	57.48	48.13
(1:4)	47.47	12.07	43.92	28.48
(1:3.9:0.1)	69.62	56.01	72.31	57.64
(1:3.8:0.2)	63.77	48.98	71.43	50.43
(1:3.7:0.3)	50.32	38.06	60.14	47.78

3.2.3. Effect of Time on Leaching Efficiency

The time-dependent leaching efficiency of the leaching reaction (60 °C, and 10 g/L) using the 1:1.9:0.1 ChCl:GLY:AA ternary DES system is given in Figure 4. It was determined that the leaching reaction achieved maximum efficiency at the 60th minute. The leaching of cathode powders utilizing binary DES, composed of an HBD and an HBA species, typically requires tens of hours or even days [42]. In the ternary system where GLY contains a carboxyl group, which has a high reducing capacity, such as AA, was used, complete dissolution of the cathode powder in the black mass was achieved in 60 min. Furthermore, in this study, black mass containing pure cathode powder was not utilized; however, the leaching process of cathode powders containing ~40% graphite by weight and exhibiting varying chemical compositions was conducted. Although the presence of graphite may reduce the leaching efficiency because it creates a physical barrier, a leaching efficiency of over 95% was achieved for all metals in 60 min.

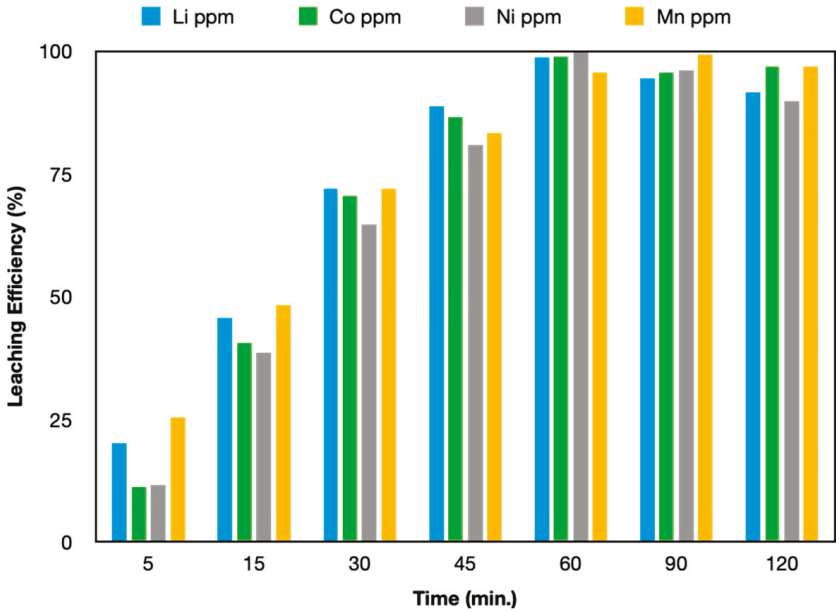


Figure 4. Time-dependent leaching efficiency of black mass (1:1.9:0.1 ChCl:GLY:AA, 60 °C, 10 g/L).

3.2.4. Effect of Temperature on Leaching Efficiency

Temperature is a crucial parameter in leaching processes involving DES. Due to the high viscosity of DES, higher temperatures are required compared to leaching reactions using inorganic acids [43]. Moreover, the viscosity of DES can be reduced either by adding water to the solution or by increasing the temperature; however, adding water may decrease leaching efficiency, as it can weaken the hydrogen bonding network within the DES [17]. In literature studies, ChCl–GLY DESs have been reported to decrease viscosities by 20-fold as the temperature increases from 20 °C to 80 °C [12]. Therefore, in this study, instead of adding water to DES, the effect of temperature on leaching efficiency was investigated. Additionally, the potential esterification of carboxyl groups in DES with the HBD must be considered when determining the operating temperature range [38]. Esterification reactions for DESs that use carboxylic acids as HBD and ChCl as HBA occur at temperatures above 60 °C [39,44]. Rodriguez et al. (2019) reported that esterification of 1%, 5%, and 9% (molar ratio) occurred in the system with the preparation of 1:2 ChCl:GLY at 60 °C, 80 °C, and 100 °C, respectively [45]. Due to these considerations, the leaching experiments in this study were limited to a temperature range between 20 °C and 60 °C, with no experiments conducted above 60 °C. The dependency of leaching efficiency on temperature is illustrated in Figure 5 (1:1.9:0.1 ChChl:GLY:AA, 60 min, and 10 g/L). Increasing the temperature from 20 °C to 60 °C caused an increase in leaching efficiencies from 24.63% to 95.56%, from 12.11% to 98.35%, from 12.9% to 98.59%, and from 12.95% to 99.68% for Li, Co, Ni, and Mn, respectively.

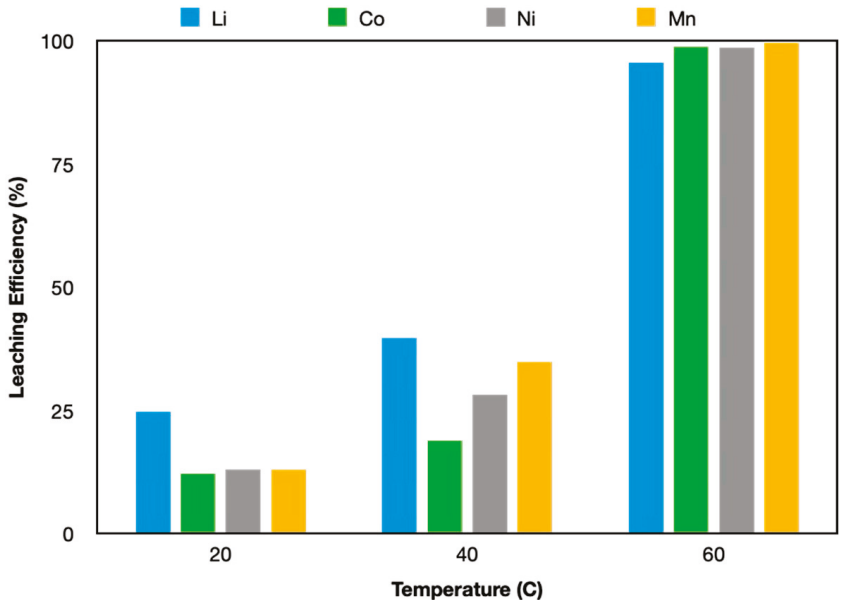


Figure 5. Temperature-dependent leaching efficiency of black mass (1:1.9:0.1 ChCl:GLY:AA, 60 min, 10 g/L).

3.2.5. Effect of Solid to Liquid Ratio on Leaching Efficiency

The effect of the solid-to-liquid ratio on leaching efficiency was investigated. The effect of 10–40 g/L solid-to-liquid ratio on leaching efficiency is given in Figure 6 (1:1.9:0.1 ChCl:GLY:AA, 60 min, 60 °C). Increasing the solid-to-liquid ratio from 10 g/L to 40 g/L resulted in a decrease in metal leaching efficiency from above 98% to 75.27%, 16.26%, 66.35%, and 39.06% for Li, Co, Ni, and Mn, respectively. At a certain solid-liquid ratio, the solution becomes saturated, and the amount of insoluble particles increases [46]. The optimum solid-liquid ratio was therefore maintained at 10 g/L.

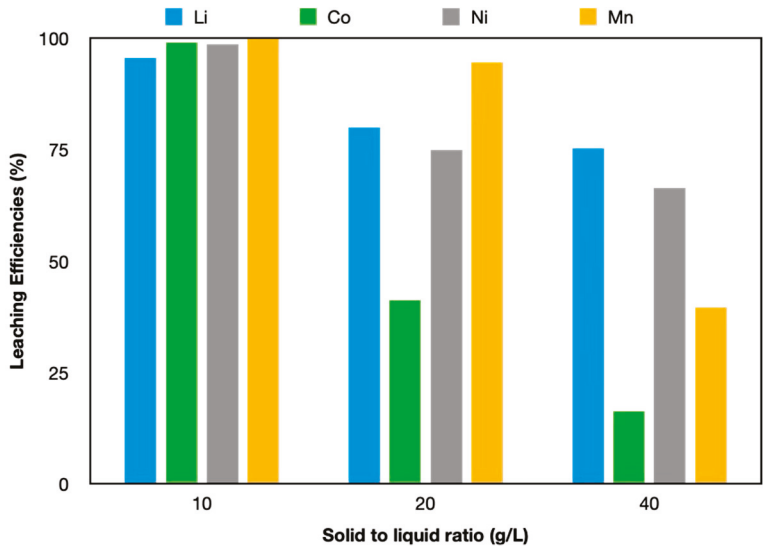


Figure 6. Effect of solid-to-liquid ratio on leaching efficiency of black mass (1:1.9:0.1 ChCl:GLY:AA, 60 min, 60 °C).

3.2.6. Leaching Kinetics

It is imperative to comprehend the kinetics of the leaching process to achieve a more profound comprehension of solid-liquid interactions and to ascertain the rate-limiting step of the reaction. A prevalent model employed for this purpose is the shrinking core model, which analyzes the interaction between solid particles and the leaching solution [44]. This model emphasizes the gradual reduction of the unreacted core within solid particles over time. This model is particularly useful in determining which stage governs the overall reaction rate during leaching. In instances where the rate-limiting step is a chemical reaction, Equation (3) is employed [47];

$$1 - (1 - x)^{\frac{1}{3}} = k_1 t. \quad (3)$$

In this equation, 'x' denotes the metal leaching rate, 't' represents time (in minutes), and 'k_1' is the reaction rate constant. Equation (4) provides a comprehensive description of the leaching process governed by chemical reaction control in dense shrinking spherical particles [47].

$$1 - (1 - x)^{\frac{1}{2}} = k_2 t. \quad (4)$$

The constants in this equation are identical to those in the previous one. Equation (5) signifies the scenario in which the reaction rate is governed by diffusion through the product layer surrounding the particles [15].

$$1 + 2(1 - x) - 3(1 - x)^{\frac{2}{3}} = k_3 t. \quad (5)$$

The leaching process was carried out with the parameters of 1:1.9:0.1 ChCl:GLY:AA, 60 min , 60 °C, 10 g/L, and the compatibility of 3 different models with the obtained leaching efficiencies was examined. The leaching kinetics of Li, Co, Ni, and Mn were evaluated using surface chemical reaction control (see Figure 7A), diffusion control (see Figure 7B), and shrinking dense particles (see Figure 7C). Additionally, kinetic model constants are presented in Table 3. However, it is difficult to conclude that any of these models accurately describes the leaching behavior of all four metals. The R values of four metals in all three models were found to be greater than 0.9 (except Ni, Diffusion), and it was thought that the kinetics of dissolution of the four metals in model 3 could be

explained. The reason for this was thought to be the use of cathode powders with different phases and chemical compositions. However, the R values for Li and Mn (>0.99) indicate a strong correlation with the surface chemical reaction model, whereas those for Co and Ni (>0.99) are in good agreement with the dense shrinking particle model. Furthermore, the reaction rate constants (k_1) for the dissolution of Li and Mn were calculated as 0.0116 and 0.0095 min^{-1} , respectively. The rate constants (k_2) for Co and Ni obtained from the diffusion-controlled model were found to be 0.016 and 0.0158 min^{-1} , respectively. Based on the obtained rate constants, the metal dissolution rates can be ranked as follows: Co > Li > Ni > Mn.

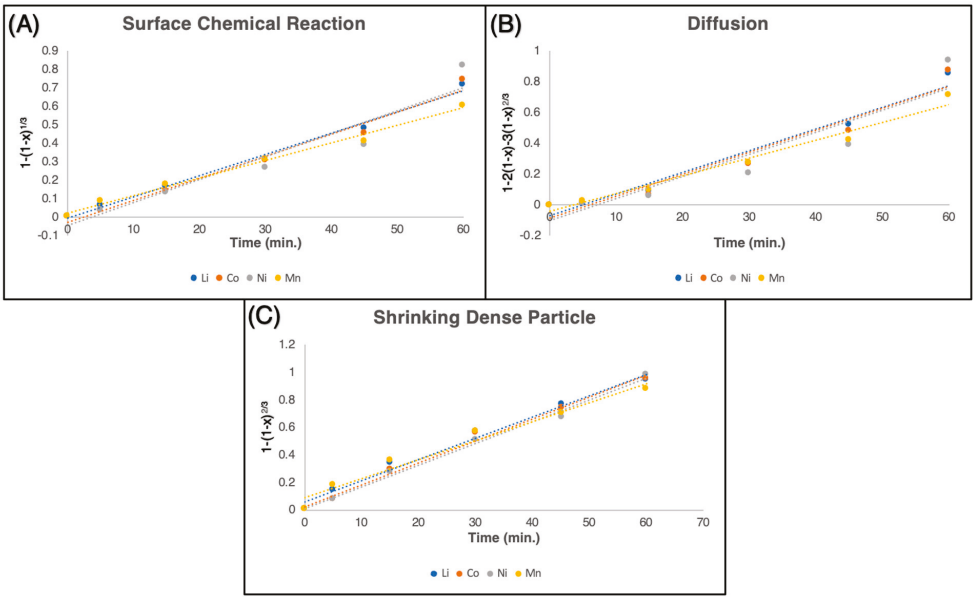


Figure 7. Leaching efficiencies' compatibility with surface chemical reaction (**A**), diffusion control (**B**), and shrinking dense particle models (**C**).

Table 3. Kinetic model fitting parameters for the leaching of Li^+ , Co^{2+} , Ni^{2+} , and Mn^{2+}.

Metals	Surface Chemical Reaction		Diffusion		Shrinking Dense Particle	
	Equation	R^2	Equation	R^2	Equation	R^2
Li	y = 0.0116x − 0.0067	0.9917	y = 0.0141x − 0.0716	0.9625	y = 0.0154x + 0.0602	0.9854
Co	y = 0.012x − 0.0282	0.9806	y = 0.0142x − 0.0859	0.9416	y = 0.016x + 0.0234	0.9914
Ni	y = 0.0124x − 0.0459	0.9231	y = 0.0143x − 0.1032	0.8676	y = 0.0158x + 0.0099	0.9935
Mn	y = 0.0095x + 0.0215	0.9907	y = 0.0116x − 0.0423	0.9735	y = 0.0138x + 0.0907	0.966

The Arrhenius equation, which is presented in Equation (6), is employed to calculate the dissolution activation energies of Li, Co, Ni, and Mn [48];

$$K_d = A \exp\left(\frac{-E_a}{RT}\right) \quad (6)$$

Here, the activation energy is denoted by E_a , the rate constant by K_d , the temperature in K by T, and the gas constant by R (8.314472 J $k^{-1}mol^{-1}$). The Arrhenius plots of ln (K_d) versus 1000/T for the leaching reactions of Li, Co, Ni, and Mn are presented in Figure 8. Moreover, the Arrhenius model constants are presented in Table 4. Based on the Arrhenius plots, activation energies for the leaching of Li, Co, Mn, and Ni were determined as 48.06, 71.06, 68.73, and 65.05 kJ/mol , respectively. Activation energy above 42 kJ/mol indicates a chemically controlled reaction, whereas values between 4.2 kJ/mol and 13 kJ/mol suggest diffusion control, and those ranging from 13 kJ/mol to 42 kJ/mol

imply mixed control [18]. The calculated activation energies for the four metals indicate that the dissolution reactions are chemically controlled.

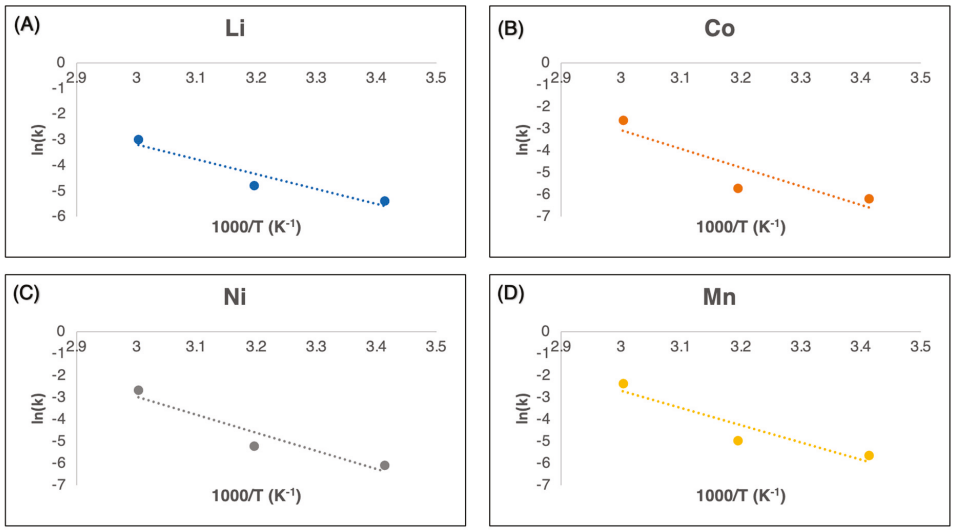


Figure 8. Arrhenius plot for Li (**A**), Co (**B**), Ni (**C**), and Mn (**D**).

Table 4. Arrhenius model fitting parameters for the leaching of Li^+ , Co^{2+} , Ni^{2+} , and Mn^{2+}.

Metals	Arrhenius Model Constant	
	Equation	R^2
Li	y = −5.7804x + 14.154	0.8975
Co	y = −8.5464x + 22.587	0.8222
Ni	y = −8.2663x + 21.844	0.9061
Mn	y = −7.8235x + 20.77	0.8708

3.2.7. Leaching Mechanism

As demonstrated in the extant literature, AA is employed in studies of the aqueous leaching of waste LIBs to reduce transition metals from +3 to +2 [49,50]. The oxidation reaction of AA is given in Figure 9 [48]. Moreover, the dissolution reactions of LCO in an aqueous system are presented in Equation (7) [51]. AA acts as a reducing agent for transition metal ions, facilitating their reduction while being oxidized to dehydroascorbic acid, thereby enhancing the leaching efficiency. In aqueous systems, AA functions not only as a reducing agent but also contributes to solvation, potentially enhancing the dissolution and mobility of metal ions [52]. However, in DES, this process may become more complex due to altered solvation dynamics and redox behavior. Carboxylic group-containing acids employed in DESs contribute to the system's acidity, functioning as leaching agents and, in certain cases, also exhibiting reducing properties [39]. Wen et al. (2023) investigated the leaching behavior of LCO cathode powders using a DES composed of ChCl and MA, demonstrating that the carboxyl groups in MA facilitated the reduction of Co^{3+} to Co^{2+} , which subsequently formed a $[CoCl_4]^{2-}$ complex with chloride anions [53]. Lu et al. (2022) reported comparable findings in a system utilizing MA and ChCl, further supporting the role of carboxyl groups in facilitating Co reduction and complexation in DES media [35]. The system utilized in this study combined AA, GLY, and ChCl, wherein AA exhibited reductive capabilities, while GLY contributed to increased solution acidity, effectively accelerating the leaching process.

$$LiCoO_{2(s)} + 4H^+_{(aq)} + e^-_{(aq)} \rightarrow Li^+_{(aq)} + Co^{2+}_{(aq)} + 2H_2O_{(l)} \quad (7)$$

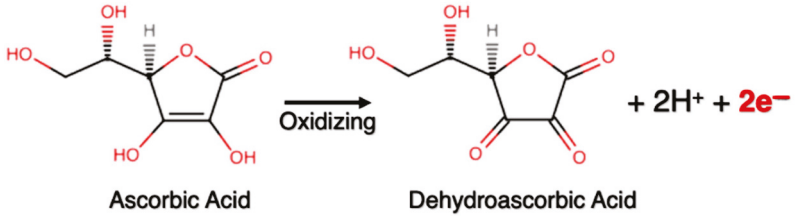


Figure 9. Oxidation reaction of ascorbic acid.

To identify the complexes that Co can potentially form following the leaching process, the bond energies between Co and various ligands were calculated. The complexes that Co can form and their bond energies are given in Figure 10. The presence of Co in tetrahedral form in DES solutions has been reported in another study [53]. The tetrahedral Co-glycolate (ΔE = 1.454 Hartree) complex exhibits a lower bonding energy compared to the corresponding Co-ascorbate (ΔE = 1.462 Hartree) complex. Following the leaching process, Co appears to exhibit a higher affinity for complexation with GLY rather than AA in the ternary DES system. The introduction of Cl^- anions into the tetrahedral coordination led to a further decrease in the bonding energies of the Co-ascorbate and Co-glycolate complexes, respectively. The $[CoCl_4]^{2-}$ complex, representing the complete occupation of tetrahedral coordination sites by Cl^- anions, exhibits the lowest bonding energy difference (ΔE = −0.413 Hartree). Based on the calculated bond energies, it is inferred that Co preferentially forms the $[CoCl_4]^{2-}$ complex with chloride anions rather than coordinating with AA or GLY. Comparable findings were reported in a separate study employing a similar methodological approach [53].

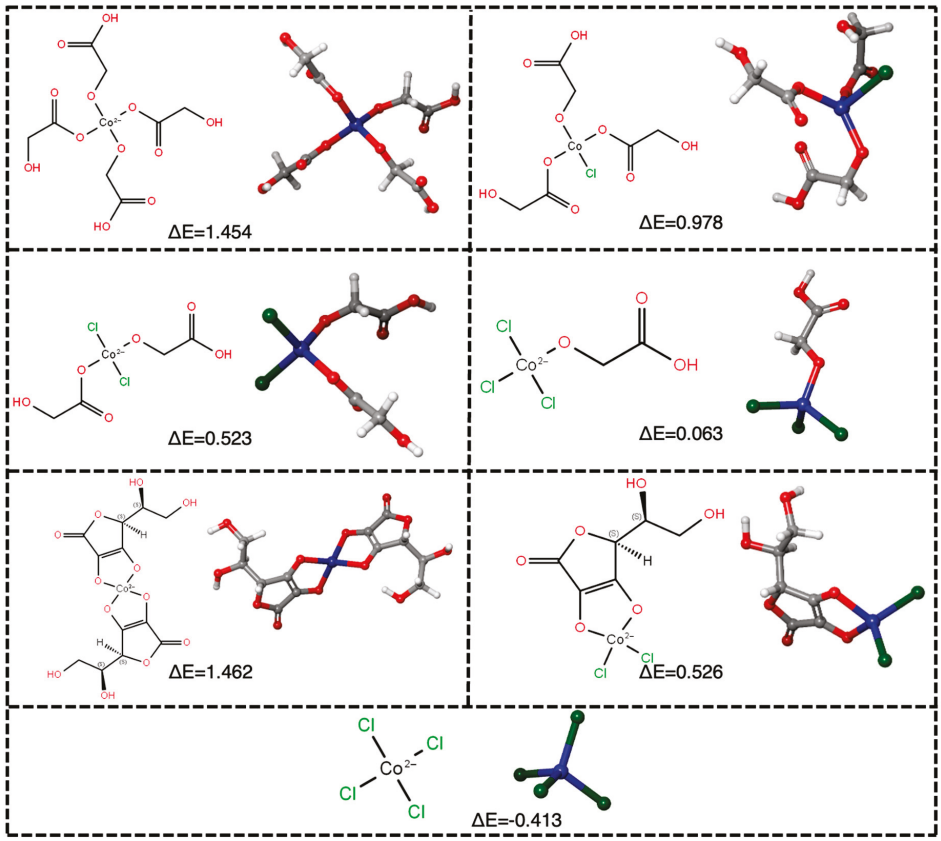


Figure 10. Potential complexes that may form after leaching.

4. Conclusions

In this study, an environmentally friendly leaching method was developed using a ternary DES system based on ChCl, GLY, and AA for the recovery of precious metals such as Li, Co, Ni, and Mn from the black mass fraction of spent lithium-ion batteries. The results showed that with the proposed 1:1.9:0.1 molar ratio ChCl:GLY:AA system, leaching efficiencies of over 95% for all metals could be achieved at 60 °C within only 1 h without applying a pre-enrichment process. Due to the reducing property of AA and the synergistic effect of the low viscosity structure of GLY, leaching kinetics were accelerated and metal solubility was optimized in DES medium. Also, as a forward-looking approach, the dissolved metal ions can be co-crystallized by antisolvent addition after adjusting their stoichiometry, enabling the regeneration of cathode precursors and closing the material recovery loop. In addition, kinetic analyses and DFT calculations showed that the leaching mechanism was controlled by chemical reactions, and Co ions predominantly formed $[CoCl_4]^{2-}$ complexes after dissolution. This study demonstrates that ternary DES systems based on environmentally friendly components such as glycolic acid and ascorbic acid can provide an effective leaching medium for the recovery of metals such as Li, Co, Ni, and Mn from lithium-ion battery waste. However, further research is needed regarding the industrial scalability, recyclability, and process integration of the method.

Author Contributions: F.N.: Methodology, Validation, Investigation, Formal analysis, Writing—original draft, Writing—review and editing. I.H.: Methodology, Validation, Investigation, Formal analysis, Writing—original draft, Writing—review and editing. E.U.: Validation, Investigation, Formal analysis, Writing—original draft, Writing—review and editing, Visualization, Conceptualization. H.N.D.: Validation, Investigation, Formal analysis. U.O.G.: Validation, Investigation, Formal analysis, Visualization. D.Y.Ö.: Formal analysis, Writing—original draft, Writing—review and editing. F.B.: Validation, Resources, Supervision, Project administration. S.G.: Validation, Resources, Supervision, Project administration. All authors have read and agreed to the published version of the manuscript.

Funding: The present study was supported by The Scientific and Technological Research Council of Turkey (TÜBİTAK) under the 2209-A University Students Research Projects Support Program (grant number: 1919B012420824).

Data Availability Statement: The datasets used and/or analyzed during the current study are available from the corresponding author upon reasonable request.

Acknowledgments: The authors thank Duygu Agaogulları for FTIR analysis.

Conflicts of Interest: The authors declare that they have no known competing financial interests or personal relationships that could have appeared to influence the work reported in this paper.

References

1. Golmohammadzadeh, R.; Faraji, F.; Rashchi, F. Recovery of Lithium and Cobalt from Spent Lithium Ion Batteries (LIBs) Using Organic Acids as Leaching Reagents: A Review. *Resour. Conserv. Recycl.* **2018** , *136* , 418–435. [CrossRef]
2. Tran, M.K.; Rodrigues, M.T.F.; Kato, K.; Babu, G.; Ajayan, P.M. Deep Eutectic Solvents for Cathode Recycling of Li-Ion Batteries. *Nat. Energy* **2019** , *4* , 339–345. [CrossRef]
3. Larouche, F.; Tedjar, F.; Amouzegar, K.; Houlachi, G.; Bouchard, P.; Demopoulos, G.P.; Zaghib, K. Progress and Status of Hydrometallurgical and Direct Recycling of Li-Ion Batteries and Beyond. *Materials* **2020** , *13* , 801. [CrossRef] [PubMed]
4. Domingues, A.M.; de Souza, R.G. Review of Life Cycle Assessment on Lithium-Ion Batteries (LIBs) Recycling. *Next Sustain.* **2024** , *3* , 100032. [CrossRef]
5. Padwal, C.; Pham, H.D.; Jadhav, S.; Do, T.T.; Nerkar, J.; Hoang, L.T.M.; Kumar Nanjundan, A.; Mundree, S.G.; Dubal, D.P. Deep Eutectic Solvents: Green Approach for Cathode Recycling of Li-Ion Batteries. *Adv. Energy Sustain. Res.* **2022** , *3* , 2100133. [CrossRef]
6. Garole, D.J.; Hossain, R.; Garole, V.J.; Sahajwalla, V.; Nerkar, J.; Dubal, D.P. Recycle, Recover and Repurpose Strategy of Spent Li-Ion Batteries and Catalysts: Current Status and Future Opportunities. *ChemSusChem* **2020** , *13* , 3079–3100. [CrossRef] [PubMed]

7. Jin, X.; Zhang, P.; Teng, L.; Rohani, S.; He, M.; Meng, F.; Liu, Q.; Liu, W. Acid-Free Extraction of Valuable Metal Elements from Spent Lithium-Ion Batteries Using Waste Copperas. *Waste Manag.* **2023** , *165* , 189–198. [CrossRef] [PubMed]
8. Li, S.; Wu, X.; Jiang, Y.; Zhou, T.; Zhao, Y.; Chen, X. Novel Electrochemically Driven and Internal Circulation Process for Valuable Metals Recycling from Spent Lithium-Ion Batteries. *Waste Manag.* **2021** , *136* , 18–27. [CrossRef] [PubMed]
9. Gao, W.; Zhang, X.; Zheng, X.; Lin, X.; Cao, H.; Zhang, Y.; Sun, Z. Lithium Carbonate Recovery from Cathode Scrap of Spent Lithium-Ion Battery: A Closed-Loop Process. *Environ. Sci. Technol.* **2017** , *51* , 1662–1669. [CrossRef] [PubMed]
10. Panda, P.; Mishra, S. Optimization of Leaching of Lithium and Cobalt from Spent Lithium-Ion Batteries by the Choline Chloride-Citric Acid/Malonic Acid DES Using Response Surface Methodology. *Environ. Res.* **2025** , *269* , 120917. [CrossRef] [PubMed]
11. Stegemann, L.; Gutscha, M. Environmental Impacts of Pyro- and Hydrometallurgical Recycling for Lithium-Ion Batteries—A Review. *J. Bus. Chem.* **2025** , *22* , 62–71. [CrossRef]
12. Li, B.; Li, Q.; Wang, Q.; Yan, X.; Shi, M.; Wu, C. Deep Eutectic Solvent for Spent Lithium-Ion Battery Recycling: Comparison with Inorganic Acid Leaching. *Phys. Chem. Chem. Phys.* **2022** , *24* , 19029–19051. [CrossRef] [PubMed]
13. Abbott, A.P.; Capper, G.; Davies, D.L.; Rasheed, R.K.; Tambyrajah, V. Novel Solvent Properties of Choline Chloride/Urea Mixtures. *Chem. Commun.* **2003** , *1* , 70–71. [CrossRef] [PubMed]
14. Cichowska-Kopczyńska, I.; Nowosielski, B.; Warmińska, D. Deep Eutectic Solvents: Properties and Applications in CO_2 Separation. *Molecules* **2023** , *28* , 5293. [CrossRef] [PubMed]
15. Peeters, N.; Binnemans, K.; Riaño, S. Solvometallurgical Recovery of Cobalt from Lithium-Ion Battery Cathode Materials Using Deep-Eutectic Solvents. *Green Chem.* **2020** , *22* , 4210–4221. [CrossRef]
16. Ma, C.; Svärd, M.; Forsberg, K. Recycling Cathode Material LiCo1/3Ni1/3Mn1/3O2 by Leaching with a Deep Eutectic Solvent and Metal Recovery with Antisolvent Crystallization. *Resour. Conserv. Recycl.* **2022** , *186* , 106579. [CrossRef]
17. Wang, J.; Lyu, Y.; Zeng, R.; Zhang, S.; Davey, K.; Mao, J.; Guo, Z. Green Recycling of Spent Li-Ion Battery Cathodes via Deep-Eutectic Solvents. *Energy Environ. Sci.* **2024** , *17* , 867–884. [CrossRef]
18. Jafari, M.; Shafaie, S.Z.; Abdollahi, H.; Entezari-Zarandi, A. Green Recycling of Spent Li-Ion Batteries by Deep Eutectic Solvents (DESs): Leaching Mechanism and Effect of Ternary DES. *J. Environ. Chem. Eng.* **2022** , *10* , 109014. [CrossRef]
19. Svigelj, R.; Dossi, N.; Grazioli, C.; Toniolo, R. Deep Eutectic Solvents (Dess) and Their Application in Biosensor Development. *Sensors* **2021** , *21* , 4263. [CrossRef] [PubMed]
20. Shi, D.; Zhou, F.; Mu, W.; Ling, C.; Mu, T.; Yu, G.; Li, R. Deep Insights into the Viscosity of Deep Eutectic Solvents by an XGBoost-Based Model plus SHapley Additive exPlanation. *Phys. Chem. Chem. Phys.* **2022** , *24* , 26029–26036. [CrossRef] [PubMed]
21. PubChem Glycolic Acid. Available online: https://pubchem.ncbi.nlm.nih.gov/compound/757 (accessed on 1 May 2025).
22. Emel'Yanenko, V.N.; Verevkin, S.P.; Stepurko, E.N.; Roganov, G.N.; Georgieva, M.K. Thermodynamic Properties of Glycolic Acid and Glycolide. *Russ. J. Phys. Chem. A* **2010** , *84* , 1301–1308. [CrossRef]
23. Kaur, P.; Rajani, N.; Kumawat, P.; Singh, N.; Kushwaha, J.P. Performance and Mechanism of Dye Extraction from Aqueous Solution Using Synthesized Deep Eutectic Solvents. *Colloids Surf. A Physicochem. Eng. Asp.* **2018** , *539* , 85–91. [CrossRef]
24. PubChem Ascorbic Acid. Available online: https://pubchem.ncbi.nlm.nih.gov/compound/54670067 (accessed on 1 May 2025).
25. Opinion, S. Scientific Opinion on the Safety and Efficacy of Vitamin C (Ascorbic Acid, Sodium Ascorbate, Calcium Ascorbate, Ascorbyl Palmitate, Sodium Calcium Ascorbyl Phosphate and Sodium Ascorbyl Phosphate) as a Feed Additive for All Animal Species Based on a Dossi submitted by DSM Nutritional Products Ltd. *EFSA J.* **2013** , *11* , 3104. [CrossRef]
26. Gęgotek, A.; Skrzydlewska, E. Antioxidative and Anti-Inflammatory Activity of Ascorbic Acid. *Antioxidants* **2022** , *11* , 1993. [CrossRef] [PubMed]
27. Garshin, A.P.; Shvaiko-Shvaikovskii, V.E. Mechanism of Oxidation of β-BN. *Sov. Powder Metall. Met. Ceram.* **1992** , *31* , 656–661. [CrossRef]
28. Uysal, E.; Dursun, H.N.; Kaya, F.; Burat, F.; Gürmen, S. Recycling of EoL Batteries with Ultrasonic Assisted Nitric-Ascorbic Acid Leaching: Experimental Design and Process Optimization. *Min. Metall. Explor.* **2025**. [CrossRef]
29. Surel, A.S.; Gul, M.F.; Uysal, E.; Yesiltepe-Ozcelik, D.; Gurmen, S. Pulse Ultrasonication Leaching Approach for Selective Li Leaching from Spent LFP Cathode Material. *Can. Metall. Q.* **2024** , *63* , 857–869. [CrossRef]
30. Neese, F.; Wennmohs, F.; Becker, U.; Riplinger, C. The ORCA Quantum Chemistry Program Package. *J. Chem. Phys.* **2020** , *152* , 224108. [CrossRef] [PubMed]
31. Stefanovic, R.; Ludwig, M.; Webber, G.B.; Atkin, R.; Page, A.J. Nanostructure, Hydrogen Bonding and Rheology in Choline Chloride Deep Eutectic Solvents as a Function of the Hydrogen Bond Donor. *Phys. Chem. Chem. Phys.* **2017** , *19* , 3297–3306. [CrossRef] [PubMed]
32. Fuzlin, A.F.; Saadiah, M.A.; Yao, Y.; Nagao, Y.; Samsudin, A.S. Enhancing Proton Conductivity of Sodium Alginate Doped with Glycolic Acid in Bio-Based Polymer Electrolytes System. *J. Polym. Res.* **2020** , *27* , 207. [CrossRef]
33. Rahmalia, W.; Shofiyani, A.; Sutiknyawati, Y.; Septiani, S. Simple Green Routes for Metal-Bixin Complexes Synthesis Using Glycerol-Based Deep Eutectic Solvent. *Indones. J. Chem.* **2022** , *22* , 1759. [CrossRef]

34. Ling, J.K.U.; Chan, Y.S.; Nandong, J.; Chin, S.F.; Ho, B.K. Formulation of Choline Chloride/Ascorbic Acid Natural Deep Eutectic Solvent: Characterization, Solubilization Capacity and Antioxidant Property. *LWT* **2020** , *133* , 110096. [CrossRef]
35. Lu, B.; Du, R.; Wang, G.; Wang, Y.; Dong, S.; Zhou, D.; Wang, S.; Li, C. High-Efficiency Leaching of Valuable Metals from Waste Li-Ion Batteries Using Deep Eutectic Solvents. *Environ. Res.* **2022** , *212* , 113286. [CrossRef] [PubMed]
36. Zhu, A.; Bian, X.; Han, W.; Cao, D.; Wen, Y.; Zhu, K.; Wang, S. The Application of Deep Eutectic Solvents in Lithium-Ion Battery Recycling: A Comprehensive Review. *Resour. Conserv. Recycl.* **2023** , *188* , 106690. [CrossRef]
37. Luo, Y.; Ou, L.; Yin, C. High-Efficiency Recycling of Spent Lithium-Ion Batteries: A Double Closed-Loop Process. *Sci. Total Environ.* **2023** , *875* , 162567. [CrossRef] [PubMed]
38. Florindo, C.; Oliveira, F.S.; Rebelo, L.P.N.; Fernandes, A.M.; Marrucho, I.M. Insights into the Synthesis and Properties of Deep Eutectic Solvents Based on Cholinium Chloride and Carboxylic Acids. *ACS Sustain. Chem. Eng.* **2014** , *2* , 2416–2425. [CrossRef]
39. Svärd, M.; Ma, C.; Forsberg, K.; Schiavi, P.G. Addressing the Reuse of Deep Eutectic Solvents in Li-Ion Battery Recycling: Insights into Dissolution Mechanism, Metal Recovery, Regeneration and Decomposition. *ChemSusChem* **2024** , *17* , e202400410. [CrossRef] [PubMed]
40. Liu, W.; Zhang, K.; Chen, J.; Yu, J. Ascorbic Acid and Choline Chloride: A New Natural Deep Eutectic Solvent for Extracting Tert-Butylhydroquinone Antioxidant. *J. Mol. Liq.* **2018** , *260* , 173–179. [CrossRef]
41. Alhadid, A.; Mokrushina, L.; Minceva, M. Influence of the Molecular Structure of Constituents and Liquid Phase Non-Ideality on the Viscosity of Deep Eutectic Solvents. *Molecules* **2021** , *26* , 4208. [CrossRef] [PubMed]
42. Huang, F.; Li, T.; Yan, X.; Xiong, Y.; Zhang, X.; Lu, S.; An, N.; Huang, W.; Guo, Q.; Ge, X. Ternary Deep Eutectic Solvent (DES) with a Regulated Rate-Determining Step for Efficient Recycling of Lithium Cobalt Oxide. *ACS Omega* **2022** , *7* , 11452–11459. [CrossRef] [PubMed]
43. Guo, M.; Deng, R.; Gao, M.; Xu, C.; Zhang, Q. Sustainable Recovery of Metals from E-Waste Using Deep Eutectic Solvents: Advances, Challenges, and Perspectives. *Curr. Opin. Green Sustain. Chem.* **2024** , *47* , 100913. [CrossRef]
44. Bilen, A.; Birol, B.; Saridede, M.N.; Kaplan, Ş.S.; Sönmez, M.Ş. Direct Microwave Leaching Conditions of Rare Earth Elements in Fluorescent Wastes. *J. Rare Earths* **2024** , *42* , 1165–1174. [CrossRef]
45. Rodriguez Rodriguez, N.; Van Den Bruinhorst, A.; Kollau, L.J.B.M.; Kroon, M.C.; Binnemans, K. Degradation of Deep-Eutectic Solvents Based on Choline Chloride and Carboxylic Acids. *ACS Sustain. Chem. Eng.* **2019** , *7* , 11521–11528. [CrossRef]
46. Ni'am, A.C.; Wang, Y.-F.; Chen, S.-W.; You, S.-J. Recovery of Rare Earth Elements from Waste Permanent Magnet (WPMs) via Selective Leaching Using the Taguchi Method. *J. Taiwan Inst. Chem. Eng.* **2019** , *97* , 137–145. [CrossRef]
47. Faraji, F.; Alizadeh, A.; Rashchi, F.; Mostoufi, N. Kinetics of Leaching: A Review. *Rev. Chem. Eng.* **2022** , *38* , 113–148. [CrossRef]
48. Morelli, M.B.; Gambardella, J.; Castellanos, V.; Trimarco, V.; Santulli, G. Vitamin C and Cardiovascular Disease: An Update. *Antioxidants* **2020** , *9* , 1227. [CrossRef] [PubMed]
49. Aaltonen, M.; Peng, C.; Wilson, B.; Lundström, M. Leaching of Metals from Spent Lithium-Ion Batteries. *Recycling* **2017** , *2* , 20. [CrossRef]
50. Li, L.; Lu, J.; Ren, Y.; Zhang, X.X.; Chen, R.J.; Wu, F.; Amine, K. Ascorbic-Acid-Assisted Recovery of Cobalt and Lithium from Spent Li-Ion Batteries. *J. Power Sources* **2012** , *218* , 21–27. [CrossRef]
51. Porvali, A.; Shukla, S.; Lundström, M. Low-Acid Leaching of Lithium-Ion Battery Active Materials in Fe-Catalyzed Cu-H_2SO_4 System. *Hydrometallurgy* **2020** , *195* , 105408. [CrossRef]
52. Chen, H.; Gu, S.; Guo, Y.; Dai, X.; Zeng, L.; Wang, K.; He, C.; Dodbiba, G.; Wei, Y.; Fujita, T. Leaching of Cathode Materials from Spent Lithium-Ion Batteries by Using a Mixture of Ascorbic Acid and HNO_3. *Hydrometallurgy* **2021** , *205* , 105746. [CrossRef]
53. Wen, Y.; He, X.; Di, S.; Liu, K.; Li, D.; Du, J. Comparative of Malonic Acid Aqueous Solution and Malonic Acid-Based Deep Eutectic Solvent for LiCoO2 Cathode Materials Recovery: Leaching Efficiency and Mechanism. *J. Environ. Chem. Eng.* **2023** , *11* , 110979. [CrossRef]

Disclaimer/Publisher's Note: The statements, opinions and data contained in all publications are solely those of the individual author(s) and contributor(s) and not of MDPI and/or the editor(s). MDPI and/or the editor(s) disclaim responsibility for any injury to people or property resulting from any ideas, methods, instructions or products referred to in the content.

minerals

MDPI

Article

Enhanced Chromite Recovery from Tailings via a Custom-Designed Shaking Table: Optimization and Performance

Savas Ozun * and Ahmet Kerim Guraslan

Department of Mining Engineering, Faculty of Engineering and Natural Sciences, Süleyman Demirel University, Isparta 32260, Türkiye

* Correspondence: savasozun@sdu.edu.tr

Abstract: Significant chromite losses to tailings in gravity separation plants arise from both suboptimal separator design and inefficient beneficiation processes, posing major challenges to resource utilization, energy efficiency, and environmental sustainability. These losses are particularly critical because the material, already comminuted to liberation size, is discarded, leading to reduced concentrate yield, wasted energy input, and increased environmental pollution. To address this issue, an industrial-scale custom-designed shaking table was developed and tested to recover marketable-grade chromite concentrate ($\geq$42% Cr_2O_3) from processing plant tailings containing 3.25%–4.25% Cr_2O_3, which had accumulated over years of chromite beneficiation. Experimental results showed that, under optimized operating parameters (320 rpm stroke frequency, 13 mm stroke length, 1° deck slope, 1300 g/L pulp density, 800 kg/h feed rate, and 7 tph wash water flow rate), Cr_2O_3 recovery increased from 8% to 27% for the first and second floor operations and from approximately 17% to 41% for the third and fourth floor operations compared with existing plant performance. The results revealed a strong interdependence between Cr_2O_3 recovery and concentrate grade, both of which are critical indicators of process efficiency. Intermediate particle sizes (−0.250 + 0.150 mm) provided the most favorable balance, yielding high recovery rates without substantially compromising the concentrated grade.

Keywords: chromite; tailings; recovery; custom-designed shaking table; optimum variables; comparison

1. Introduction

Chromium is a naturally occurring element in the Earth's crust and is present in approximately 25 different minerals. Among these, chromite is the most common and contains the highest chromium content [1]. It is a critical mineral for several key industries essential to modern life, including the chemical, metallurgical, refractory, and foundry sectors. The production of stainless steel is the primary driver of ferrochrome demand, accounting for approximately 94% of global chromium consumption [2,3].

Globally, there are over 12 billion tons of marketable chromite reserves, with the majority hosted in stratiform-type deposits. Podiform deposits constitute the second largest source of chromite reserves, while laterites—weathering products of peridotite—contribute minimally to global chromite production [4–8]. Chromite-bearing ores are commonly associated with gangue minerals like olivine, serpentine, chlorite-group minerals, feldspars, and pyroxenes, with specific gravities ranging from approximately 2.6 to 4 g/cm^3 [9]. Processing generally involves comminution to liberate chromite particles, followed by concentration to achieve marketable Cr_2O_3 grades exceeding 34%, which can be directly used in industrial applications.

Numerous studies have employed gravity separation techniques for the beneficiation of chromite ores. These studies highlight the effectiveness of various gravity methods, such as shaking tables, spirals, jigs, and dense media separation, in concentrating chromite [10–14]. The significant density difference between chromite (3.58–5.09 g/cm^3) [15,16] and its associated gangue minerals makes gravity concentration the most widely employed and well-established beneficiation method. This approach enables the economical separation of valuable chromite particles from gangue while allowing precise control over operational parameters to achieve higher concentrate grades [17–21]. Among various gravity separation techniques, shaking tables are particularly preferred for chromite beneficiation because they combine relatively low operating costs with operational simplicity and minimal maintenance requirements compared to alternative methods [22]. They operate on the flowing film principle, where a thin slurry layer moves across a riffled deck, enabling density-driven stratification and differential motion of particles for effective separation. Although they offer high separation efficiency, particularly for fine- and medium-sized particles, the process, like other flowing film-based methods, is highly sensitive to feed rates. Mono-layer feeding, where particles are distributed in a single layer, enhances separation performance and enrichment efficiency by ensuring direct interaction between particles and the flowing film, allowing gravity to act more selectively [23]. In contrast, industrial operations often prioritize throughput over selectivity, using multi-layer feeding in which particles interact with one another rather than the separating medium, thereby reducing concentrate purity [2,24].

With the depletion of high-grade ores that can be directly used after mining, the enrichment of fine-grained and low-grade ore reserves has become increasingly important to meet industrial demand [25]. Consequently, lower-grade ores can be upgraded for industrial applications using suitable beneficiation techniques, depending on the degree of particle liberation and the nature of the associated gangue minerals [2,26]. At the same time, critical design parameters of shaking tables—such as stroke, stroke length, and inclination—are often fixed or difficult to adjust in industrial settings. Inadequate control over these variables reduces separation efficiency and leads to substantial chromite losses to tailings, even though these particles incur almost no comminution cost. Such losses not only represent a loss of valuable material but also contribute to environmental risks and storage challenges [3], prompting both industrial practice and academic research to increasingly focus on developing strategies for minimizing chromite losses in tailings during gravity separation [5,13,14,21,27].

This study focuses on recovering chromite from plant tailings using a custom-designed, industrial-scale shaking table that was both modified and operationally optimized for enhanced performance. The novelty lies in combining the valorization of low-grade tailings with the development of a shaking table offering on-site adjustment of critical parameters, such as stroke, stroke length, and slope, features typically absent or highly constrained in conventional systems. This adaptability enables more efficient chromite recovery under challenging conditions, particularly at higher strokes and shorter stroke lengths, which exceed the capabilities of existing plant tables. The research specifically aimed to produce marketable chromite concentrate (>42% Cr_2O_3) from tailings, identify optimal operating parameters, and benchmark the new design against current plant equipment. By targeting the recovery of approximately 10 million tons of accumulated tailings (3.25%–4.25% Cr_2O_3, comparable to run-of-mine ore) from a long-standing mining operation in Bursa, the study provides a practical, cost-effective pathway for improving chromite beneficiation efficiency.

2. Materials and Methods

2.1. Taking Samples from the Tailings Storage Area

The physical conditions of the tailings storage area were first evaluated to establish an optimal starting point for reprocessing, as the tailings originated from previous plant operations, including grinding, screening, classification, and gravity separation. Samples were systematically collected from storage areas 1–3 (Figure 1) using a 5 m × 5 m grid sampling method with JCB-type backhoe loaders (Rochester, UK). Before testing, samples from different storage areas were combined using a Bobcat mini loader, then subdivided into representative samples applying alternate shovel sampling and coning–quartering for laboratory analysis.

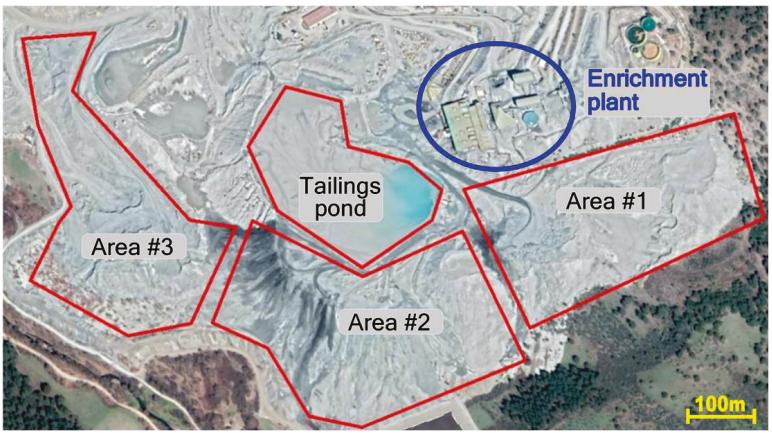


Figure 1. Chromite enrichment plant and tailings storage area.

For particle size adjustment, the mills previously employed for grinding were operated at low speeds (10 rpm) to disperse and disintegrate any agglomerated particles before the tests. In some cases, a small proportion of grinding balls (<5% by volume) was added to break down larger ore fragments, ensuring a uniform particle size distribution for subsequent processing.

2.2. Petrographic and XRD (X-Ray Diffraction) Analyses

The investigated chrome spinel-bearing ultramafic rock is identified as serpentinized dunite. Petrographic and XRD analyses were conducted to determine the mineralogical composition of the rock. The XRD results reveal that the rock consists of forsterite (olivine), serpentine (antigorite, chrysotile), chromite, and magnetite minerals (Figure 2). Thin-section analysis (Figure 3) indicates that olivine has undergone extensive serpentinization, with more than 50% of the original olivine minerals altered to serpentine. However, tiny relict olivine minerals (from 0.300 to 0.020 mm) are still observable. Under crossed polarized light, olivine exhibits third- to fourth-order interference colors, while appearing colorless under plane polarized light. Disseminated Cr-spinel crystals are mainly opaque and dispersed within the serpentine matrix. The chromian spinels are mainly subhedral to anhedral in shape and fine- to medium-grained (ranging in size from 1.5 mm to 0.005 mm, average < 0.350 mm). They display pull-apart structures, with fractures filled with serpentine minerals.

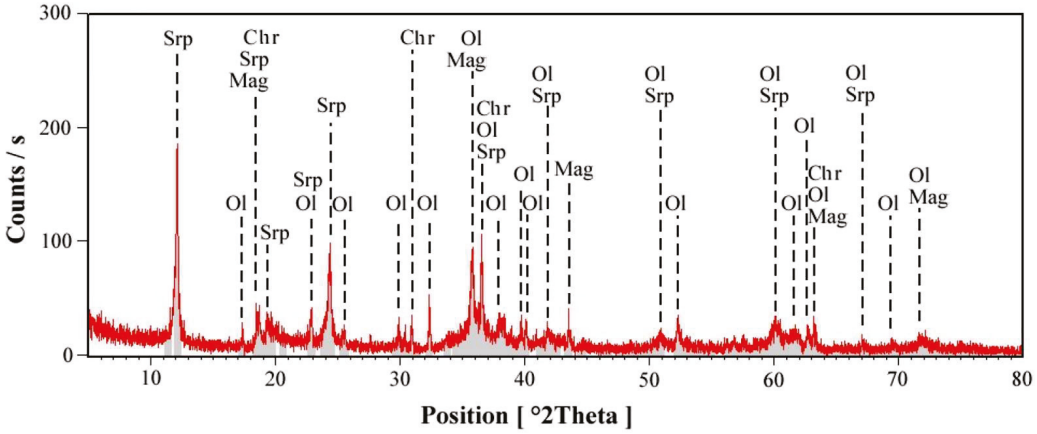


Figure 2. X-ray pattern of as received tailings sample (Ol: olivine, Chr: chrome spinel, Srp: serpentine, Mag: magnetite).

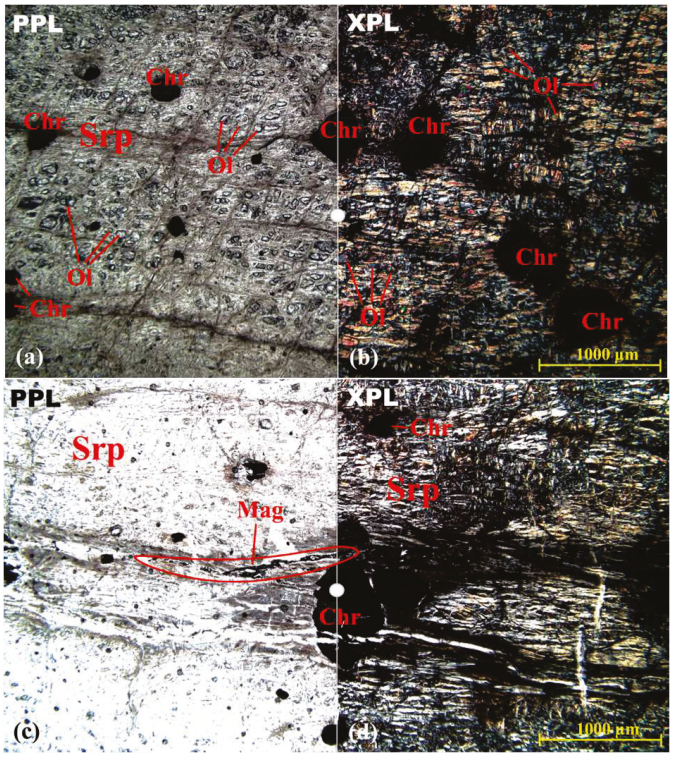


Figure 3. Photomicrographs of the sample in (**a**,**c**) plane polarized light (PPL) and (**b**,**d**) crossed polarized light (XPL) (Ol: olivine, Chr: chrome spinel, Srp: serpentine, Mag: magnetite).

2.3. XRF (X-Ray Fluorescence) Analysis

Chemical analyses of the as-received tailings sample (used as the feed) and the concentrate, middling, and waste samples obtained from the experiments were conducted using a Thermo Fisher Scientific Niton XL3t XRF (Waltham, MA, USA) analyzer. Calibration with standards of known composition before measurements ensured high analytical accuracy and minimized error. The results for the as-received tailings sample are presented in Table 1.

Table 1. Chemical analysis of the as-received tailings sample.

Component	%
Cr_2O_3	4.14
FeO	6.11
SiO_2	36.82
MgO	38.3
CaO	0.95
Al_2O_3	1.4

2.4. Particle Size Analysis

The particle size distribution of the tailing sample used in the experimental tests was determined by wet sieving. The size distribution and corresponding Cr_2O_3% content of each size range are given in Table 2. According to the results, the Cr_2O_3% content varied between 1.61% and 5.90%. The lowest Cr_2O_3 content was obtained in larger particle sizes, while the grade increased as the particle size decreased, resulting in the highest Cr_2O_3 grade with −0.150 mm particle size. Given that the Cr_2O_3 grade for the +0.500 mm size was below 1% and accounted for less than 0.6% of the total feed, the sample finer than 0.500 mm was used throughout the study.

Table 2. Size distribution of the as-received tailings sample.

Particle Size (mm)	Weight (%)	∑ Undersize (%)	Cr_2O_3 (%)	Cr_2O_3 Distribution (%)
+1	0.28	100.00	1.61	0.11
−1 + 0.850	0.05	99.72	1.73	0.02
−0.850 + 0.710	0.06	99.68	1.86	0.03
−0.710 + 0.600	0.23	99.61	2.01	0.11
−0.600 + 0.500	0.48	99.38	2.46	0.28
−0.500 + 0.425	8.70	98.90	2.55	5.36
−0.425 + 0.355	15.38	90.21	2.65	9.84
−0.355 + 0.300	8.89	74.82	3.35	7.19
−0.300 + 0.250	15.32	65.93	3.70	13.68
−0.250 + 0.212	3.71	50.62	4.13	3.70
−0.212 + 0.180	6.12	46.90	4.28	6.32
−0.180 + 0.150	9.17	40.78	4.32	9.56
−0.150 + 0.125	3.71	31.62	5.49	4.91
−0.125 + 0.106	6.17	27.91	5.81	8.65
−0.106 + 0.090	4.35	21.74	5.76	6.04
−0.090 + 0.075	3.51	17.40	5.68	4.82
−0.075 + 0.063	3.17	13.88	5.87	4.50
−0.063 + 0.053	1.64	10.71	5.81	2.29
−0.053 + 0.045	2.20	9.07	5.90	3.13
−0.045 + 0.038	2.84	6.88	5.73	3.93
−0.038	4.04	4.04	5.67	5.53
Total	**100**		**4.14**	

2.5. Shaking Table Customization and the Methods Applied

The shaking tables in the existing plant have been in operation for many years and exhibit limited flexibility in adjusting key operating parameters such as stroke, stroke length, and deck slope. Furthermore, mechanical fatigue has reduced their overall operational efficiency. To address these limitations, while preserving the principal design characteristics of the plant-scale shaking table, specifically the deck dimensions (488 cm × 183 cm) and the riffle configuration on the deck (3 mm high and spaced 6 mm apart), a customized shaking table with easily adjustable high stroke speeds, variable stroke lengths, and an adjustable slope mechanism (Table 3) was designed and manufactured for this study. Several components were integrated to optimize operation, including a digital display

speed driver (Figure 4a), a lever-type transmission for easy stroke adjustment (Figure 4b), and a jointed and hinged assembly enabling precise control of deck inclination (Figure 4c). The deck slope was measured by a digital display inclinometer (Figure 4d).

Table 3. Operating variables of the customized shaking table.

Variables	Values
Strokes (rpm)	≤450 rpm
Length of strokes (mm)	3–28 mm
Deck slope (°)	>0 ± 0.05

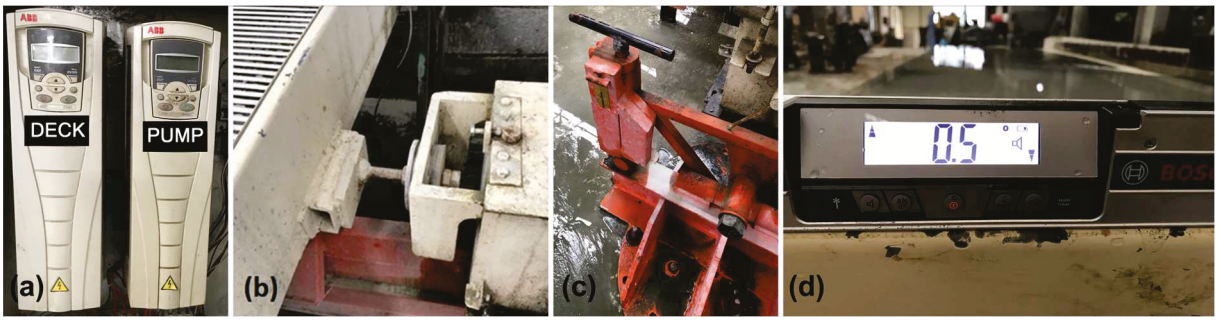


Figure 4. Variable control mechanisms of the custom-designed shaking table included: (**a**) a speed driver, (**b**) a lever-type transmission for stroke length adjustment, (**c**) a slope adjustment system, and (**d**) a digital inclinometer.

A schematic diagram and photographs of the custom-designed shaking table are presented in Figure 5a,b. To improve operational control, a mechanism comprising a pump and feeding cone was implemented, allowing the table to operate in a closed circuit until equilibrium was achieved under the specified variables during pulp feeding. To prevent particle settling and clogging at the cone outlet, a mixing mechanism and pinch valve system were integrated into the feeding cone, ensuring the pulp maintained the desired density before entering the table. Product collection chutes positioned around the table facilitated the transfer (recirculation) of waste, middling, and concentrate streams back to the pump through a return pipe system, thereby maintaining a continuous feed to the cone. In addition, spare outlet systems equipped with sampling valves were installed on the chutes, enabling the collection of waste, middling, and concentrate samples once steady-state operation was reached under the designated parameters.

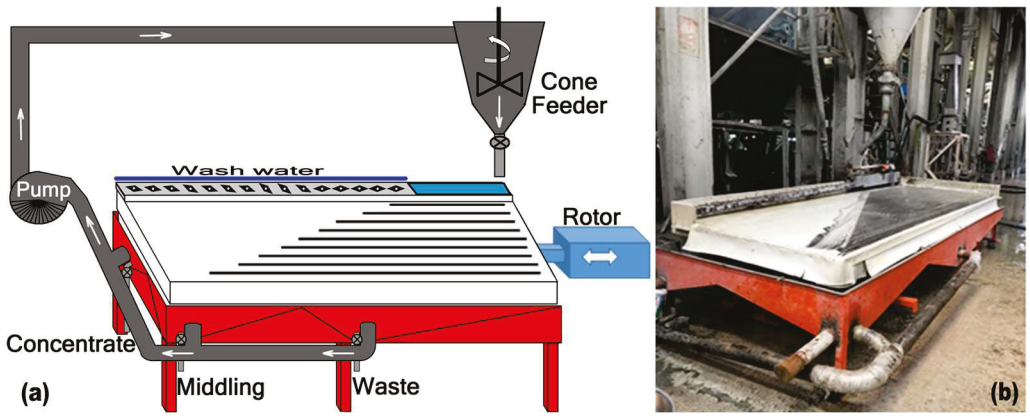


Figure 5. The custom-designed shaking table (**a**) schematic and (**b**) real view.

The shaking table setup was operated in a closed circuit until the operating variables reached equilibrium. Subsequently, samples were simultaneously collected from the concentrate, middling, and waste outlets using sampling valves (concentrate/middling and waste) over an average period of 10 s. After collection, each product was oven-dried at 100 ± 10 °C, weighed after drying, and analyzed by XRF to determine its chemical composition.

3. Results and Discussion

This study was conducted in two distinct phases. The first phase focused on utilizing existing plant facilities to recover a commercially viable chromite concentrate from tailings using a Wilfley-type shaking table operated within the mechanical constraints of the current processing equipment. The second phase aimed to improve process efficiency through the design, modification, and operation of a custom-designed shaking table. Results from the existing plant setup were systematically compared with those obtained using the custom-designed shaking table. In addition, key variables influencing chromite recovery from tailings were identified, and their optimal operating conditions were determined using the custom-designed shaking table.

3.1. Processing of the Tailings with the Existing Plant Facilities

Before conducting experimental tests with the custom-designed shaking table, the separation process was carried out under existing plant conditions using a standard Wilfley-type shaking table operated within the mechanical limitations of the facility. As shown in the chromite enrichment plant flowsheet (Figure 6), feed material with a particle size of −0.500 mm was initially processed on the first group of tables (1st–2nd floors). The middlings from this stage were subsequently directed to the next table group (3rd floor) for additional chromite recovery, while the 4th floor tables operated in a closed circuit to minimize chromite losses from the preceding stages.

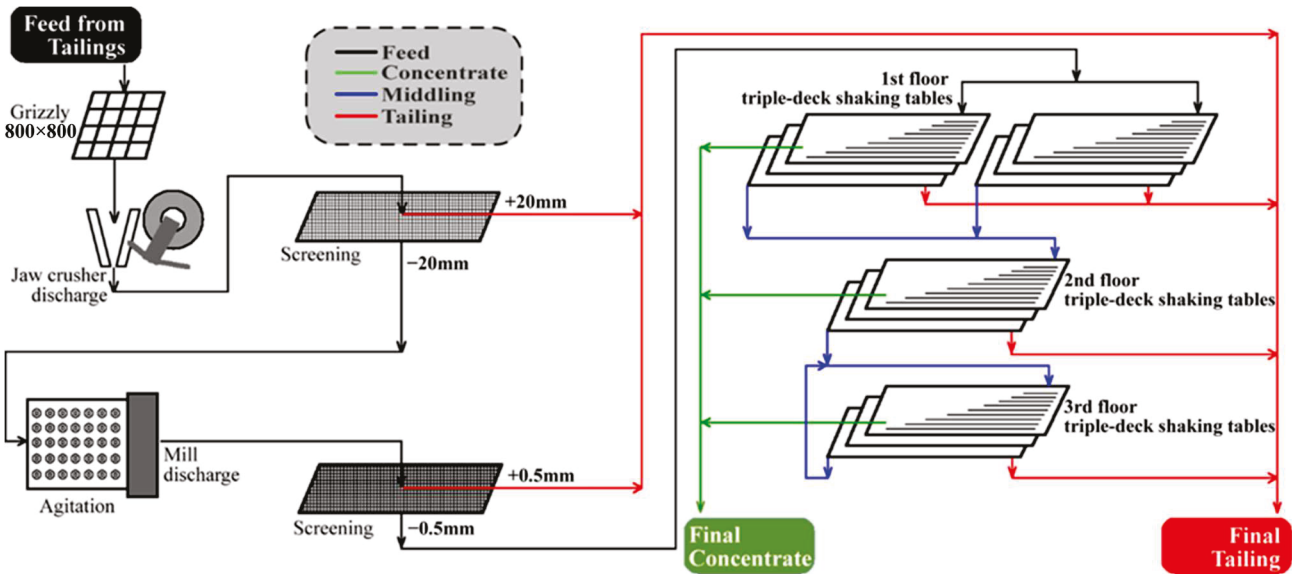


Figure 6. Flowsheet of the chromite enrichment plant.

The primary objective of this phase was to produce a marketable-grade chromite concentrate (>42% Cr_2O_3) while maximizing recovery and minimizing losses to waste. The operational process variables applied during testing are presented in Table 4. Under optimal operating conditions, the 1st–2nd floor tables achieved a Cr_2O_3 recovery of approximately 8%, whereas the 3rd and 4th floor tables, which processed the middlings (about 65% of the 1st–2nd floor table feed), contributed an additional 17% Cr_2O_3 recovery.

Table 4. Key variables for maximizing chromite recovery from tailings under existing plant conditions.

Variables	Values
Feed grade (Cr_2O_3%)	4.14 ± 0.05
Strokes (rpm)	260
Length of strokes (mm)	16
Deck slope (°)	1.5 ± 0.5
Pulp density (g/L)	1200
Feed rate (kg/h)	1050
Wash-water flow rate (tph)	8 ± 1

3.2. Processing of the Tailings with a Custom-Designed Shaking Table

Analysis of chromite recovery from tailings using the existing plant revealed several challenges that limited the achievement of high Cr_2O_3 yields. The operational inefficiencies were attributed to constraints in the design and adjustable parameters of the existing shaking tables used during the concentration process. To overcome these limitations, an industrial-scale shaking table was designed, customized, and fabricated, featuring adjustable low-to-high stroke frequencies, variable stroke lengths, and a conveniently adjustable deck slope, all intended to improve Cr_2O_3 recovery from tailings with greater efficiency. This custom-designed unit was subsequently employed to determine the optimal operational parameters, including stroke, stroke length, slope, pulp density, and feed particle size range, that significantly influence Cr_2O_3 recovery. The results obtained from this setup were then compared with those achieved under the existing plant conditions.

3.2.1. Effect of Stroke Rate on Chromite Recovery

Particles in contact with the surface of the shaking table are transported in the direction of table motion through frictional forces. This shaking motion, which facilitates the transport of mineral particles, is characterized by its asymmetry [23], consisting of a slower forward stroke and a faster backward stroke. Under standard operating conditions, the table is operated at 250–300 rpm. In the initial phase of this study, the variables listed in Table 5, known to influence the separation process, were kept constant to evaluate the effect of stroke speed (rpm) on chromite recovery from processing plant tailings.

Table 5. Variables used to determine the optimum table stroke.

Variables	Values
Length of strokes (mm)	13
Deck slope (°)	1.0
Pulp density (g/L)	1300
Feed rate (kg/h)	500
Wash-water flow rate (tph)	7
Strokes (rpm)	280–360

As shown in Figure 7, chromite recovery from the enrichment plant tailings exhibited an inverse relationship with the shaking table stroke rate: recovery decreased as stroke increased. The Cr_2O_3 recovery ranged from 10% to 22%, highlighting the significant influence of stroke on separation performance. At the lowest stroke rate of 280 rpm, the shaking action was insufficient to promote effective stratification of the dense chromite particles behind the riffles. Consequently, these particles were entrained into the middling zone and mixed with gangue minerals (primarily olivine) due to the scavenging effect of the wash water, resulting in the lowest recovery of approximately 10%.

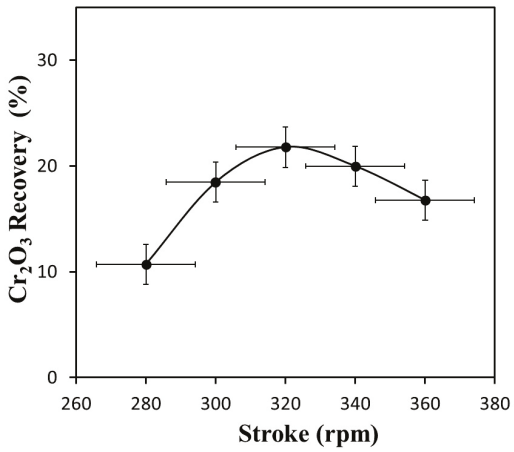


Figure 7. Effect of the shaking table stroke on Cr_2O_3 recovery from tailings.

With increasing shaking table stroke, Cr_2O_3 recovery improved, and at 320 rpm, chromite particles were effectively directed into the concentrate zone without intermixing with the middling product. Under these conditions, a distinct separation layer was formed, resulting in higher recovery rates. However, a further increase in stroke speed to 360 rpm led to the intrusion of gangue minerals, primarily olivine, into the concentrate zone, producing a broad separation band and a subsequent decline in Cr_2O_3 recovery from the tailings. Considering that the tailings were processed without additional grinding, one of the factors limiting further recovery improvement is the presence of unliberated particles. These particles likely reduced the efficiency of gravity separation, as they are less prone to report to the concentrate fraction.

3.2.2. Effect of Stroke Length on Chromite Recovery

In gravity concentration using a shaking table, stroke length is a key operational variable that significantly influences particle stratification and separation efficiency by affecting particle movement according to size and density differences. For coarser feed materials, longer strokes enhance the transport of heavier particles toward the concentrate end, whereas shorter strokes are more effective for finer feeds [9]. Based on this principle, the present study investigated the effect of stroke length, ranging from 7 mm to 16 mm, on the separation performance, Cr_2O_3 recovery from tailings, and resulting concentrate grade. During these experiments, all other operating parameters, including the previously determined optimum stroke rate of 320 rpm, were held constant as listed in Table 6. The results are presented graphically in Figure 8.

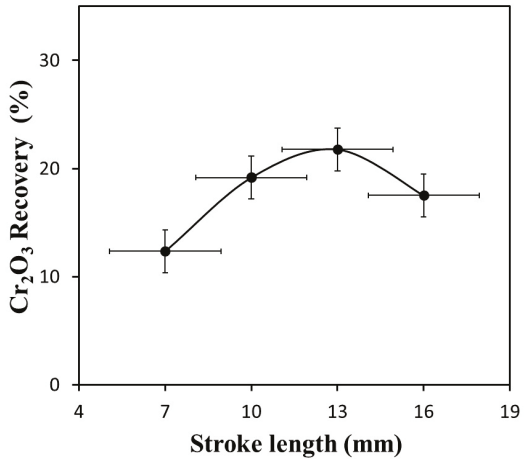


Figure 8. Effect of stroke length on Cr_2O_3 recovery from tailings.

Table 6. Variables used to determine the optimum stroke length.

Variables	Values
Strokes (rpm)	320
Deck slope (°)	1.0
Pulp density (g/L)	1300
Feed rate (kg/h)	500
Wash water flow rate (tph)	7
Length of strokes (mm)	7–16

The experimental results indicated that Cr_2O_3 recovery from the tailings was strongly affected by the shaking table stroke length. At short stroke lengths (7–10 mm), heavier chromite particles predominantly remained in the middling zone and failed to reach the concentrate area, resulting in Cr_2O_3 recoveries below 13% and 19%, respectively. Increasing the stroke length enhanced particle transport and broadened the collection band, promoting more efficient separation. When the stroke length was set to 13 mm, Cr_2O_3 recovery increased to approximately 22%. However, further increasing the stroke length to 16 mm caused chromite particles to bypass the riffles, designed to create a hindered settling region toward the concentrate, and shift into the middling and reject zones. Under these conditions, effective separation on the deck surface was not achieved, leading to a decline in Cr_2O_3 recovery to below 17%.

3.2.3. Effect of Shaking Table Slope on Chromite Recovery

Deck slope is a key parameter influencing Cr_2O_3 recovery, as it must be optimized according to the properties of both valuable and gangue minerals, including particle size and density. Increasing the table slope accelerates water flow, which in turn affects the lateral movement of particles across the deck. Higher slopes are generally more suitable for coarser feed materials, whereas near-horizontal slopes are preferred for finer fractions. Considering that the d_{80} of the feed was -0.325 mm, shaking table slopes ranging from 0.5° to 2.0° were evaluated to assess their effect on chromite recovery from the tailings. The operating variables applied during these tests are summarized in Table 7, and the results are presented graphically in Figure 9.

Table 7. Variables used to determine the optimum shaking table slope.

Variables	Values
Strokes (rpm)	320
Length of strokes (mm)	13
Pulp density (g/L)	1300
Feed rate (kg/h)	500
Wash-water flow rate (tph)	7
Deck slope (°)	0.5–2.0

The results demonstrated a clear influence of deck slope on chromite recovery from tailings. At the minimal slope of 0.5°, reduced water flow and increased water thickness hindered effective stratification, causing chromite particles to move irregularly and mix with gangue in the reject zone, resulting in Cr_2O_3 recovery of below 11.5%. Increasing the slope to 1° enhanced stratification behind the riffles, promoting more efficient transport of chromite particles to the concentrate zone and yielding recovery values exceeding 20%. However, further increases in slope to 1.5° and 2.0° accelerated water flow, displacing additional gangue minerals toward the reject zone. Although these steeper slopes produced higher concentrate grades, the separation bands became narrower, rendering the process

more sensitive to minor variations during concentrate collection, which could significantly affect final concentrate quality.

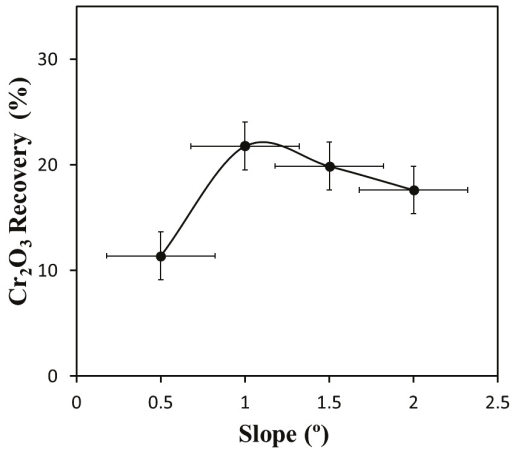


Figure 9. Effect of shaking table slope on Cr_2O_3 recovery from tailings.

3.2.4. Effect of Pulp Density on Chromite Recovery

Maintaining the appropriate solid–water balance is crucial for effective gravity concentration. Pulp density, expressed as the percentage of solids in a solid–liquid mixture, directly affects the slurry viscosity. When pulp density exceeds the optimal value, increased viscosity reduces fluidity, preventing most minerals from stratifying behind the riffles. Conversely, low pulp densities allow fine heavy particles to be carried with the lighter particles toward the reject zone. As a result, gravity concentration equipment operates most efficiently within the narrow range of pulp densities, and even slight deviations from this range can significantly reduce separation efficiency [25]. This part of the study investigated the effect of varying pulp densities on chromite recovery from tailings. Tests were conducted with pulp densities ranging from 1100 to 1400 g/L, while previously established optimum values for stroke, stroke length, and slope were maintained. The tested variables and corresponding results are summarized in Table 8 and presented graphically in Figure 10.

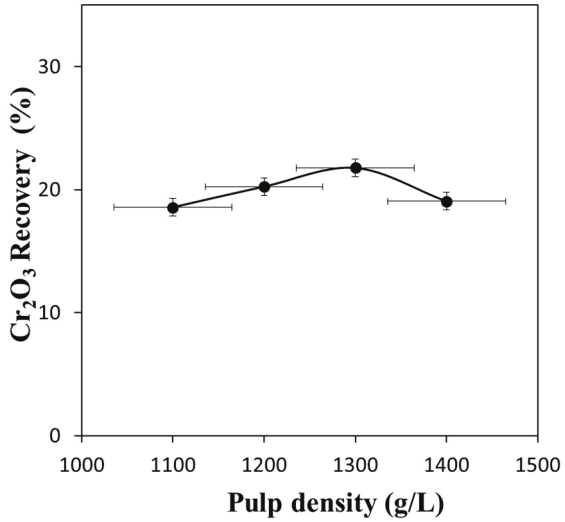


Figure 10. Effect of pulp density on Cr_2O_3 recovery from tailings.

Table 8. Variables used to determine the optimum pulp density.

Variables	Values
Strokes (rpm)	320
Length of strokes (mm)	13
Deck slope (°)	1.0
Feed rate (kg/h)	500
Wash water flow rate (tph)	7
Pulp density (g/L)	1100–1400

The results indicate that at a low pulp density (1100 g/L), chromite fines were largely carried down the slope with the water, predominantly entering the waste zone due to excessive water content, which limited the recovery of marketable-grade concentrate. Increasing the pulp density enhanced Cr_2O_3 recovery, reaching an optimum at 1300 g/L. However, further increasing the pulp density to 1400 g/L caused chromite particles to be displaced toward the waste and middling zones due to enhanced mechanical carrying effects, ultimately reducing the overall yield. These findings highlight the critical role of pulp density in balancing mineral transport and separation efficiency, demonstrating that both under- and over-dilution of the pulp can adversely affect Cr_2O_3 recovery.

3.2.5. Effect of Feed Rate on Chromite Recovery

For mineral processing equipment to be economically viable, it must operate at optimal efficiency and capacity. Operating below the ideal capacity results in lost economic value, reduced production of marketable product per unit time, and higher operating costs, whereas exceeding optimal capacity decreases effectiveness and separation efficiency. Consequently, achieving the highest possible Cr_2O_3 yield requires operating the shaking table at its optimum feed rate. Based on the optimum variables determined earlier in this study (Table 9), enrichment tests were carried out with feed rates ranging from 500 to 1200 kg/h to both maximize processing capacity and identify the most effective feed rate for shaking table operation.

Table 9. Variables used to determine the optimum feed rate.

Variables	Values
Strokes (rpm)	320
Length of strokes (mm)	13
Deck slope (°)	1.0
Pulp density (g/L)	1300
Wash water flow rate (tph)	7
Feed rate (kg/h)	500–1200

The optimal conditions determined in this study were initially applied at a feed rate of 500 kg/h, with the wash water flow rate maintained at 7 tph, based on existing plant conditions and preliminary tests. The results showed that increasing the feed rate from 500 kg/h to 800 kg/h substantially enhanced Cr_2O_3 recovery (Figure 11). At a 500 kg/h, Cr_2O_3 recovery was approximately 22%, whereas increasing the feed rate to 800 kg/h increased recovery to over 28%. This improvement can be attributed to the fixed wash water rate of 7 tph, which was relatively high for the lower feed rate and caused chromite particles to be washed away into the reject zone. At the higher feed rate, gangue minerals were displaced toward the middling and reject zones, resulting in more efficient separation and higher Cr_2O_3 recovery values.

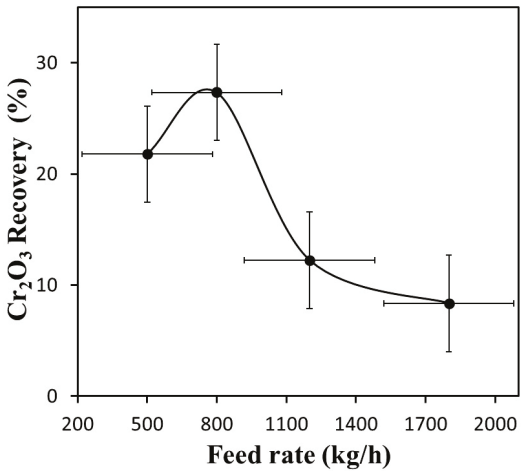


Figure 11. Effect of feed rate on Cr_2O_3 recovery from tailings.

However, further increasing the feed rate to 1200 kg/h caused chromite particles to be transported along with gangue minerals without effective separation, resulting in their accumulation in the middling and reject zones and preventing the production of a marketable-grade concentrate. At these higher feed rates, the shaking table riffles, designed to create hindered settling conditions, were unable to retain the chromite particles effectively, allowing them to escape to the reject zone. Combined with the insufficient wash water relative to the increased feed, this led to a sharp decline in Cr_2O_3 recovery, dropping below 10%. These findings highlight the critical balance required between feed rate and wash water flow to maintain effective separation and maximize recovery in shaking table operations.

3.2.6. Effect of Wash Water Flow Rate on Chromite Recovery

Insufficient wash water flow hinders the effective removal of low-density gangue minerals from high-density valuable minerals, resulting in low-grade concentrate. Conversely, excessive wash water can displace high-density minerals toward the low-density fraction, leading to significant losses of valuable material to waste and reducing Cr_2O_3 recovery [28]. In this part of the study, the previously established optimal operational parameters were maintained (Table 10), while the effect of varying wash water flow rates (6–9 tph) on Cr_2O_3 recovery was systematically evaluated. The results (Figure 12) emphasize the critical balance between wash water flow and mineral density required to achieve optimal separation and maximize chromite recovery.

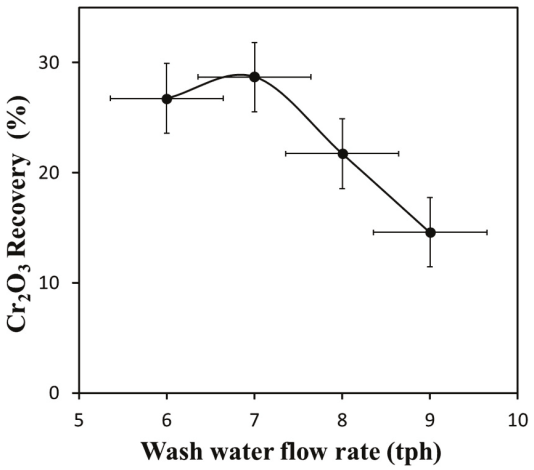


Figure 12. Effect of wash water flow rate on Cr_2O_3 recovery from tailings.

Table 10. Variables used to determine the optimum wash water flow rate.

Variables	Values
Strokes (rpm)	320
Length of strokes (mm)	13
Deck slope (°)	1.0
Pulp density (g/L)	1300
Feed rate (kg/h)	800
Wash water flow rate (tph)	6–9

The experimental results demonstrated that the wash water flow rate has a substantial effect on the efficiency of the separation process. At the lowest flow rate of 6 tph, water was insufficient to achieve effective separation, resulting in poorly defined concentrate, middling, and reject zones on the shaking table surface and low overall recovery. Under these conditions, careful control was required to prevent mixing olivine with chromite and to produce a marketable-grade concentrate, further limiting recovery. Increasing the wash water flow rate to 7 tph improved the separation: lighter gangue minerals were effectively displaced toward the middling and reject zones, enabling easier attainment of marketable concentrate grades and higher Cr_2O_3 recoveries compared to the lower flow rate. However, further increasing the wash water flow to 8–9 tph caused chromite particles to be carried into the middling or reject zones due to excessive water, thereby reducing separation efficiency and causing Cr_2O_3 recovery to drop sharply below 15%. These results underscore the critical need to balance wash water flow with feed characteristics to optimize both recovery and concentrate quality in shaking table operations.

3.3. Comparison of the Custom-Designed Shaking Table Performance with Existing Plant Conditions

Previous results (Section 3.1) indicated that under existing plant conditions, the 1st and 2nd floor shaking tables produced a maximum chromite concentrate of less than 1% of the feed, corresponding to a maximum Cr_2O_3 recovery of 8%. Approximately 65% of the feed, classified as middlings in the first step, was subsequently reprocessed using the 3rd and 4th floor shaking tables to recover marketable-grade concentrate and minimize chromite losses. This part, therefore, aimed to compare the performance of the existing plant shaking tables with that of the custom-designed shaking table in terms of Cr_2O_3 recovery. The optimized operating parameters for the custom-designed shaking table and the corresponding results are summarized in Table 10 and presented in Figure 13, respectively.

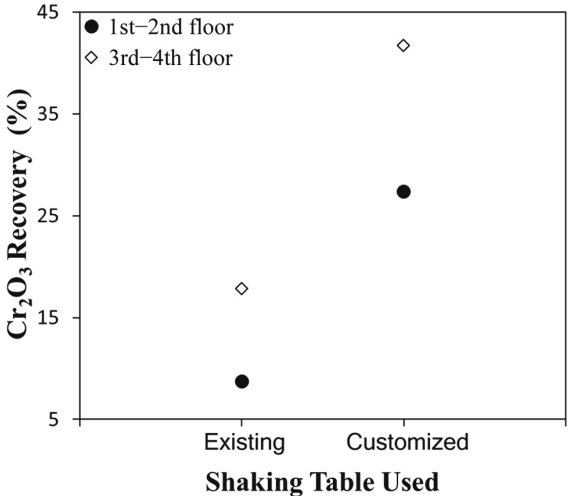


Figure 13. Comparison of Cr_2O_3 recovery under existing plant conditions and using the custom-designed shaking table.

The primary objective of the enrichment processes was to obtain marketable chromite concentrate from the plant tailings. Under existing plant conditions, the 1st and 2nd floor shaking tables achieved a maximum Cr_2O_3 recovery of only 8%, indicating substantial chromite losses. This low recovery can be attributed to mechanical fatigue from prolonged operation and design limitations of the existing tables, which restricted their separation efficiency. In contrast, the use of a custom-designed shaking table with optimized operating parameters significantly enhanced Cr_2O_3 recovery, increasing it to over 27%. This improvement highlights the importance of equipment optimization in tailings processing and demonstrates the potential economic gains without additional mining or grinding. Moreover, the proportion of middlings sent to the 3rd and 4th floor shaking tables was reduced by 40%, reflecting more efficient separation and lower material recirculation, which collectively enhance overall plant performance.

When evaluating the recovery of marketable-grade chromite concentrate from the middlings of the 1st and 2nd floor tables, the 3rd and 4th floor shaking tables under existing plant conditions achieved only approximately 17% Cr_2O_3 recovery. In contrast, reprocessing these middlings using the custom-designed shaking table substantially increased recovery to over 40%. This result underscores the critical role of tailored equipment design in capturing chromite particles that would otherwise remain unextracted and emphasizes the potential of customized solutions to improve mineral utilization and promote more sustainable processing practices.

3.4. Processing of the Tailings Classified into Narrow Particle Size Ranges: Effect of Feed Particle Size on Chromite Recovery Using a Custom-Designed Shaking Table

Gravity concentration equipment, including jigs, spirals, and shaking tables, typically operates on feed materials classified into narrow particle size ranges to minimize the influence of particle size on recovery [24]. Each method achieves optimal efficiency only when operated under conditions specifically adjusted for the target particle size fraction. Consequently, careful optimization of both operational parameters and particle size characteristics is essential to achieve peak separation performance. While the optimal particle size ranges for gravity separation are broadly recognized, the quantitative relationship between particle size and separation efficiency remains insufficiently explored.

In this phase of the study, tailings enrichment was conducted using a custom-designed shaking table after classifying the feed into four narrow particle size fractions: $-0.500 + 0.355$ mm, $-0.355 + 0.250$ mm, $-0.250 + 0.150$ mm, and -0.150 mm. The previously established optimal operational variables (Table 11) were applied consistently across all fractions to evaluate the effect of particle size on Cr_2O_3 recovery. The results clearly demonstrated that size-dependent particle behavior governs the efficiency of chromite–gangue separation (Figure 14). Effective separation was driven by hindered settling and selective layering, which were most pronounced in the $-0.250 + 0.150$ mm size fraction. Within this optimal range, the significant specific gravity differential between chromite and the lighter gangue (e.g., olivine, serpentine) promoted efficient separation, yielding high recoveries while maintaining concentrate quality, with peak Cr_2O_3 recovery exceeding 50%. In contrast, the $-0.355 + 0.250$ mm fraction yielded a lower recovery of approximately 45%, attributed to incomplete stratification and localized turbulence that disrupted consistent layer formation. Recovery sharply declined to ~16% for the -0.150 mm fraction due to the process inefficiencies inherent to fine particle processing. As fine or slow-settling particles remained suspended, they increased pulp viscosity. This elevated viscosity directly impaired separation in two ways: it enhanced the entrainment of gangue minerals, preventing their clean rejection, and it reduced the visual clarity of mineral bands on the deck, hindering precise mechanical separation [24]. Similarly, the coarsest fraction ($-0.500 + 0.355$ mm) exhibited poor separation due to hindered particle mobility and erratic movement on the

deck surface. These findings corroborate classical stratification theory [29], demonstrating that gravity separation efficiency is governed by a complex interplay between particle characteristics (size, shape, and density) and hydrodynamic conditions [30]. Ultimately, particle size was identified as the most influential parameter controlling Cr_2O_3 recovery on the custom-designed shaking table.

Table 11. Optimized operating variables for the custom-designed shaking table.

Variables	Values
Strokes (rpm)	320
Length of strokes (mm)	13
Deck slope (°)	1.0
Pulp density (g/L)	1300
Feed rate (kg/h)	800
Wash water flow rate (tph)	7

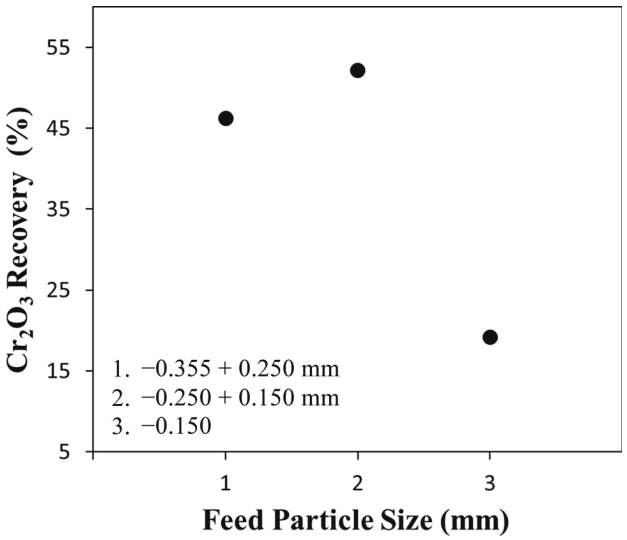


Figure 14. Effect of feed particle size distribution on Cr_2O_3 recovery.

4. Summary and Conclusions

This study clearly demonstrates the substantial potential of a custom-designed shaking table to enhance chromite recovery from plant tailings significantly. By redesigning the conventional table for improved usability and operational flexibility, the research provides a practical solution to both mitigate environmental pollution associated with tailings while economically valorizing chromite minerals that would otherwise be lost—critically, without additional mining or grinding costs.

The optimized operating parameters—320 rpm table speed, 1° inclination, 13 mm amplitude, 1300 g/L pulp density, 800 kg/h feed rate, and 7 tph wash water flow—resulted in significant performance gains. Under these conditions, Cr_2O_3 recovery increased from approximately 8% to 27% for the 1st–2nd floor tables and from roughly 17% to over 40% for the 3rd–4th floor table groups. Consequently, a marketable-grade chromite concentrate was produced from tailings (average 4.15 $\pm$ 0.05% Cr_2O_3), effectively more than doubling the recovery rates achieved under existing plant conditions.

The study also emphasizes that separation efficiency is fundamentally governed by feed particle size. Classifying the tailings into discrete size fractions markedly improved Cr_2O_3 recovery. The −0.250 + 0.150 mm fraction exhibited optimal performance, driven by hindered settling and selective layering, achieving a recovery of $\geq$50% without compromising concentrate grade, followed by the −0.355 + 0.250 mm fraction (~44%).

Overall, this research demonstrates the effectiveness of a custom-designed shaking table and provides mineral processing plants with a technically viable and economically attractive approach to substantially enhance chromite recovery from challenging tailings. These findings support improved resource utilization and contribute to more sustainable mining operations.

Author Contributions: Conceptualization, S.O.; Methodology, S.O.; Software, S.O.; Validation, S.O.; Formal analysis, S.O. and A.K.G.; Investigation, S.O. and A.K.G.; Resources, A.K.G.; Data curation, S.O.; Writing—original draft, S.O.; Writing—review & editing, S.O.; Visualization, S.O.; Supervision, S.O.; Project administration, S.O. All authors have read and agreed to the published version of the manuscript.

Funding: The APC was partially funded by SDU-FBY-2018-6472.

Data Availability Statement: The original contributions presented in this study are included in the article. Further inquiries can be directed to the corresponding author.

Acknowledgments: The authors gratefully acknowledge ŞETAT Mining for their support, for providing the tailings samples used in this study, and for facilitating the experimental tests conducted as part of this research. The authors would also like to express their sincere appreciation to O. Elitok, E.B. Tuncay, and U. Memis for their valuable contributions and efforts in the characterization of the samples.

Conflicts of Interest: The authors declare no conflict of interest.

References

1. Taşlıgil, N.; Şahin, G. Chrome in Türkiye in terms of economic geography. *Eur. J. Soc. Sci.* **2011**, *4*, 82–108.
2. Murthy, Y.R.; Tripathy, S.K.; Kumar, C.R. Chrome ore beneficiation challenges & opportunities—A review. *Miner. Eng.* **2011**, *24*, 375–380. [CrossRef]
3. Guraslan, A.K. Recovery of Saleable Concentrate from Chromite Processing Plant Tailing in Bursa/Orhaneli. Master's Thesis, Süleyman Demirel University, Institute of Natural and Applied Sciences, Isparta, Turkey, 2019.
4. Papp, J.F.; Lipin, B.R. Chromium and Chromium Alloys. In *Kirk-Othmer Encyclopedia of Chemical Technology*; Othmer, K., Ed.; John Wiley & Sons: Hoboken, NJ, USA, 2001.
5. Guney, A.; Onal, G. Atmaca, New aspect of chromite gravity tailing re-processing. *Miner. Eng.* **2001**, *14*, 1527–1530. [CrossRef]
6. Papp, J.F. *Chromium—A National Mineral Commodity Perspective, Report: USGS Numbered Series. Open-File Report*; Geological Survey (U.S.): Reston, VA, USA, 2007; p. 48.
7. Loock, M.M.; Beukes, J.P.; van Zyl, P.G. A Survey of Cr(VI) Contamination of Surface Water in the Proximity of Ferrochromium Smelters in South Africa. *Water SA* **2014**, *40*, 709–716. [CrossRef]
8. USGS, U.S. Geological Survey, Mineral Commodity Summaries. *Chromium* **2025**, 58–59.
9. Can, I.B.; Ozsoy, B.; Ergun, S.L. Developing an optimum beneficiation route for a low-grade chromite ore. *Physicochem. Probl. Miner. Process.* **2019**, *55*, 865–878. [CrossRef]
10. Alaee, N.H.; Sargheyni, J.; Pezeshkan, M. Kianoush, Design and optimization of a spiral separator for enhanced chromite recovery and sustainability. *Clean. Eng. Technol.* **2025**, *24*, 100880. [CrossRef]
11. Ozcan, O. The use of a reflux classifier for chromite ores: Assessment of different circuit alternatives at pilot scale. *Physicochem. Probl. Miner. Process.* **2025**, *61*, 203747. [CrossRef]
12. Murthy, Y.R.; Tripathy, S.K. Process optimization of a chrome ore gravity concentration plant for sustainable development. *S. Afr. Inst. Min. Metall.* **2020**, *120*, 261–268. [CrossRef]
13. Cicek, T.; Cocen, I. Applicability of Mozley gravity separator (MGS) to fine chromite tailings of Turkish chromite concentrating plants. *Miner. Eng.* **2002**, *15*, 91–93. [CrossRef]
14. Çiçek, T.; Cöcen, I.; Engin, V.T.; Cengizler, H.; Şen, S. Technical and economical applicability study of centrifugal force gravity separator (MGS) to Kef chromite concentration plant. *Miner. Process. Extr. Metall. Trans. Inst. Min. Metall. Sect. C* **2008**, *117*, 248–255. [CrossRef]
15. Schacht, C. *Refractories Handbook*, 1st ed.; Schacht, C., Ed.; CRC Press: Boca Raton, FL, USA, 2004.
16. Rivera, O.; Garbers-Craig, A. Morphological and compositional changes of chromite as it descends in the black top of a platinum group metals smelter. *Miner. Eng.* **2023**, *201*, 108221. [CrossRef]

17. Jones, T.; Barker, P. Efficient enhanced gravity separation using the Kelsey centrifugal jig. In Proceedings of the 39th Annual Meeting of the Canadian Mineral Processors, Ottawa, ON, Canada, 23–25 January 2007; Folinsbee, J., Ed.; The Canadian Institute of Mining, Metallurgy and Petroleum (CIM): Westmount, QC, Canada, 2007; pp. 259–394.
18. Ozyurt, M.; Cebeci, Y.; Ergün, Ş.L. Recovery of chromite from concentrator plant tailings. *Sci. Min. J.* **2023**, *62*, 17–21. [CrossRef]
19. Richards, R.C.; MacHunter, D.M.; Gates, P.J.; Palmer, M.K. Gravity separation of ultra-fine (−0.1mm) minerals using spiral separators. *Miner. Eng.* **2000**, *13*, 65–77. [CrossRef]
20. Tripathy, S.K.; Murthy, Y.R.; Singh, V.; Farrokhpay, S.; Filippov, L.O. Improving the quality of ferruginous chromite concentrates via physical separation methods. *Minerals* **2019**, *9*, 667. [CrossRef]
21. Tripathy, S.K.; Ramamurthy, Y.; Sahu, G.P.; Tathavadkar, V. Ultra fine chromite concentration using spiral concentrator. In Proceedings of the XI International Seminar on Mineral Processing Technology (MPT-2010), NML, Jamshedpur, India, 15–17 December 2010; pp. 144–150.
22. Aras, A.; Taner, H.A. Investigation of chromite ore beneficiation possibilities with different gravity concentrators. *Rud.-Geološko-Naft. Zbornik.* **2023**, *38*, 127–134. [CrossRef]
23. Gupta, A.; Yan, D. Gravity separation. In *Mineral Processing Design and Operations An Introduction Second Edition*; Elsevier: Amsterdam, The Netherlands, 2016.
24. Wills, B.A.; Napier-Munn, T. *Wills' Mineral Processing Technology*, 7th ed.; Butterworth-Heinemann: Oxford, UK, 2006.
25. Izerdem, D. Low-Grade Chromite Beneficiation through Spiral Concentration: A Review from the Turkish Market Perspective. *Miner. Process. Extr. Metall. Rev.* **2024**, *46*, 436–456. [CrossRef]
26. Curry, J.A.; Ismay, M.J.L.; Jameson, G.J. Mine operating costs and the potential impacts of energy and grinding. *Miner. Eng.* **2014**, *56*, 70–80. [CrossRef]
27. Abaka-Wood, G.B.; Quast, K.; Zanin, M.; Addai-Mensah, J.; Skinner, W. A study of the feasibility of upgrading rare earth elements minerals from iron-oxide-silicate rich tailings using Knelson concentrator and Wilfley shaking table. *Powder Technol.* **2019**, *344*, 897–913. [CrossRef]
28. Tripathy, S.K.; Murthy, Y.R.; Singh, V. Characterisation and separation studies of Indian chromite beneficiation plant tailing. *Int. J. Miner. Process.* **2013**, *122*, 47–53. [CrossRef]
29. Woollacott, L.C.; Silwamba, M. An experimental study of size segregation in a batch jig. *Miner. Eng.* **2016**, *94*, 41–50. [CrossRef]
30. Little, L.; Wiese, J.; Becker, M.; Mainza, A.; Ross, V. Investigating the effects of particle shape on chromite entrainment at a platinum concentrator. *Miner. Eng.* **2016**, *96–97*, 46–52. [CrossRef]

Disclaimer/Publisher's Note: The statements, opinions and data contained in all publications are solely those of the individual author(s) and contributor(s) and not of MDPI and/or the editor(s). MDPI and/or the editor(s) disclaim responsibility for any injury to people or property resulting from any ideas, methods, instructions or products referred to in the content.

minerals

MDPI

Article

Recycling Copper (Cu) from Waste Automotive Printed Circuit Boards (WPCBs) After Characterization and Liberation Study by Mineral Processing Techniques

Mahsa Pourmohammad [1,*], Josep Oliva [1], Hernan Anticoi [1], Carlos Hoffmann Sampaio [1], Pura Alfonso [1], César Valderrama [2,3], Jose Luis Cortina [2,3] and Percy Escalante [1]

[1] Department of Mining, Industrial and ICT Engineering, Universitat Politècnica de Catalunya Barcelona Tech (UPC), Av. Bases de Manresa 61-73, 08242 Manresa, Spain
[2] Chemical Engineering Department, Escola d'Enginyeria de Barcelona Est (EEBE), Universitat Politècnica de Catalunya (UPC)-BarcelonaTECH, C/Eduard Maristany 10-14, Campus Diagonal-Besòs, 08930 Barcelona, Spain
[3] Barcelona Research Center for Multiscale Science and Engineering, Campus Diagonal-Besòs, 08930 Barcelona, Spain
* Correspondence: mahsa.pourmohammad.golloujeh@upc.edu

Abstract: Waste printed circuit boards (WPCBs) are one of the fastest-growing waste streams and pose a significant environmental challenge while also representing a valuable secondary resource due to their rich metal content, particularly copper (Cu). Since effective recovery of metals requires mechanical pre-treatment and advanced characterization, WPCB boards were subjected to size reduction and then characterized through X-ray fluorescence (XRF), inductively coupled plasma optical emission spectroscopy (ICP-OES), scanning electron microscopy (SEM-EDS), and mineral liberation analysis (MLA). Results indicated that copper is predominantly found in coarser particle sizes due to its ductility, while glass fibers and ceramics dominate finer fractions. Liberation studies revealed that Cu is essentially free in fine particles (<100 μm) but tends to remain locked in coarser fractions. Based on these results, gravity separation methods were employed to concentrate the copper: coarse particles (>300 μm) were treated on a shaking table, achieving a Cu recovery of 95%, while fine particles (<300 μm) were processed using a multi-gravity separator (MGS), with recoveries of 94% for 100 × 300 μm and 81.5% for <100 μm size fractions. This study presents a gravity-based separation strategy that combines shaking tables and MGS to optimize Cu recovery from automotive WPCBs. To the authors' knowledge, the MGS application for WPCBs has received little attention, despite its strong potential for separating this type of waste. The proposed methodology enhances the concentration and purity of the metallic fraction (in this case, Cu), especially in fine particles, which are challenging to work with, while reducing environmental impacts through minimal chemical use, thereby contributing to sustainable e-waste recycling.

Keywords: characterization; multi gravity separator (MGS); waste printed circuit boards (WPCBs); recycling: shaking table

1. Introduction

Waste electrical and electronic equipment (WEEE) is among the fastest growing waste streams in the European Union, increasing at a rate of 3%–5% annually. Globally, it is also one of the most rapidly expanding waste streams in terms of volume and environmental impact [1,2]. Waste printed circuit boards (WPCBs) are crucial components of

these electronic waste streams. Although they comprise only 3%–6% of global e-waste, these devices contain valuable recyclable materials, including plastics, glass, and metals such as copper, silver, gold, and palladium [3,4]. This makes e-waste a potential economic resource, often referred to as an "urban mine" [5–8]. The total e-waste stream is approximately 40 billion euros; WPCBs contribute over 40% of the total metal value. The potential revenue from recycling WPCBs is estimated at $21.200 per ton [1]. WPCBs have a high metal concentration, containing around 20% copper, 1000 ppm silver, 250 ppm gold, and 110 ppm palladium by mass. In contrast, an average mine yields only 0.6% copper (Cu), 215 ppm silver (Ag), 1 ppm gold (Au), and 2.7 ppm palladium (Pd). However, they contain various toxic substances, including heavy metals such as cadmium (Cd), lead (Pb), mercury (Hg), and Arsenic (As), as well as persistent organic pollutants (POPs) and brominated flame retardants (BFRs) [4,9,10]. This highlights the dual significance of waste WPCBs as a valuable secondary resource and a concern for environmental regulations. Therefore, recovering precious metals from WPCBs is economically and environmentally beneficial, as the e-waste problem remains unresolved, especially in developing countries [11–13].

Recycling WPCBs is not an easy process due to the varying mechanical properties of the WPCB compositions [14–16]. Pre-treatment methods, such as mechanical processing and dismantling, not only help to address this challenge by reducing impurities but also reduce the reagent consumption during recycling [3,9,17,18]. Processes such as impact, compression, shearing, stretching, tearing, and bending apply energy to modify materials, resulting in reduced particle sizes, morphological changes, exfoliation, or phase transformations. These changes enhance the effectiveness of hydrometallurgical and bio-metallurgical treatments [19,20]. So, optimizing WPCB communication strategies is essential and aligns with the United Nations' Sustainable Development Goals (SDGs), particularly SDG 12—Responsible Production and Consumption. Enhancing physical separation methods for WPCB recycling promotes sustainability by conserving resources, improving infrastructure, and benefiting human health and environmental quality [6,21–23].

Another main challenge in WPCB recycling is proper characterization of their composition, distribution, and composition liberation, as WPCBs are heterogeneous [5]. They can contain up to 60 different elements, consisting of approximately 40% metals—including copper (Cu), lead (Pb), nickel (Ni), silver (Ag), platinum (Pt), and gold (Au)—along with 30% plastics and 30% ceramics [9,24]. Various characterization methods have been explored, like acid digestion [25,26]. However, X-ray fluorescence (XRF) is also widely used due to its non-destructive nature, speed, and ease of particle manipulation [25,27,28]. Additionally, imaging techniques such as microscopy and scanning electron microscopy (SEM) aid in analyzing particle distribution and liberation [26,29,30].

In the mineral industry, image analysis has shifted towards automated procedures lately, using automated analyzers coupled with electron microscopes, such as MLA and QEMSCAN, to study composition liberation. MLA stands out as an invaluable tool for qualitative and quantitative characterization, including composition associations, particle size, and composition liberation. This system was developed to analyze the liberation of compositions and has attracted significant attention from both industry and academia. However, it is used for determining the degree of liberation of mechanically processed PCB particles and for compositional characterization of complex electronic waste, such as batteries [5,29,31,32].

Other techniques, such as Quantitative Evaluation of Materials by Scanning Electron Microscopy (QEMSCAN), Automated Material Identification and Classification System (AMICS), Tescan Integrated Mineralogical Analyzer (TIMA), and X-ray microtomography (μCT), also provide valuable insights to analyze the degree of liberation of a composi-

tion [31,33]. These non-destructive characterization methods, and their use to understand the association of metals/non-metals across different size fractions, demonstrate their importance for characterizing electronic waste. Therefore, accurate characterization is crucial for quantifying metals and non-metals in extraction processes, assessing losses, determining extraction yield, optimizing recovery efficiency, and evaluating the feasibility of large-scale implementation [34,35].

Although various mineral processing techniques, including magnetic and electrostatic separation, column air classification, flotation, and gravity-based methods such as jigging, tabling, falcon concentrator, sink–float separation, etc., have been employed to extract metals from the crushed WPCBs due to the effective minimization of the air pollution while enhancing metal recovery, none of them mentioned the capacity of the multi-gravity separator (MGS) technique usage to recover Cu from automotive WPCBs, with a focus on fine particles [3,11,21,26,30,36–45]. Gravity concentration methods, renowned for their environmental friendliness (no chemical reagents required and no further heating needed), low capital, and operating costs, are widely used as a pre-treatment step in WPCB recycling. It should be noted that it is one of the oldest methods for separating compositions based on differences in specific gravity. Thus, since metals and non-metals (NMF) existing in the crushed WPCBs exhibit significant differences in specific gravity, this makes the low-cost gravity separation methods, such as tabling [9,36,46] or MGS, a viable option for separating heavy metal particles from relatively lighter plastic and ceramic particles [36,47].

The MGS operates on principles similar to a shaking table but utilizes rotational motion to generate centrifugal forces stronger than gravity. This enhanced force enables more efficient separation, especially at finer particle sizes [48]. MGS is an advanced gravity concentration technique that combines centrifugal acceleration with the forces acting on a conventional shaking table to concentrate materials. The separation chamber of the MGS consists of a cylindrical drum with a to-and-fro shaking mechanism. With the front end elevated, the inclined drum allows the material to flow towards the opposite end, rotated at a specific speed, generating centrifugal forces on the particles. Due to their higher settling rates, heavier particles form initial layers on the drum surface, while lighter particles overlay them. At this point, the material bed inside the drum contains successive layers, with heavier particles in the innermost positions and lighter ones on top. Fresh water is continuously sprayed onto the settled bed at the front of the drum, facilitating the flowing film concentration. The outer layers of the lighter materials are selectively washed and collected in the tailings launder at the back end of the drum. The heavier material bed, along with any entrapped coarser and lighter particles, is scraped toward the front end by a rotating spiral scraper mechanism. During this scrapping process, wash water helps further separate the heavy material bed, ensuring that the coarser and lighter materials are washed into the tailings before the heavy materials are discharged into the front-end launder. The combined forces acting on the MGS drum allow for repeated concentrations of materials based on their differential specific gravity before the products are discharged. This study aimed to exploit the specific gravity differences between copper-bearing materials and gangue for efficient separation in the MGS process [49].

The shaking tables consist of a sloping deck with a riffled surface. A motor powers a small arm that shakes the table along its length, parallel to the riffle and rifle pattern. This longitudinal shaking motion includes a slow forward stroke and a rapid return strike. The riffles are arranged in such a manner that heavy material is trapped and conveyed parallel to the direction of the oscillation. Water is added to the top of the table perpendicular to the table's motion. The heaviest and coarsest particles are collected at the end of the table, while the lightest and finest particles wash over the riffles and to the bottom edge. Between these two extremes, particles of medium size and density—known as middlings—are

also separated. The process sorts materials into concentrate, middlings, and waste based on the difference in the specific density of the grains. Shaking tables are widely used in mineral processing to concentrate different metal ores and coal preparation. It is also used for the cost-effective recovery of metals from crushed WPCBs. These devices are often used downstream of other gravity concentration equipment, such as Reichert spirals, jigs, and centrifugal gravity concentrators, for final cleaning before refining or the sale of the product [50–53].

This study aims to propose a process combining two gravity concentration methods —shaking table and MGS—with high cut efficiency in terms of mass recovery and metal content in the final products. According to the literature review, the MGS, as a gravity separation method, has received no attention, to the authors' knowledge, despite its strong separation potential and compatibility for recovering fine Cu particles from automotive WPCBs, which is often a limit for the other separation methods. MGS, with the combined effects of rotation and pulsation, produces cleaner separation boundaries, higher-purity metal concentrates, and non-metal tails with fewer contaminants. So, this means less need for downstream hydrometallurgical refining. In addition, water use is efficient as thin-film flow requires relatively little water. Moreover, most of the work focused on coarse particles (>300 μm). In contrast, this study focused on MGS to physically recover Cu from fine particles (<300 μm), which can substitute for the concentration in subsequent steps, such as hydrometallurgical, pyrometallurgical, and bio-metallurgical treatments, which mainly concentrate the metals. Those are not environmentally friendly and slower, respectively. Moreover, by maximizing the Cu recovery physically as a preconcentration, the subsequent efficiency of the further processes, like pyrometallurgical and hydrometallurgical processes, will be improved. Finally, a green process flowsheet was proposed to enrich the copper content in WPCBs, utilizing a shaking table and MGS.

2. Materials and Methods

2.1. Materials

In this study, automotive WPCB boards were selected after manual disassembly of electronic components (such as resistors, capacitors, diodes, transistors, connectors, and chips) and cutting them into small pieces with simple workshop tools like a hammer, mallet, standard pliers, and bolt cutter to reduce material variability and simplify the crushing process.

2.2. Methodology

2.2.1. Comminution

Simple workshop tools were used to disassemble the components from the boards. Then, a knife crusher with adjustable knife spacing (0.15–0.2 cm) was used to control the size reduction of the samples. In addition, a Kenwood Easy Chop Chopper (0.5 L container, two speeds, four blades, 500 W) was used to crush the samples to finer particle sizes. Samples with particles smaller than 1.18 mm were characterized and subjected to liberation analysis, while larger particles were reprocessed through additional crushing until all materials were reduced to below 1.18 mm, and then they proceeded to the separation steps (Figure 1). The quartering technique was applied to ensure representative sampling in subsequent analyses.

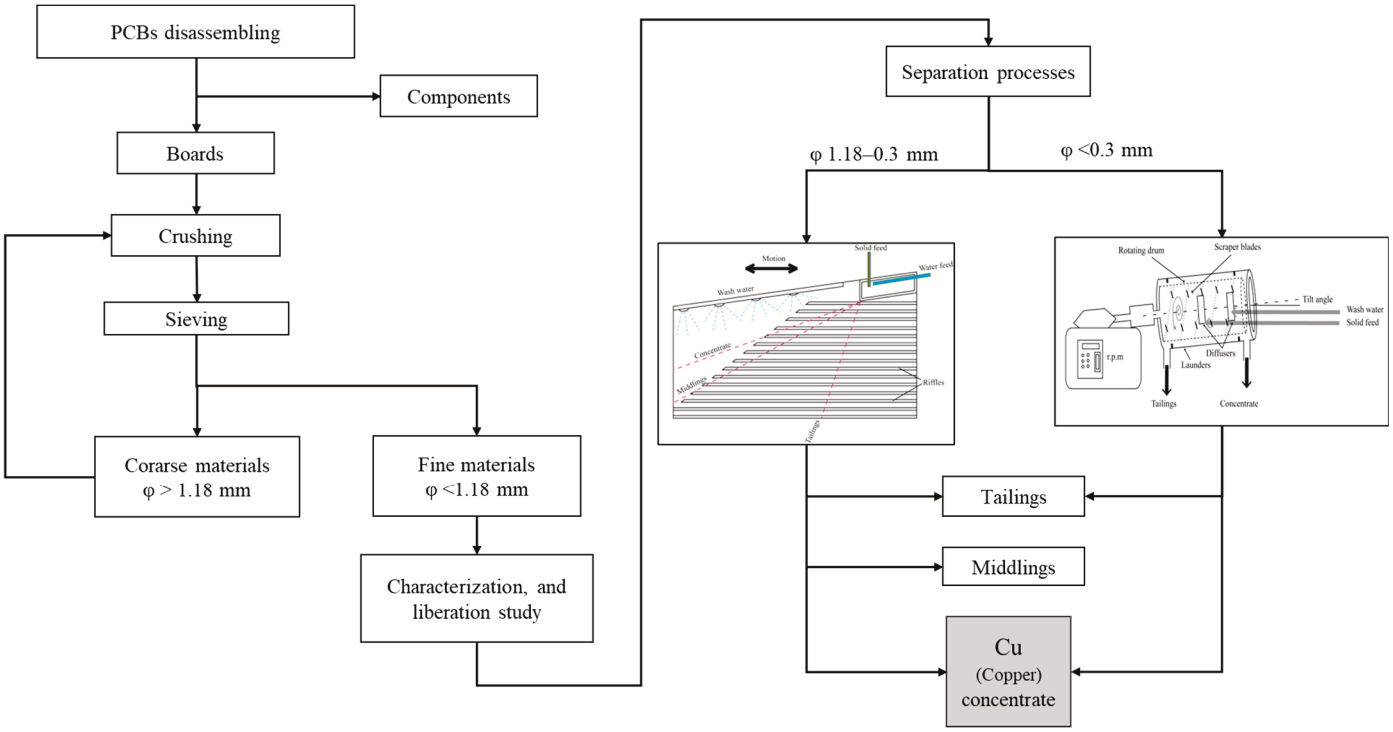


Figure 1. Preparation plan for the recovery of copper from WPCBs.

2.2.2. Characterization and Liberation Study

Various characterization techniques were employed to analyze the resulting WPCB powder. The process began with size distribution analysis using 1180, 500, 250, and 100 µm sieves. Then, to characterize the chemical composition, semiquantitative X-ray fluorescence (XRF) analysis was performed using the Epsilon 1 model from Malvern Panalytical (Malvern, The Netherlands) to determine the metal content in the WPCB powder. For XRF analysis, powder samples were analyzed, and the compositions were defined as elements and oxides in the program created for WPCBs. The study was carried out with three repetitions to ensure the accuracy of the results. For the quantitative identification of precious metals, samples were digested in a microwave using an aqua regia solution (3:1 volume ratio of hydrochloric acid (37% pure) to nitric acid (67% pure)). The digested solution was then analyzed using inductively coupled plasma optical emission spectroscopy (ICP-OES) with the 5100 ICP-OES model from Agilent Technologies (Santa Clara, CA, USA).

At the end, the morphological and compositional distributions of the powder were analyzed using optical microscopy and scanning electron microscopy (SEM) with energy-dispersive spectroscopy (EDS). These analyses were conducted using a field emission scanning electron microscope (FESEM) (JEOL JSM 7001F-JEOL LTD Chome-1-2, Tokyo, Japan) paired with an energy-dispersive spectrometer (EDS; Oxford X-Max, 20 mm^2 window, Oxford Instruments Abingdon OX13 5QX, Oxford, UK) for qualitative assessment. To study the degree of liberation, mineral liberation analysis (MLA) is used at the SEM-MLA facility at Memorial University of Newfoundland (St. John's, NL, Canada). The study used FEI MLA 650FEG equipment to assess composition associations quantitatively, composition locking, and particle shape factors, all of which are crucial for subsequent separation processes.

2.2.3. Separation

Based on the WPCB compositions' liberation degree and density, a Holman–Wilfley Ltd. (Redruth, Cornwall, UK) shaking table was used for coarse particles > 300 μm (300 × 1180 μm). In comparison, an MGS was selected for fine particles < 300 μm to separate copper from non-metallic materials. The feed is divided into two particle size ranges for MGS tests: 100 × 300 μm and <100 μm.

The shaking table begins with a 20%–25% mass pulp fed from the feed box, moving along the table with wash water. Due to the vibrating mechanism, particles undergo diagonal movement, where size and density differences determine their separation. The process involves a slow forward stroke and a rapid return, ultimately collecting small, dense particles at the left end of the table. In contrast, larger, lighter particles are collected opposite the feed box. Figure 2 illustrates the cross-section of the shaking table. The Wilfley model shaking table can effectively separate metal and plastic materials within a 100 μm to 1000 μm particle size range [36]. In this study, the process was applied to materials within the 300 × 1180 μm particle size range. Four key factors, process water flow rate (L/m), wash water flow rate (L/m), deck angle (°), and motion frequency (Hz), influencing the copper recovery of the concentrate, middlings, and tailings were evaluated. Process water flow rate between 4 and 8 (L/m); wash water flow rate between 4 and 12 (L/m); deck angle from 2 to 5 (°); and motion frequency 50–60 (Hz) were tested. To facilitate separation, gutters were placed in the concentrate collection and tailings discharge areas with partitions to separate the collected products. After separation, the collected fractions were filtered and dried at 90 °C in an oven. The final products were classified into a heavy fraction (copper concentrate), middlings (copper and plastic), and a light fraction (plastic).

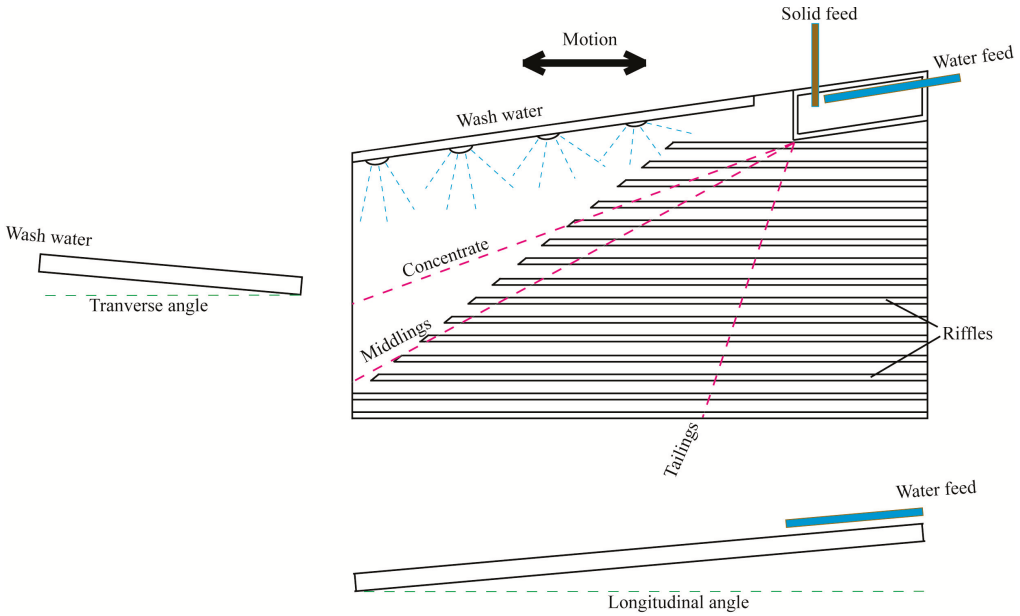


Figure 2. The cross-section figure of the shaking table.

The MGS setup used in this study includes a feed tank equipped with a stirrer, a peristaltic pump for delivering feed to a pilot-scale MGS unit, and sample containers for collecting concentrate and tailings samples. Figure 3 presents a cross-sectional view of the MGS. Solids and water were combined in measured proportions to achieve a solids consistency of 20%–25% by weight in the feed tank. Three factors of water flow rate (L/m), movement frequency (strokes/min), and longitudinal slope angle (°) were studied to reach the highest Cu recovery. Water flow rates of 0.5–2 L/min, movement frequencies of 200–300 strokes/min, and longitudinal slope angles of 3°–5° were examined. During operation, the feed slurry,

consisting of WPCB particles smaller than 300 µm, was continuously pumped into the drum steadily, ensuring the top-size-to-small-size ratio remained below 20%. Samples from the concentrate and tailings streams were collected under steady-state conditions and reached after 5 min of operation. These samples were filtered, dried, and analyzed for total copper content.

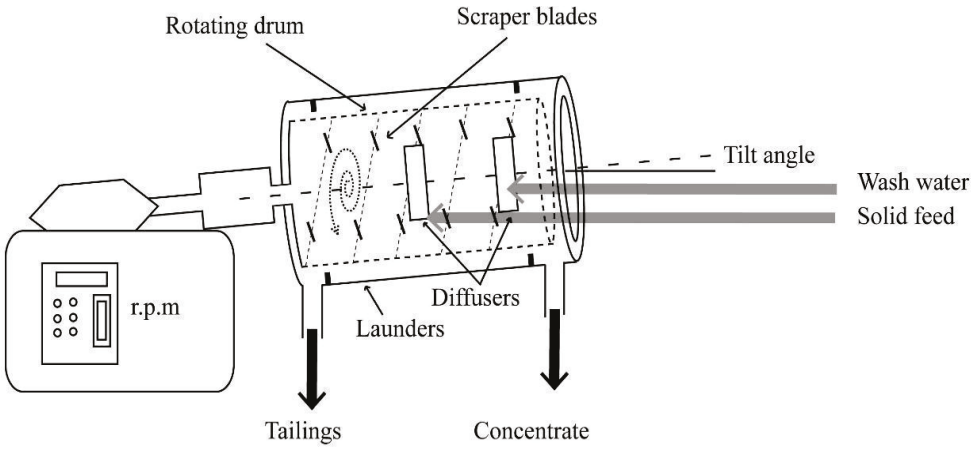


Figure 3. The cross-section figure of the MGS.

3. Results and Discussion

3.1. Sample Preparation

After disassembling the WPCBs, the mass balance indicated that approximately 61.6% of the WPCBs consist of boards, while the remaining 38.4% are components (Figure 4a). This breakdown is crucial for recovery and recycling, indicating that most WPCBs are boards [54].

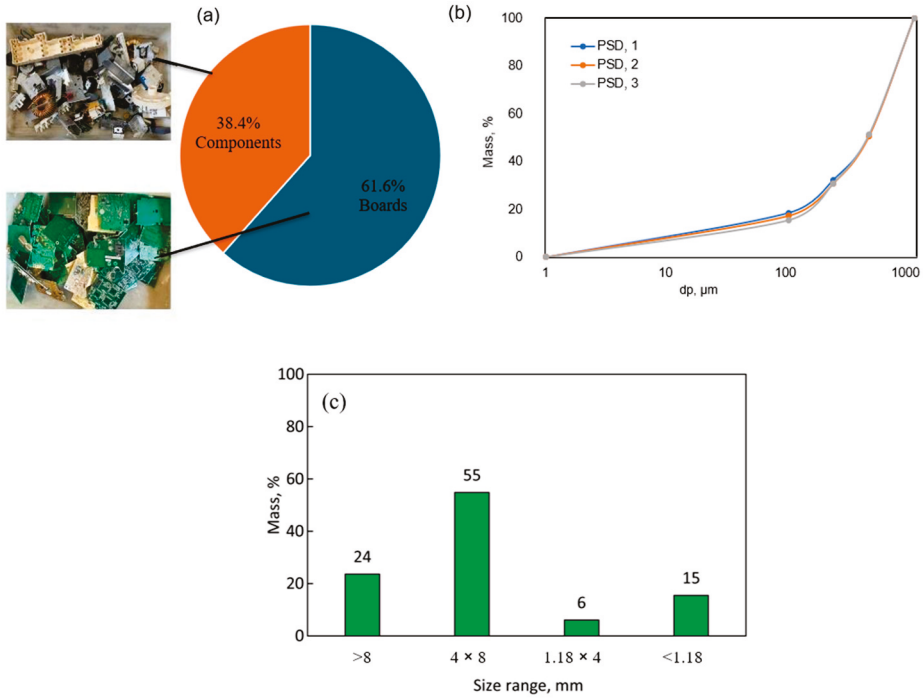


Figure 4. (**a**) disassembling the WPCBs, (**b**) PSD of the crushed WPCBs, (**c**) results of the crushing with the Easy Chop Chopper.

Then, the boards resulting from this disassembling proceeded to the crushing step. Since the Easy Chop Chopper crusher was found to be ineffective for crushing WPCBs, the crushing process continued with the knife crusher until all samples were reduced to particles smaller than 1.18 mm. Figure 4c. shows the results of the Easy Chop Chopper crusher. As shown in the results, it produced coarser (>8 mm, 24%) and medium-sized fragments (8–4 mm, 55%).

The particle size distribution (PSD) of the crushed materials was determined to analyze the crushing process using sieves of 1180, 500, 250, and 100 µm. Figure 4b shows the results of the PSD analysis of the crushing processes, with three repetitions. The steep rise in larger particle sizes suggests that most of the material mass is concentrated in the larger particle fractions, approximately 67.6% of the particles were larger than 250 µm. In comparison, 32.3% were smaller than 250 µm. As less fine material was produced, it can be concluded that the comminution process was environmentally friendly.

3.2. Characterization

During crushing, the classified sample was examined in the laboratory under an optical microscope without reflected light to analyze each size class. The results revealed that the finest size (−63 µm) could not be observed with the optical microscope without reflected light (Figure 5f). However, as the particle size range increases, the resolution improves (Figure 5e,d). In coarser size classes (100 × 150 µm and 150 × 250 µm), no visible interlocking was detected (Figure 5c,d), although in the 250 × 500 µm and 500 × 1180 µm size fractions, numerous recognizable clusters were observed, highlighted by red circles (Figure 5a,b). These clusters consist of interconnected materials, likely due to metal pins coated with other metals or metal bundles compressed with adhesive [6].

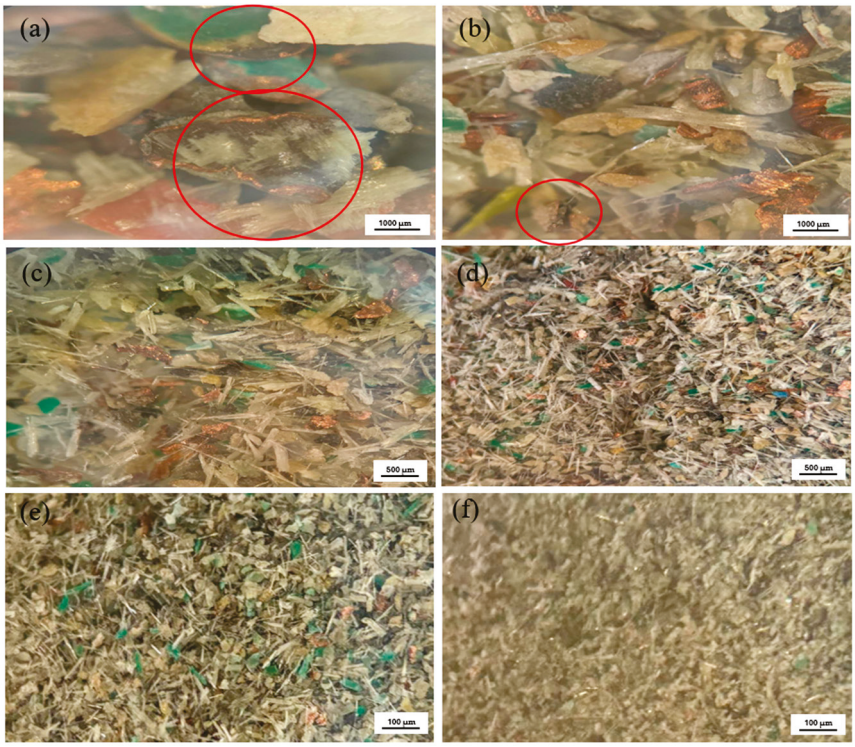


Figure 5. Different-sized fractions of the crushed WPCBs under optical microscopy. (**a**) 500 × 1180 µm, (**b**) 250 × 500 µm, (**c**) 150 × 250 µm, (**d**) 100 × 150 µm, (**e**) 63 × 100 µm, (**f**) −63 µm.

Then, WPCB powder was examined under a microscope with reflected light to compare with the results from optical microscopy without light. The results from the optical microscope with reflected light reveal remarkable images (Figure 6). Non-metallic com-

ponents, such as glass fibers and ceramics, did not transmit light, so they appeared black or gray, whereas metals reflected light, making them colorful and shiny. It is evident that depending on the type of metal, the reflected color varies; for example, the orange color is associated with copper particles. Moreover, unlocked metals and locked metals containing non-metal particles are clearly visible in this Figure. In Figure 6c,d, the red circles indicate locked metal with non-metal particles, while the green circle marks a free metal particle.

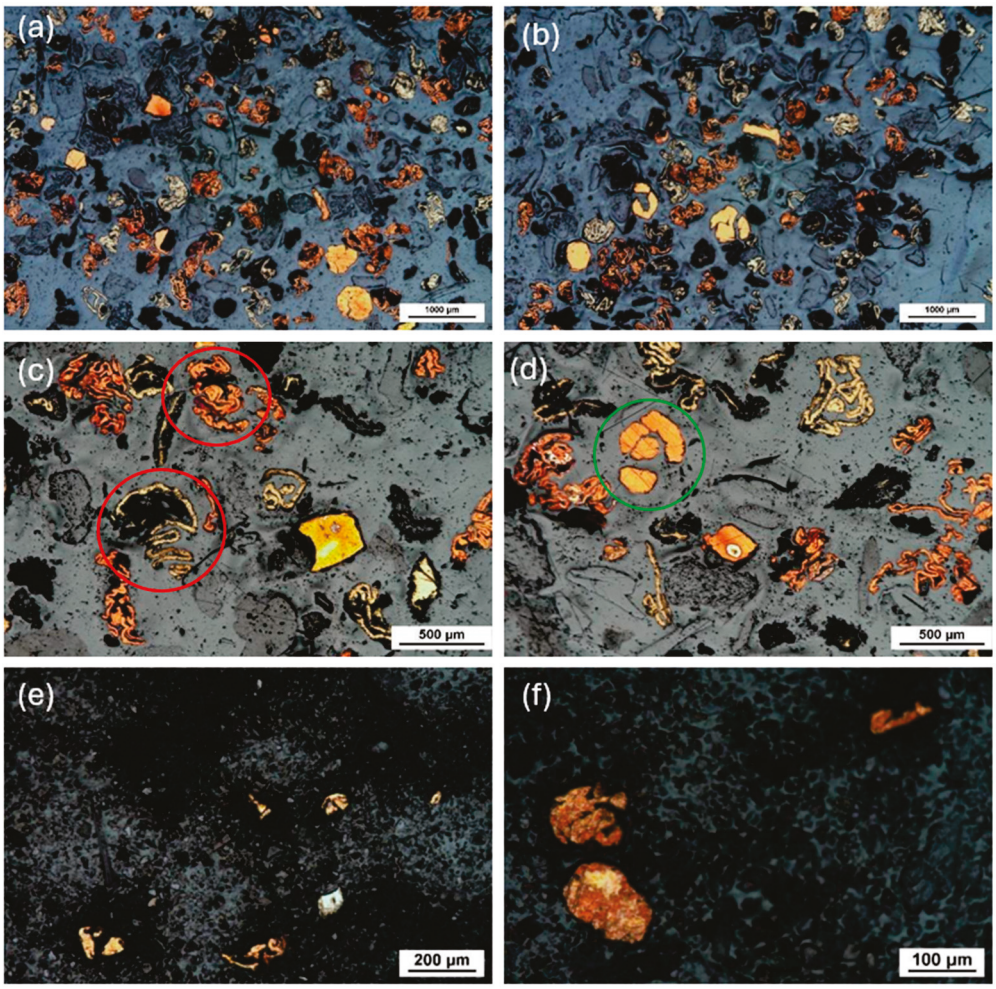


Figure 6. WPCB powder under an optical microscope with reflected light at different magnifications. (**a**,**b**) WPCB powder with ×5 magnification, (**c**,**d**) WPCB powder with × 10 magnification, (**e**,**f**) WPCB powder with ×20 magnification.

To study the distribution of the compositions and the morphology of the crushed WPCBs, SEM-EDS was conducted on the feed and various-sized fractions of WPCBs, as illustrated in Figure 7. According to SEM-EDS analysis, WPCBs mainly consist of glass fibers embedded in resins containing SiO_2, Al_2O_3, and CaO [3,6], which appear in all classifications as bar- and spherical-shaped particles (gray color). Moreover, there are particles in white colors that correspond to metals that are more liberated at finer particle sizes (Figure 7a,b). However, Cu particles appear more agglomerated with glass fibers in the coarse particle sizes (Figure 7c,d). As particle size increases, the agglomeration of both metal and non-metal components also increases.

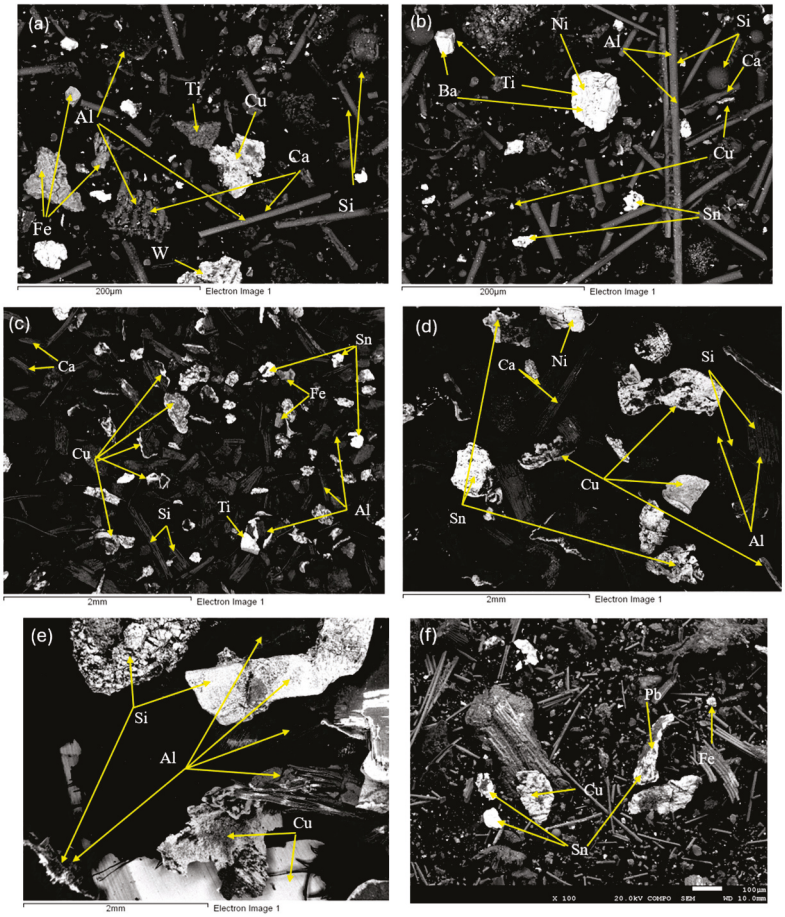


Figure 7. SEM-EDS analysis of the feed and different particle size ranges of WPCBs. (**a**,**b**) −100 µm, (**c**) 100 × 250 µm, (**d**) 250 × 500 µm, (**e**) 500 × 1180 µm, (**f**) feed.

To analyze the major compositions of the WPCBs, XRF analysis was carried out on feed WPCBs and different size fractions of crushed WPCBs in three repetitions. Since the average standard deviation of the repeated analyses was less than 0.7%, the results were considered trustworthy. The results have been selected to be presented in both oxides and elements (Table 1). Based on the XRF results, the major elements of the feed are SiO_2, CaO, Cu, Br, and Al_2O_3 at 35%, 13.6%, 11.1%, 9.4%, and 6.4%, respectively. Copper is the primary metal in WPCB due to its high electrical and thermal conductivity. From the results shown in Table 1, it can be inferred that the Cu percentage is higher in coarser meshes than in finer ones [11]. This phenomenon is attributed to the "ductility" and "workability," showing how much a specific metal or alloy can elongate without rupturing. Thus, due to the higher ductility, a higher portion of the Cu is found in the coarser meshes [3].

It should be noted that industries use different types of copper foil, each with distinct advantages and drawbacks. Electrodeposited (ED) and rolled annealed (RA) copper are the most commonly used foils. The primary difference between them lies in their grain structure. ED copper has a vertical grain structure, which makes it more susceptible to cracking due to stress concentration in the valleys between sharp surface peaks. Cracks can quickly spread along these boundaries. In contrast, RA copper has a horizontal grain structure with a smoother surface, reducing stress concentrators. However, once a crack forms, it must pass through multiple grain boundaries to fracture the entire copper structure [6]. So, this variation in copper types affects crushing and separation efficiency, explaining why not all the Cu is fully liberated during processing. Moreover, Fe during the crushing step cracks and becomes finer due to the lower ductility, thereby decreasing its percentage in the coarse phase. In addition, CaO + SiO_2, as glass fibers and ceramic parts,

follows the same approach. The contents of SiO_2 and CaO are reported to be higher in the finer fraction than in the coarse one. This indicates that a significant number of ceramics and glass fibers became very fine during the comminution due to their brittleness [3].

Table 1. XRF determination of the crushed WPCBs in wt%.

	<100, μm	**100 × 250, μm**	**250 × 500, μm**	**500 × 1180, μm**	**Feed, μm**
Al_2O_3	6.8	7.4	7.9	8.9	6.4
CaO	15.0	11.6	10.6	8.7	13.6
SiO_2	36.1	25.7	23.2	19.9	35.0
Fe_2O_3	2.9	1.4	0.7	0.5	1.6
Cu	4.8	13.2	13.0	18.9	11.0
Br	5.7	12.9	13.0	10.9	9.4
Sb	0.16	0.21	0.23	0.25	0.22
Ba	1.4	0.9	0.3	0.2	0.5
W	5.9	4.5	3.5	2.1	3.8

In the following, ICP-OES analysis was used to determine metals with small amounts, such as Au, Ag, Sn, Pb, Co, Ti, and Ni, as the XRF was not able to measure them accurately. Table 2 shows the analysis results of feed and WPCBs with different particle size ranges, with an average standard deviation of less than 0.5%. As can be seen, the amounts of precious metals such as Au and Ag are high. It can be seen that precious metals in WPCBs are many times more abundant than in their respective natural ores [55,56].

Table 2. Chemical composition of the crushed WPCBs using ICP-OES in wt%.

	<100, μm	**100 × 250, μm**	**250 × 500, μm**	**500 × 1180, μm**	**Feed, μm**
			ppm		
Au	846.79	149.38	176.32	69.45	400.64
Ag	116.68	236.79	185.84	397.74	236.84
Pb	455.14	640.74	889.85	714.07	747.33
Co	23.23	13.60	25.13	27.01	38.99
			%		
Sn	1.60	2.33	3.36	4.23	3.24
Ni	0.42	0.40	0.58	1.12	0.65
Ti	0.19	0.14	0.07	0.08	0.12

After determining the sample compositions by XRF and ICP, the samples were sent for MLA analysis to determine the accurate liberation degree of mechanically processed WPCBs. MLA images were obtained from MLA across three particle size ranges—300 × 1180 μm, 100 × 300 μm, and −100 μm—for further separation processes. Although the distribution of compositions and the morphology of the crushed WPCBs were analyzed by SEM-EDS, MLA is a technique that provides qualitative and quantitative characterization, including associations among compositions, particle size, and composition liberation. So, as a final stage of the characterization and for beginning the separation step, MLA analysis has been carried out.

As the XRF analysis showed, the major metal in this WPCB is Cu, so the first study explicitly presents the liberation of Cu for subsequent separation steps. The Cu liberation by particle size corresponds to the distribution of particles (wt%) by the grade class of Cu within the WPCBs, as illustrated in Figure 8. The graphs show the distribution of Cu in WPCBs. The X-axis, considering eleven grades ranging from 0%–10% to 90%–99%, as well

as a 100% grade class for fully liberated particles. The Y-axis shows the distribution in wt. (%), which means how much of the total material (by weight) falls into each grade in different particle size ranges. The Z-axis presents the particle size ranges (μm), in other words, the size of the particles in μm.

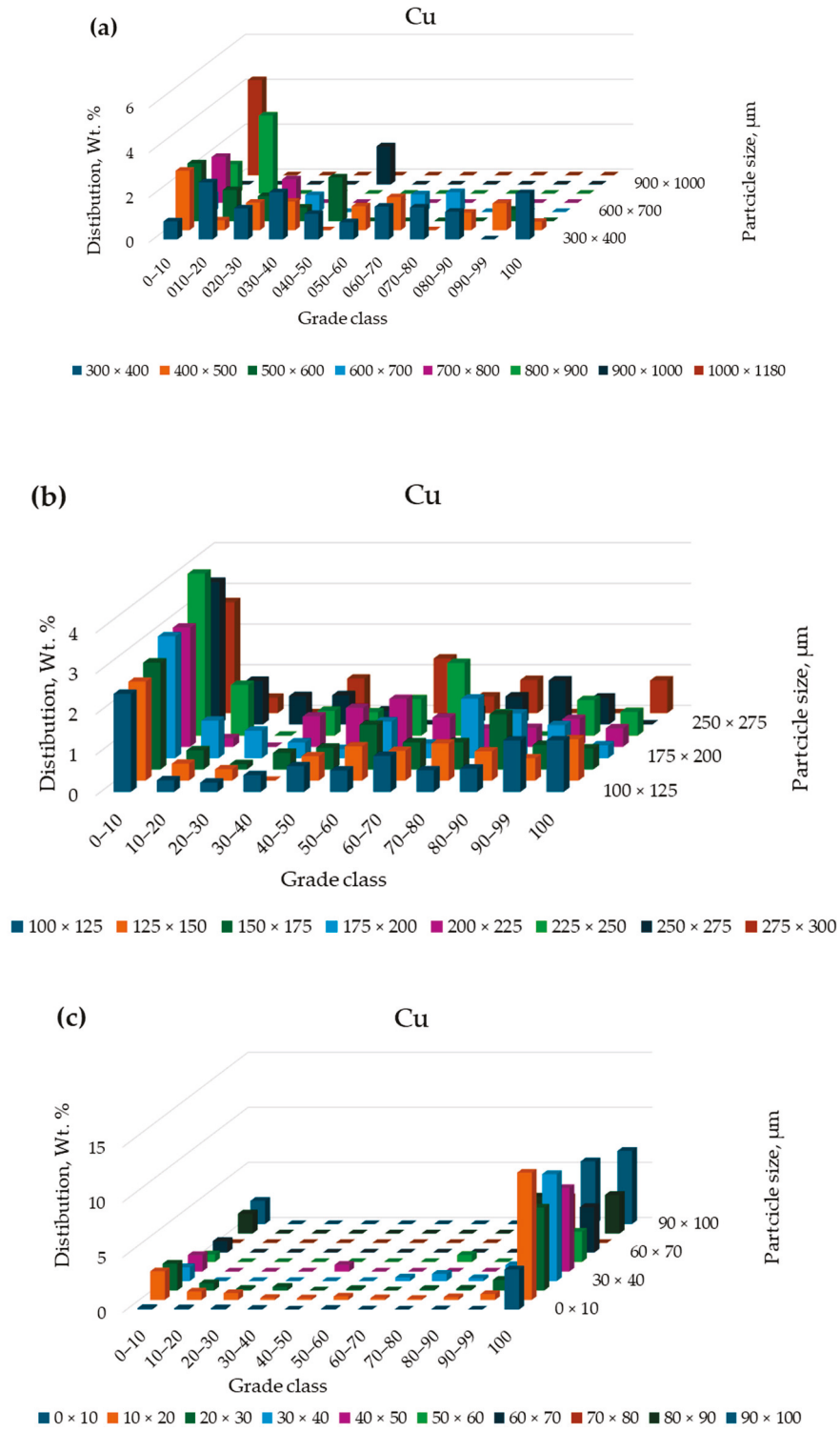


Figure 8. The liberation degree of Cu in 3 different particle sizes. (**a**) 300 × 1180 μm, (**b**) 100 × 300 μm, (**c**) −100 μm.

The analysis of the particles smaller than 100 μm (Figure 8c) shows that most of the particles are completely liberated, 57.04%. They are accumulated in the grade class 100%.

This means that a large number of particles are formed only by copper (grade class 100%). The concentration of these particles in a gravity concentration process is expected to recover concentrates with high copper contents and high copper mass recovery. In contrast, 13.59% of particles with Cu have a low grade (0%–10%), indicating that 13.59% are not liberated. The liberation degree of Cu particles smaller than 100 μm was analyzed by dividing the particles into 10 μm size intervals. Each interval represents a range of particle diameters (0 × 10, 10 × 20, 20 × 30, 30 × 40, 40 × 50, 50 × 60, 60 × 70, 70 × 80, 80 × 90, 90 × 100 μm). As can be seen in Figure 8c, particles smaller than 10 μm are a dark blue color. Then particles with particle sizes of 10 × 20 μm are orange in color, etc. It makes it easier to interpret the liberation degree of each particle size range in Wt%.

On the other hand, in the other two size ranges (300 × 1180 μm and 100 × 300 μm—Figure 8a,b), a large number of particles are in the grade classes in the middle of the figure (20–30, 30–40 . . . 70–80) indicating a low copper liberation (these particles are called Middlings), 33.06% and 36.86% of 300 × 1180 μm and 100 × 300 μm size ranges are middlings, respectively. Only 10% of particles with Cu in 100 × 300 μm size ranges have a grade class of 100%, indicating total liberation. In both cases, it is expected to concentrate low copper contents and low copper mass recovery, especially in the size range 100 × 300 μm (Figure 8b), which presents a large amount of middlings. The liberation degree of Cu particles with 100 × 300 μm size ranges was analyzed by dividing the particles into 25 μm size intervals. Each interval represents a range of particle diameters (100 × 125, 125 × 150, 150 × 175, 175 × 200, 200 × 225, 225 × 250, 250 × 275, 275 × 300 μm). It should be explained that the groups were determined by evaluating the data, and the best group was selected based on each particle size. As shown in Figure 8b, particle sizes of 100 × 125 μm are shown in a dark blue color. Then, particle sizes of 125 × 150 μm are the orange color, etc.

On the other hand, Figure 8b presents a large number of particles in the grade class 0%–10%, 33.75%. This means that almost half of the waste particles are not liberated. They present a maximum of 10% of copper. If they are removed in a gravity concentration process (waste material), the copper content will increase in the concentrate. Moreover, 54.86% of particles with Cu in the 300 × 1180 μm size range have a grade of 0–20. It means that half of the coarse particles are mostly locked. The liberation degree of Cu particles with 300 × 1180 μm size ranges was analyzed by dividing the particles into 100 μm size intervals. Each interval represents a range of particle diameters (300 × 400, 400 × 500, 500 × 600, 600 × 700, 700 × 800, 800 × 900, 900 × 1000, 1000 × 1180 μm). As shown in Figure 8a, particle sizes of 300 × 400 μm are the dark blue color. Then the particle sizes of 400 × 500 μm are shown in orange color, etc.

Secondly, the Cu association with other components in three particle size ranges is analyzed in Figure 9. Associations refer to the percentage of the extent of the boundaries of composition in contact with free surfaces or other compositions [57].

The figure shows that 96.32% of Cu in particles smaller than 100 μm have a free surface, while the remaining 3.68% are associated with other compositions, primarily Ca + Al + SiO. This is the flotation size range, and good results could be achieved with flotation due to the free surface. In the 100 × 300 μm size fraction, 72.03% of Cu have a free surface, with 27.97% associated mainly with bromide. For particles in the 300 × 1180 μm size range, 66.18% of Cu have a free surface, while 33.82% are predominantly associated with bromide. The results indicate that the free surface (orange color) dominates in all particle sizes, meaning most of the Cu has a free surface. However, as particle size increases, the proportion of Cu with a free surface decreases, confirming the liberation study findings that the degree of liberation of Cu decreases with increasing particle size.

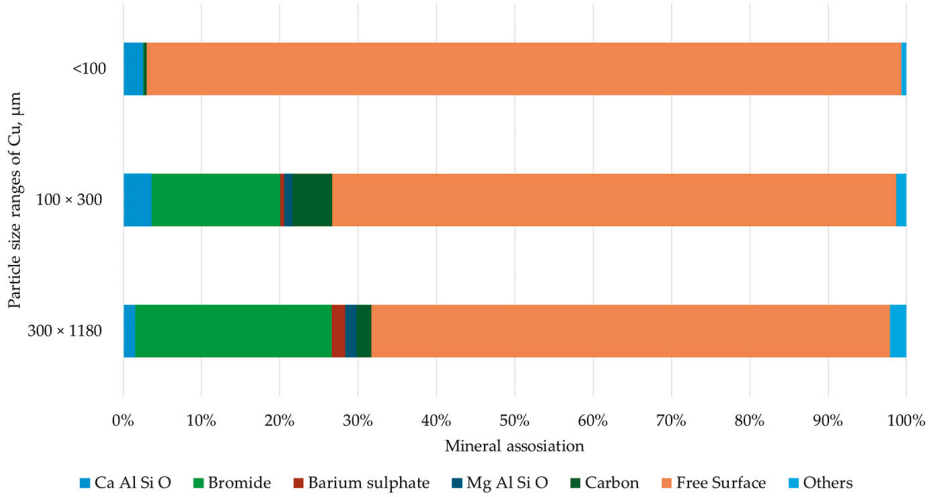


Figure 9. Cu association analysis in three different particle size ranges in wt%.

Lastly, the cumulative mass of Cu in different particle size ranges was measured (Figure 10). The cumulative theoretical recovery obtained through MLA estimates the amount of valuable compositions that could be recovered in a separation process, based on its degree of liberation from the waste [58]. This recovery can be calculated from the grade and/or the free surface, as both factors influence the efficiency of the concentration process. A higher degree of liberation or greater free surface area of the compositions imply potentially higher recovery. Both methods help predict the efficiency of composition recovery by considering the composition's quantity and physical liberation.

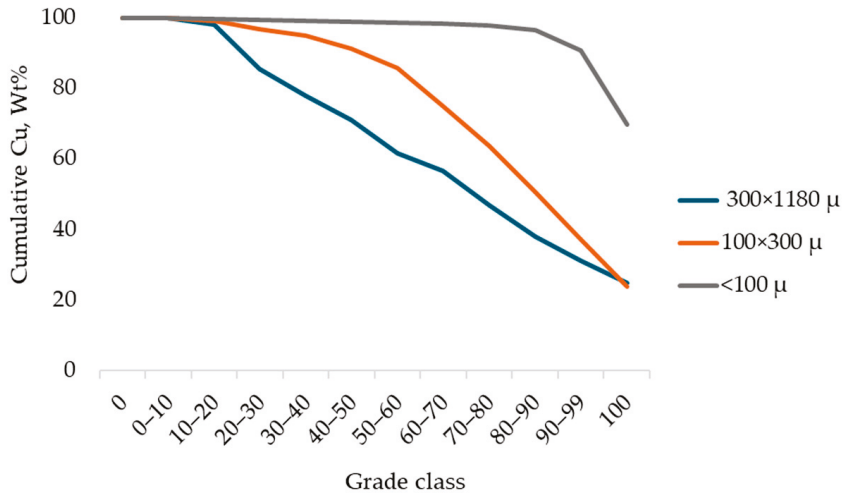


Figure 10. Cumulative mass of the Cu in different particle size ranges.

The Cu cumulative graph shows that as the Cu grade decreases (100 to 0), the cumulative mass of copper increases across all three particle size ranges (almost 20 to 100 wt%). The finer particle size (gray line) retains a higher cumulative mass of Cu across most Cu grade ranges, while the coarser particles (blue line) show the lowest cumulative Cu mass. This suggests that Cu is more liberated in the fine fractions than in the coarse fractions. Although the finest particle size has the most liberated Cu, the other particle size ranges have approximately the same number of liberated particles in the 100% grade class.

To conclude, coarse samples with particle sizes ranging from 300 to 1180 µm present a Cu content of 9.65% (Table 3). Of this Cu mass, 24.68% is in the 100% grade class, indicating that these Cu particles are completely liberated. Additionally, 22.18% falls within the

70%–99% grade classes (grade classes 70–80, 80–90, and 90–99 in Figure 10), meaning they are partially liberated. This work assumes that particles in grade classes above 70% exhibit sufficient liberation to be concentrated using gravimetric processes. A significant portion of this particle size range—38.50%—falls within the 20%–70% grade classes, while a small fraction, around 14.64%, has a grade of less than 20%. Cu particles in grade classes below 20% are thoroughly mixed, showing low Cu liberation and making their separation by gravity concentration difficult. Table 3 presents the Cu content of WPCBs determined by MLA techniques across three particle size ranges. It determines the quantitative volume or weight percentages of composition phases in a sample. It describes the actual composition, rather than the normative (theoretical) composition calculated from chemical data.

Table 3. Cu content in three different particle sizes by MLA techniques.

Particle Size Ranges, μm	wt%
300 × 1180	9.65
100 × 300	4.58
<100	4.25

Samples with particle sizes ranging from 100 to 300 μm contain 4.58% Cu (Table 3), of which 23.71% is completely liberated, falling within the 100% grade class (Figure 10—orange curve). Additionally, 40% have a grade between 70% and 99%, indicating that the particles are partially liberated. Meanwhile, 31.10% of the particles fall within the 30–70% grade classes, while less than 5.19% have a grade below 30%.

For finer samples with particle sizes less than 100 μm containing 4.25% Cu (Table 3), 69.69% of this material is entirely liberated (Figure 10—gray curve), grade class of 100%. Furthermore, 28.12% falls within the 70%–99% grade classes, indicating partial liberation of the particles. Only a small fraction, 2.19%, is in the grade class below 70%, indicating limited particle liberation.

3.3. Separation

After accurate characterization of the classified feeds, particles in the size range 300 × 1180 μm were beneficiated on a shaking table, and particles in the size range smaller than 300 μm were beneficiated in an MGS.

The shaking table concentration with the coarse particles (300 × 1180 μm) shows that Cu can be recovered by 14.78% (Cu content) and 95.01% (Cu recovery) in the concentrate, the middlings present 0.70% (Cu content) and 4.53% (Cu recovery), and the waste 0.07% (Cu content) and 0.46% (Cu recovery). The test's average standard deviation indicates that the data are reliable. The average standard deviations of the concentrate, middlings, and tailings were 2.2%, 1.5%, and 0.65%, respectively. It is possible to say that most of the particles with grade classes over 70% are in the concentrate, with grade classes between 30 and 70% in the middlings, and with grade classes under 30% in the waste.

Optimal recovery is achieved with a higher water flow rate and a lower deck angle [35], since the process targets a high-recovery clean product. Increasing the deck angle and decreasing the water flow rate negatively impact the efficiency. On the other hand, as the deck angle increases, efficiency decreases in the concentrate while rising in the middlings, as shown in Table 4.

Table 4. Shaking table results.

					Concentration			Middlings			Waste		
Mass, g	**Deck Angle, θ**	**Frequency, Hz**	**Wash Water, L/min**	**Process Water, L/min**	**Mass, %**	**Cu, %**	**Cu R, %**	**Mass, %**	**Cu, %**	**Cu R, %**	**Mass, %**	**Cu, %**	**Cu R, %**
296.4	1	60	12	8	37.9	30.7	94.6	53.4	0.9	4.1	8.7	1.9	1.4
298.2	2	60	12	8	36.9	40.1	95	38.7	1.8	4.5	24.4	0.3	0.5
312.5	3	60	12	8	43.6	47.7	73.2	39.9	18.4	26	16.5	1.5	0.8
322.9	4	40	2	4	45.2	42	83	46.5	7.8	15.9	8.4	3	1.1
300.9	5	50	2	4	44.7	47.8	82.1	23.5	17.3	15.7	31.8	1.8	2.3
319.2	5	60	4	4	29.4	56.7	60.9	40.3	24.5	36.1	30.3	2.7	3

The MGS has been carried out on two particle size ranges: 100 × 300 μm and smaller than 100 μm. Table 5 presents the concentration results of the MGS tests. The MGS concentration with the coarse particles (100 × 300 μm) shows that Cu can be recovered by 6.89% (Cu content) and 94% (Cu recovery) in the concentrate and 0.44% (Cu content) and 6% (Cu recovery) in the waste. The MGS concentration with the fine particles (−100 μm) shows that Cu can be recovered by 3.81% (Cu content) and 81.5% (Cu recovery) in the concentrate and 0.87% (Cu content) and 18.5% (Cu recovery) in the waste. According to the average standard deviation of the tests, the data are reliable. An average standard deviation of the concentrate and tailings was 1.2% and 0.4%, respectively. Optimal recovery is achieved with a lower wash water flow rate and a lower deck angle, since the process aims for a high-recovery clean product with a low-grade rejectable tailings stream.

Table 5. MGS results.

				Concentration			Waste		
Mass, g	**Wash Water, L/min**	**Drum Revolutions, rpm**	**Deck Angle, θ**	**Mass, %**	**Cu, %**	**Cu R, %**	**Mass, %**	**Cu, %**	**Cu R, %**
<100 μm									
106.2	0.5	300	2.4	52.4	7.3	81.5	47.6	1.8	18.5
203.3	0.5	295	3	17.8	18.4	65.3	82.2	2.1	34.7
195.8	0.9	290	2.94	8.5	19.2	40.9	91.5	2.6	59.1
100 × 300 μm									
86.7	0.5	300	2.4	59.8	11.5	94	40.1	1.1	6
153.4	0.5	300	3.4	21.4	40.1	80.4	78.6	2.7	19.6
202.7	0.5	305	3	17.2	37.9	56.9	82.8	6	43.1

The proposed flowsheet for Cu beneficiation using a shaking table and MGS is shown in Figure 11. The following data are presented in the figure: Mtot is the total mass in the fraction; Cucont is the copper content in the fraction; Cumetal is the mass of copper presented in the fraction; and Curec is the metallurgical mass balance of the copper in relation to the feed (total is 100%).

It is possible to observe in Figure 11 that 44.32% of the total mass of the feed goes to the concentrates: 10.67% of the concentrate of the MGS in the fraction 100 to 300 μm, 11.25% in the fraction −100 μm, and 22.40% of the concentrate of the shaking table. These concentrates (44.32% of the total mass) present a mean copper content of 10.10%, with 93.81% of the copper mass from the feed (15.41% of the MGS 100 × 300 μm; 8.99% of the MGS −100 μm, and 69.41% of the shaking table). This means it is possible to recover 93.81% of the copper using a flowsheet like that.

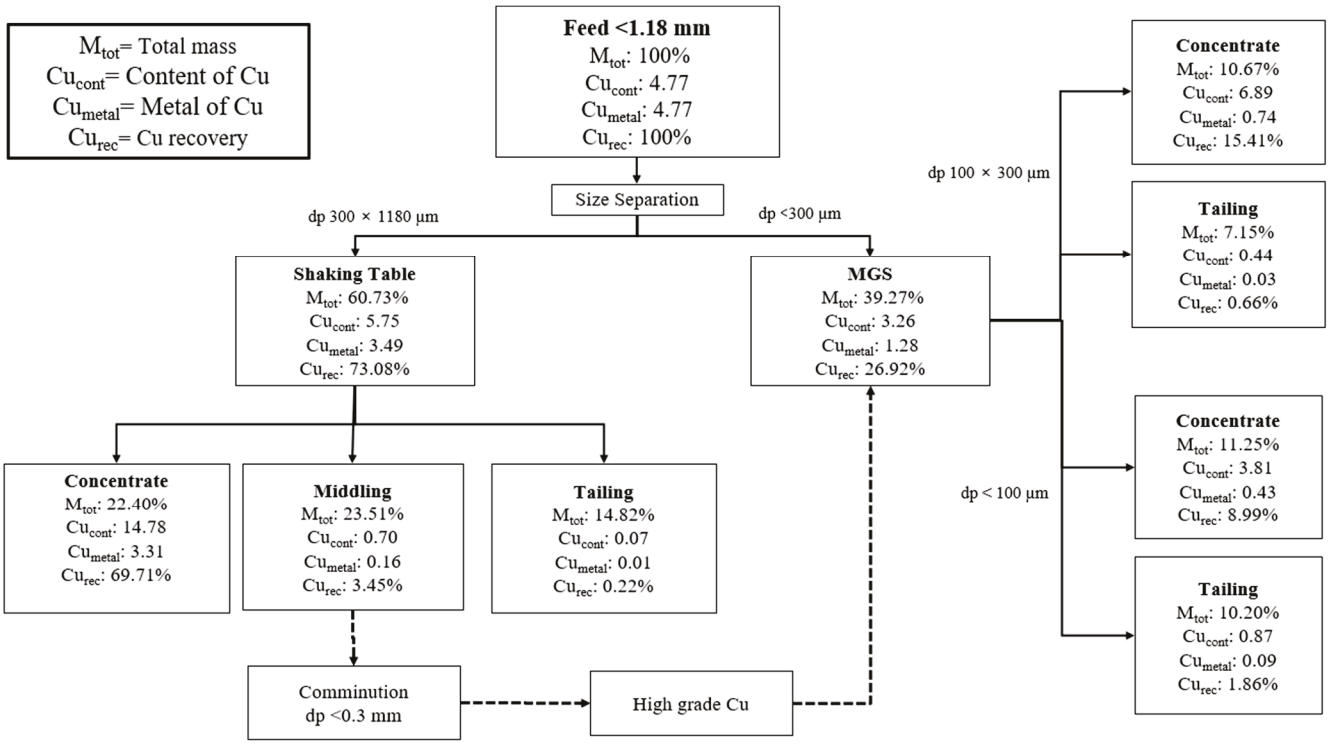


Figure 11. Proposed flowsheet for Cu beneficiation.

The tailings of the tests (MGS, fraction 100 × 300 µm and fraction −100 µm; and the shaking table) present a mass of 32.17% of the feed (7.15%, MGS, fraction 100 × 300; 10.20%, MGS, fraction −100; and 14.82% of the shaking table). The mean copper content of these tailings is 0.29%, with only 2.74% of the copper in the feed. The amount of copper discarded in the tailings is relatively small, demonstrating good liberation of waste particles and good cutting efficiency.

It is also possible to generate middlings in the shaking table (23.51% of the total mass; 0.7% of copper content; 3.45% mas of the copper in the feed) that can be added to the tailings or comminuted to a top size of 300 µm and sent to the MGS feed for more intense concentration.

As mentioned before, this flowsheet tries to propose more environmentally friendly processes. In terms of chemical usage, other methods such as flotation and leaching [59–62] use chemicals such as acids, collectors, and frothers, but this process reduces chemical use to zero, thereby reducing environmental impact and lowering costs, especially on a large scale. The large-scale industrial use of the chemical will add to the cost of recycling processes for these kinds of wastes; however, this flowsheet uses differences in the specific gravity of the waste to separate metals from non-metals, which seems more industrial.

Ogunniyi et al. (2009) used the flotation technique without collectors or frothers, but the Cu recovery did not reach 70% [63]. In another study by Chen et al. (2023), 93.8% of the Cu was recovered by reverse flotation with ultrasonic assistance, which uses ultrasonic to increase the energy consumption, and it will increase the costs at the end [64]. However, some studies prove that with proper optimization of flotation conditions, high recoveries (up to 95%) are achievable [65,66]. However, as mentioned, the environmental and economic aspects remain problems. Moreover, the particle size ranges in these studies are limited; however, our study covers a broader range.

Ismail Mohammad et al. (2025) studied the effect of solvent pre-treatment on the leaching of copper, especially for larger particle sizes [67]. The results were not satisfactory: 47.3% Cu recovery without pre-treatment and 87.65% with pre-treatment. Magoda et al. (2024) used a two-step bioleaching process to recover Cu [60]. However, the particle size

was limited to the 38–150 μm fraction, and the Cu recovery was 68.2%. Other difficulties in this work include maintaining pH and temperature, as each microbial group has a strict optimal range (acidic for acidophiles, alkaline for cyanobacteria) [68]. We suppose that the combination of the Cu recovered from our work with leaching in the following steps can provide better results with less environmental impact and at a lower cost.

Bilesan et al. (2021) combined a hydrocyclone with the dilution-gravity method (DGM) for recovering precious and base metals from fine particle sizes (<75 μm) of the WPCBs [26]. However, the total copper recovery of 72% was achieved. So, compared to the MGS, it has a limited particle size, lower Cu recovery, and an additional cost due to the use of the DGM.

Xian et al. (2021) used heated printed circuit boards via an enhanced gravity concentrator falcon (SB40) and a high-gradient magnetic separator to recover Cu and iron (Fe), and they earned 74.02% Cu recovery and 78.11% Fe recovery [69]. In addition to the lower recovery gained compared to our work, the heating process is not environmentally friendly and releases toxic gases.

It is important to note that some losses occur primarily due to the generation of fines and the flat particles, with a nearly two-dimensional shape of metal particles produced during crushing. These particles exhibit poor settling behavior in the wet circuit. Additionally, ultrafine plastic particles create challenges in the wet circuit by clustering and trapping small metal particles, further affecting separation efficiency [11].

Furthermore, the selective separation of heavy metals such as zinc, brass, and gold was not the focus of this study. Instead, the primary objective was to minimize the environmental impact of electronic waste and ensure the efficient recovery of copper resources [32]. Future studies could explore the separation of precious metals like gold and silver, since considerable quantities were prevalent in the WPCBs. These noble metals in WPCBs are the primary economic driver for e-waste recycling [70–73]. Additionally, non-metallic fractions (NMFs) should not be overlooked, as they can serve as safe and effective fillers in various composites with thermoset and thermoplastic resin matrices, adding them to concrete to enhance the engineering properties of concrete such as strength, durability, shrinkage, and permeability, offering an environmentally friendly solution [74–77].

Lastly, it is suggested that the recovered copper from this flowsheet be sent for further treatment, such as pyrometallurgical processing, to eliminate impurities and meet the requirements of the industry's smelting process [78].

4. Conclusions

This study developed and evaluated a two-stage gravity separation process for recovering copper from waste printed circuit boards (WPCBs), combining a shaking table for coarse particles (>300 μm) and a multi-gravity separator (MGS) for fine particles (<300 μm). After mechanical pre-treatment and comprehensive characterization, X-ray fluorescence (XRF), inductively coupled plasma optical emission spectroscopy (ICP-OES), scanning electron microscopy (SEM-EDS), and mineral liberation analysis (MLA) were performed, which were critical in understanding the feed material composition locking and association.

Quantitative separation results highlight the efficiency of the proposed flowsheet. The shaking table achieved 95.01% Cu recovery in the coarse fraction, while the MGS produced 94% Cu recovery for the 100–300 μm fraction and 81.5% Cu recovery for particles below 100 μm. When integrated, the two-unit flowsheet successfully recovered 93.81% of the total Cu into clean concentrates representing 44.32% of the total mass, while only 2.74% of the copper was discarded in tailings. These outcomes confirm that gravity separation, when preceded by appropriate comminution and liberation analysis, can produce high-quality Cu concentrates with minimal environmental impact.

The efficiency of the multi-gravity separator as a physical beneficiation technique for the recovery of Cu from fine particles was proven. The proposed methodology enhances the concentration and purity of the metallic fraction (in this case, Cu), especially in fine particles, which are challenging to work with, while reducing environmental impacts through minimal chemical use, thereby contributing to sustainable e-waste recycling.

Results of the characterization show that the MLA technique is an effective and accurate method for characterizing complex materials like WPCBs and offering detailed insights into compositions, particle liberation, and shapes, etc. Secondly, a high concentration of precious metals such as Au and Ag highlights its potential for future recovery and recycling.

For future work, the research can be extended in several promising directions. First, the separation of other precious metals, such as gold and silver, identified in significant quantities by ICP-OES, should be investigated, as they are a primary economic driver of e-waste recycling. Second, the valorization of the non-metallic fraction (NMF) should be explored, for instance, as a filler in construction composites or concrete to enhance material properties.

Author Contributions: Conceptualization, M.P.; Methodology, J.O. and C.H.S.; Software, M.P. and P.E.; Validation, M.P., J.O. and C.H.S.; Formal analysis, J.O., H.A. and C.H.S.; Investigation, M.P.; Resources, J.O. and C.H.S.; Data curation, M.P. and P.E.; Writing—original draft, M.P.; Writing—review & editing, J.O., H.A., C.H.S., P.A., C.V., J.L.C. and P.E.; Visualization, M.P., H.A. and P.A.; Supervision, J.O., H.A., C.H.S. and P.A.; Project administration, J.O., C.H.S., C.V. and J.L.C.; Funding acquisition, J.O., C.H.S., C.V. and J.L.C. All authors have read and agreed to the published version of the manuscript.

Funding: This research was funded by MICIU/AEI/10.13039/501100011033/FEDER, UE, grant number: PID2024-158241OB-I00.

Data Availability Statement: The original contributions presented in this study are included in the article. Further inquiries can be directed to the corresponding author.

Acknowledgments: The authors would like to thank the Agencia Estatal de Investigación del Ministerio de Ciencia e Innovación for funding the project under grant number PID2021-127028OB-I00. This work is part of Maria de Maeztu Units of Excellence Programme CEX2023-001300-M/funded by MCIN/AEI/10.13039/501100011033.The authors belong to the 2021-SGR 01041 (RiiS) and 2021-SGR 00596 (R2EM) research groups financed by the AGAUR, Generalitat de Catalunya.

Conflicts of Interest: The authors declare no conflicts of interest.

References

1. Kumar, A.; Holuszko, M.E.; Janke, T. Characterization of the non-metal fraction of the processed waste printed circuit boards. *Waste Manag.* **2018**, *75*, 94–102. [CrossRef] [PubMed]
2. Pourmohammad, M.; Oliva, J.; Anticoi, H.; Hoffmann Sampaio, C.; Alfonso, P.; Valderrama, C.; Cortina Pallas, J.L. The Characterization of Black Mass from Spent Lithium-Ion Scooter Batteries Using Multi-Analytical Techniques. *Recycling* **2025**, *10*, 54. [CrossRef]
3. Nekouei, R.K.; Pahlevani, F.; Rajarao, R.; Golmohammadzadeh, R.; Sahajwalla, V. Two-step pre-processing enrichment of waste printed circuit boards: Mechanical milling and physical separation. *J. Clean. Prod.* **2018**, *184*, 1113–1124. [CrossRef]
4. Van Yken, J.; Cheng, K.Y.; Boxall, N.J.; Sheedy, C.; Nikoloski, A.N.; Moheimani, N.R.; Kaksonen, A.H. A comparison of methods for the characterization of waste-printed circuit boards. *Metals* **2021**, *11*, 1935. [CrossRef]
5. Otsuki, A.; Mensbruge, L.D.L.; King, A.; Serrano, S.; Fiore, L.; Bonifazi, G. Non-destructive characterization of mechanically processed waste printed circuit boards—Particle liberation analysis. *Waste Manag.* **2020**, *102*, 510–519. [CrossRef]
6. Abbadi, A.; Rácz, A.; Bokányi, L. Exploring the comminution process of waste printed circuit boards in recycling; a review. *J. Mater. Cycles Waste Manag.* **2024**, *26*, 1326–1348. [CrossRef]
7. Ji, X.; Yang, M.; Wan, A.; Yu, S.; Yao, Z. Bioleaching of Typical Electronic Waste—Printed Circuit Boards (PCBs): A Short Review. *Int. J. Environ. Res. Public Health* **2022**, *19*, 7508. [CrossRef]

8. Mori de Oliveira, C.; Bellopede, R.; Tori, A.; Zanetti, G.; Marini, P. Gravity and Electrostatic Separation for Recovering Metals from Obsolete Printed Circuit Board. *Materials* **2022**, *15*, 1874. [CrossRef]
9. Sarvar, M.; Slarirad, M.M.; Shabani, M.M. Characterisation and mechanical separation of metals from computer Printed Circuit Board (PCBs) based on mineral processing methods. *Waste Manag.* **2015**, *45*, 246–257. [CrossRef]
10. Palmieri, R.; Bonifazi, G.; Serranti, S. Recycling-oriented characterization of plastic frames and printed circuit boards from mobile phones by electronic and chemical imaging. *Waste Manag.* **2014**, *34*, 2120–2130. [CrossRef] [PubMed]
11. Das, A.; Vidyadhar, A.; Mehrotra, S.P. A novel flowsheet for the recovery of metal values from waste printed circuit boards. *Resour. Conserv. Recycl.* **2009**, *53*, 464–469. [CrossRef]
12. Oke, E.A.; Potgieter, H. Discarded e-waste/printed circuit boards: A review of their recent methods of disassembly, sorting and environmental implications. *J. Mater. Cycles Waste Manag.* **2024**, *26*, 1277–1293. [CrossRef]
13. Keleş, B.; Dinç, N.I.; Dursun, H.N.; Burat, F.; Ulusoy, U. The effect of particle geometry (size & shape) on the recovery of gold and copper metallic particles from end-of-life random access memory cards by flotation. *Waste Manag.* **2024**, *179*, 66–76. [CrossRef]
14. Otsuki, A.; Gonçalves, P.P.; Stieghorst, C.; Révay, Z. Non-destructive characterization of mechanically processed waste printed circuit boards: X-ray fluorescence spectroscopy and prompt gamma activation analysis. *J. Compos. Sci.* **2019**, *3*, 54. [CrossRef]
15. Touze, S.; Guignot, S.; Hubau, A.; Devau, N.; Chapron, S. Sampling waste printed circuit boards: Achieving the right combination between particle size and sample mass to measure metal content. *Waste Manag.* **2020**, *118*, 380–390. [CrossRef]
16. Ghosh, B.; Ghosh, M.K.; Parhi, P.; Mukherjee, P.S.; Mishra, B.K. Waste Printed Circuit Boards recycling: An extensive assessment of current status. *J. Clean. Prod.* **2015**, *94*, 5–19. [CrossRef]
17. Wang, L.; Li, Q.; Sun, X.; Wang, L. Separation and recovery of copper from waste printed circuit boards leach solution using solvent extraction with Acorga M5640 as extractant. *Sep. Sci. Technol.* **2018**, *54*, 1302–1311. [CrossRef]
18. Yoo, J.; Jeong, J.; Yoo, K.; Lee, J.; Kim, W. Enrichment of the metallic components from waste printed circuit boards by a mechanical separation process using a stamp mill. *Waste Manag.* **2009**, *29*, 1132–1137. [CrossRef] [PubMed]
19. Veit, H.M.; Juchnes, N.C.; Scherer, J. Use of Gravity Separation in Metals Concentration from Printed Circuit Board Scraps. Metallurgy and materials. *Rem Revista Escola de Minas* **2014**, *67*, 73–79. [CrossRef]
20. Burat, F.; Özer, M. Physical separation route for printed circuit boards. *Physicochem. Probl. Miner. Process.* **2018**, *54*, 554–566. [CrossRef]
21. Keglevich de Buzin, P.J.W.; Ambrós, W.M.; Schadach de Brum, I.A.; Candiota Tubino, R.M.; Hoffmann Sampaio, C.; Oliva Moncunill, J. Development of a Physical Separation Route for the Concentration of Base Metals from Old Wasted Printed Circuit Boards. *Minerals* **2021**, *11*, 1014. [CrossRef]
22. Zhu, X.; Zhang, L.; Dong, S.; Kou, W.; Nie, C.; Lyu, X.; Qiu, J.; Li, L.; Liu, Z.; Wu, P. Mechanical activation to enhance the natural floatability of waste printed circuit boards. *Waste Manag.* **2020**, *109*, 222–230. [CrossRef]
23. Ogunniyi, I.; Vermaak, M.; Groot, D. Chemical composition and liberation characterization of printed circuit board comminution fines for beneficiation investigations. *Waste Manag.* **2009**, *29*, 2140–2146. [CrossRef]
24. Arshadi, M.; Yaghmaei, S.; Mousavi, S.M. Content evaluation of different waste PCBs to enhance basic metals recycling. *Resour. Conserv. Recycl.* **2018**, *139*, 298–306. [CrossRef]
25. Hubau, A.; Chagnes, A.; Minier, M.; Touzé, S.; Chapron, S.; Guezennec, A.G. Recycling-oriented methodology to sample and characterize the metal composition of waste Printed Circuit Boards. *Waste Manag.* **2019**, *91*, 62–71. [CrossRef]
26. Bilesan, M.R.; Makarova, I.; Wickman, B.; Repo, E. Efficient separation of precious metals from computer waste printed circuit boards by hydrocyclone and dilution-gravity methods. *J. Clean. Prod.* **2021**, *286*, 125505. [CrossRef]
27. Ichikawa, S.; Hirokawa, Y.; Kurisaki, T.; Nakamura, T. Characterization of a printed-circuit board by X-ray fluorescence and X-ray diffraction analyses for metal recovery. *Spectrochim. Acta Part B At. Spectrosc.* **2023**, *210*, 106819. [CrossRef]
28. Agbim, A.; Schumacher, K.A.; Sharp, N.; Paul, R.; Corzo, R. Elemental characterization of electronic waste: A review of research methodologies and applicability to the practice of e-waste recycling. *Waste Manag.* **2024**, *187*, 91–100. [CrossRef]
29. Gonçalves, P.P.; Otsuki, A. Determination of liberation degree of mechanically processed waste printed circuit boards by using the digital microscope and SEM-EDS analysis. *Electronics* **2019**, *8*, 1202. [CrossRef]
30. Zhang, G.; He, Y.; Feng, Y.; Zhang, T.; Wang, H.; Zhu, X. Recovery of residual metals from fine nonmetallic fractions of waste printed circuit boards using a vibrated gas-solid fluidized bed. *Sep. Purif. Technol.* **2018**, *207*, 321–328. [CrossRef]
31. Escalante, P.; Oliva, J.; Anticoi, H.; Hoffmann Sampaio, C.; Mohanty, K. Characterization of mineralogical impurities in a carbonate-rich material using MLA. *Miner. Eng.* **2025**, *230*, 109409. [CrossRef]
32. Vanderbruggen, A.; Gugala, E.; Blannin, R.; Bachmann, K.; Serna-Guerrero, R.; Rudolp, M. Automated mineralogy as a novel approach for the compositional and textural characterization of spent lithium-ion batteries. *Miner. Eng.* **2021**, *169*, 106924. [CrossRef]
33. Donnelly, L.; Pirrie, D.; Power, M.; Menzies, A. Phase Characterisation for Recycling of Shredded Waste Printed Circuit Boards. *Recycling* **2025**, *10*, 157. [CrossRef]

34. Sun, Z.H.I.; Xiao, Y.; Sietsma, J.; Agterhuis, H.; Visser, G.; Yang, Y. Characterisation of metals in the electronic waste of complex mixtures of end-of-life ICT products for development of cleaner recovery technology. *Waste Manag.* **2015**, *35*, 227–235. [CrossRef]
35. Lancaster, S.T.; Sahlin, E.; Oelze, M.; Ostermann, M.; Vogl, J.; Laperche, V.; Touze, S.; Ghestem, J.; Dalencourt, C.; Gendre, R.; et al. Evaluation of X-ray fluorescence for analysing critical elements in three electronic waste matrices: A comprehensive comparison of analytical techniques. *Waste Manag.* **2024**, *190*, 496–505. [CrossRef]
36. Gok, Ö.; Akar Sen, G. Recovery of copper from printed circuit boards (PCBs) using shaking table. *J. Serbian Chem. Soc.* **2023**, *88*, 1039–1053. [CrossRef]
37. Duana, C.; Wen, X.; Shi, C.; Zhao, Y.; Wen, B.; He, Y. Recovery of metals from waste printed circuit boards by a mechanical method using a water medium. *J. Hazard. Mater.* **2009**, *166*, 478–482. [CrossRef]
38. Estrada-Ruiz, R.H.; Flores-Campos, R.; Gámez-Altamirano, H.A.; Velarde-Sánchez, E.J. Separation of the metallic and non-metallic fraction from printed circuit boards employing green technology. *J. Hazard. Mater.* **2016**, *311*, 91–99. [CrossRef]
39. Veit, H.M.; Diehl, T.R.; Salami, A.P.; Rodrigues, J.S.; Bernardes, A.M.; Teno'rio, J.A.S. Utilization of magnetic and electrostatic separation in the recycling of printed circuit boards scrap. *Waste Manag.* **2005**, *25*, 67–74. [CrossRef]
40. Farajzadeh, S.; Chelgani, S.C. Gravity separation by falcon concentrator- an over review. *Sep. Sci. Technol.* **2022**, *57*, 2145–2164. [CrossRef]
41. Guo, C.; Wang, H.; Liang, W.; Fu, J.; Yi, X. Liberation characteristic and physical separation of printed circuit board (PCB). *Waste Manag.* **2011**, *31*, 2161–2166. [CrossRef]
42. Tanısalı, E.; Özer, M.; Burat, F. Precious Metals Recovery from Waste Printed Circuit Boards by Gravity Separation and Leaching. *Miner. Process. Extr. Metall. Rev.* **2020**, *42*, 24–37. [CrossRef]
43. Palav, S.D.; Torres, A.; Biegler, L.T. Systematic conceptual design strategies for the recovery of metals from E-waste. *Front. Chem. Eng.* **2024**, *6*, 1388456. [CrossRef]
44. Lopez-Paneque, A.M.; Gallardo Garcia-Orta, V.H.; Gallardo, J.M.; Sepulveda-Ferrer, R.E.; Chicardi, E. The Influence of Electrostatic Separation Parameters on the Recovery of Metals from Pre-Crushed PCBs. *Metals* **2025**, *15*, 826. [CrossRef]
45. Abbadi, A.; Bokanyi, L. Flotation of comminuted waste printed circuit boards particles—A review. *Miner. Eng.* **2025**, *233*, 109642. [CrossRef]
46. Kumar, A.; Holuszko, M.E.; Janke, T. Assessing the Applicability of Gravity Separation for Recycling of Non-Metal Fraction from Waste Printed Circuit Boards. *Adv. Sustain. Syst.* **2022**, *6*, 2000231. [CrossRef]
47. Das, S.K.; Ellamparuthy, G.; Kundu, T.; Angadi, S.I.; Rath, S.S. A comprehensive review of the mechanical separation of waste printed circuit boards. *Process Saf. Environ. Prot.* **2024**, *187*, 221–239. [CrossRef]
48. Fitzpatrick, R.; Hegarty, P.; Fergusson, K.; Rollinson, G.; Xie, W.; Mildren, T. Optimisation of a Multi-Gravity Separator with Novel Modifications for the Recovery of Ferberite. *Minerals* **2018**, *8*, 191. [CrossRef]
49. Bhaskar, K.U.; Rao1, K.K.; Govindarajan1, B.; Barnwal1, J.P.; Rao, T.C. Studies on multi-gravity separator for rejection of acid insoluble in a copper concentrate. *Eur. J. Miner. Process. Environ. Prot.* **2005**, *5*, 35–47.
50. Mori de Oliveira, C.; Bellopede, R.; Tori, A.; Marini, M.P. Study of Metal Recovery from Printed Circuit Boards by Physical-Mechanical Treatment Processes. *Mater. Proc.* **2021**, *5*, 121. [CrossRef]
51. Burt, R.O. *Gravity Concentration Technology*; Developments in Mineral Processing; Elsevier Science Ltd.: Amsterdam, The Netherlands, 1984; Volume 5.
52. Gupta, A.; Yan, D.S. *Mineral Processing Design and Operations: An Introduction*, 1st ed.; Elsevier Science: Amsterdam, The Netherlands, 2006.
53. Franke, D.M.; Suponik, T.; Nuckowski, P.M.; Dubaj, J. Evaluation of the efficiency of metal recovery from printed circuit boards using gravity processes. *Physicochem. Probl. Miner. Process.* **2021**, *57*, 63–77. [CrossRef]
54. Lee, J.; Kim, Y.; Lee, J. Disassembly and physical separation of electric/electronic components layered in printed circuit boards (PCB). *J. Hazard. Mater.* **2012**, *241–242*, 387–394. [CrossRef]
55. Huang, Y.F.; Chou, S.L.; Lo, S.L. Gold recovery from waste printed circuit boards of mobile phones by using microwave pyrolysis and hydrometallurgical methods. *Sustain. Environ. Res.* **2022**, *32*, 6. [CrossRef]
56. Wang, R.; Zhang, C.; Zhao, Y.; Zhou, Y.; Ma, E.; Bai, J.; Wang, J. Recycling gold from printed circuit boards gold-plated layer of waste mobile phones in "mild aqua regia" system. *J. Clean. Prod.* **2021**, *278*, 123597. [CrossRef]
57. Cardenas-Vera, A.; Hesse, M.; Möckel, R.; Merker, R.G.; Heinig, T.; Phan, Q.V. Investigation of Sensor-Based sorting and selective comminution for pre-concentration of an unusual parisite-rich REE ore, South Namxe, Vietnam. *Miner. Eng.* **2022**, *177*, 107371. [CrossRef]
58. Sandmann, D.; Gutzmer, J. Use of Mineral Liberation Analysis (MLA) in the Characterization of Lithium-Bearing Micas. *J. Miner. Mater. Charact. Eng.* **2013**, *1*, 285–292. [CrossRef]
59. Yao, Y.; Zhou, K.; He, J.; Zhu, L.; Zhao, Y.; Bai, Q. Efficient recovery of valuable metals in the disposal of waste printed circuit boards via reverse flotation. *J. Clean. Prod.* **2021**, *284*, 124805. [CrossRef]

60. Magoda, K.; Nomngongo, P.N.; Mekuto, L. Two-Step Bio-Dissolution of Metals from Printed Circuit Boards Using Acidophilic Iron- and Sulfur-Oxidizing Mesophiles. *Recycling* **2024**, *9*, 6. [CrossRef]
61. Tan, Q.; Liu, L.; Yu, M.; Li, J. An innovative method of recycling metals in printed circuit board (PCB) using solutions from PCB production. *J. Hazard. Mater.* **2020**, *390*, 121892. [CrossRef]
62. Ajiboye, A.E.; Olasehinde, F.E.; Adebayo, O.A.; Ajayi, O.J.; Ghosh, M.K.; Basu, S. Extraction of Copper and Zinc from Waste Printed Circuit Boards. *Recycling* **2019**, *4*, 36. [CrossRef]
63. Ogunniyi, I.O.; Vermaak, M.K.G. Investigation of froth flotation for beneficiation of printed circuit board comminution fines. *Miner. Eng.* **2009**, *22*, 378–385. [CrossRef]
64. Chen, L.; He, J.; Zhu, L.; Yao, Q.; Sun, Y.; Guo, C.; Chen, H.; Yang, B. Efficient recovery of valuable metals from waste printed circuit boards via ultrasound-enhanced flotation. *Process Saf. Environ. Prot.* **2023**, *169*, 869–878. [CrossRef]
65. He, J.; Duan, C. Recovery of metallic concentrations from waste printed circuit boards via reverse floatation. *Waste Manag.* **2017**, *60*, 618–628. [CrossRef] [PubMed]
66. Ogunniyi, I.O.; Vermaak, M.K.G. Froth Flotation for Beneficiation of Printed Circuit Boards Comminution Fines: An Overview. *Miner. Process. Extr. Met. Rev.* **2009**, *30*, 101–121. [CrossRef]
67. Ismail Mohamed, A.T.; Schimperna, G.; Cantoni, G.; Demichelis, F.; Fino, D.; Perucchini, S.; Rubertelli, F.; Laviano, F. Effect of Solvent Pre-Treatment on the Leaching of Copper During Printed Circuit Board Recycling. *Recycling* **2025**, *10*, 80. [CrossRef]
68. Magoda, K.; Mekuto, L. Biohydrometallurgical Recovery of Metals from Waste Electronic Equipment: Current Status and Proposed Process. *Recycling* **2022**, *7*, 67. [CrossRef]
69. Xian, Y.; Tao, Y.; Ma, F.; Zhou, Y. Recovery of Metals from Heat-Treated Printed Circuit Boards via an Enhanced Gravity Concentrator and High-Gradient Magnetic Separator. *Materials* **2021**, *14*, 4566. [CrossRef]
70. Priya, A.; Hait, S. Comprehensive characterization of printed circuit boards of various end-of-life electrical and electronic equipment for beneficiation investigation. *Waste Manag.* **2018**, *75*, 103–123. [CrossRef] [PubMed]
71. Wang, R.; Fan, G.; Zhang, C. Process and systematic study of gold recovery from flexible printed circuit boards (FPCBs) using a choline chloride–ethylene glycol system. *Waste Manag.* **2024**, *178*, 351–361. [CrossRef] [PubMed]
72. Ilkhani, Z.; Aiouache, F. Bioleaching of Gold from Printed Circuit Boards: Potential Sustainability of Thiosulphate. *Recycling* **2025**, *10*, 87. [CrossRef]
73. Martinez-Ballesteros, G.; Valenzuela-García, G.L.; Gómez-Alvarez, A.; Encinas-Romero, M.A.; Mejía-Zamudio, F.A.; Rosas-Durazo, A.D.J.; Valenzuela-Frisby, R. Recovery of Ag, Au, and Pt from Printed Circuit Boards by Pressure Leaching. *Recycling* **2021**, *6*, 67. [CrossRef]
74. Marques, A.C.; Marrero, J.M.C.; Malfatti, C.F. A review of the recycling of non-metallic fractions of printed circuit boards. *SpringerPlus* **2013**, *2*, 521. [CrossRef] [PubMed]
75. Kaya, M. Recovery of metals and nonmetals from electronic waste by physical and chemical recycling processes. *Waste Manag.* **2016**, *57*, 64–90. [CrossRef] [PubMed]
76. Krishnan, S.; Bhagavatula, S.G.K.; Karingamanna, J.; Madhavan, M.K. An Experimental Investigation into the Performance of Concrete and Mortar with Partial Replacement of Fine Aggregate by Printed Circuit Board (PCB) E-Waste. *Recycling* **2025**, *10*, 138. [CrossRef]
77. Flores-Campos, R.; Deaquino-Lara, R.; Rodríguez-Reyes, M.; Martínez-Sánchez, R.; Estrada-Ruiz, R.H. The Use of Nonmetallic Fraction Particles with the Double Purpose of Increasing the Mechanical Properties of Low-Density Polyethylene Composite and Reducing the Pollution Associated with the Recycling of Metals from E-Waste. *Recycling* **2024**, *9*, 56. [CrossRef]
78. Primary Copper Smelting: National Emissions Standards for Hazardous Air Pollutants (NESHAP), EPA Unitaed States Environmental Protection Agency. Available online: https://www.epa.gov/stationary-sources-air-pollution/primary-copper-smelting-national-emissions-standards-hazardous-air#:~:text=Rule%20Summary,-Alert&text=Primary%20copper%20smelting%20is%20the,50%20percent%20from%20these%20sources (accessed on 14 November 2025).

Disclaimer/Publisher's Note: The statements, opinions and data contained in all publications are solely those of the individual author(s) and contributor(s) and not of MDPI and/or the editor(s). MDPI and/or the editor(s) disclaim responsibility for any injury to people or property resulting from any ideas, methods, instructions or products referred to in the content.

minerals

MDPI

Article

Preliminary Study of Geochemical, Mineralogical and Magnetic Susceptibility Properties of Flotation Tailings from the Pb-Zn-Cu-Ag Rudnik Mine, Serbia

Stefan Petrović [1,*], Nenad Nikolić [2], Jovica Stojanović [3], Vesna Cvetkov [1], Vladimir Simić [1], Jovana Malbašić [1], Ljiljana Obrenović [4] and Dragana Životić [1,*]

[1] University of Belgrade, Faculty of Mining and Geology, Đušina 7, 11000 Belgrade, Serbia; vesna.cvetkov@rgf.bg.ac.rs (V.C.); vladimir.simic@rgf.bg.ac.rs (V.S.); jovana.malbasic@rgf.bg.ac.rs (J.M.)
[2] University of Belgrade, Institute for Multidisciplinary Research, Kneza Višeslava 1, 11030 Belgrade, Serbia; nnikolic@imsi.bg.ac.rs
[3] Institute for Technology of Nuclear and Other Mineral Raw Materials, Bulevar Franš d'Eperea 86, 11000 Belgrade, Serbia; j.stojanovic@itnms.ac.rs
[4] Rudnik and Flotation Rudnik doo, Miše Mihajlovića 2, 32313 Rudnik, Serbia; ljobrenovic@contangorudnik.rs
* Correspondence: stefan.petrovic@rgf.bg.ac.rs (S.P.); dragana.zivotic@rgf.bg.ac.rs (D.Ž.)

Abstract: Samples of flotation tailings generated during the exploitation and processing of Zn–Pb–Cu–Ag ore from the Rudnik mine (Serbia) were investigated for their mineralogical, geochemical, and magnetic susceptibility properties. The flotation tailings consist of a complex mineral assemblage, including silicates, carbonates, sulfides, phosphates, sulfates, oxides, hydroxides, and native elements. Quartz, calcite, and orthoclase dominate the coarse fraction (>400 μm), accompanied by epidote, Ca-garnet, and Ca-clinopyroxene. Sulfide minerals are concentrated in finer fractions (<400 μm), with pyrite and arsenopyrite being the most abundant, followed by pyrrhotite, sphalerite, galena, and chalcopyrite. These sulfides occur as dispersed grains within a silicate–carbonate matrix. Post-depositional oxidative alteration is moderately developed, with pyrite replaced by hematite, galena by cerussite, and chalcopyrite by malachite. Geochemical analyses reveal that SiO_2 (avg. 38.98 wt%), Fe_2O_3 (avg. 23.68 wt%), Al_2O_3 (avg. 8.95 wt%), CaO (avg. 9.03 wt%) and MgO (avg. 1.50 wt%) dominate the composition. Economically significant metals include Zn (avg. 0.47 wt%), Pb (avg. 0.20 wt%), Cu (avg. 0.11 wt%), Ag (max. 19 μg/g), and Bi (max. 130 μg/g). Mass magnetic susceptibility shows a strong correlation with S (r = 0.92), Co (r = 0.90), and Bi (r = 0.87); moderate correlation with Fe_2O_3, Al_2O_3, and As; and negative correlation with Mn, TiO_2, Zn, and Pb. The ferromagnetic phase most likely originates from pyrrhotite, as well as hematite formed during pyrite alteration and goethite.

Keywords: flotation tailings; Rudnik mine; mineralogy; geochemistry; magnetic susceptibility

1. Introduction

Mine tailings are increasingly recognized as a potential source of mineral raw materials in response to increasing metal demand and the need for sustainable resource management. Their characterization and the recovery of valuable components have become an important aspect of contemporary resource and environmental policies [1]. Mine tailings often contain significant amounts of metals that could not be recovered with the technologies available at the time of mining, were not economically viable, or were not analyzed—or could not be analyzed—at that time. In Serbia, tailings generated from polymetallic Pb–Zn mines are the second largest source of waste in the metal mining sector, due to an annual ore production

of approximately 500 thousand tonnes [2]. Despite their potential as secondary sources of metals, tailings from polymetallic deposits in Serbia have received limited scientific attention [3,4]. Until recently, only flotation tailings from the Grot mine had been the subject of preliminary investigation [5]. More recent studies have examined flotation tailings from the Rudnik mine, including mineralogical and environmental assessments [6] and the flotation behavior of minerals [7–9].

The Rudnik mine, situated in central Serbia, is one of the most prominent and long-standing polymetallic mining sites. It hosts economically significant concentrations of Pb, Zn, Cu, and Ag, and has been continuously exploited since 1953, with a total of more than 14 million tonnes of ore extracted to date [10]. The mine exploits a distal skarn deposit formed during Oligocene to Early Miocene magmatic-hydrothermal activity, consistent with other deposits associated with volcano-intrusive complexes in the Balkan Peninsula [11–13]. Sulfide ore is predominantly hosted within epidote-bearing skarn and occurs as massive bodies, stockwork veinlets, and disseminated mineralization. The main sulfide minerals include sphalerite, galena, and chalcopyrite, with pyrrhotite, arsenopyrite, and pyrite as common gangue phases. Metal concentrations in ore vary considerably, ranging from 0.94 to 5.66 wt% Pb, 0.49 to 4.49 wt% Zn, 0.08 to 2.18 wt% Cu, and 50 to 297 μg/g Ag [14].

Decades of mining and flotation processing of polymetallic ore have resulted in a tailings storage facility covering ~30 ha, with over 11 million tonnes (7 million m^3) of material deposited to date (Figure 1a,b). These flotation tailings, representing the residual fraction after the beneficiation of PbS, ZnS, and $CuFeS_2$ concentrates, has evolved from initially supporting only Pb and Zn recovery to including Cu concentrates since 1988. Their mineralogical composition and heterogeneity position them simultaneously as a potential secondary resource and as a factor influencing long-term environmental impact. Consequently, the tailings storage facility represents both a challenge and an opportunity—requiring proper management to mitigate ecological risks while offering scope for revalorization through modern processing technologies. In this context, characterization becomes essential for advancing sustainable resource management and circular economy strategies.

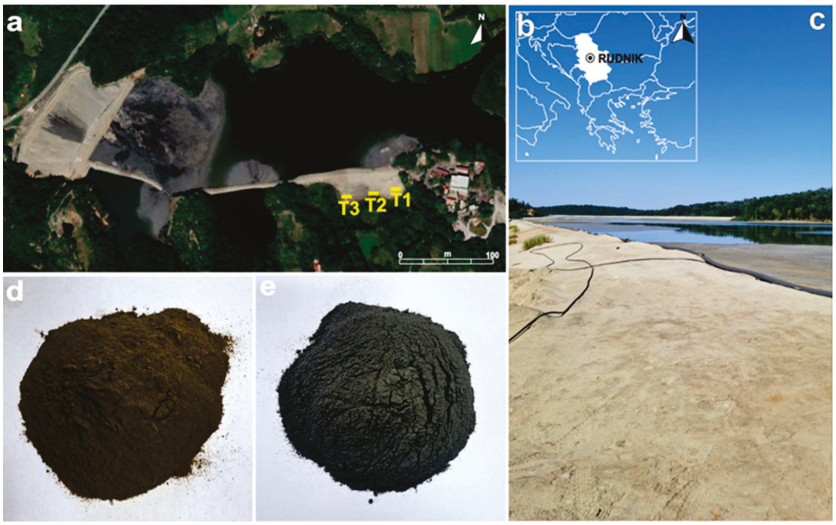


Figure 1. (**a**) Satellite image of the Rudnik mine flotation tailings showing the positions of sampled trenches (T1, T2, T3), source: Google Maps [15]. (**b**) Location of the Rudnik flotation tailings in the Republic of Serbia, SE Europe. (**c**) Field photograph of the mine flotation tailings site. (**d**) Sample brown-colored flotation tailings. (**e**) Sample grey-colored flotation tailings.

The present study provides the first comprehensive dataset on the mineralogical, geochemical, and magnetic susceptibility properties of flotation tailings samples from the Rudnik mine, thereby strengthening the knowledge base required for sustainable management and the potential valorization of tailings as secondary raw material sources in the future.

2. Materials and Methods

2.1. Sampling

Samples were obtained from three vertical trenches excavated within the tailings body, which occupies the bed of a former dry creek (Figure 1a). In total, 16 samples were collected (Table 1). Trench T1 was sampled at 0.5 m intervals, whereas trenches T2 and T3 were sampled at 1 m intervals to evaluate vertical heterogeneity within the flotation tailings. Mineralogical and geochemical analyses, as well as magnetic susceptibility, were carried out for each depth interval. This approach enables the assessment of vertical variations in composition.

Table 1. Details of flotation tailings samples, including trench, sample designation, depth, and material description.

Trench	Samples ID	Depth (m)	Material Description
T1	T1.1	0.0–0.5	Grey material
	T1.2	0.5–1.0	
	T1.3	1.0–1.5	
	T1.4	1.5–2.0	
	T1.5	2.0–2.5	Brown material
	T1.6	2.5–3.0	
	T1.7	3.0–3.5	Grey material, interbedded with Brown
	T1.8	3.5–4.0	
T2	T2.9	0.0–1.0	Grey material
	T2.10	1.0–2.0	
	T2.11	2.0–3.0	Brown material
	T2.12	3.0–4.0	Grey material
T3	T3.13	0.0–1.0	Grey material
	T3.14	1.0–2.0	
	T3.15	2.0–3.0	Brown material
	T3.16	3.0–4.0	Grey material

2.2. Granulometrical Analysis

Granulometric analysis was performed on two composite samples. The first composite (TC1) was prepared from 50 g of individual samples consisting of brown material and mixture of grey and brown material (samples T1.5, T1.6, T1.7, T7.8, T2.11, T3.15), while the second composite (TC2) was prepared from the same weight of grey material (samples T1.1, T1.2, T1.3, T1.4, T2.9, T2.10, T2.12, T3.13, T3.14, T3.16). Both composite samples were homogenized and analyzed.

The grain-size distribution of the two composite samples was determined by dry sieving in the laboratory. The homogenized material was separated into nine fractions: F1 = 0–0.045 mm, F2 = 0.045–0.063 mm, F3 = 0.063–0.09 mm, F4 = 0.09–0.125 mm, F5 = 0.125–0.25 mm, F6 = 0.25–0.5 mm, F7 = 0.5–0.71 mm, F8 = 0.71–1 mm, and F9 = 1–2 mm.

2.3. X-Ray Diffraction (XRD)

X-ray diffraction analyses were performed on a "PHILIPS" X-ray diffractometer, model PW-1710 (Malvern Panalytical, Malvern, UK), with a curved graphite monochromator and a scintillation counter. The intensities of diffracted CuKα X-rays (λ = 1.54178 Å) were measured at room temperature in intervals of 0.02°2θ and a time of 1 s in the range from 4 to 65°2θ. The X-ray tube was operated at a voltage of 40 kV and a current of 30 mA, while the slits for directing the primary and diffracted beams were set to 1 mm and 0.1 mm, respectively.

2.4. Optical and Scanning Electron Microscopy with Energy Dispersive Spectroscopy (SEM-EDS)

Optical analyses were performed at the University of Belgrade, Faculty of Mining and Geology, using a Zeiss Axio Imager 2 reflected light microscope, and at the Institute for Technology of Nuclear and Other Mineral Raw Materials (ITNMS), using a Carl Zeiss-Jena JENAPOL-U polarizing microscope for both reflected and transmitted light. Samples were subsequently examined with a scanning electron microscope (SEM, JSM-6610LV, JEOL Inc., Tokyo, Japan) operated at 20 kV. Mineral identification was supported by energy-dispersive X-ray spectrometry (EDS, Xplore 30, Oxford Instruments, Abingdon, UK), with a detection limit of approximately 0.1 wt% based on internal standards. Backscattered electron (BSE) micrographs were used to evaluate mineral homogeneity and identify potential zoning features.

2.5. X-Ray Fluorescence (XRF)

The chemical composition analyses of the selected samples were performed using the SPECTRO Xepos C energy dispersive X-ray fluorescence (ED-XRF) spectrometer, with an air-cooled X-ray tube with a thick Pd/Co binary alloy anode operating at 50 kV voltage and at tube power of 50 W. The analyses were conducted on 5 grams of unfused, fine-grained powder samples.

2.6. Fourier-Transform Infrared Spectroscopy (FTIR)

The FTIR spectra of the fine-grained powder materials were recorded using a Perkin Elmer Spectrum Two equipped with the Universal ATR accessory. The spectrum of each powder sample was recorded in the mid-infrared range 1600–400 cm^{-1} with 20 scans and a spectral resolution of 4 cm^{-1}.

2.7. Inductively Coupled Plasma Optical Emission Spectrometry (ICP-OES)

Selected elements (Ca, Mg, Cu, Pb, Zn, Co, Ni, Mn, Cr, Ba, As, Bi, and Ag) were analyzed with a PERKIN-ELMER AVIO 200 ICP-OES, which uses a vertical plasma engineered to handle even the most difficult, high-matrix samples without dilution. A full-wavelength field detector simultaneously measured spectral ranges around the lines of interest. Sample digestion and preparation were carried out using an acid mixture (HNO_3:HCl = 3:1). The detection limit of the AVIO 200 ICP-OES is in the μg/L (ppb) range, typically 0.1–100 μg/L depending on the element. The procedure for preparation of a calibration curve included 5 values depending on the range of concentration that is expected. Standard reference material OREAS 135 [16] was used for quality control.

2.8. Laboratory Measurement of Magnetic Susceptibility (MS)

Magnetic susceptibility was measured at room temperature (~20 °C) under a low magnetic field of 400 A/m using an MFK-1A Kappabridge (AGICO Instruments, Brno, Czech Republic) with a sensitivity of 2×10^{-8} SI. Volume magnetic susceptibility was determined on dry samples of fixed volume (20 cm^3). Sample mass was measured with a Radwag AS 220 R2 Plus analytical balance, accurate to four decimal places, to calculate

mass magnetic susceptibility. Each sample was measured five times, and the mean value was used for further analysis. Before measurements, the magnetic susceptibility of the plastic bag and instrument holder was determined and used to correct the final values.

3. Results

3.1. Grain Size Distribution

Grain size analysis of composite samples TC1 and TC2 revealed that both samples have a similar distribution, with slightly over 90% of the material being finer than 0.5 mm (Table 2 and Figure 2). The main difference is that the brownish colored material contains approximately twice the amount of the <0.063 mm fraction.

Table 2. Grain size distribution of composite flotation tailings samples.

Sieve, mm	TC1, %	TC2, %
F9: 1.0–2.0	100.0	100.0
F8: 0.710–1.0	97.6	96.2
F7: 0.500–0.710	97.0	94.5
F6: 0.250–0.500	92.7	91.1
F5: 0.125–0.250	76.4	76.3
F4: 0.090–0.125	53.8	54.3
F3: 0.063–0.090	32.0	31.6
F2: 0.045–0.063	17.3	8.1
F1: <0.045	10.6	5.1

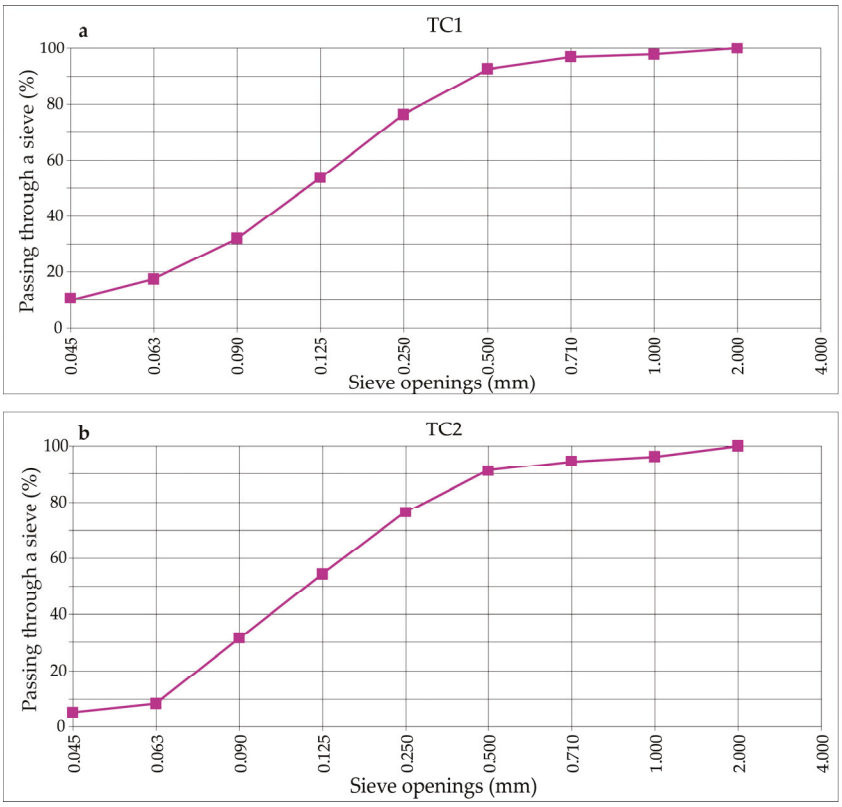


Figure 2. Diagram of grain size distribution of composite flotation tailings samples TC1 (**a**) and TC2 (**b**) from the Rudnik mine.

3.2. Mineralogy

3.2.1. X-Ray Diffraction (XRD)

X-ray diffraction (XRD) analysis of flotation tailings samples reveals a consistent and complex mineral assemblage predominantly composed of silicate, carbonate, sulfate, and sulfide minerals (Figure 3, Table 3). Quartz and calcite are the most abundant phases across all samples. Sulfide minerals, including pyrite, sphalerite, chalcopyrite, galena, pyrrhotite, and arsenopyrite, are also present. Accessory minerals such as chlorite, dolomite, and gypsum were also identified, and minor diffraction peaks indicate the presence of additional gangue minerals, including kaolinite or related clays, plagioclase, orthoclase, muscovite, anatase, and goethite.

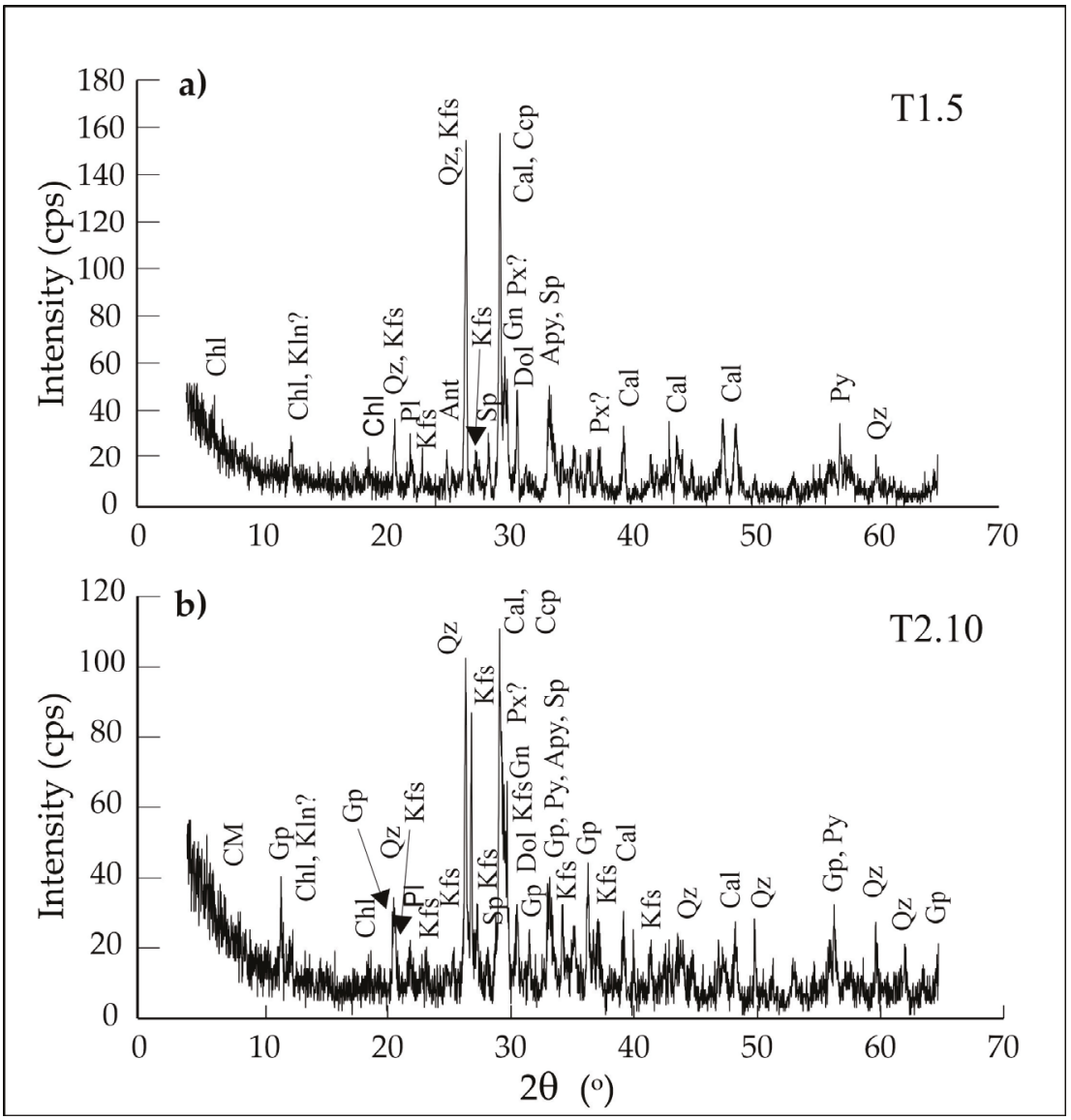


Figure 3. Representative XRD diffractograms of flotation tailings samples from the Rudnik mine: (**a**) sample T1.5, (**b**) sample T2.10. Abbreviations [17]: Apy—arsenopyrite, Ccp—chalcopyrite, Gn—galena, Py—pyrite, Qz—quartz, Sp—sphalerite, Kfs—K-feldspar, Ant—anatase, Gp—gypsum, Chl—chlorite, Kln—kaolinite, Pl—plagioclase, Cal—calcite, CM—clay mineral, Px—pyroxene. ?—possible presence, but not confirmed.

Table 3. Mineral identification based on optical microscopy, SEM-EDS, and XRD analyses. Abundance categories are defined as follows: Major—minerals present as dominant phases in the samples (>25%); Moderate—minerals regularly observed in moderate quantities (5%–25%); Minor—minerals present in low quantities (1%–5%); Trace—minerals observed only sporadically or in specific samples (<1%).

Group	Mineral	Confirmation Method	Relative Abundance in the Samples															
			T1.1	T1.2	T1.3	T1.4	T1.5	T1.6	T1.7	T1.8	T2.9	T2.10	T2.11	T2.12	T3.13	T3.14	T3.15	T3.16
Silicates, phosphates, carbonates, sulfates	Quartz	XRD, Optical, SEM-EDS, FTIR	major	major	moderate	moderate	moderate	major	major	major	major	major	moderate	major	major	major	major	major
	Calcite	XRD, Optical, SEM-EDS, FTIR	moderate	major	major	major	major	major	major	major	major	major	major	major	major	major	major	major
	Epidote	SEM-EDS				trace	trace	trace			trace	trace	trace			trace	trace	trace
	Ca-garnet	SEM-EDS		trace	moderate	moderate	trace				moderate	moderate	moderate	trace			trace	trace
	Orthoclase (K-feldspar)	XRD, SEM-EDS, FTIR	major	major	moderate	moderate	major	major	major	major	major	major	major	major	major	major	major	major
	Ca-clinopyroxene	SEM-EDS	moderate	moderate	moderate	moderate	moderate	moderate	moderate	moderate	moderate	moderate	moderate	moderate	moderate	moderate	moderate	moderate
	Apatite	SEM-EDS				trace	trace				trace	trace	trace					
	Zircon	SEM-EDS										trace						
	Gypsum	XRD		trace	trace													
	Chlorite	XRD	trace		trace	trace	trace	trace	trace	trace	trace			trace	trace	trace	trace	trace
	Plagioclase	XRD										trace	trace	trace				
Sulfides and native, elements	Pyrite	XRD, Optical, SEM-EDS	major	major	major	major	major	major	major	major	major	major	major	major	major	major	major	major
	Arsenopyrite	XRD, Optical, SEM-EDS	major	trace	trace	major	major	major	major	major	major	major	major	major	major	major	major	major
	Pyrrhotite	XRD, Optical, SEM-EDS	major	trace	trace	trace	major	major	major	major	major	trace	trace	trace	major	major	trace	trace
	Sphalerite	XRD, Optical, SEM-EDS	trace	moderate	moderate	moderate	major	major	trace	major	trace	trace	moderate	trace	trace	trace	moderate	trace
	Chalcopyrite	XRD, Optical, SEM-EDS	trace	trace	trace	trace	major	trace	trace	trace	trace	trace	trace	trace	major	major	trace	trace
	Galena	XRD, Optical, SEM-EDS	trace	trace	moderate	moderate	major	trace	trace	moderate	trace	trace	moderate	moderate	major	trace	moderate	trace
	Native bismuth	Optical, SEM-EDS			trace		trace	trace										
	Native silver	Optical, SEM-EDS			trace	trace				trace				trace				
	Native copper	Optical, SEM-EDS											trace	trace				
	Pentlandite	Optical, SEM-EDS				trace	trace	trace							trace			
	Hematite	Optical, SEM-EDS	major	major	major	trace	trace	trace	trace	trace	major	major	major	trace	major	major	trace	trace
	Bismite	Optical, SEM-EDS			trace		trace	trace							trace			
	Cerussite	SEM-EDS									trace	trace						
	Malachite	SEM-EDS									trace	trace						
	Anatase	XRD				trace	trace	trace										
	Goethite	XRD, SEM-EDS													trace			

major moderate minor trace

3.2.2. FTIR Analysis

The Fourier transform infrared spectroscopy (FTIR) was used for profiling the mine tailings samples' components. The component identification based on characteristic band vibrations in the fingerprint region of 1600–400 cm^{-1} is shown in Figure 4. In the fingerprint region, the most intensive broad complex band in the 1100–950 cm^{-1} range is assigned to the in-plane Si–O–Si stretching vibration in silicates. The bands at ca 1163, 1086 (shoulder), doublet 799 and 778, are assigned to stretching and banding vibrations in quartz. The strong and wide band at 1440–1420 cm^{-1} is assigned to carbonates. Specifically, bands 876 and 712 cm^{-1} are assigned to calcite. The intensities of quartz and carbonate bands suggest that those minerals are the most abundant, which is consistent with optical and XRD investigations. In addition, the bands belonging to feldspar and sulfates are also observed, the latter consistent with the gypsum identified by XRD.

3.2.3. Optical and Scanning Electron Microscopy with Energy Dispersive Spectroscopy (SEM-EDS)

Optical and SEM-EDS analyses support the XRD results and provide additional insight into the textural and spatial relationships among the identified minerals (Table S1 in Supplementary Materials). The tailings comprise a heterogeneous mixture of sulfides, native elements, and secondary oxidation products, embedded within a matrix dominated by silicates and carbonates (Figure 5a). According to optical examination, most grains range in size from 100 to 300 μm. Sulfides and their alteration products often appear as finer particles (<100 μm), with occasional larger grains, whereas silicates and carbonates typically form coarser particles (>400 μm).

Quartz is the most abundant, occurring as large, homogeneous and euhedral grains. It is commonly associated with sulfide minerals, particularly pyrite and sphalerite, where it occurs in interstitial spaces relative to the sulfides (Figure 5a,b).

Calcite, epidote, garnet, and orthoclase are also common, most frequently occurring as dispersed grains of various sizes (Figure 5a,b). Ca-pyroxenes, represented by diopside-hedenbergite, occur as subhedral to euhedral grains, although they are present only in minor quantities. Apatite and zircon appear as small, very rare, and dispersed grains.

Pyrite and arsenopyrite represent the most abundant sulfide minerals within the tailings, predominantly occurring as isolated grains and, to a lesser extent, as intergrowths with silicate phases (Figure 5c). Pyrite grains display considerable size variability, commonly reaching coarse dimensions of up to 400 μm. These grains are homogeneous, with rare inclusions of chalcopyrite and galena, which appear as droplet-shaped inclusions up to 40 μm in length. Partial to complete oxidation of pyrite is frequent, with hematite frequently present as a secondary alteration mineral (Figure 5a,b). Arsenopyrite occurs as isolated, homogeneous, and unaltered grains of sizes comparable to pyrite (Figure 5c).

Pyrrhotite is less abundant relative to pyrite and arsenopyrite and often associated with galena, sphalerite, and chalcopyrite (Figure 5d). It occasionally contains flame- or vein-like pentlandite exsolutions less than 5 μm in length.

Among economically significant sulfides, sphalerite is the most prevalent. It occurs as individual grains that host chalcopyrite inclusions ranging from 10 to 40 μm and, less frequently, as co-occurrence with other minerals, especially sulfides such as galena and chalcopyrite (Figure 5e). Sphalerite grains range from below 50 μm to 500 μm in size.

Galena is commonly observed in complex intergrowths with sphalerite, chalcopyrite, and various silicate, oxide, and carbonate minerals, while isolated grains are subordinate. Its grain size ranges from 50 to 250 μm. Sometimes, galena is associated with native bismuth, native silver, and bismite (Figure 5f,g). Secondary alteration along some grain boundaries is evidenced by the occurrence of cerussite (Figure 5h).

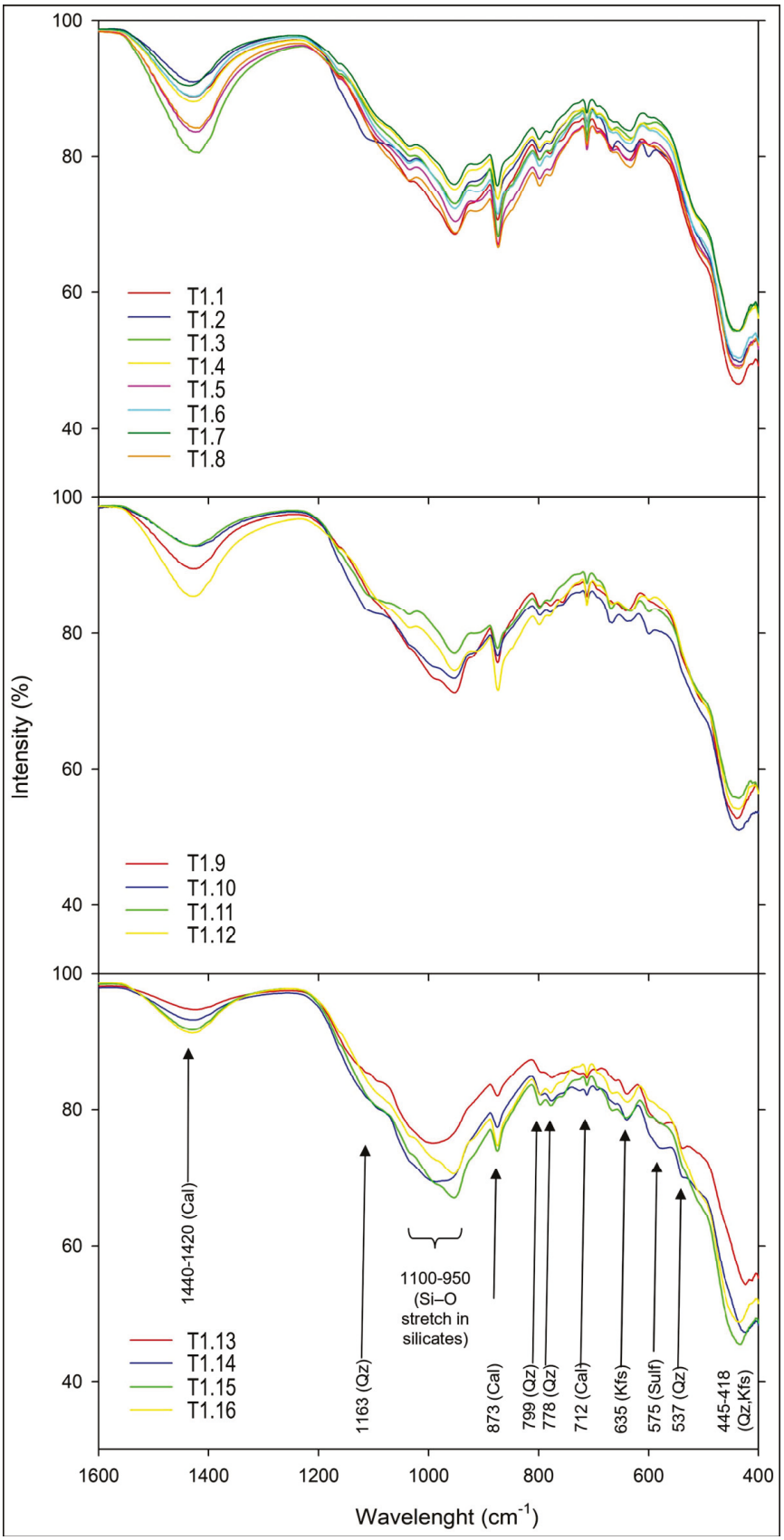


Figure 4. FTIR spectra in the fingerprint region (1600–400 cm^{-1}) of flotation tailing from the Rudnik mine. Abbreviations [17]: Cal—calcite, Kfs—K-feldspar, Qz—quartz, Sulf—sulfates.

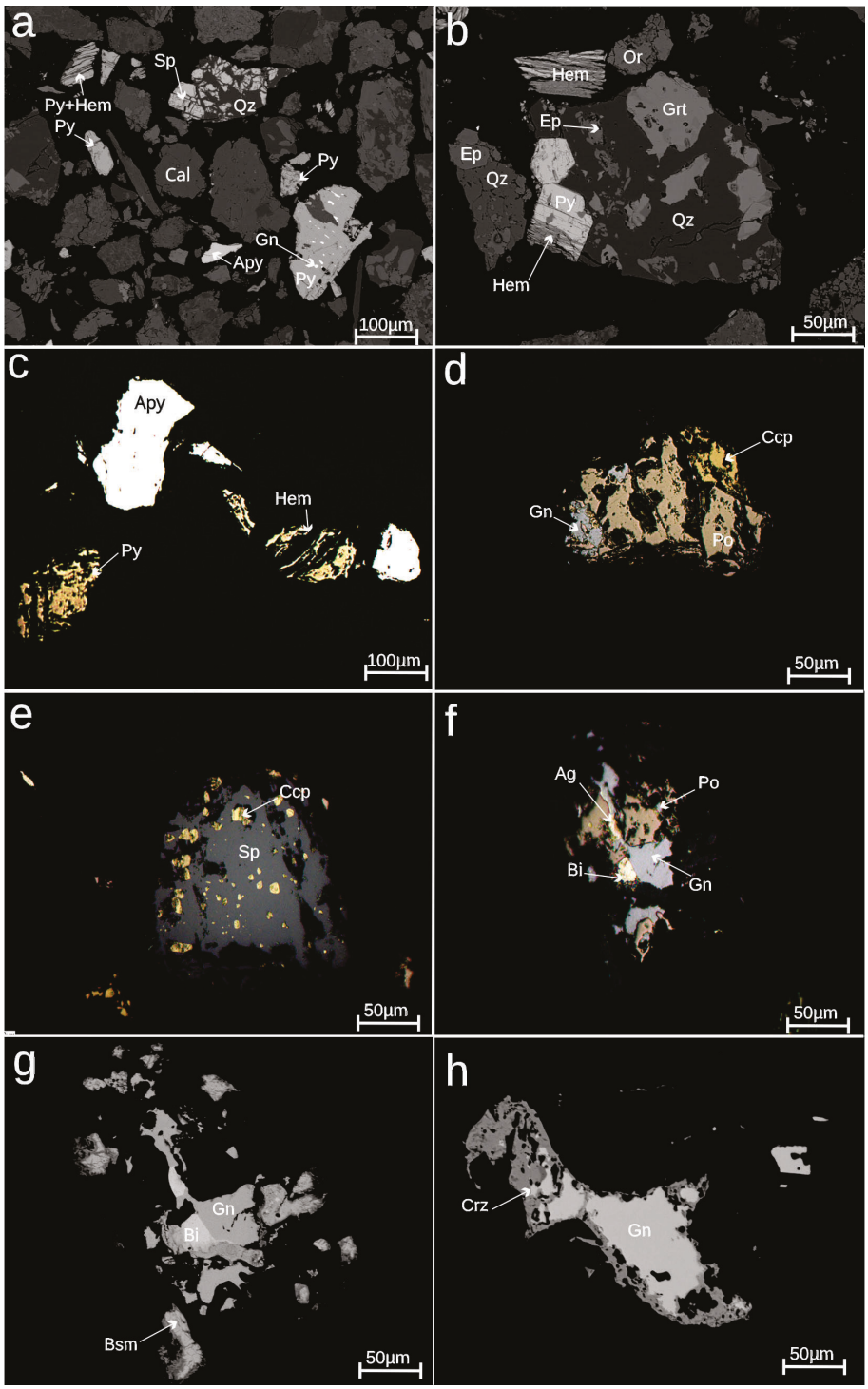


Figure 5. Photomicrographs ((**a**–**d**): reflected light; (**e**–**h**): backscattered electron images) of tailings from the Rudnik mine. (**a**) Quartz and calcite grains associated with sulfides in the flotation tailings; (**b**) quartz grain associated with garnet, pyrite, epidote, and hematite; (**c**) pyrite and arsenopyrite grains; (**d**) Co-occurrence of pyrrhotite, chalcopyrite, and galena; (**e**) sphalerite grain with chalcopyrite inclusions; (**f**) pyrrhotite with galena hosting inclusions of native silver and native bismuth; (**g**) galena grain associated with native bismuth and bismite; (**h**) galena grain partly altered to cerussite along the rim. Abbreviations [17]: Ag—native silver; Apy—arsenopyrite; Bi—native bismuth; Bsm—bismite; Ccp—chalcopyrite; Crz—cerussite; Ep—epidote; Gn—galena; Grt—garnet; Hem—hematite; Or—orthoclase; Po—pyrrhotite; Py—pyrite; Qz—quartz; Sp—sphalerite.

Chalcopyrite forms fine impregnations within sphalerite or as small inclusions and co-occurrence with pyrrhotite and sphalerite (Figure 5d,e). Grain sizes range from submicron

to 100 μm. The chalcopyrite is rarely altered, although minor malachite coatings have been present on some grain surfaces.

3.3. Geochemistry

The most abundant oxide in all samples is SiO_2 (33.81–44.30 wt%; Table 4; Figure 6), followed by Fe_2O_3 (19.02–28.74 wt%), Al_2O_3 (7.69–10.57 wt%), CaO (4.49–12.88 wt%) and MgO (1.24–1.91 wt%). Sulfur (S) contents vary widely (2.20–12.30 wt%). Among the metals, Zn shows the highest enrichment (0.21–0.79 wt%), followed by Pb (0.14–0.32 wt%) and Cu (0.05–0.17 wt%). Manganese (Mn) is present in moderate amounts (0.104–0.189 wt%), whereas Cr is consistently low ($\leq$0.036 wt%). Arsenic (As) displays a broad range (0.012–0.732 wt%). Nickel (Ni) (0.011–0.023 wt%) and Co (0.003–0.007 wt%) contents remain consistently low. Bismuth (Bi) is present in trace but potentially significant amounts (0.002–0.013 wt%), while Ag content is lower (6 to 19 μg/g).

Pearson correlation analysis is performed to assess the relationships among oxides, elements, and magnetic susceptibility (MS) (Figure 7).

Strong positive correlations ($r \geq 0.7$) are between SiO_2 and Al_2O_3 (r = 0.87). Al_2O_3 is also positively correlated with Ni (r = 0.71), while Fe_2O_3 shows strong positive correlations with Cu (r = 0.82), Bi (r = 0.87), and Co (r = 0.79). Sulfur (S) is strongly correlated with Co (r = 0.97) and Bi (r = 0.91), while with Cu and Ag (r = 0.81), as well as Zn and Mn (r = 0.79), also show strong positive correlations. Ni is strongly correlated with As (r = 0.89), and Bi with Co (r = 0.97). Ag is positively correlated with Cr (r = 0.77) and Zn (r = 0.71).

Moderate positive correlations ($0.4 \leq r < 0.7$) are between SiO_2 and Ni (r = 0.61) and As (r = 0.55), Al_2O_3 and S (r = 0.50) and As (r = 0.63), Fe_2O_3 and S (r = 0.71) and Cr (r = 0.55), S and Cu (r = 0.53) and Cr (r = 0.45), Cu and Pb (r = 0.61) and Co (r = 0.62), Ni and SiO_2 (r = 0.61) and Al_2O_3 (r = 0.71), Co and Cr (r = 0.49), Cr and Cu (r = 0.64) and Fe_2O_3 (r = 0.55), Ag and Pb (r = 0.54) and Mn (r = 0.43).

Table 4. Major oxide, sulfur, and metal contents, and mass magnetic susceptibility (MS) in flotation tailings samples from the Rudnik mine (oxides and sulfur contents determined by XRF; metals contents by ICP-OES).

	T1.1	**T1.2**	**T1.3**	**T1.4**	**T1.5**	**T1.6**	**T1.7**	**T1.8**	**T2.9**	**T2.10**	**T2.11**	**T2.12**	**T3.13**	**T3.14**	**T3.15**	**T3.16**	**AV**	**SD**
SiO_2 (%)	44.30	35.74	35.10	35.10	34.45	40.23	43.01	37.24	43.87	38.31	33.81	37.66	41.73	41.30	43.23	38.73	38.99	3.60
TiO_2 (%)	0.55	0.50	0.45	0.48	0.52	0.53	0.48	0.52	0.47	0.52	0.53	0.47	0.37	0.45	0.63	0.52	0.50	0.06
Al_2O_3 (%)	9.98	8.30	7.69	7.96	7.82	8.71	9.05	8.13	9.43	8.66	7.84	8.22	10.17	10.24	10.57	9.26	8.88	0.96
Fe_2O_3 (%)	21.31	23.02	22.59	25.17	25.88	21.31	23.31	23.31	19.02	22.88	25.45	23.45	28.74	27.31	21.02	20.59	23.40	2.58
CaO (%)	9.49	10.30	12.54	9.63	10.71	9.30	9.48	9.53	7.91	9.27	8.65	12.88	4.49	5.11	7.56	7.62	9.03	2.23
MgO (%)	1.68	1.46	1.36	1.34	1.46	1.43	1.43	1.41	1.69	1.83	1.33	1.33	1.24	1.46	1.91	1.71	1.50	0.20
S (%)	2.20	2.24	3.28	5.05	4.54	2.94	3.99	4.25	4.22	3.11	2.66	2.93	12.30	10.90	4.16	3.49	4.52	2.90
Cu (%)	0.059	0.100	0.153	0.137	0.161	0.085	0.070	0.144	0.047	0.069	0.127	0.103	0.171	0.139	0.075	0.049	0.106	0.042
Pb (%)	0.15	0.21	0.23	0.26	0.25	0.14	0.15	0.28	0.14	0.16	0.32	0.25	0.20	0.15	0.21	0.17	0.20	0.06
Zn (%)	0.24	0.70	0.79	0.76	0.72	0.40	0.32	0.68	0.25	0.27	0.70	0.70	0.27	0.22	0.24	0.21	0.47	0.24
Co (%)	0.003	0.003	0.003	0.004	0.004	0.003	0.003	0.004	0.003	0.003	0.003	0.003	0.007	0.007	0.003	0.003	0.004	0.001
Ni (%)	0.016	0.011	0.013	0.014	0.014	0.012	0.012	0.013	0.023	0.015	0.012	0.011	0.018	0.019	0.018	0.017	0.015	0.003
Mn (%)	0.164	0.161	0.189	0.180	0.177	0.150	0.164	0.164	0.123	0.145	0.156	0.188	0.105	0.104	0.119	0.132	0.151	0.028
Cr (%)	0.018	0.016	0.021	0.036	0.036	0.021	0.022	0.025	0.019	0.017	0.015	0.016	0.027	0.025	0.017	0.016	0.022	0.007
Ba (%)	0.003	0.002	0.002	0.001	0.002	0.001	0.001	0.001	0.001	0.001	0.001	0.001	0.002	0.002	0.001	0.001	0.001	0.001
As (%)	0.132	0.034	0.039	0.040	0.035	0.012	0.014	0.016	0.732	0.266	0.065	0.032	0.541	0.550	0.195	0.163	0.179	0.228
Bi (%)	0.004	0.004	0.004	0.006	0.007	0.003	0.004	0.005	0.002	0.003	0.003	0.004	0.013	0.012	0.002	0.002	0.005	0.003
Ag (μg/g)	8	11	16	19	16	11	12	15	11	8	12	13	14	13	8	6	12	3
MS [10^{-6} m^3kg^{-1}]	1.465	1.997	1.528	2.230	2.766	2.034	2.428	1.673	2.363	0.687	1.217	1.502	4.643	4.724	1.965	1.991	2.201	1.093

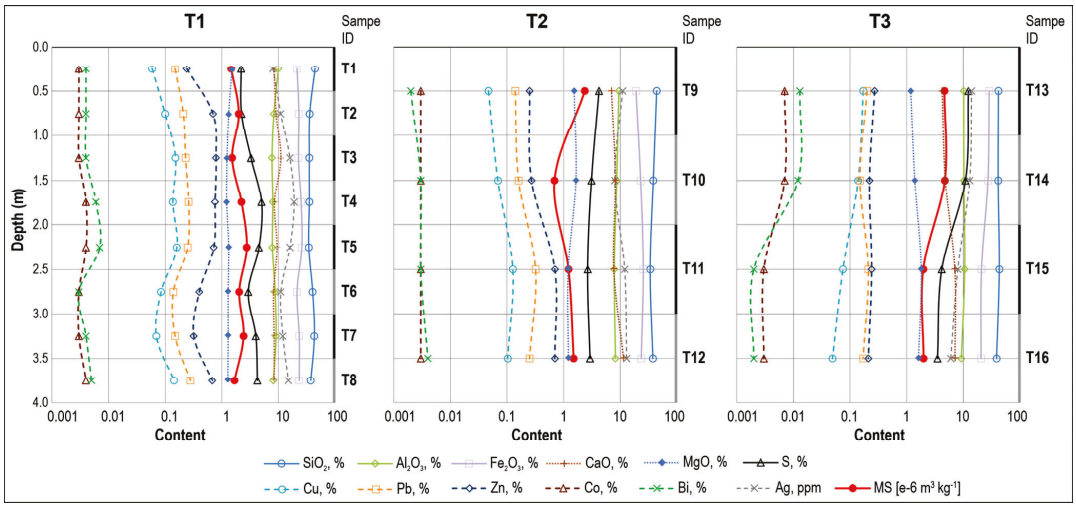


Figure 6. Distribution of major oxides, selected elements, and magnetic susceptibility (MS) in flotation tailings samples from the Rudnik mine.

Strong negative correlations ($r \leq -0.7$) are between SiO_2 and Zn ($r = -0.86$) and Pb ($r = -0.76$), Al_2O_3 and Zn ($r = -0.88$), Mn and Al_2O_3 ($r = -0.82$) and Ni ($r = -0.76$), and Zn and Ni ($r = -0.69$).

Moderate negative correlations ($-0.7 < r \leq -0.4$) are between TiO_2 and Fe_2O_3 ($r = -0.55$), S ($r = -0.63$), Co ($r = -0.61$), and Cu ($r = -0.46$), S and Mn ($r = -0.64$), Cu and Al_2O_3 ($r = -0.33$), as well as Ag and SiO_2 ($r = -0.51$), TiO_2 ($r = -0.50$), and Al_2O_3 ($r = -0.530$).

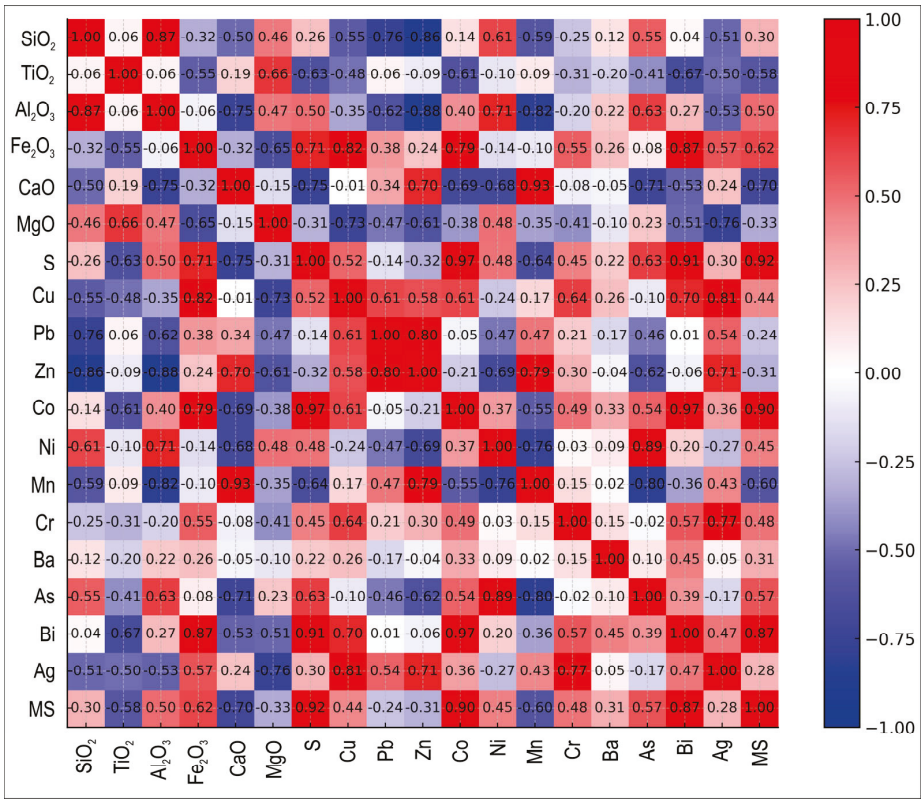


Figure 7. Correlation matrix of oxides, elements and magnetic susceptibility (MS) of flotation tailings samples from the Rudnik mine. The color bar on the right represents the values of the correlation coefficient (r) between pairs of variables (in this case, chemical elements, oxides and magnetic susceptibility).

3.4. Magnetic Susceptibility

Mass magnetic susceptibility (MS) values of the flotation tailings show considerable variability, ranging from 0.687×10^{-6} $m^3 \cdot kg^{-1}$ to 4.724×10^{-6} $m^3 \cdot kg^{-1}$, with an average of 2.201×10^{-6} $m^3 \cdot kg^{-1}$ (Table 4). The highest MS values were recorded in samples T3.13 and T3.14, whereas the lowest were observed in T2.10 and T2.11. This variability reflects differences in geochemical and mineralogical composition, particularly the abundance of iron-rich ferromagnetic minerals (in general), which show an affinity toward specific metals (Figure 6).

Correlation analysis was performed using MS and bulk geochemical data for all analyzed tailings samples (Figure 7). Strong positive correlations were identified between MS and S (r = 0.92), Co (r = 0.90), Bi (r = 0.87), and Ag (r = 0.87). Moderate positive correlations with MS were observed for Fe_2O_3 (r = 0.62), As (r = 0.57), Cr (r = 0.48), Al_2O_3 (r = 0.50), Cu (r = 0.45), and Ni (r = 0.45). Moderate negative correlations were recorded for Mn (r = -0.60) and TiO_2 (r = -0.58), while Zn exhibited only a weak negative correlation with MS (r = -0.31). These trends are consistent with sample-level observations; for instance, T3.13 and T3.14, which show the highest MS values, also display elevated concentrations of S and Co, reflecting the strong positive correlations identified. No elements show strong negative correlations with MS ($r \leq -0.7$).

4. Discussion

The polymetallic ore from the Rudnik mine is characterized by complex co-occurrence of gangue and ore minerals, which can adversely influence ore processing efficiency [18,19]. In the analyzed flotation tailings samples, no significant variations in the distribution of mineral phases were observed. The major minerals—calcite, quartz, and K-feldspar—were consistently present, accompanied by epidote, Ca-garnet, and Ca-pyroxene, which reflects the skarn-type mineralogy of the primary ore [13,20]. These minerals were commonly associated with sulfides, which were either embedded within or dispersed throughout a predominantly silicate–carbonate matrix. Among the sulfides, pyrite, arsenopyrite, and pyrrhotite are dominant, followed by sphalerite, galena, and chalcopyrite.

Post-depositional oxidative alteration is most pronounced near the surface, where atmospheric exposure promotes the oxidation of sulfides. Similar alteration features are also observed at several depths within the tailings, mainly in material that was previously exposed at the surface and later buried by younger tailing material. Pyrite is particularly susceptible, frequently replaced by hematite along grain boundaries or via pseudomorphosis, illustrating natural weathering processes [21]. Galena and chalcopyrite are likewise transformed, forming cerussite and malachite, respectively, whereas other sulfides remain relatively unaltered, resulting in heterogeneous oxidation patterns throughout the tailings. Compared with nearby sites, oxidation in the Rudnik flotation tailings appears relatively limited [22].

The geochemical data corroborate these mineralogical and petrographic observations. Elevated SiO_2 and Al_2O_3 contents confirm the prevalence of silicate and aluminosilicate minerals (Table 2), while increased Fe_2O_3 and S concentrations in the upper part of T3 indicate a significant abundance of iron sulfides such as pyrite and pyrrhotite. Sulfur concentrations vary considerably (2.20–12.30 wt%), reflecting vertical heterogeneity in sulfide distribution (Table 4; Figure 6). Base metal contents—Zn (up to 0.79 wt%), Pb (up to 0.32 wt%), and Cu (up to 0.17 wt%)—provide further evidence of inefficiencies in historical ore processing. Although present at low concentrations, trace elements such as Ag and Bi may still hold economic significance for potential future recovery.

The sulfur content along the vertical profile of the trenches T2 and T3 indicates a decrease with depth, reflecting the progressive decomposition of sulfide minerals over time

(i.e., with depth) and the migration of liberated sulfur as sulfate via pore waters within the tailings body.

Correlation analysis provides further insights into the geochemical controls of the tailings. The strong positive correlation between SiO_2 and Al_2O_3 (r = 0.87) is typical of aluminosilicate minerals (feldspars), which, together with quartz, dominate the gangue matrix. Conversely, strong positive correlations between Fe_2O_3 and Cu, Bi, and Co, as well as between S and Co and Bi, highlight the controlling role of sulfide phases—chiefly pyrite, pyrrhotite, and arsenopyrite—in the geochemical behavior of these elements [23]. Correlations such as Cu–Ag, Zn–Mn, and Ni–As further reflect well-documented mineralogical linkages, including chalcopyrite with Ag, sphalerite with Mn, and arsenopyrite with Ni and As [24,25]. The very strong correlation between Bi and Co (r = 0.97) suggests a close association within Fe-sulfide phases, with possible implications for the recovery of critical metals [26]. Negative correlations between SiO_2/Al_2O_3 and Zn/Pb highlight the contrast between the silicate–carbonate matrix, which is poor in metals, and the sulfide phases, which serve as the primary hosts of base metals. Similarly, negative correlations between Mn and Al_2O_3/Ni indicate that Mn is linked to carbonate and oxide minerals, whereas Ni is predominantly controlled by the presence of sulfides.

Magnetic susceptibility (MS) data further support the observed geochemical and mineralogical patterns in the analyzed samples. Pyrrhotite is strongly ferromagnetic, in contrast to pyrite and arsenopyrite, which are diamagnetic to weakly paramagnetic; this explains why pyrrhotite is the only mineral capable of generating high MS values in the flotation tailings material. Accordingly, Fe-sulfide–rich samples (e.g., T3.13 and T3.14) display the highest recorded MS values, consistent with their elevated sulfur contents (12.3% and 10.90%, respectively), confirming that the abundance of pyrrhotite exerts primary control over the magnetic response. Pyrrhotite is the main carrier of the magnetic signal, while its alteration products—hematite and goethite—may provide a secondary but measurable contribution [27]. In contrast, samples dominated by the silicate–carbonate matrix show markedly lower MS values, as minerals such as quartz, calcite, and K-feldspar have negligible or zero susceptibility and therefore diminish the overall magnetic signal. Overall, MS patterns are consistent with the mineralogical assemblage and demonstrate that variations in mineral distribution—particularly the proportion of pyrrhotite relative to non-magnetic gangue minerals—govern the magnetic properties of the flotation tailings.

The relatively low metal concentrations and the complex intergranular associations of the sulfide minerals indicate that economically viable metallurgical processing of the tailings is limited. In contrast, the high abundance of other minerals (quartz, calcite and orthoclase) and their fine grain size (~90% smaller than 0.5 mm) suggests the potential use of the tailings as low-value aggregates in the construction industry. This approach enables material valorization despite the low metal content and provides a sustainable solution for tailings management.

5. Conclusions

The flotation tailings of the Rudnik mine exhibit mineralogical and geochemical characteristics that reflect the complexity of the processed primary ore, the efficiency of mineral liberation and phase selectivity during flotation, as well as post-depositional alterations, including sulfide oxidation and the formation of secondary minerals. Key findings include the following:

- Complex mineral associations and microtextural intergrowths of rock-forming minerals with sulfides hinder efficient flotation of the primary ore.
- Flotation tailings are dominated by quartz, calcite, orthoclase and accompanied by Ca-garnets, Ca-pyroxenes and epidote. Economically valuable sulfides—sphalerite,

galena, and chalcopyrite—are mostly present in fractions finer than 400 μm (mostly below 100 μm) and occur as dispersed grains within a silicate–carbonate matrix. Post-depositional oxidation is moderately developed; pyrite is often replaced by hematite, galena by cerussite, and chalcopyrite by malachite, while other sulfides remain relatively unaltered.

- High SiO_2 and Al_2O_3 contents confirm the dominance of silicate and aluminosilicate minerals, whereas elevated Fe_2O_3 and S reflect the presence of iron sulfides. Zn, Pb, and Cu concentrations are below 1%, while minor elements such as Ag and Bi, although present at low levels, may hold future economic potential.
- Mass magnetic susceptibility data support the mineralogical observations: samples with higher Fe_2O_3 and S show elevated susceptibility, whereas samples with lower Fe_2O_3 exhibit reduced susceptibility, consistent with XRD and SEM-EDS analyses.
- Given the relatively low metal concentrations and the complex intergranular associations of the minerals, the most realistic immediate valorization pathway is the use of the tailings as low-value construction aggregates. Future research will include various mineral processing techniques for further characterization and evaluation of the tailings. Selective pre-treatment for trace-metal recovery could also be investigated as a secondary option following detailed characterization and a technical–economic assessment.

Supplementary Materials: The following supporting information can be downloaded at: https://www.mdpi.com/article/10.3390/min15121287/s1, Representative SEM-EDS spectra of the minerals; Table S1: Chemical composition of mineral phases measured with SEM-EDS method and presented in oxides wt% normalized; Table S2: Chemical composition of mineral phases measured with SEM-EDS method in wt% normalized.

Author Contributions: Conceptualization, S.P., V.S. and D.Ž.; methodology, N.N., J.S., V.C., J.M. and Lj.O.; validation, V.S. and D.Ž.; formal analysis, N.N., J.S., V.C. and Lj.O.; writing—original draft preparation, S.P. and V.S.; writing—review and editing, V.C., D.Ž. and N.N.; project administration, V.S. All authors have read and agreed to the published version of the manuscript.

Funding: This research was funded by the Science Fund of the Republic of Serbia, GRANT 7522—REASONING and the Ministry of Science, Technological Development and Innovation of the Republic of Serbia (Grant numbers: 451-03-136/2025-03/200126; 451-03-136/2025-03/200053; 451-03-136/2025-03/200023).

Data Availability Statement: All data generated or analyzed during this study are included in this published article and are available upon request from the corresponding author.

Acknowledgments: The permission to take samples and the determination of selected trace elements by the "Rudnik i flotacija Rudnik" Company is gratefully acknowledged.

Conflicts of Interest: Author Ljiljana Obrenović was employed by the company Rudnik and flotation Rudnik doo. The remaining authors declare that the research was conducted in the absence of any commercial or financial relationships that could be construed as a potential conflict of interest.

References

1. European Commission. Mining Waste; European Commission—Environment. Available online: https://environment.ec.europa.eu/topics/waste-and-recycling/mining-waste_en#law (accessed on 20 September 2025).
2. Gavrilovic, D. *Statistical Yearbook of the Republic of Serbia*; Statistical Office of the Republic of Serbia: Belgrade, Serbia, 2024; 446p.
3. Steiner, T.M.C.; Bertrandsson Erlandsson, V.; Šajn, R.; Melcher, F. Preliminary chemical and mineralogical characterization of tailings from base metal sulfide deposits in Serbia and North Macedonia. *Geol. Croat.* **2022**, *75*, 291–302. [CrossRef]
4. Šajn, R.; Ristović, I.; Čeplak, B. Mining and metallurgical waste as potential secondary sources of metals—A case study for the West Balkan region. *Minerals* **2022**, *12*, 547. [CrossRef]

5. Djokić, B.V.; Jović, V.; Jovanović, M.; Ćirić, A.; Jovanović, D. Geochemical behaviour of some heavy metals of the Grot flotation tailing, Southeast Serbia. *Environ. Earth Sci.* **2012**, *66*, 933–939. [CrossRef]
6. Abramović, F.; Cvetkov, V.; Ilić, A.; Životić, D. Korelacija magnetnog susceptibiliteta i sadržaja metala u flotacijskom jalovištu. In Proceedings of the 18. Kongres Geologa Srbije "Geologija Rešava Probleme", Divčibare, Serbia, 1–4 June 2022; pp. 23–24.
7. Lazić, P.; Nikšić, Đ.; Miković, B.; Tomanec, R. Copper minerals flotation in flotation plant of the "Rudnik" mine. *Podzemni Rad.* **2019**, *35*, 23–35. [CrossRef]
8. Lazić, P.; Nikšić, D.; Tomanec, R.; Vučinić, D.; Cvetičanin, L. Chalcopyrite floatability in flotation plant of the Rudnik mine. *J. Min. Sci.* **2020**, *56*, 119–125. [CrossRef]
9. Nikšić, D.; Lazić, P.; Kostović, M. Flotability of chalcopyrite from the Rudnik deposit. *J. Min. Sci.* **2021**, *57*, 523–530. [CrossRef]
10. Popović, R.; Umeljić, G. *Metallogeny of the Rudnik Mountain, Position in Time and Space*; Rudnik doo: Belgrade, Serbia, 2015; p. 224.
11. Cvetković, V.; Šarić, K.; Pécskay, Z.; Gerdes, A. The Rudnik Mts. volcano-intrusive complex (central Serbia): An example of how magmatism controls metallogeny. *Geol. Croat.* **2016**, *69*, 89–99. [CrossRef]
12. Hoerler, J.; Von Quadt, A.; Burkhard, R.; Peytcheva, I.; Cvetković, V.; Baker, T. The Karavansalija mineralized center at the Rogozna Mountains in SW Serbia: Magma evolution and time relationship of intrusive events and skarn Au±Cu–Pb–Zn mineralization. *Front. Earth Sci.* **2022**, *9*, 798701. [CrossRef]
13. Petrović, S.; Bakker, R.J.; Cvetković, V.; Jelenković, R. Multiphase evolution of fluids in the Rudnik hydrothermal-skarn deposit (Serbia): New constraints from study of quartz-hosted fluid inclusions. *Mineral. Petrol.* **2024**, *118*, 461–482. [CrossRef]
14. Stojanović, J.; Radosavljević-Mihajlović, A.; Radosavljević, S.; Vuković, N.; Pačevski, A. Mineralogy and genetic characteristics of the Rudnik Pb-Zn/Cu, Ag, Bi, W polymetallic deposit (Central Serbia)—New occurrence of Pb (Ag) Bi sulfosalts. *Period. Mineral.* **2016**, *85*, 121–135.
15. Google. Google Maps. Available online: https://www.google.com/maps (accessed on 29 September 2025).
16. OREAS 135. Available online: https://www.oreas.com/crm/oreas-135/ (accessed on 18 November 2025).
17. Whitney, D.L.; Evans, B.W. Abbreviations for names of rock-forming minerals. *Am. Mineral.* **2010**, *95*, 185–187. [CrossRef]
18. Fuerstenau, D.W.; Phatak, P.B.; Kapur, P.C.; Abouzeid, A.Z. Simulation of the grinding of coarse/fine (heterogeneous) systems in a ball mill. *Int. J. Miner. Process.* **2011**, *99*, 32–38. [CrossRef]
19. Little, L.; Mainza, A.N.; Becker, M.; Wiese, J.G. Using mineralogical and particle shape analysis to investigate enhanced mineral liberation through phase boundary fracture. *Powder Technol.* **2016**, *301*, 794–804. [CrossRef]
20. Stojanović, J.N.; Radosavljević, S.A.; Tošović, R.D.; Pačevski, A.M.; Radosavljević-Mihajlović, A.S.; Kašić, V.D.; Vuković, N.S. A review of the Pb-Zn-Cu-Ag-Bi-W polymetallic ore from the Rudnik orefield, Central Serbia. *Geol. Anal. Balk. Poluostrva* **2018**, *79*, 47–69. [CrossRef]
21. Garcia, C.; Ballester, A.; Gonzalez, F.; Blázquez, M.L. Pyrite behaviour in a tailings pond. *Hydrometallurgy* **2005**, *76*, 25–36. [CrossRef]
22. Zdravković, A.; Cvetković, V.; Pačevski, A.; Rosić, A.; Šarić, K.; Matović, V.; Erić, S. Products of oxidative dissolution on waste rock dumps at the Pb-Zn Rudnik mine in Serbia and their possible effects on the environment. *J. Geochem. Explor.* **2017**, *181*, 160–171. [CrossRef]
23. Vaughan, D.J.; Corkhill, C.L. Mineralogy of sulfides. *Elements* **2017**, *13*, 81–87. [CrossRef]
24. George, L.L.; Cook, N.J.; Ciobanu, C.L. Partitioning of trace elements in co-crystallized sphalerite–galena–chalcopyrite hydrothermal ores. *Ore Geol. Rev.* **2016**, *77*, 97–116. [CrossRef]
25. George, L.L.; Cook, N.J.; Crowe, B.B.; Ciobanu, C.L. Trace elements in hydrothermal chalcopyrite. *Mineral. Mag.* **2018**, *82*, 59–88. [CrossRef]
26. Godirilwe, L.L.; Gayratov, B.; Jeon, S.; Shibayama, A. Utilization of pyrite-rich tailings in sulfation roasting for efficient recovery of copper, nickel, and cobalt from smelter slag. In Proceedings of the 11th World Congress on Mechanical, Chemical, and Material Engineering (MCM 2025), Paris, France, 19–21 August 2025.
27. Dunlop, D.J.; Özdemir, Ö. *Rock Magnetism: Fundamentals and Frontiers*; Cambridge University Press: Cambridge, UK, 1997.

Disclaimer/Publisher's Note: The statements, opinions and data contained in all publications are solely those of the individual author(s) and contributor(s) and not of MDPI and/or the editor(s). MDPI and/or the editor(s) disclaim responsibility for any injury to people or property resulting from any ideas, methods, instructions or products referred to in the content.

MDPI AG
Grosspeteranlage 5
4052 Basel
Switzerland
Tel.: +41 61 683 77 34

Minerals Editorial Office
E-mail: minerals@mdpi.com
www.mdpi.com/journal/minerals



Disclaimer/Publisher's Note: The title and front matter of this reprint are at the discretion of the Guest Editors. The publisher is not responsible for their content or any associated concerns. The statements, opinions and data contained in all individual articles are solely those of the individual Editors and contributors and not of MDPI. MDPI disclaims responsibility for any injury to people or property resulting from any ideas, methods, instructions or products referred to in the content.





Academic Open
Access Publishing

mdpi.com

ISBN 978-3-7258-8660-9